Università degli Studi di Parma

PhD in Science and Technology of Innovative Materials
XX° Cycle

Disciplinary scientific sector "CHIM04"

HOST-GUEST SUPRAMOLECULAR POLYMERS BASED ON PHOSPHONATE CAVITANDS

Coordinator: Prof. Manfredo Manfredi

Supervisor: Prof. Enrico Dalcanale

Author: Dr. Roger Yebeutchou Mbanda

“Chance Favours the Prepared Mind”

Alexander Fleming

A toi maman

contents

Chapter 1

INTRODUCTION

Chapter 2

COMPLEXATION STUDIES OF PHOSPHONATE CAVITANDS

Chapter 3

HOST-GUEST DRIVEN SELF-ASSEMBLY OF SUPRAMOLECULAR HOMOPOLYMERS

Chapter 4

SELF-ASSEMBLY OF SUPRAMOLECULAR COPOLYMERS VIA HOST-GUEST INTERACTIONS AND METAL-COORDINATION

Chapter 5

HIGHLY SELECTIVE MONOMETHYLATION OF PRIMARY AMINES PROMOTED BY HOST-GUEST COMPLEXATION

Chapter 1

General introduction

Non covalent interactions are increasingly being used for the self-assembly of well-defined supramolecular architectures and molecular materials. Such interactions are important in polymer science where hydrogen bonding and other weak interactions are pivotal in determining polymer properties and in the design of new polymer architectures.[1] Supramolecular polymers[2] may have advantages over traditional polymers because of the reversible nature of the non-covalent interactions that hold them together. Because these materials are made up of small molecules, they could flow like small molecules at elevated temperatures or in dilute solution.[3] Also, they might respond differently to high levels of stress, since the interactions holding the chain together are constantly being broken and reformed. Moreover, thanks to the reversibility of the non-covalent interactions in supramolecular polymers, the materials should reach a thermodynamically favorable state with the maximum possible cross-linking. In a conventional network the cross-links are irreversible, which leads to polymers that cannot easily adjust to changing environmental stresses and often leaves behind a high degree of un-reacted functionalities.

The design of supramolecular polymers has several elements to it. The most important aspect is the choice of the interactions that will hold the monomers together. The interaction must be stronger than the van der Waal's forces between the polymer chains, but weak enough to allow

reversible dissociation under a reasonable stress. However, the interactions used always rely on the cooperative phenomenon of many weak interactions, which lack directionality, giving rise to microphase-separated structures or gelation due to network formation.[4] For linear supramolecular polymers,[5] it is a prerequisite to have strong and highly directional, reversible interactions in order to construct materials that include a reversible alternative for the covalent bond.

This thesis is organized as follow:

Chapter 2. In this chapter we chose the type of interaction (host-guest interactions based tetraphosphonate cavitands[6]), we devised the synthetic procedure of the Tiiii cavitand,[7] and studied the host-guest complexation processes with different techniques to verify if this type of interaction has the requisites for application in the self-assembly host-guest polymers.

Chapter 3. This chapter describes the design and the synthesis of the monomer units for the self-assembly of linear supramolecular homopolymers, their self-assembly and characterization in the solid state and in solution.

Chapter 4. This chapter describes the design and synthesis of the monomer units for the self-assembly of linear and cross-linked supramolecular copolymers, and their characterization.

Chapter 5. In this chapter, we exploited the high association constants recorded in the complexation of N-methylammonium salts by Tiiii phosphonate cavitands to segregate the monomethylated products of the monomethylation reactions of primary amines. In this way, high selective monomethylation of primary aliphatic, cyclo-aliphatic and aromatic amines was obtained.

References

[1] a) C. Hilger, M. Dräger, R. Stadler, *Macromolecules* **1992**, *25*, 2498; b) A. Aggeli, M. Bell, N. Boden, J. N. Keen, P. F. Knowles, T. C. B. McLeish, M. Pitkeathly, S. E. Radford, *Nature*, **1997**, *386*, 259-262.

[2] C. Fouquey, J.–M. Lehn, A.–M. Levelut, *Adv. Mater.*, **1990**, *2*, 254-257; J. S. Moore, *Curr. Opin. Solid. State Mater. Sci.*, **1996**, *1*, 777-788; N. Zimmerman, J. S. Moore, S. C. Zimmerman, *Chem. Ind.*, **1998**, 604-610.

[3] C. B. St Pourcain, A. C. Griffin, *Macromolecules*, **1995**, *28*, 4116-4121.

[4] M. Möller, J. Omeis, E. Mühleisen, in *Reversible Polymeric Gels and Related Systems*, P. S. Russo, Ed. (ACS Symp. Ser. 350, American Chemical Society, Washington DC, 1987), chap. 7.

[5] J.-M. Lehn, Macrom. Chem. Macrom. Symp., **1993**, *69*, 1.

6 P. Delange, J.-P. Dutasta. *Tetrahedron Lett.*, **1995,** 60, 36, 9325-9328.

7 R. Pinalli, M. Suman, E. Dalcanale, *Eur. J. Org. Chem.*, **2004,** 451-462.

Chapter 2

COMPLEXATION STUDIES OF PHOSPHONATE CAVITANDS

2.1 Introduction

Molecular receptors are host molecules capable of binding or recognizing selectively guest molecules, which nature varies from neutral to cationic and anionic. The design and development of the receptors to facilitate recognition requires considerable effort and in recent years many papers have appeared in this very important area of chemistry. Many different receptors based on cryptands[1], crown ethers[2], calixarenes[3], ciclodextrins[4] and cyclic poliamines[5] are described in the literature. Considerable attention has been paid to molecular receptors based bridged resorcinarenes, named cavitands. The name cavitands was given in 1983 by Cram[6] to the class of synthetic organic compounds with enforced cavities of molecular dimensions. The choice of recognition sites in cavitands receptors is pivotal. Resorcinarenes are convenient molecular platforms for the construction of cavitand receptors. They can be easily prepared in high yield by the acid-catalyzed reactions between resorcinol and either aliphatic or aromatic aldehydes.[7] The flexible resorcinarene can be rigidified by reacting its four couples of adjacent phenolic oxygen with different bridging groups. Different phosphorous bridged-cavitands have been synthesized in the last years. By changing the degree of

oxidation of the phosphorous it is possible to tune their complexation properties. P(III) phosphonito cavitands are stabilized by transition metals and was used in catalysis.[8] P(V) phosphonate cavitands are divided in two groups: phosphonate PO and thiophosphonate PS which are able to recognize respectively hard and soft metals. Due to the versatility of the phosphorus atoms, many synthetic receptors have been equipped with it. In this Chapter, we will focus our attention to a single class of cavitands, the phosphonate ones.

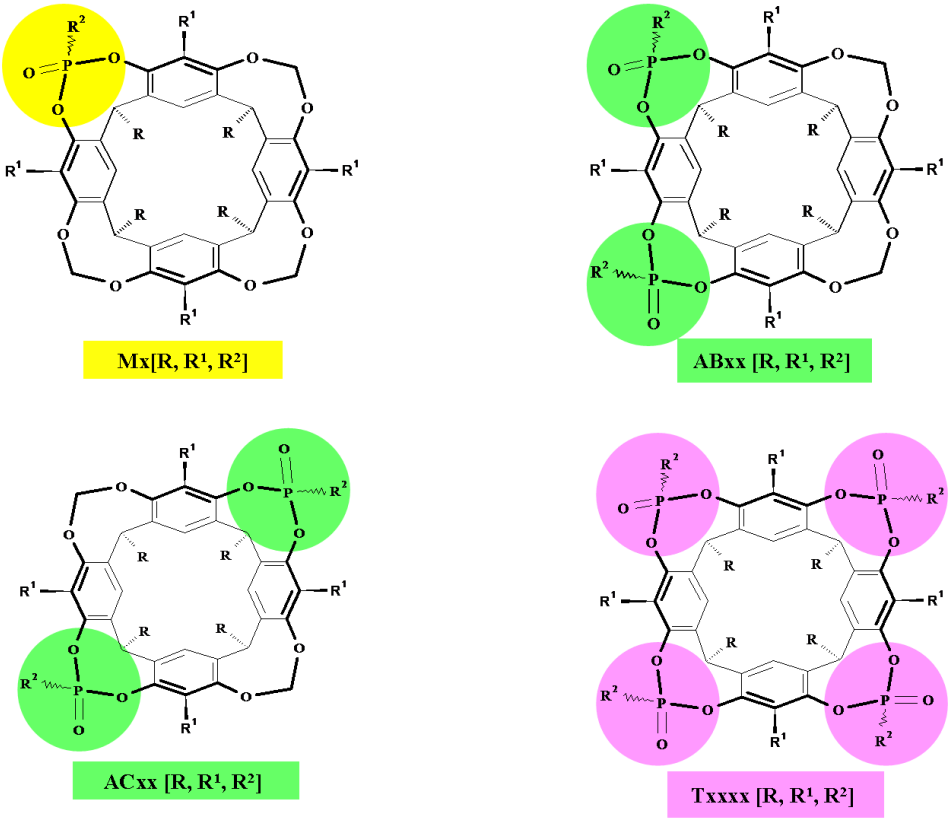

Figure 1. Nomenclature of the phosphonate cavitands

Before delving into the subject, it is important to define the nomenclature of the phosphorous-bridged cavitands based on resorcinarene skeletons. Such nomenclature summarizes the number and relative positions of phosphorous bridges, their stereochemistry, and the type of substituents at the lower rim, at the apical positions, and on the phosphorous bridges, respectively, in a single term.[9] Figure 1 reports a survey of the structure for phosphonate cavitands. The first, capital letters define the number and positions of bridges second, lower case letters define the in-out stereochemistry at each P center, and R, R^1, and R^2 in brackets define the substituents at the lower rim, in apical positions, and on the P stereocenters respectively. For the corresponding tetrathiophosphonate cavitands the term S is adopted (Tiiii→TSiiii).

The first attempt to synthesize phosphonate-cavitands was carried out by Cram's group in the 1980s by reacting a methyl-footed resorcinarene[10] with dichlorophenylphosphonate[11]. The complex mixture obtained was not investigated further, due to the difficulties to isolate the different diastereoisomers formed. Some years later, Dalcanale and coworkers reported the preparation and characterization of several tetraphosphate-cavitands[12] using methyl-footed resorcinarenes as molecular platforms (Scheme 1).

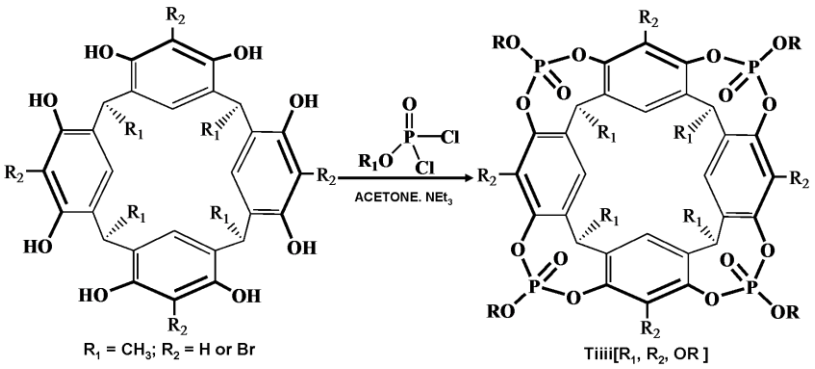

Scheme 1. Synthesis of tetraphosphate-cavitands.

The reaction conducted with a series of aryl dichlorophosphates in dry acetone or THF in the presence of an excess of triethylamine as base, resulted in all cases in the formation of five of the six possible diastereomers (Figure 2) observed via HPLC analysis of the crude reaction (Table 1).

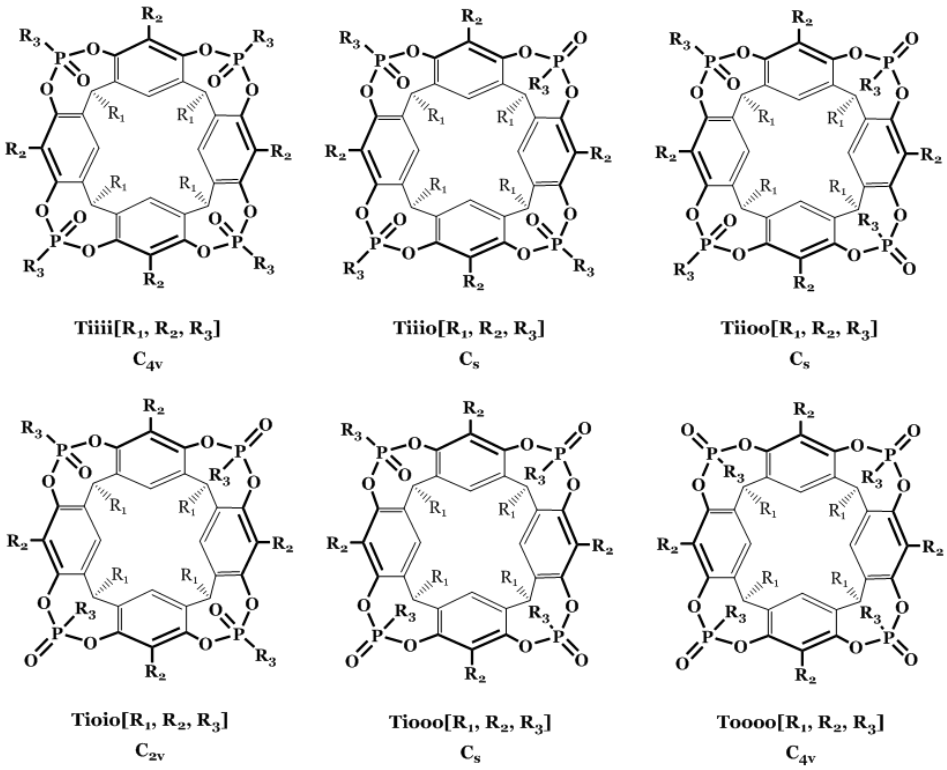

Figure 2. The six possible diastereomers of tetraphosphonate cavitands.

The reactions (4-12) in Table 1 occur with good yield (>50%) and the various isomers having different orientations of the P=O groups, either inward (i) or outward (o) with respect to the cavity was identified by a combination of ^{1}H NMR, ^{13}C NMR, and ^{31}P NMR spectroscopy. The number of phosphorous and hydrogen atom resonances reflects the

different symmetries of the six diastereomers, and combination of the two allowed the univocal identification of the Tiioo and Tioio isomers.

	R_1	R_2	a iiii	b iiio	c iioo	d ioio	e iooo	f oooo	overall isolated yield, %
3	ethoxy	H			33[a]	25[a]	42[a]		12
4	4-methylphenoxy	H	<1	17	18	18	38	8	80
5	4-*tert*-butylphenoxy	H		14	39	12	32	3	75
6	4-chlorophenoxy	H		22	27	18	33		80
7	2-phenylphenoxy	H	10	34	26	17	13		50
8	2,6-diisopropyl-phenoxy	H		52	22	13	13		55
9	2,4,6-trimethyl-phenoxy	H		50	20	18	12		58
10	4-methylphenoxy	Br		22	20	21	34	3	70
11	4-*tert*-butylphenoxy	Br		30	27	16	27		68
12	4-chlorophenoxy	Br		33	28	14	25		65

Table1. Isomer distribution of phosphate cavitands via HPLC analysis.

To distinguish further between the two remaining pairs of diastereoisomers (Tiiii vs Toooo and Tiiio vs Toooi), chemical shift differences must be considered: the protons directed inward with respect to the cavity experience a strong and diagnostic high-field shift. ^{13}C NMR and ^{1}H NMR relaxation time experiments independently confirmed the attribution.[13] The crystal structure of Tioio[CH_3, H, OTol] was resolved, confirming the attribution.[14]

The iiii isomer that possesses the best qualifications as molecular receptor thank to the four P=O groups converging toward the center of the cavity is not formed in the case of phosphate cavitands. In order to change the distribution in favour of iiii or iiio isomers, bromide were introduced in apical positions of starting resorcinarenes but as shown in Table 1 (**10**-**12**) no change of the isomers distribution is evident. At this point, the attention was turned toward phosphonate cavitands.

The stereoselective synthesis of Tiiii isomer was achieved by Dutasta[15] and co-workers in 1995 using toluene as solvent in the presence of 0.2 equivalents of N-methylpyrrolidine (NMP) (Scheme 2).

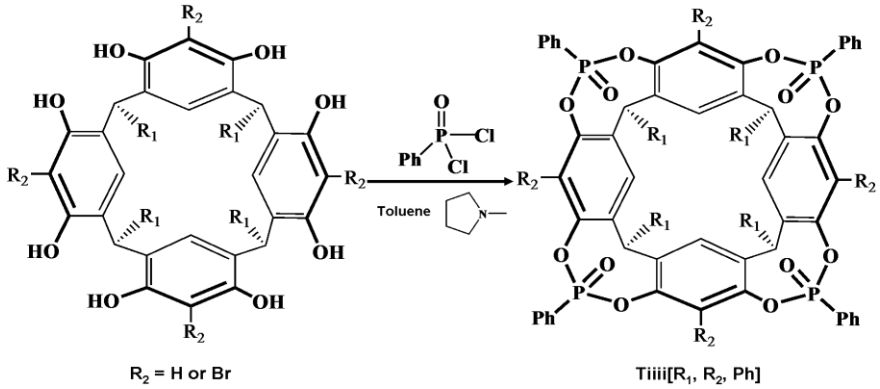

Scheme 2. Stereoselective synthesis of phosphonate cavitands.

In this case Tiiii isomer was obtained in 25% of yield with only a minor amount of Tiiio isomer present. The complexation studies with these cavitands provided good results and high association constants $>10^7$ M^{-1} was recorded for alkali, alkali earth and ammonium salts, obtained from extraction methods. Several tetraphosphonate-cavitands have been synthesized with a similar procedure isolating both the Tiiii and Tiiio isomers in good yield[16] without traces of the other four isomers (Table 2).

	R_2	R_1	iiii(%)	iiio(%)
A	H	CH_3	25	-
B	H	CH_2CH_2Ph	51	5
C	H	n-$C_{11}H_{23}$	38	3
D	H	$(CH_2)_7$ OC_6H_4-o-NO_2	40	-
E	H	$(CH_2)_7$ OC_6H_4-p-NO_2	31	-
F	Br	n-$C_{11}H_{23}$	-	44

Table 2. Yields and stereoisomer distribution of tetraphosphonate-cavitands using the Dutasta procedure.

The introduction of four bromines in apical positions of the starting resorcinarene strictly influences the stereochemistry of the reaction since only the iiio isomer was obtained (Table 2F).

In a different experiment, a resorcinarene was allowed to react with $PhPOCl_2$ in toluene in presence of 10 equivalents of triethylamine (Table 3B). In this case Tiiii and Tiiio isomers were obtained in 28.5% and 7% yield respectively.

	R_2= H R_1	amines	solvents	Tiiii	Tiiio
A	$CH_2CH_2C_6H_5$	NMP	Toluene	53	9
B	$CH_2CH_2C_6H_5$	Et_3N	Toluene	28.5	7
C	CH_3	Et_3N	acetone	0	0
D	CH_3	NMP	acetone	0	0

Table 3. Influence of the solvent/amine pair in the stereochemistry of the bridging reaction of resorcinarenes with $PhPOCl_2$.

The same reactions were made in acetone as solvent in presence of 10 eq of NMP and the results were the same as reported by Dalcanale previously (Table 3C and D); no trace of Tiiii and Tiiio isomers were observed. These results led to conclude that the solvent/amine pair is crucial in the stereochemistry of the bridging reaction of resorcinarenes with dichlorophenylphosphine oxide.

In a different approach Puddephatt and coworkers proposed the stereoselective synthesis of tetraphosphonito cavitands by reacting resorcinarenes with dichlorophenylphosphine in diethyl ether as solvent and in presence of pyridine as base[17] (Scheme 3).

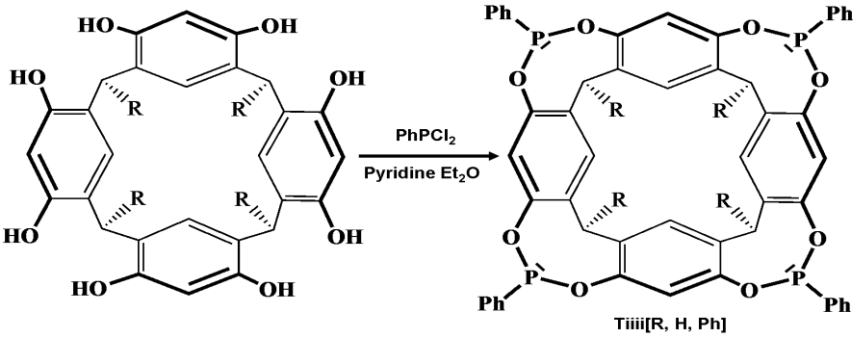

Scheme 3. Stereoselective synthesis of Tiiii phosphonito cavitands.

The formation of the Tiiii isomer with all phenyl groups directed outward and ion pairs directed inward the center of the cavity is preferred as predicted by theoretical calculations.[18] The stereochemistry is consistent with the observation in the ^{31}P NMR spectrum of a singlet corresponding to a unique product formed. This type of phosphorous-cavitands was used as ligand for transition metals coordination.[19]

Using the Puddephatt procedure, Nifantyev Group's synthesized the first amidothiophosphonate cavitand in two steps (Scheme 4): resorcinarene reacts initially with tris(diethylamino) phosphine giving rise to Tiiii isomer of amidophosphonito cavitands (Scheme 4a) in 72% yield, followed by in situ oxidation of phosphonito cavitands with sulphur (Scheme 4b) leading selectively to the formation of TSiiii amidothiophosphonate cavitands in 95% yield[20].

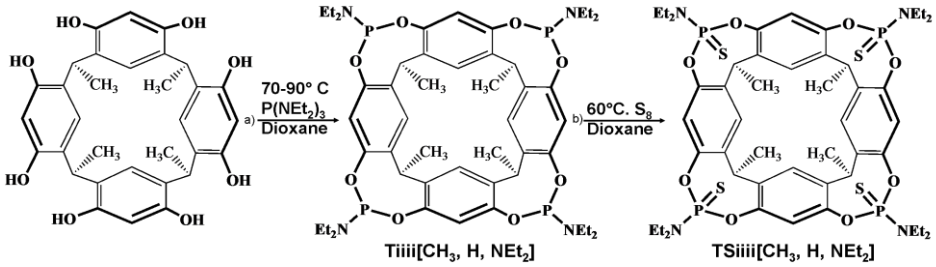

Scheme 4. Stereoselective synthesis of TSiiii thioamidophosphonate cavitands.

The Nifantyev procedure was modified by Dutasta group for the stereoselective synthesis of the first TSiiii thiophosphonate cavitand (Scheme 5). Reaction of resorcinarenes with $PhPCl_2$ in diethyl ether in presence of pyridine afforded exclusively the Tiiii phosphonito cavitand (Scheme 5a). Its subsequent *in situ* oxidation with sulfur proceeded with retention of configuration and led to the thiophosphonate cavitand TSiiii[$C_{11}H_{23}$, H, Ph] in 52% yield after column chromatography.[21]

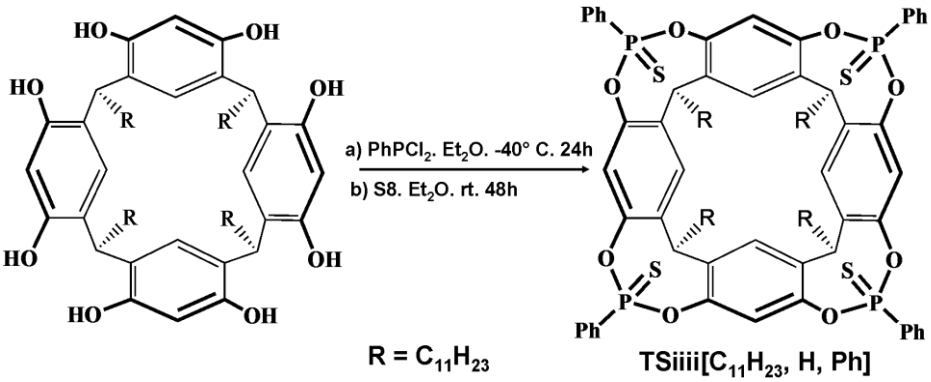

Scheme 5. Sterereoselective synthesis of TSiiii thiophosphonate cavitands.

The ionophoric properties of cavitand TSiiii[$C_{11}H_{23}$, H, Ph] toward soft metals were studied and thus they were used for the extraction of Ag, Hg, Pb, Cu, Ni. Co, Zn, Cd, Co, Ti picrate salts with good results.[22]

Reactions of substitution of sulphur with oxygen on phosphonate moiety using H_2O_2[23], peracids[24], and peroxide[25] on the phosphorous atoms are reported in literature. By tuning the reaction conditions, the substitution can occur either with retention or inversion of the configuration.

In particular, the Dutasta Group obtained the conversion of P=S in P=O moiety with retention of configuration by reacting thiophosphonate-cavitand with H_2O_2 in refluxed toluene (Scheme 6).[26]

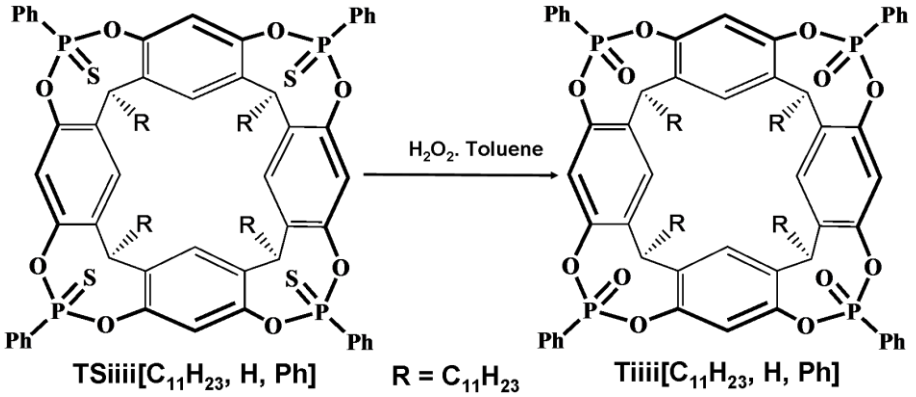

Scheme 6. Conversion TSiiii thiophosphonate cavitands to Tiiii phosphonate cavitands with retention of configuration.

In conclusion two methods were used for the stereoselective synthesis of Tiiii cavitands. The first one is the templating method that requires the use of N-methylpyrrolidine/toluene pair while the second one combines the Puddephatt and Nefantyev procedures leading to the unique Tiiii isomer.

2.2 Results and Discussion

2.2.1 Stereoselective synthesis of thiophosphonate and phosphonate cavitands

A part of diastereoselective synthesis of Tiiii and TSiiii cavitands was done in Lyon in collaboration with the group of Prof. J.-P. Dutasta of the ENS de Lyon (Ecole Normal Supérieure of Lyon).

In this chapter, we report a comprehensive study of the molecular recognition properties of Tiiii phosphonate cavitands toward ammonium and methyl pyridinium salts.

The study is articulated in two different items:

1) An accurate design and selection of the hosts and guests, in order to mimic host-guest polymerization events at the molecular level.

2) A survey of the major characterization techniques for this type of host-guest complexation, in order to obtain a suitable palette of tools to be applied to the polymerization case (Chapter 3).

The model cavitand Tiiii[C_3H_7, CH_3, Ph] was synthesized as host and the cavitands TSiiii[($3C_3H_7$ + CH_3-Py^+ X^-), CH_3, Ph] were synthesized as methyl pyridinium guests to study the dimerization processes (Figure 3).

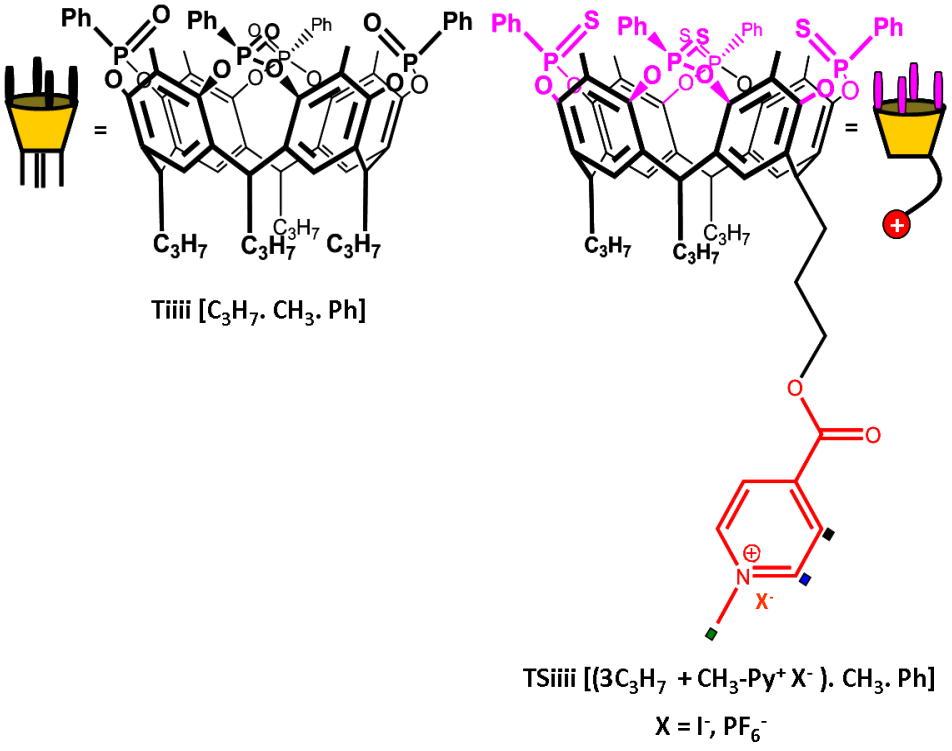

Figure 3. Target host and guest molecules for dimerization studies.

Synthesis of **TSiiii[($3C_3H_7$ + CH_3-Py^+ X^-), CH_3, Ph]**. The guest cavitands TSiiii[($3C_3H_7$ + CH_3-Py^+ X^-), CH_3, Ph] were synthesized following a six steps procedure.

Synthesis of mixed-footed resorcinarene. This class of resorcinarenes are obtained from the acid-catalyzed condensation reaction of methyl resorcinol with a mixture 1:3 of 2,3-dihydrofuran and an aldehyde.[27] In this specific case, a mixture 3:1 of butanal and 2,3-dihydrofuran was added to a solution of methyl resorcinol in methanol, and then a mixture 1:1 of a solution of HCl 12M in water and methanol was slowly added and heated at reflux (Scheme 7). Two sequential chromatographic separations on silica gel are necessary to isolate the pure mono-hydroxyl footed resorcinarene **1** in low yield 15%. Propyl-footed resorcinarene **2** has also been separated in 13% yield.

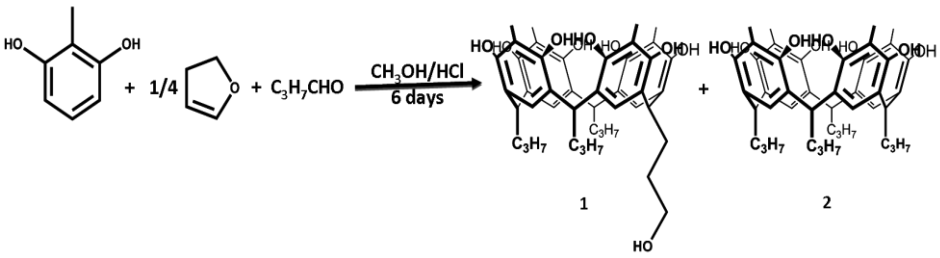

Scheme 7. Synthesis of resorcinares 1 and 2.

Selective upper rim protection of the mono-hydroxyl footed resorcinarene 1. Since the eight phenolic hydroxyl groups at the upper rim can interfere with the functionalization of the hydroxyl group at the lower rim, their preliminary protection is necessary before lower rim functionalization.[28] We adopted the silyl-bridged protection because it is easy to introduce, stable enough to allow the lower rim functionalization and easy to remove. We chose a resorcinarene with four methyls in apical positions for three reasons: i) to deepen the cavity, ii) strengthen the CH-π interactions between the host and the methyl pyridinium group, and

especially iii) to obtain a silyl-bridged cavitand stable enough to support further reaction conditions until deprotection reaction. Since the hydroxyl phenol groups on resorcinarene decreases the yield of the purification on silica gel, we performed the silyl-bridged reaction on the crude reaction of condensation. The reaction proceeds well using dichlorodimethyl silane as bridging agent in dry pyridine (Scheme 8).

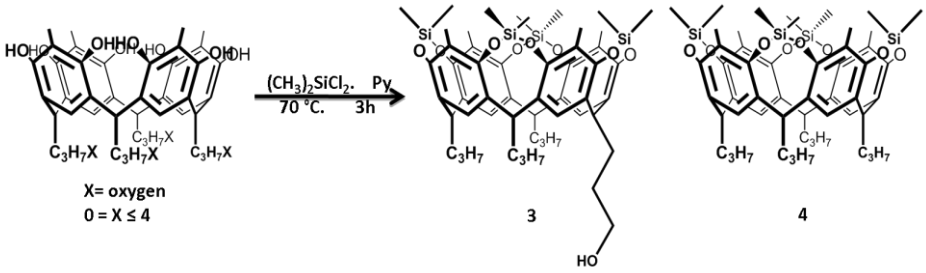

Scheme 8. Upper rim protection of resorcinarenes

In this way mono-hydroxyl footed silyl-bridged cavitand **3** was obtained directly in 29 % yield after chromatographic separation, together with propyl-footed silyl-bridged cavitand **4** in 16 % yield. The ^{1}H NMR spectrum of the product shows the presence of two new singlets, one at -0.7 ppm characteristic of Si-CH_3 that point inside the cavity and the other one at 0.4 ppm characteristic of Si-CH_3 that point outside of the cavity.

Lower rim functionalization. The isonicotinoyl moiety is introduced at lower rim by reacting, silyl-cavitand **3** with an excess of isonicotinoyl chloride hydrochloride in pyridine, affording the product as yellowish powder in 90% yield after crystallization from a mixture 2:1 of water and acetonitrile (Scheme 9).

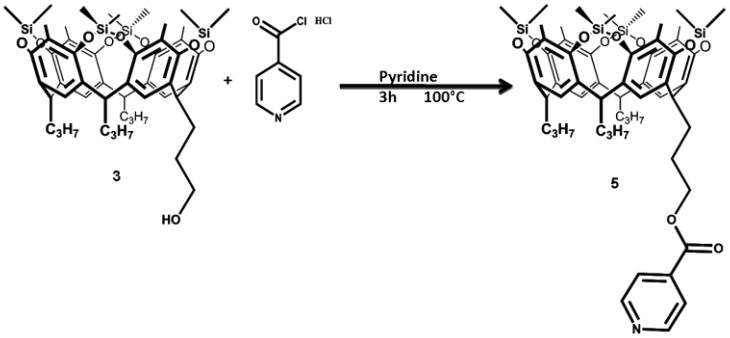

Scheme 9. Lower rim functionalization of mono-hydroxyl-footed silyl-cavitand 3.

Upper rim deprotection. The upper rim deprotection is a very easy reaction that occurs in DMF, using of a solution of HF in water as deprotecting agent (Scheme 10). The crude reaction is purified by simply crystallization from a mixture 1:1 of acetonitrile and water, affording the mono-pyridyl footed resorcinarene **6** in yield 81%.

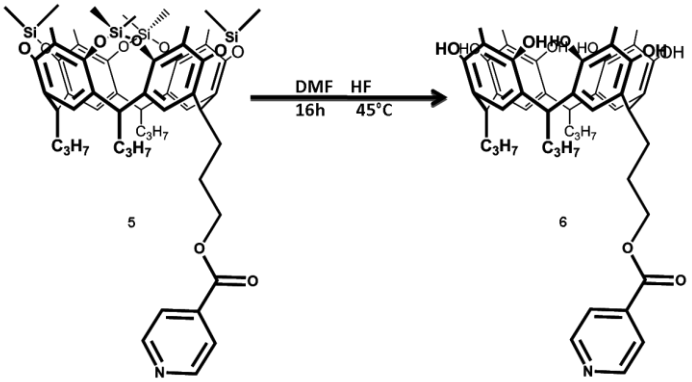

Scheme 10. Upper rim deprotection of mono-pyridyl footed silyl-cavitand 6.

Upper rim functionalization. We used the Dutasta[21] procedure described above to bridge with thiophosphonate moieties the upper rim of mono-pyridyl footed resorcinarene. In the reaction with the mono-pyridyl-footed resorcinarene **6**, the phosphoryl groups were attached to

the resorcinarene skeleton to produce the cavitand Tiiii [($3C_3H_7$ + py), CH_3, Ph] by using a two step synthesis (Scheme 11). The phosphonito-cavitand P(III) Tiiii [($3C_3H_7$ + py), CH_3, Ph], which was obtained by reacting mono-pyridyl-footed resorcinarene **6** with 4.1 equivalents of dichlorophenylphosphine (Scheme 11a), gave the thiophosphonate-cavitand TSiiii [($3C_3H_7$ + py), CH_3, Ph] after *in situ* treatment with an excess of S_8 (Scheme 11b) in yield 70%.

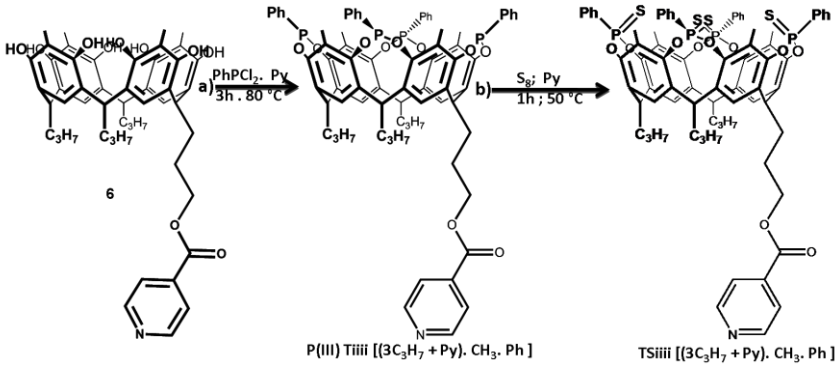

Scheme 11. Two step synthesis of cavitand TSiiii [($3C_3H_7$ + py), CH_3, Ph].

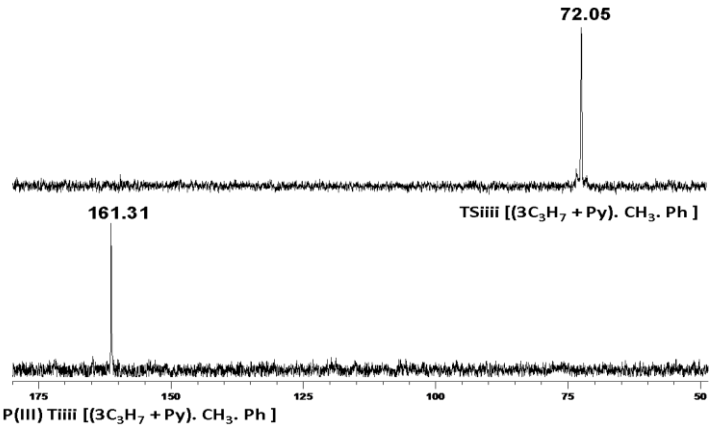

Figure 4. Formation of TSiiii [($3C_3H_7$ + py), CH_3, Ph] monitored via ^{31}P NMR in $CDCl_3$.

The reaction was monitored via ^{31}P NMR which spectrums show the complete *in situ* oxidation of the cavitand P(III) Tiiii [($3C_3H_7$ + py), CH_3, Ph] to the cavitand TSiiii [($3C_3H_7$ + py), CH_3, Ph] by looking at the diagnostic shift of the phosphorous signal from 161.31 to 72.05 ppm (Figure 4).

Methylation of the pyridine moiety. The cavitand TSiiii [($3C_3H_7$ + py^+I^-), CH_3, Ph] is obtained by methylation reaction of the pyridine moiety using and excess of methyl iodide as methylating agent in refluxing acetonitrile (Scheme 12a). The reaction affords quantitatively the product.

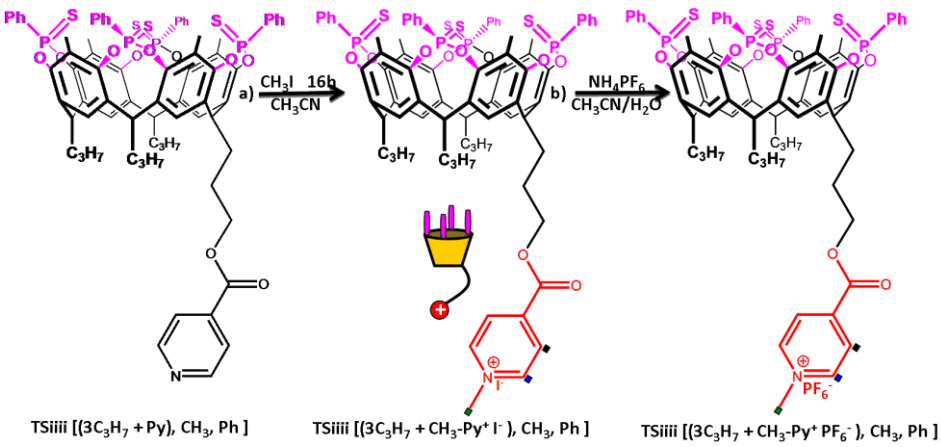

Scheme 12. Methylation reactions of TSiiii [($3C_3H_7$ + py), CH_3, Ph] (a) and exchange reaction of counterions (b).

The hexafluorophosphate counterion was introduced via ion exchange reaction using ammonium hexafluorophosphate. Cavitand TSiiii [($3C_3H_7$ + $Py^+PF_6^-$), CH_3, Ph] was obtained in 90% yield after re-crystallization in a mixture acetonitrile and water (Scheme 12b). The presence of the PF_6^- anion is proven by the multiplet at the ^{31}P NMR integrating for one phosphorous (see experimental section). The ^{31}P NMR signals of the P=S

groups in the methylated products show a minimal variation of chemical shift compared to that of the non methylated precursors (Figure 5). This indicates that the methyl pyridinium moiety is not complexed inside the TSiiii cavities.

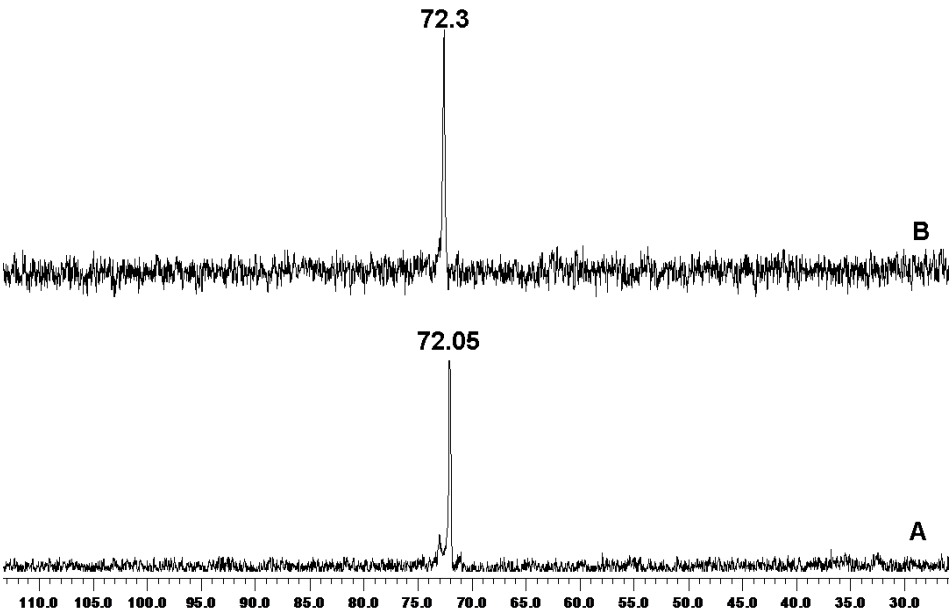

Figure 5. ^{31}P NMR in $CDCl_3$ of TSiiii cavitands before (A) and after (B) methylation.

This assertion is confirmed by the crystal structure of the cavitand TSiiii [($3C_3H_7$ + $py^+PF_6^-$), CH_3, Ph] obtained by a slow diffusion of water in a suspension of the cavitand in acetonitrile that was resolved in collaboration with Prof. Geremia of the University of Trieste.

The crystal structure of cavitand TSiiii [($3C_3H_7$ + $Py^+PF_6^-$), CH_3, Ph] confirms the NMR experimental data; at the upper rim the four P=S groups point all inside the cavity, at the lower rim there are three C3 alkyl chains and one C3 alkyl chain linked to a methyl-isonicotinium moiety. The crystal packing analysis shows that the counterion

hexafluorophosphate fit the lower rim and they are orientated in such a way that a P-F bond is directed toward the center of the cavity. In particular, a fluorine atom interacts with the CH_2 moieties of the alkyl chains through weak hydrogen bonds (Figure 6a) with a minimum distance F-H of 2.6 ± 0.02 Å. The anion located in a crystallographic symmetry center, links couple of cavitands through their lower rims (Figure 6b).

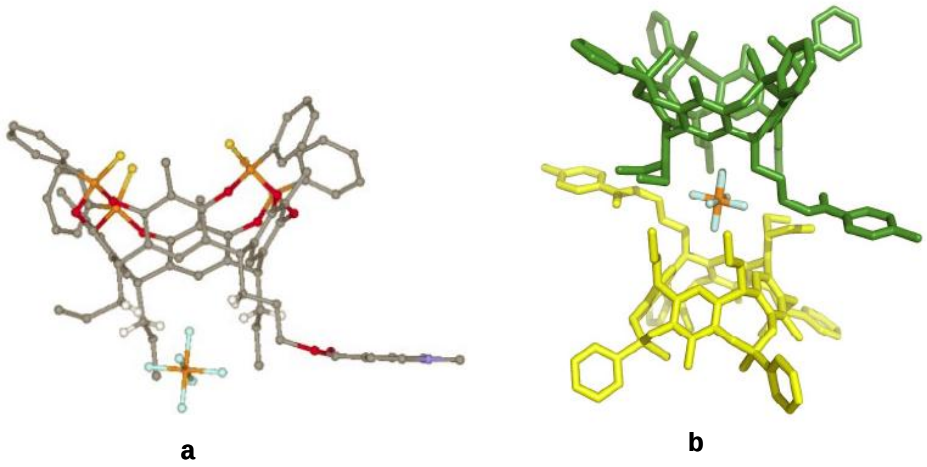

Figure 6. Crystal structure and section of crystal packing of cavitand TSiiii [($3C_3H_7$ + Py^+ PF_6^-), CH_3, Ph] that show a) interaction between PF_6^- and CH_2 of the alkyl chains; b) couple of cavitands hold together by the counterion.

In the crystal packing, couples of cavitands orientated with the cavities in opposite directions are related by a further inversion center. These couples are assembled through the methyl pyridinium moieties which partially close the cavity of the symmetry related molecule forming weak ion-dipole interactions between the positive charge of the N^+ of the methyl pyridinium moiety and the P=S bonds (Figure 7a). Probably the methyl pyridinium moiety never enters inside the cavity because of the steric hindrance of the sulphur groups that block the entrance of the

cavities. The simultaneous presence of the above interactions leads to the formation of supramolecular chain arrangement in which the chains are parallel to the 101 crystallographic directions (Figure7b). This arrangement of cavitands in the crystal packing highlighted the lack of specific host-guest interactions between the cavities and the methyl pyridinium groups.

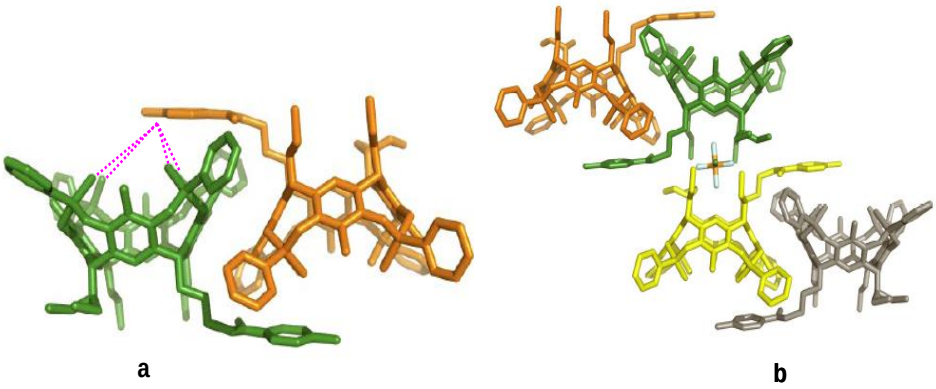

Figure 7. Crystal packing of the cavitand TSiiii [($3C_3H_7$ + py^+ PF_6^-), CH_3, Ph] shows a) the N^+-S=P ion-dipole interactions between a couple of cavitands and b) arrangement of the cavitands along the 101 crystallographic axis

Synthesis of the cavitand Tiiii[C_3H_7, CH_3, Ph]. As reported by Dutasta[16], fours bromines in apical positions of a resorcinarene lead to the formation of the non desired diastereomer Tiiio (Table 3F) by employing Ph(Cl_2)PO as bridging agent. By substituting the four bromines in apical positions with four methyls, the same result obtained by Dutasta was observed. So the two step synthesis to prepared TSiiii cavitand[21] followed by substitution reaction of sulphurs with oxygen reported by Dutasta for the synthesis of Tiiii[R_1, H, Ph][26] was used. Scheme 13 shows the first step.

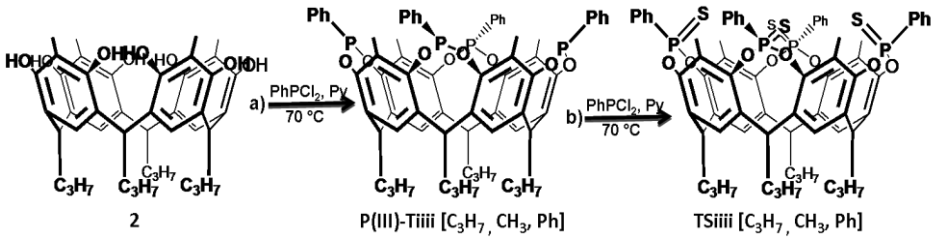

Scheme 13. Stereoselective synthesis of cavitand TSiiii[C_3H_7, CH_3, Ph].

Resorcinarene **2** reacts with 4.1 equivalents of dichlorophenylphosphine in pyridine (Scheme 13 a), leading to the formation of only Tiiii phosphonito cavitand confirmed by the ^{31}P NMR performed on crude reaction that shows a single peak at 162 ppm diagnostic of Tiiii isomer (Figure 9a). Subsequent in situ oxidation with S_8 occurs with retention of configuration leading to the cavitand TSiiii[C_3H_7, CH_3, Ph] in 70 % yield. The iiii configuration of the P=S bond is confirmed by a single peak at ^{31}P NMR at 72 ppm (Figure 9b). In collaboration with Dr Chiara Massera of the University of Parma, the crystal structure of cavitand TSiiii[C_3H_7, CH_3, Ph] was obtained and resolved (figure 8).

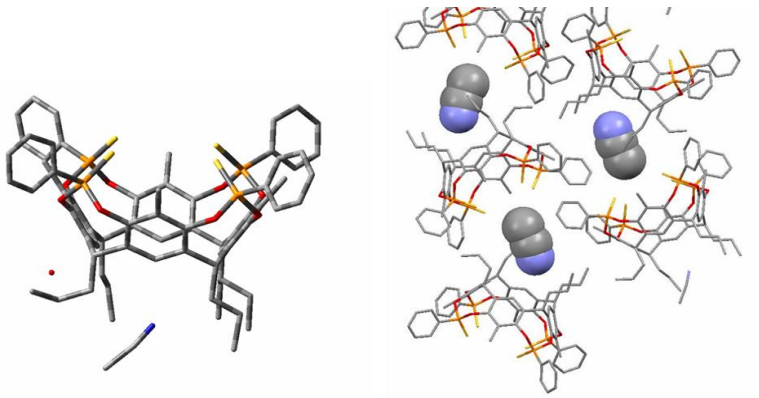

Figure 8. Crystal structure (a) and crystal packing (b) of the cavitand TSiiii[R_1, CH_3, Ph].

The structure of the cavitand TSiiii[C_3H_7, CH_3, Ph] confirms the NMR experimental data; at the upper rim the four P=S groups point all inside the cavity and there are four C3 alkyl chains at the lower rim. The compound crystallizes with water and acetonitrile as solvent molecules. The acetonitrile does not enter the cavity (Figure 8a) due to the steric hindrance of the sulphur atoms. The crystal packing shows how the acetonitrile fills the empty spaces left in the lattice (Figure 8b).

Substitution of sulphur with oxygen. The sulphur was substituted with oxygen using the MCPBA (meta chloro perbenzoic acid) as oxygen carrier. The reaction occurred in chloroform affording after 30 min and purification on silica gel column chromatography the cavitand Tiiii[C_3H_7, CH_3, Ph] in 60 % yield. A small amount of Tiiio isomer is formed but it was not isolated. Figure 8 shows the progress of the reaction from the resorcinarene **2** to the final Tiiii[C_3H_7, CH_3, Ph] monitored via ^{31}P NMR.

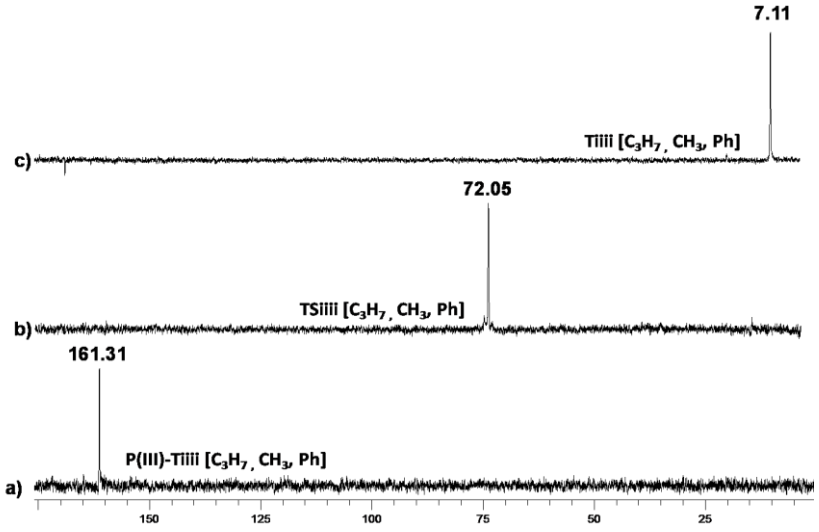

Figure 9. ^{31}P NMR monitoring of the bridging reaction of the resorcinarene 2 to form cavitand Tiiii[C_3H_7, CH_3, Ph] in $CDCl_3$.

This synthetic route performed by Dutasta to prepare diastereoselectively the Tiiii tetraphosphonate cavitands is effective and also gives good yield but, requires two steps and especially two chromatographic separations. Since The Tiiii tetraphosphonate cavitands interacts strongly with several alkali and alkali earth metals,[15] purifications on silica gel chromatography lead to the formation of Na^+, and K^+ complexes of Tiiii[C_3H_7, CH_3, Ph].

New synthetic route for diastereoselective synthesis of Tiiii cavitands. The new synthetic route was performed, by reacting the resorcinarene **2** with dichlorophenylphosphine (Scheme 14a), followed by direct *in situ* oxidation of P(III)-Tiiii product with an excess of a water solution of H_2O_2 at room temperature (Scheme 14b). In order to absorb the reaction heat avoiding secondary reactions that can lead to the formation of undesired by-products, chloroform was added to the reaction mixture. This reaction affords quantitatively the desired Tiiii product by simply re-crystallization of the crude reaction in a mixture 1:1 acetonitrile and bi-distilled water.

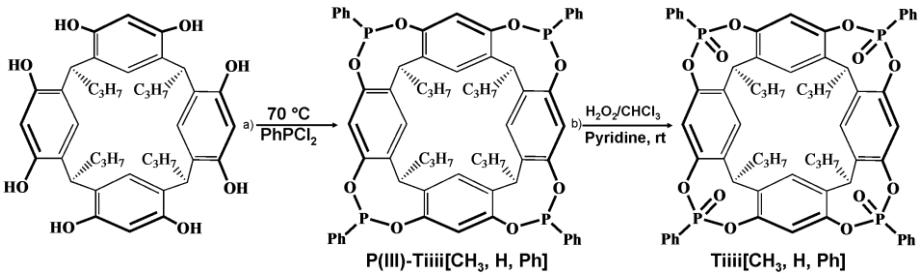

Scheme 14. New procedure for the stereoselective synthesis of phosphonate cavitand Tiiii[C_3H_7, CH_3, Ph].

We compared the ^{31}P NMR of cavitand Tiiii[C_3H_7, CH_3, Ph] obtained by using the Dutasta procedure and that obtained by using the new one step synthesis and the result is summarized in Figure 10.

Since the complexation of alkali and alkali earth metals by Tiiii cavitands leads to the down-field shift of the phosphorous signal (fast exchange conditions), we can conclude that the cavity of the cavitand obtained by using the new synthetic route is metals and other pollutants free.

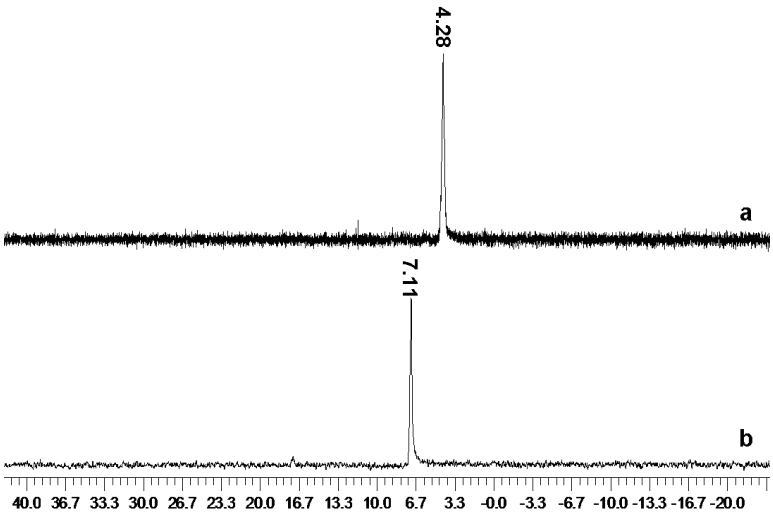

Figure 10. a) ^{31}P NMR of the cavitand Tiiii[C_3H_7, CH_3, Ph] obtained by using the new one step synthetic route b) ^{31}P NMR of the same cavitand obtained by using the two step synthetic route of Dutasta procedure both in $CDCl_3$.

The cavitand Tiiii[C_3H_7, CH_3, Ph] was crystallized from a mixture 9:1 of acetonitrile and water, and in collaboration with Dr. Chiara Massera of the University of Parma, the crystal structure was obtained and resolved (Figure 11).

The crystal structure clearly shows that, cavitand Tiiii[R_1, CH_3, Ph] consists of a tetraphosphonate cavitand, that crystallizes with two acetonitrile molecules located on the quaternary symmetry axis of the cavity, one in the upper part and the other one among the C3 chains. The first acetonitrile interacts with the phenyl rings forming the cavity *via*

CH-π interactions; even if the acetonitrile hydrogen could not be refined, it is possible to calculate their position and estimate a CH···centroid distance and angle of 3.075 Å and 162.6° respectively; the P=O···N distance is of 3.791 Å. The packing shows the presence of two series of channels along the c axis, filled by the acetonitrile molecules.

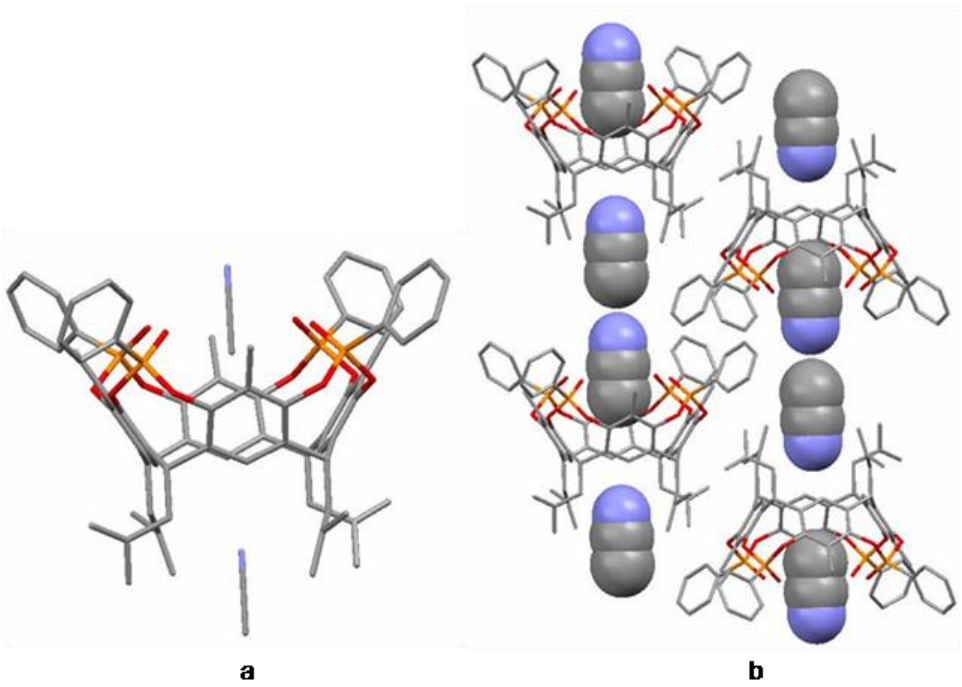

Figure 11. a) Molecular structure of cavitand cavitand Tiiii[R_1, CH_3, Ph]; b) Crystal packing along the c axis. Hydrogen are omitted for clarity;

Figure 12 reports the top view of the crystal structure of cavitand Tiiii[C_3H_7, CH_3, Ph] (Figure 12a) compared to that of cavitand TSiiii[C_3H_7, CH_3, Ph] (Figure 12b). It shows the availability of the Tiiii[C_3H_7, CH_3, Ph] cavity for guest recognition and the steric hindrance of the sulphur atoms that close the cavity of the cavitand TSiiii[C_3H_7, CH_3, Ph] preventing acetonitrile inclusion.

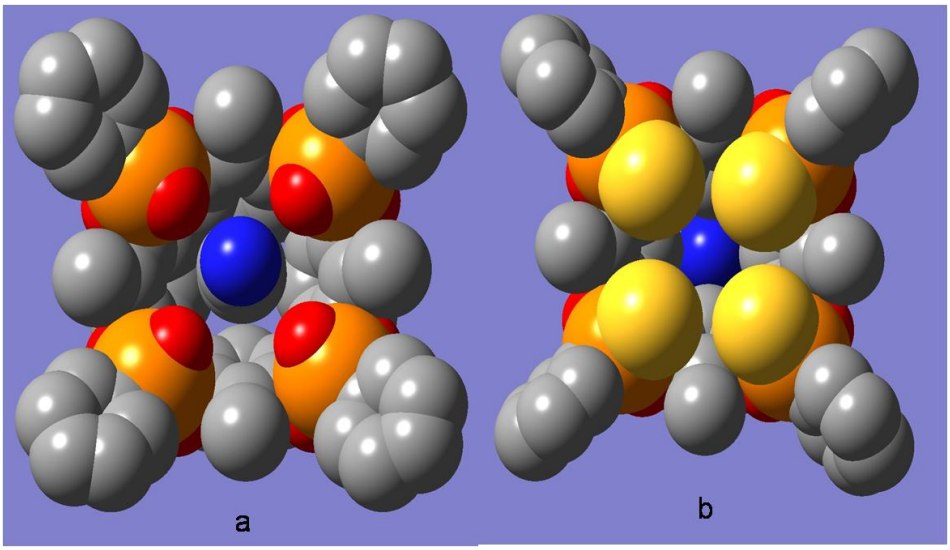

Figure 12. Top space filling view of the a) cavitand Tiiii[C_3H_7, CH_3, Ph] (with acetonitrile inside the cavity) b) and cavitand TSiiii[C_3H_7, CH_3, Ph] (with the cavity empty).

Synthesis of ammonium and pyrididinium guests. For the complexation studies, we synthesized and used a wide range of guests based on ammonium, N-methyl ammonium and methyl pyridinium salts. The isonicotinium systems **8A,** and **8B** were synthesized in two steps; the first step is the esterification of the isonicotinoyl chloride hydrochloride with methanol and butanol respectively affording respectively **7A** and **7B**, followed by methylation reaction in acetonitrile with methyl iodide, affording the corresponding isonicotinium iodide salts. In order to study the counterion effect in the complexation studies, the corresponding PF_6^- **9A, 9B** were obtained by ion-exchange reaction with NH_4PF_6, which leads to the precipitation of the products in a mixture acetonitrile-water as solvent. Ditopic guest **11** was synthesized from **10** using the same

procedure described above and hexan-1,6-diol. Ion-exchange reaction using NH_4PF_6 led to the ditopic guest **12**.

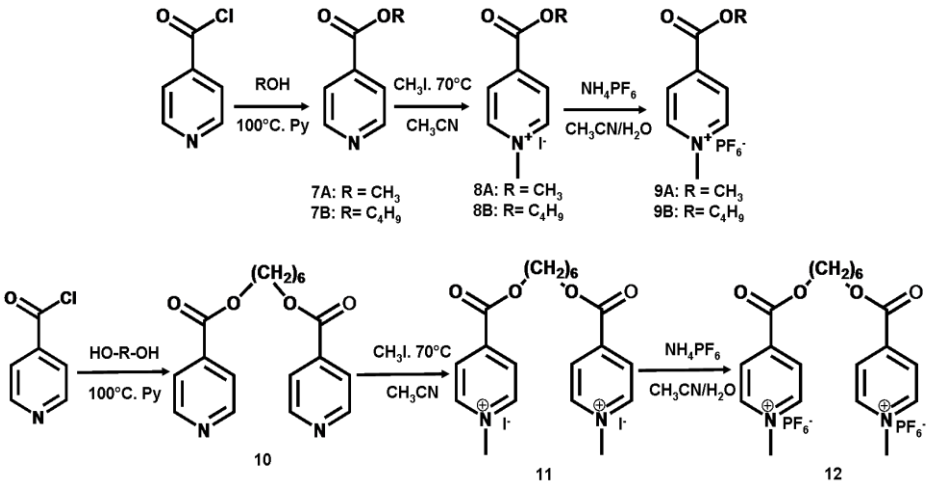

Scheme 15. Synthesis of the isonicotinium salts.

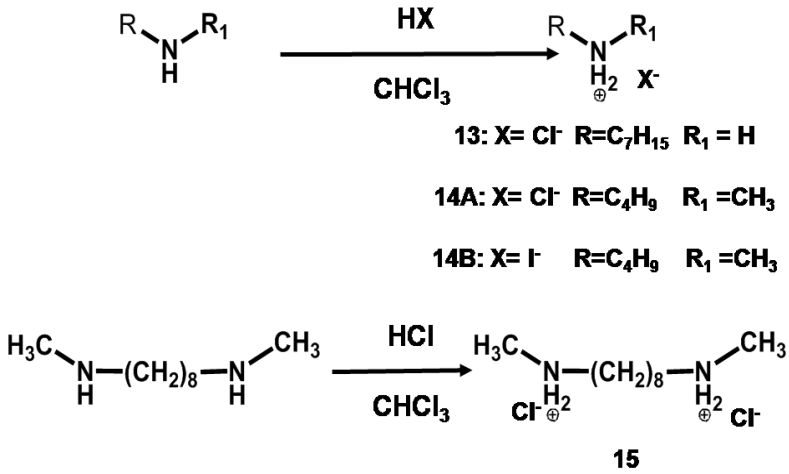

Scheme 16. Synthesis of the ammonium salts.

The ammonium salts **13, 14A** and **14B** were synthesized by salification reaction of the corresponding amines with HCl or HI depending on the

desired counterion. The corresponding ditopic ammonium salt **15** was synthesized by salification reaction of the N,N-dimethyloctyldiamine with HCl.

2.2.2 Complexation studies

Tiiii cavitands bind strongly many cations. In the case of ammonium ions, the driving force of complexation is H-bonding plus ion-dipole interactions. When a methyl group is present, it fits into the cavity adding CH-π interactions to the others present (Figure 13).

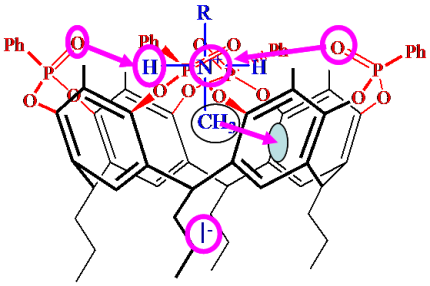

Figure 13. H-bonding, ion-dipole and CH_3-π interactions between the Tiiii cavitand and N-methylammonium salts.

In this part of the chapter, we report the qualitative studies of the complexation of Tiiii cavitands via NMR. Moreover we evaluated electrochemically and photophysically the qualitative and quantitative effects of self-assembly and disassembly on the complexation of N-methyl pyridinium system. Finally we report the thermodynamics studies of complexation via titration calorimetric (ITC).

2.2.2.1 Complexation studies via NMR

NMR titrations can provide a quantitative evaluation of K_{ass} in the range $10\text{-}10^4$.[29] Above these values other techniques are used due to the high

dilution required to evaluate the K_{ass}. In fact NMR operates in $1/K_{ass}$ as concentration regime. When the concentration is below 10^{-4} M the NMR is not any more a suitable technique. Since the ammonium salts are complexed by the Tiiii cavitands with association constant higher than 10^7 as reported by Dutasta group,[15] the complexation studies via NMR are limited to a qualitative evaluation. To perform these studies cavitand Tiiii[C_3H_7, CH_3, Ph] was used as host molecule. As ammonium salt we chose N-methylbuthylammonium iodide **14B** for its solubility in apolar solvents such as chloroform or methylenechloride in which high association constants can be recorded. Figure 14 shown the ^{1}H NMR of the **14B**-Tiiii[C_3H_7, CH_3, Ph] complex.

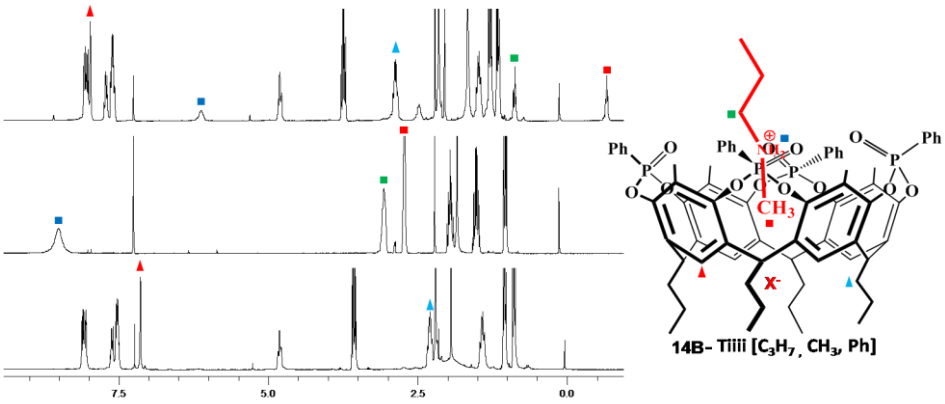

Figure 14. ^{1}H NMR of the 14B-Tiiii[C_3H_7, CH_3, Ph] complex.

The inclusion of the guest inside the cavity of the host is evidenced by the up-field shift of the guest signals. Especially the C**H**$_3$, N**H**$_2$ and C**H**$_2$NH$_2$ moieties (blue, red and green square) that undergo a large up-field shift due to the shielding effect of the cavity. Particularly diagnostic is the up-field shift of the N-CH_3 group ($\Delta\delta > 3$ ppm), which in the complex resonates at the negative chemical shift values (Figure 14).

The aromatic resorcinarene protons are down-field shifted due to the proximity of the positively charged guest. The de-shielding effect of the

charged guest inside the cavity also affects the phosphorous signal that undergoes more than 4 ppm down-field shift (Figure 15).

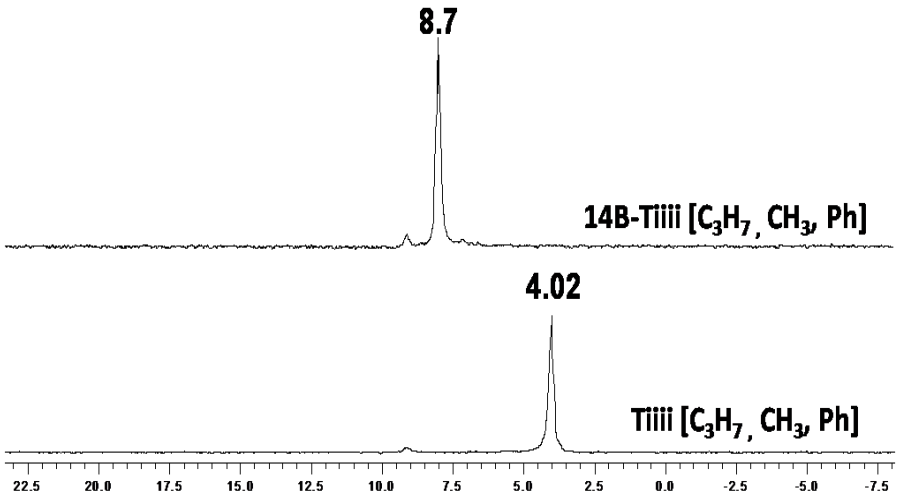

Figure 15. ^{31}P NMR in $CDCl_3$ of the 14B-Tiiii[C_3H_7, CH_3, Ph] complex.

The complexation of pyridinium systems were studied using N-methylbutylisonicotinium iodide **8B** as guest for its solubility in both polar and apolar solvents.

We can see again the up-field shift of the guest signals. Particularly diagnostic is also in this case the shift of the signal of the CH_3 pyridinium moiety, which moves more than 4 ppm up-field (red square). The down-field shift of the resorcinarene protons at the ^{1}H NMR (Red triangle) (Figure 16a), and that of phosphorous ^{31}P NMR (Figure 16b), are related to the positive charge of the guest.

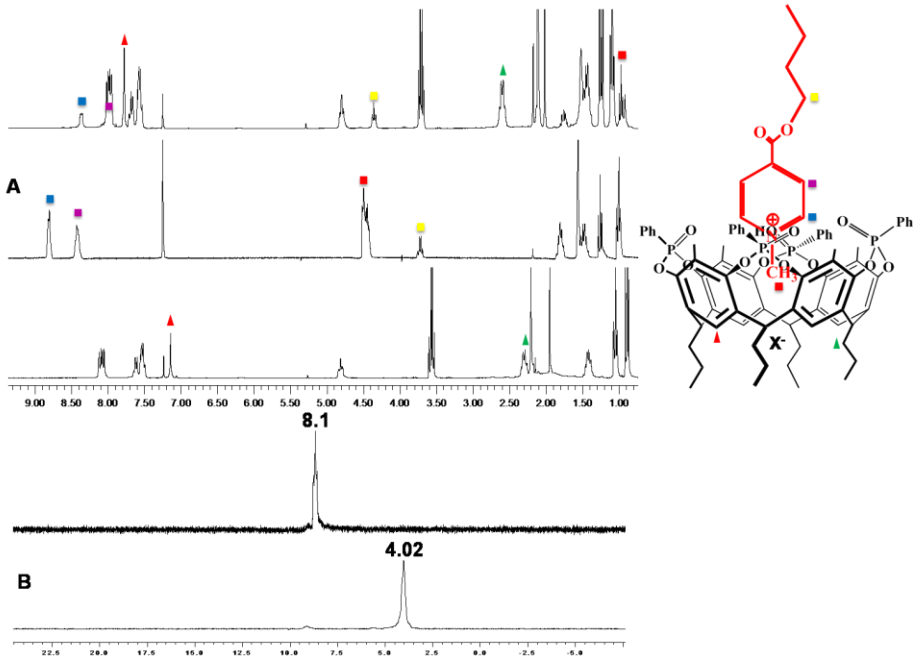

Figure 16. A) ^{1}H NMR and B) ^{31}P NMR of the 8B- Tiiii[C_3H_7, CH_3, Ph] complex in $CDCl_3$.

2.2.2.2 Photophysical and Electrochemical properties of the Host-guest Complexes

These studies were performed in collaboration with prof. Credi of the University of Bologna. For this work the cavitand Tiiii[C_3H_7, CH_3, Ph] was chosen as host, and two different guests were selected thanks to their photophysical and electrochemical sensibility and compatibility. The first guest is the N-methylmethylisonicotinium hexafluorophosphate **9A,** while the second one is the methyl viologen hexafluorophosphate **16,** which synthesis was already reported in our group (Figure 17).[30]

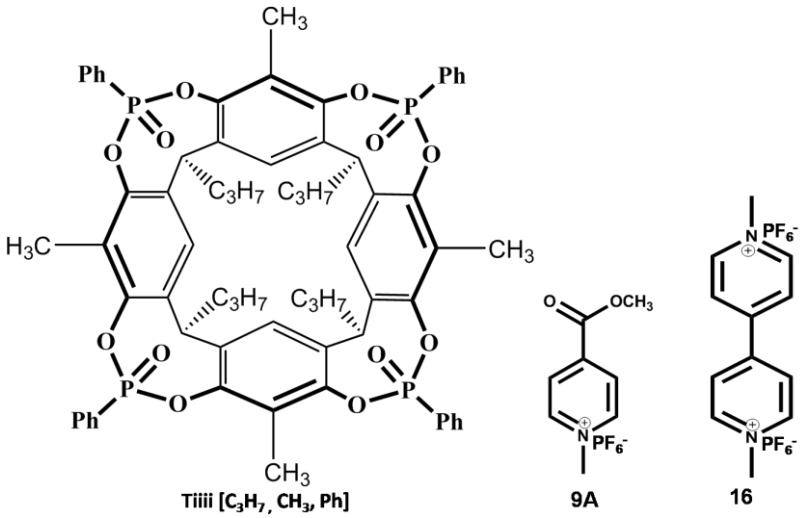

Figure 17. Cavitand host, monotopic guest 9A and ditopic guest 16.

First of all we must examine photochemically and electrochemically the individual compounds under working conditions (room temperature). These data are resumed in Table 4 and shown in Figure 18.

	Spectroscopic data					Electrochemical data[d]			
Compound	Absorption[a]		Luminescence[a]						
	λ_{max}/nm	ε/M^{-1}cm^{-1}	λ_{max}/nm	τ/ns	Φ	E^{I} [e]/ V vs SCE	Nr. of electrons	E^{II} [e]/ V vs SCE	Nr. of electrons
Tiiii[C_3H_7, CH_3, Ph]	272	9000	303	2.5	0.06	[f]	[f]	[f]	[f]
9A	274	4500	[b]	[b]	[b]	–0.65	1. *r*	–1.52	1. *i*
16	260[c]	20000[c]	353[c]	0.9[c]	0.02[c]	–0.21[g]	1. *r*	–0.77[g]	1. *r*

Table 4. [a] Air equilibrated CH_2Cl_2 solution. [b] Not luminescent. [c] Air equilibrated CH_3CN solution. [d] Electrochemical data for the different compounds (10^{-3} M) in CH_2Cl_2, 0.1 M tetrabutylammonium hexafluorophosphate as supporting electrolyte, glassy carbon electrode. [e] For reversible processes, denoted with r, halfwave potential values are reported; for irreversible processes, denoted with i, potential values estimated from DPV peaks are reported. Ferrocene was used as an

internal reference, $E_{Fc}+_{//Fc}$ = 0.51 V vs SCE. [f] Not electroactive. [g] Data referred to 1,1'-dioctyl-4,4'-bipyridinium because of the very low solubility of 16 in CH_2Cl_2.

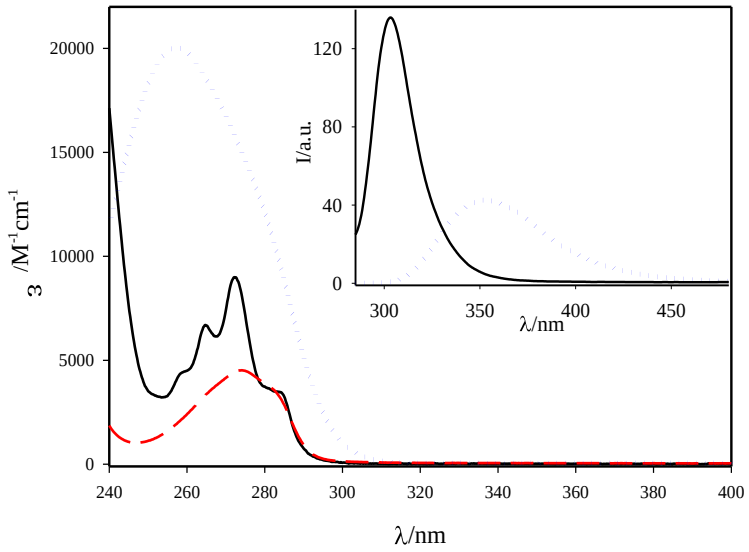

Figure 18. Absorption and fluorescence (inset) spectra of cavitand Tiiii[C_3H_7, CH_3, Ph] (full line) and guests 9A (dashed line) and ditopic guest 16 (dotted line) in CH_2Cl_2 at room temperature. For the fluorescence spectra, excitation was performed at the corresponding absorption maximum.

Photophysical properties.

9A-Tiiii[C_3H_7, CH_3, Ph] Complex. The absorption spectrum of a 1:1 mixture of cavitand Tiiii[C_3H_7, CH_3, Ph] and **9A** is slightly different from the sum of the absorption spectra of the isolated species (Figure 19). Specifically, the appearance of an absorption tail in the 280-310 nm regions suggests the occurrence of some electronic interactions between Tiiii[C_3H_7, CH_3, Ph] and **9A**.

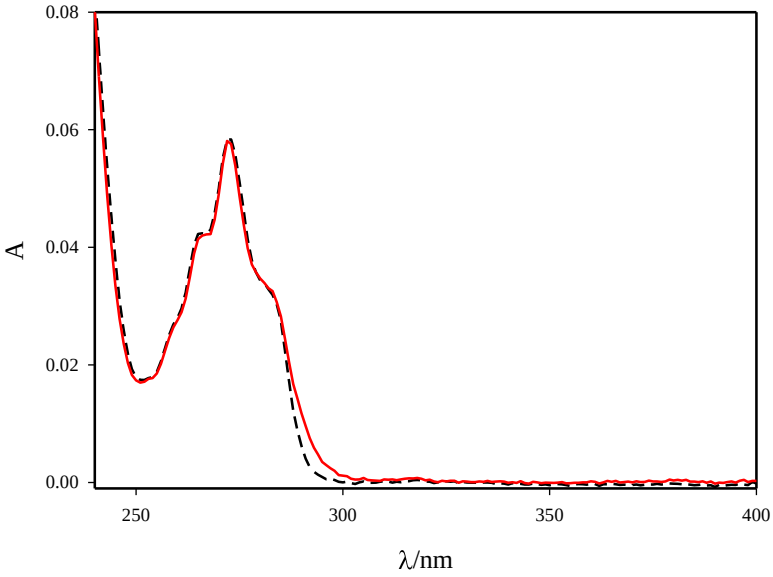

Figure 19. Absorption spectrum of a 1:1 mixture of Tiiii[C_3H_7, CH_3, Ph] and 9A, each 5.0×10^{-6} M (full line), and sum of the absorption spectra of the individual species at the same concentration (dashed line) in CH_2Cl_2 at room temperature.

Titration of Tiiii[C_3H_7, CH_3, Ph] with **9A** leads to absorption spectral changes which, however, are dominated by the absorbance increase due to addition of the guest. Instead, the fluorescence band of Tiiii[C_3H_7, CH_3, Ph] is strongly quenched upon addition of **9A** (Figure 20). The titration curve points to the formation of an adduct with 1:1 stoichiometric and Log*K* = 6.6 ± 0.1 [($K_a \approx (4 \pm 0.27)10^6$)]. It can be noticed that a fluorescence emission, corresponding to ca. 11% of the initial intensity, is still observed at the end of the titration. Such an emission is assigned to the cavitand. A careful comparison of the band shape of the fluorescence of Tiiii[C_3H_7, CH_3, Ph] and that of the **9A**-Tiiii[C_3H_7, CH_3, Ph] adduct shows that these bands are similar, but not identical; specifically, the band of **9A**-Tiiii[C_3H_7, CH_3, Ph] complex has a more pronounced low-energy tail. Since the absorption spectra do not shows evident charge-transfer bands for the **9A**-Tiiii[C_3H_7, CH_3, Ph]

adduct, and energy transfer from Tiiii[C_3H_7, CH_3, Ph] to **9A** should be almost isoergonic, it is likely that the quenching takes place by a photo-induced electron-transfer process from an excited state localized on cavitand Tiiii[C_3H_7, CH_3, Ph] and the electron accepting guest **9A**. The quenching rate constant can be estimated as follows:

$k_q = 1/\tau_0 \, (I_0/I - 1)$ (1)

where τ_0 and I_0 are the luminescence lifetime and intensity of Tiiii[C_3H_7, CH_3, Ph] in the absence of **9A**, and I is the luminescence intensity of the **9A**-Tiiii[C_3H_7, CH_3, Ph] assembly. According to our results, k_q = 3.3×10^9 s^{-1} (Eq. 1).

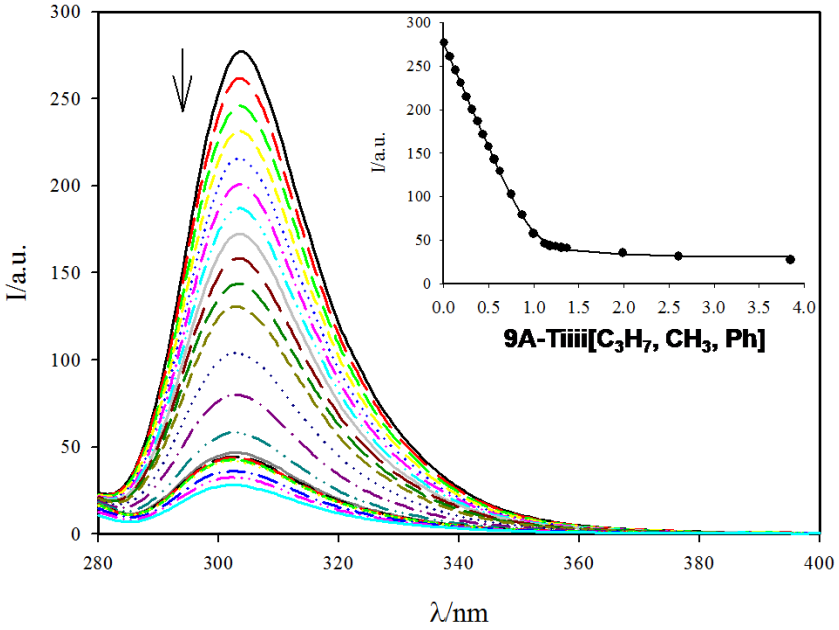

Figure 20. Fluorescence changes (λ_{exc} = 272 nm) upon titration of 1 (1.56×10^{-5} M) with 9A in CH_2Cl_2 at room temperature. The inset shows the titration curve obtained by reading the fluorescence intensity at 304 nm.

16-Tiiii[C_3H_7, CH_3, Ph] Complex. Owing to the poor solubility of **16** in CH_2Cl_2, we have initially performed complexation experiments in CH_3CN. However, spectroscopic titrations indicate that no complexation of **16** by cavitand Tiiii[C_3H_7, CH_3, Ph] occurs in acetonitrile solution. But similar experiments with the same solvent and the same guest via NMR indicated that indeed the system aggregates also in CH_3CN (see Chapter 4.2.3).

Addition of **16** to a CH_2Cl_2 solution of Tiiii[C_3H_7, CH_3, Ph] causes changes in the absorption and luminescence spectra (Figure 21) that are consistent with the formation of an adduct between these components.

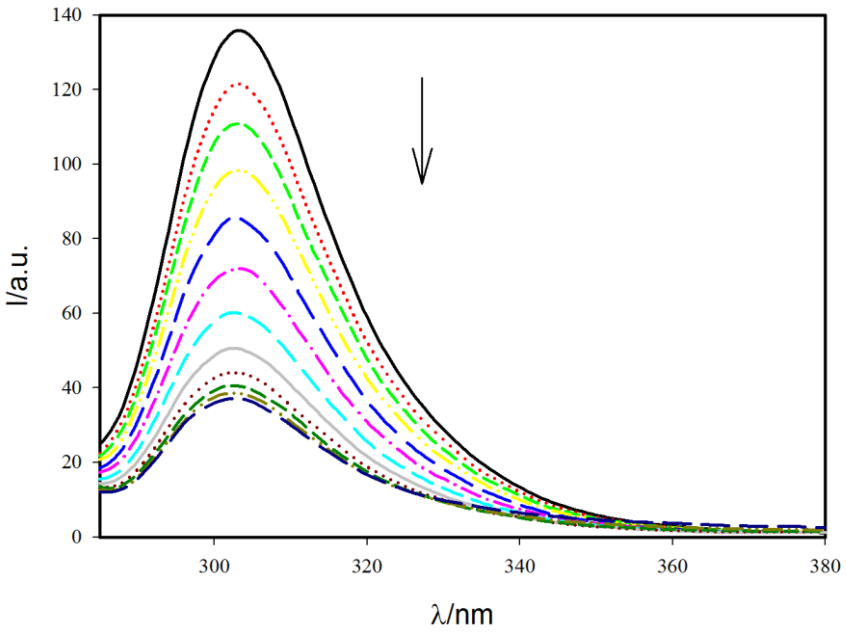

Figure 21. Fluorescence spectral changes (λ_{ex} = 271 nm) observed upon titration of a 7.8×10^{-6} M CH_2Cl_2 solution of Tiiii[C_3H_7, CH_3, Ph] with small aliquots of a concentrated solution of 16 in MeCN.

Specifically, both the fluorescence of Tiiii[C_3H_7, CH_3, Ph] and **16** are quenched when the components are mixed. The decrease of fluorescence

of the free cavitand is over after addition of 0.5 equivalents of **16** (Figure 22a); concomitantly, the fluorescence of free **16** is not observed until after the addition of more than 0.5 equivalents of guest (Figure 22b). All these observations point to the formation of a 2:1 adduct in which two cavitands encapsulate one methylviologen species.

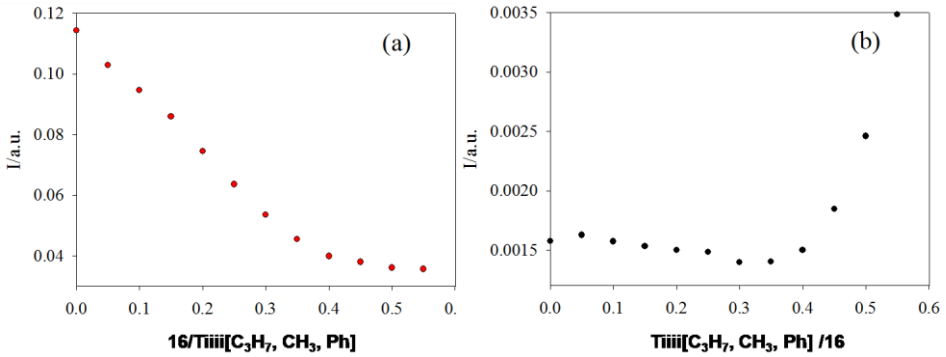

Figure 22. Fluorescence titration curves (CH_2Cl_2, room temperature) obtained from the intensity at (a) 310 nm, i.e., emission of Tiiii[C_3H_7, CH_3, Ph] , and (b) 370 nm, i.e., emission of 16. Excitation was performed at 271 nm.

The reverse titration, namely, addition of cavitand Tiiii[C_3H_7, CH_3, Ph] to a solution of **16**, also gives interesting results. First of all, the absorption spectrum of a very dilute solution of **16** in CH_2Cl_2 shows a band in the near UV much broader than that observed in MeCN, with a red-side tail reaching down to 400 nm (Figure 23). This behaviour is most likely related to aggregation phenomena involving the poorly soluble **16** species. Addition of Tiiii[C_3H_7, CH_3, Ph] causes the progressive disappearance of the red-side absorption tail and the quenching of the luminescence band of **16** (Figure 23). As it can be seen from the titration curve (Figure 23, inset) the quenching of the methylviologen luminescence both in the 1:1 and in the 2:1 adducts is complete, suggesting a value of k_q exceeding 5×10^{10} s^{-1} (eq. 1). The luminescence characteristic of free Tiiii[C_3H_7, CH_3, Ph] does not show

up until more than two equivalents have been added. The fluorescence titration plot (Figure 23, inset) is consistent with the formation of two adducts, with 1:1 and 2:1 (host:guest) stoichiometries, respectively. Clearly, complexation by Tiiii[C_3H_7, CH_3, Ph] prevents the formation of aggregates of **16** species in CH_2Cl_2. The stepwise stability constants for the 1:1 and the 2:1 complexation result to be LogK_1 = 6.3 ± 0.1 and LogK_2 = 6.3 ± 0.3, respectively. This result shows that complexation of methyl viologen by the first cavitand does not hamper the association of a second cavitand molecule; i. e. the two binding events are disconnected.

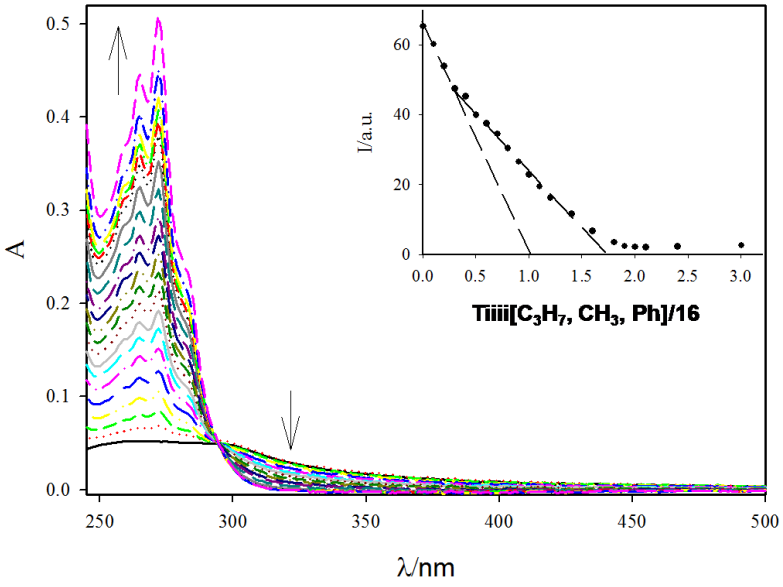

Figure 23. Absorption spectral changes observed upon titration of 16 (1.2 x 10^{-5} M) with 1 in CH_2Cl_2 at room temperature. The inset shows the fluorescence titration curve obtained from the emission intensity of 16 at 334 nm upon excitation at 300 nm.

The titration of **16** by Tiiii[C_3H_7, CH_3, Ph] was also performed in CH_2Cl_2/MeCN 8:2 (*v*/*v*) in order to afford good solubility of

methylviologen and avoid its intermolecular aggregation. Under these conditions, the absorption spectrum of **16** is almost identical to that observed in MeCN, thereby showing no aggregation. The changes in the luminescence bands of Tiiii[C_3H_7, CH_3, Ph] and **16** are similar to those observed in pure CH_2Cl_2 and are consistent with the formation of 1:1 and 2:1 adducts, albeit with slightly lower stability constants (LogK_1 = 6.00 ± 0.04 and LogK_2 = 5.6 ± 0.1, respectively). Most likely, the solvophobic effects responsible for the insertion of **16** into the cavity of Tiiii[C_3H_7, CH_3, Ph] are diminished by the presence of 20% MeCN. This observation is in agreement with the fact that self-assembly in these systems is mainly driven by solvophobic effects.

Since the electrochemical experiments are performed in the presence of a large amount of supporting electrolyte, we investigated the self-assembly of Tiiii[C_3H_7, CH_3, Ph] and **16** in the presence of 0.1 M of tetrabutylammonium hexafluorophosphate ($TBAPF_6^-$). The presence of such an electrolyte lowers the stability constant for both the 1:1 and 2:1 adducts (LogK_1 = 5.16±0.03 and LogK_2 = 3.9±0.7, respectively), presumably because the high ionic strength increases the polarity of the medium, thereby decreasing the solvent effects that drive the self-assembly. Moreover we can consider, as another interpretation, that the $TBAPF_6^-$ forms ion-dipole interactions (N^+---O=P) (see crystal structure depicted in Figure7) acting as competitive guest, decreasing both K_{ass}.

Electrochemical properties.

The electrochemical data for the examined compounds in CH_2Cl_2/$TBAPF_6$ at room temperature are gathered in Table 4. The cavitand Tiiii[C_3H_7, CH_3, Ph] is not electroactive in the potential window

examined (from –1.8 V to +1.8 V vs SCE). The methyl pyridinium guest **9A** shows two reduction processes, and no oxidation. The first reduction process is reversible and mono-electronic ($E'_{1/2}$ = –0.65 V); the second one also involves the exchange of one electron and is poorly reversible (E''_{p} = –1.52 V). Since methyl viologen, **16**, is not soluble enough in CH_2Cl_2 in order to perform voltammetric experiments, 1,1′-dioctyl-4,4′-bipyridinium (dioctylviologen) was employed as a model[31] for the electroactive bipyridinium unit **16**. On the other hand, dioctylviologen cannot be used as a guest for Tiiii[C_3H_7, CH_3, Ph], because the two octyl chains can neither be accommodated in the inner space of the cavitand nor pierce its lower rim. Dioctylviologen shows[32] two reversible mono-electronic reduction processes with $E'_{1/2}$ = –0.21 V and $E''_{1/2}$ = –0.77 V vs SCE.

9A- Tiiii[C_3H_7, CH_3, Ph] complex. The addition of one equivalent of Tiiii[C_3H_7, CH_3, Ph] to a solution of **9A** causes a shift of the first reduction process of the guest to more negative potentials, and a decrease of the corresponding current intensity (Figure 24). These observations are in agreement with the fact that **9A** forms a complex with the cavitand. The second reduction process, however, is not affected by the presence of Tiiii[C_3H_7, CH_3, Ph], suggesting that one-electron reduction of the guest leads to disassembly of the complex. This behaviour can be accounted for by considering that one-electron reduction of **9A** affords a neutral species which affinity for the CH_2Cl_2 solvent should be much higher than that of the cationic form. Moreover, the electron-acceptor character of the guest is strongly diminished upon reduction, thereby weakening the electron donor-acceptor interactions that can possibly take place with the electron-rich aromatic walls of the cavitand.

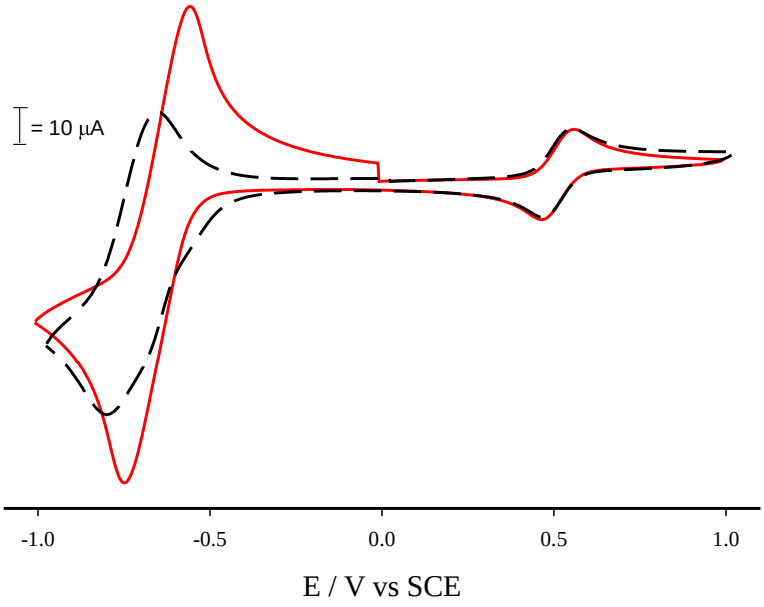

Figure 24. Cyclic voltammoletric curves for the first reduction of 9A alone (full line) and in the presence of one equivalent of Tiiii[C_3H_7, CH_3, Ph] (dashed line). The reversible wave at +0.51 V is that of ferrocene. Conditions: 1.2×10^{-3} M, CH_2Cl_2/TBAPF$_6$, glassy carbon electrode.

In order to confirm whether one-electron reduction of the guest leads to complex disassembly, spectroelectrochemical experiments have performed. The absorption spectrum of the monoreduced species (Figure 25), obtained upon electrolysis of **9A** at –1.1 V vs an Ag pseudo-reference electrode, shows two intense bands with λ_{max} = 304 and 395 nm. The shape of the absorption bands arising from reduction of the **9A** guest in the **9A**-Tiiii[C_3H_7, CH_3, Ph] adduct (Figure 24) is identical to that of the absorption bands obtained for free mono-reduced species. Had the monoreduced guest remained into the cavity of Tiiii[C_3H_7, CH_3, Ph], its absorption spectrum would have been affected in some way – for example, by shifting of the band maxima. Therefore, the spectroelectrochemical results confirm that the **9A**-Tiiii[C_3H_7, CH_3, Ph] complex is disassembled upon one-electron reduction of the guest.

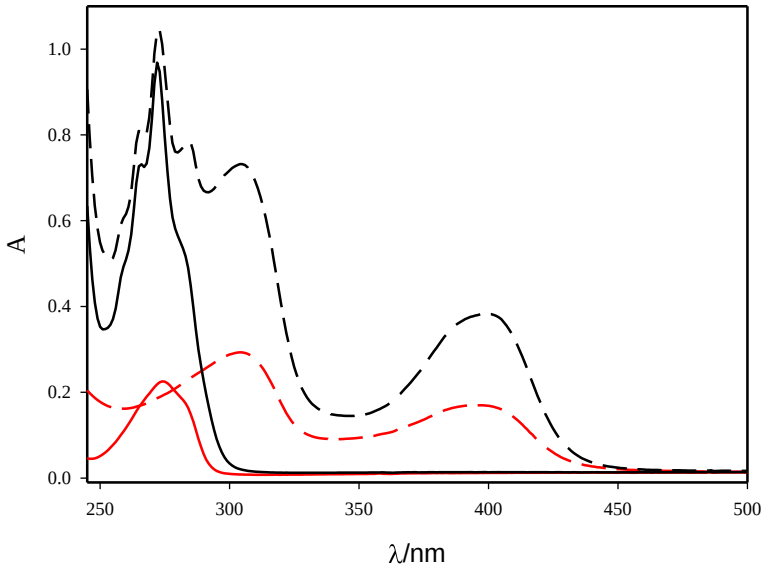

Figure 25. Red curves: absorption spectra of 9A before (full line) and after (dashed line) one electron reduction. Black curves: absorption spectra of the 9A-Tiiii[C_3H_7, CH_3, Ph] adduct before (full line) and after (dashed line) one-electron reduction of the 9A guest. Electrolysis was performed in CH_2Cl_2/TBAPF$_6$ at –1.1 V vs an Ag pseudo-reference electrode. The concentration of 9A alone (red curves) was 2.3×10^{-3} M, whereas that of Tiiii[C_3H_7, CH_3, Ph] and 9A in the mixture (black curves) was 3.8×10^{-3} M; the optical path length was 180 μm.

16-Tiiii[C_3H_7, CH_3, Ph] complex. In the presence of two equivalents of Tiiii[C_3H_7, CH_3, Ph], the methylviologen guest **16** can be dissolved in CH_2Cl_2 to a concentration sufficient for voltammoletric experiments. Under these conditions, the first reduction process of **16** is considerably shifted to more negative potentials compared to the same process in the dioctylviologen model compound (Figure 26). This observation is in agreement with the fact that **16** forms a stable 1:2 complex with the cavitand. The second reduction process takes place at the same potential observed for the corresponding process in dioctylviologen (Figure 26). This observation again suggests that one-electron reduction of the guest

leads to disassembly of the complex, for the same reasons discussed in the case of the previous system.

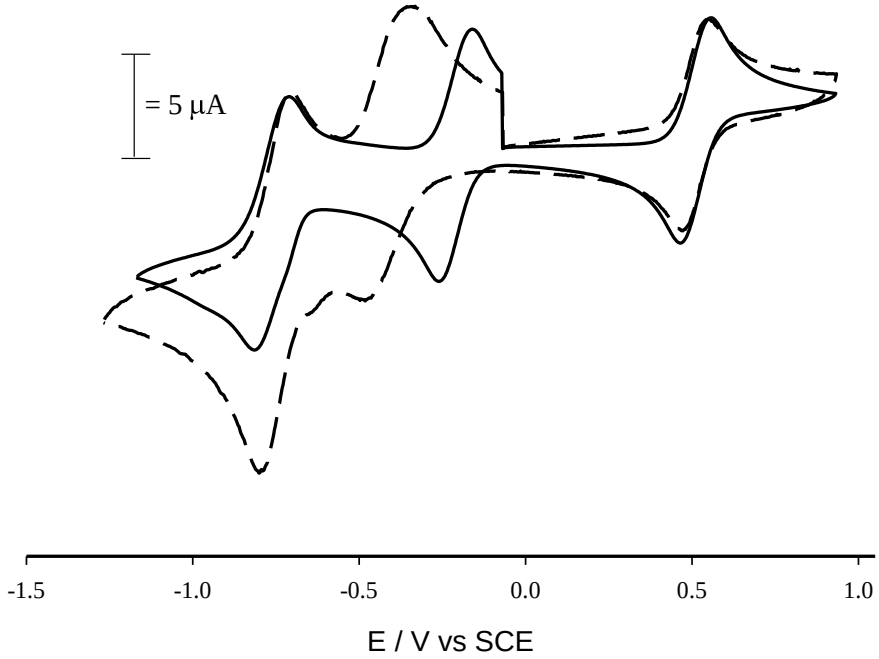

Figure 26. Cyclic voltammoletric curves for reduction of dioctylviologen alone (full line) and of 16 in the presence of two equivalents of Tiiii[C_3H_7, CH_3, Ph] (dashed line). The reversible wave at +0.51 V is that of ferrocene. Conditions: 1.05×10^{-3} M, CH_2Cl_2/TBAPF$_6$, glassy carbon electrode.

Spectroelectrochemical experiments confirm indeed this hypothesis. The absorption spectrum of the monoreduced **16** species (Figure 27), obtained upon electrolysis of **16** at –0.5 V vs an Ag pseudo-reference electrode, shows the typical[31] absorption spectrum of the bipyridinium radical cation, with two intense and structured bands peaking at λ_{max} = 399 and 605 nm. The absorption spectral shape obtained upon reduction of the **16-**Tiiii[C_3H_7, CH_3, Ph] complex in the same conditions is identical to that of free monoreduced dioctylviologen. Had the monoreduced species remained into the cavity of Tiiii[C_3H_7, CH_3, Ph], its absorption spectrum

would have been affected in some way. Therefore, the spectroelectrochemical results confirm that the **16**-Tiiii[C_3H_7, CH_3, Ph] complex is disassembled upon one-electron reduction of the guest.

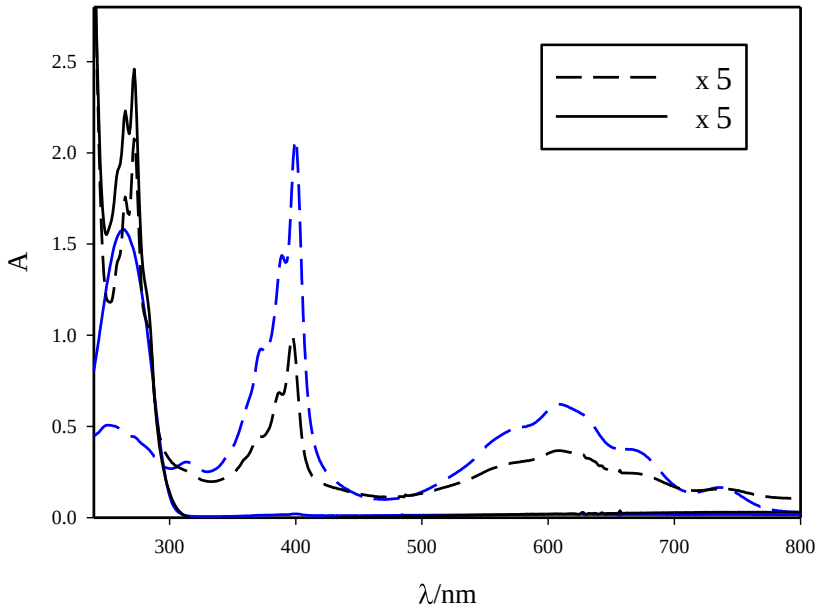

Figure 27. Blue curves: absorption spectra of dioctylviologen before (full line) and after (dashed line) one-electron reduction. Black curves: absorption spectra of the 16-Tiiii[C_3H_7, CH_3, Ph] adduct before (full line) and after (dashed line) one-electron reduction of the 16 guest; these two spectra are multiplied by a factor of 5 to facilitate comparison. Electrolysis was performed in CH_2Cl_2/TBAPF$_6$ at –1.1 V vs an Ag pseudo-reference electrode. The concentration of dioctylviologen alone (blue curves) was 4.1×10^{-3} M, whereas those of 1 and 16 in the mixture (black curves) were 1.1×10^{-3} M and 5.5×10^{-4} M, respectively; the optical path length was 180 μm.

In conclusion, the formation of stable complexes between cavitand Tiiii[C_3H_7, CH_3, Ph] and mono- and bis-methylpyridinium guests (**9A,** and **16** respectively) in dichloromethane solution has been demonstrated. The complexes have 1:1 stoichiometry in the case of the mono-methyl

pyridinium guest, whereas the bis-methyl pyridinium guest is complexed by two cavitand molecules. The main driving force for such self-assembly processes is ascribed to solvophobic effects experienced by the positively charged guests in the apolar solvent. Formation of the complexes affects substantially the photophysical and electrochemical properties of the molecular components. Specifically, the luminescence observed of the free host and guest species is strongly quenched when they get associated.

Electrochemical experiments show that one-electron reduction of the guests leads to decomplexation. Since the mono-electronic reduction of the investigated guests is reversible, the self-assembly and disassembly of such complexes can be electrochemically controlled. These results are of interest because they constitute the first steps towards the construction of supramolecular materials (e.g., supramolecular polymers) that can be assembled and disassembled under control of an external stimulation.

2.2.2.3 Thermodynamic of formation of Host-Guest complexes

The ITC experiments were done in Spain in collaboration with the group of Prof. Javier de Mendoza of the ICIQ (Instituto Catalán de Investigaciòn Quìmica) of Tarragona.

The thermodynamic of association are characterized by association constant (Ka) and stoichiometry (n) using NMR, electrochemistry, photo-physic and other methods. Among these methods ITC is an powerful tool for determining with high precision all the thermodynamic parameters such as the free energy (ΔG), the enthalpy (ΔH), entropy (ΔS) and heat

capacity (ΔCP) as well as association constant (Ka) and stoichiometry (n).

General Aspects of ITC

Recently, the advent of several highly sensitive titration calorimeters has generated much interest in this technique.[33]

An ITC instrument consists of two identical cells composed of a highly efficient thermal conducting material surrounding by an adiabatic jacket which is usually cooled by water bath (Figure 28). Sensitive thermopile/thermocouple circuits detect temperature differences between the two cells and between the cells and the jacket. Heaters located on both cells and the jacket activated when necessary to maintain identical temperature between all components. In an ITC experiments the cavitand solution is placed in the sample cell. The reference cell contains only the solvent used for dissolution. A signal < 1 mW generated by the heater located in the reference cell before the injection of the titrant, activates the heater located on the sample and this represents the baseline signal. The direct observable measured in an ITC experiment is the time-dependent input of the power required to maintain equal temperatures in the sample and reference cell.

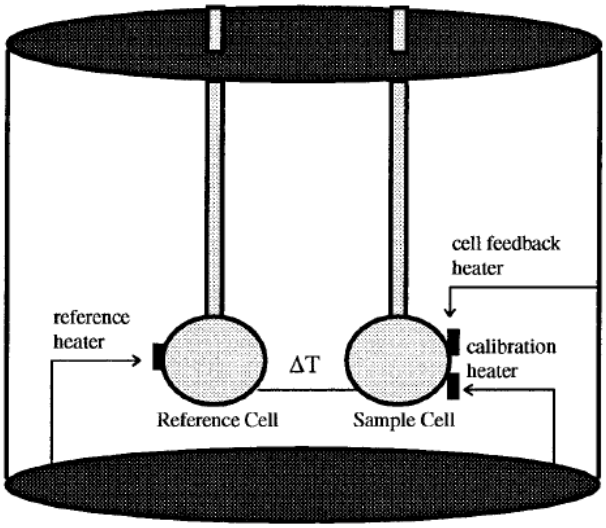

Figure 28. Schematic diagram of an ITC instrument

The experimental titration curves were analyzed through the standard model of a single set of identical sites, according to which the total evolved heat in the solution cell, Q (active cell volume V_0) is given by:

$$Q = \frac{nM_t \Delta H^0 V_0}{2}\left[1+\frac{X_t}{nM_t}+\frac{1}{nK_{eq}M_t}-\sqrt{\left(1+\frac{X_t}{nM_t}+\frac{1}{nK_{eq}M_t}\right)^2-\frac{4X_t}{nM_t}}\right] \quad (2)$$

where n is the number of identical sites, X_t and M_t are the total concentration of the guest and the host, respectively, and K_{eq} is the equilibrium constant given by $K_{eq} = \Theta / (1-\Theta)$ [illegible], where Θ is the fractional saturation, related to the total concentration of complexed sites of the host by ($n\,\Theta\, M_t$). The value of Q can be calculated for a given set of n, K_{eq}, and ΔH^0 values at the end of the every injection and can be compared with the experimental one, allowing the optimization of those parameters. The heat involved in the reaction is provided in kJ mol^{-1} of injectant (in our case mole of guest).

Thermodynamic parameters in methanol.

ITC (Isothermal Titration Calorimetry) experiments were carried out in degassed methanol to measure the thermodynamic parameters associated with the inclusion process, ΔH corresponding to the total heat evolved or absorbed in the inclusion process: Keq, ΔG, ΔS, and the stoichiometry n corresponding to the inflection point of the plot Q *vs* molar ratio (Figure 29), which are the perfect sigmoids in this solvent, allowing the accurate determination of n.

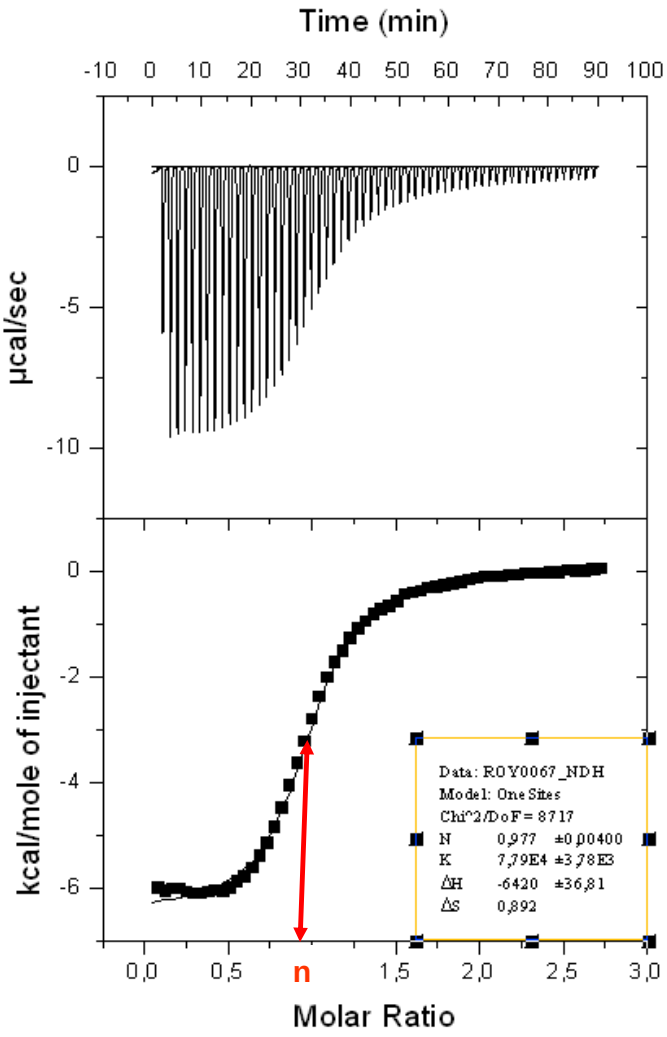

Figure 29. Experimental plot of a titration of the cavitand Tiiii[C_3H_7, CH_3, Ph] with a guest in methanol.

Cavitand Tiiii[C_3H_7, CH_3, Ph] was used as host molecule. Monotopic ammonium salts **13, 14A, 14B** ditopic ammonium salt **15,** monotopic methyl pyridinium salts **8B, 9B** , and ditopic methyl pyridinium salt **12,** were used as guest molecules. Table 5 summarized the results obtained.

	K_{ass} (M^{-1})	ΔH($KJmol^{-1}$)	TΔS($KJmol^{-1}$)	ΔG($KJmol^{-1}$)	n
13: $C_7H_{15}NH_3Cl$	$(3 \pm 0.5)10^3$	-10.13 ± 0.88	9.76 ±1.22	-19.82 ± 0.41	0.89 ± 0.05
14A: $C_4H_9NH_2CH_3Cl$	$(3.9 \pm 0.7)10^5$	-16.1 ± 0.5	15.81 ± 0.81	-31.9 ± 0.44	0.93 ± 0.02
14B: $C_4H_9NH_2CH_3I$	$(2.6 \pm 0.2)10^5$	-17.1 ± 0.2	13.8 ± 0.3	-30.9 ± 0.19	0.89 ± 0.01
15:$(CH_3NH_2)_2(CH_2)_8Cl_2$	$(2.14 \pm 0.3)10^6$	-37.41 ± 1.1	-0.9 ± 0.7	-37.05 ± 0.35	0.45 ± 0.004
9B: 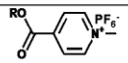	$(8.6 \pm 0.43)10^4$	-16.4 ± 0.03	11.73 ± 0.01	-28.13 ± 0.12	0.91 ± 0.015
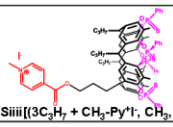 TSiiii[($3C_3H_7$ + CH_3-Py$^+$I$^-$, CH_3, Ph]	$(8.16 \pm 0.6)10^4$	-11.86 ± 0.35	16.1 ± 0.4	-28 ± 0.18	1.01 ± 0.01
8B: 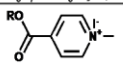	$(9.25 \pm 0.96)10^4$	-17.11 ± 0.05	11.21 ± 0.01	-28.73 ± 0,25	0.88 ± 0.01
12: 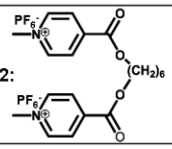	$(1.6 \pm 0.21)10^5$	-31.7 ± 0.8	-1.9 ± 0.7	-29.9 ± 0,32	0.49± 0.013

Table 5. Thermodynamic parameters of host-guest complexation processes in methanol.

Since the $K_{ass} < 10^8$ M^{-1}, all these parameters can be determined with good precision.[34] The average values for the thermodynamic parameters are given in Table 5.

The excellent agreement between the experimental values for n and the expected ones certifies the quality of the titration experiments.

Observing Table 5, we notice that the complexation processes between the cavitand Tiiii[C_3H_7, CH_3, Ph] and the monotopic guests **8B, 9B, 13, 14A, 14B** are both enthalpy and entropy driven. We would expect that the formation of host-guest complexes diminish the freedom of both components and are unfavourable intrinsically from the entropic point of view but the decrease in entropy is however, compensated to large extent by desolvation of both host and guest involved.[35] The desolvation cannot

explain alone the high values of entropy recorded (in some case higher than the enthalpy). Probably also the conformational freedom of the host, guest, host-guest complexes and the counterion must be taken into account. In fact, in the complexation processes of the ditopic guests (**12** and **15**) whose final products show reduced conformational liberty due to the more pre-organization of the dimeric complex, the entropic loss is not longer balanced by the desolvation. In polar solvents such as methanol, there are not enthalpic and entropic differences between the counterions (Cl^-, I^-, and PF_6^-) likely because they are well solvated and move freely in solution. Comparing the ammonium salt **13** and the N-methylammonium salt **14A** in this solvent, we can observe that, CH_3 group linked to the nitrogen of the amine contributes in two ways on the thermodynamic point of view:

- An enthalpy increase ≈ 6 $kJ.mol^{-1}$ due to the addition of a new interaction (CH-π) between the π electrons of the aromatic rings of the resorcinarene skeleton, and the CH_3 linked to the ammonium salt.

- An entropy advantage of ≈ 6 $kJ.mol^{-1}$ probably due to the release of a higher amount of coordinated solvent into the bulk for **14A** that possesses the additional CH_3 group which enhances the solvation sphere.

These two contributions lead consequently to the growth of two orders magnitude of the association constant.

The isonicotinium salt **8B** cannot make hydrogen bonding, but possesses an enthalpy similar to that of ammonium salt **14B.** Probably the isonicotinium salts can make additional CH-π interaction with the CH_3 in the apical position of the resorcinarene (Figure 30).

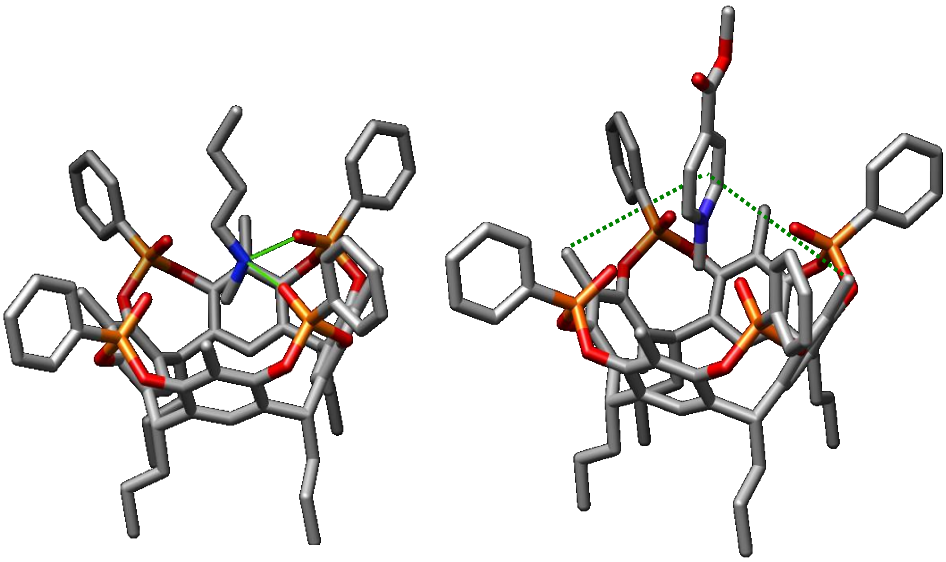

Figure 30. Molecular modelling shows CH_3: π interactions between apical CH_3 of resorcinarene ring and π electrons of pyridinium salt and hydrogen bonding between Tiiii[C_3H_7, CH_3, Ph] and 14B.

The entropy of the complexation of the two guests is slightly different likely owing to the different solvation sphere of the complexed residue fitting inside the cavity and the different conformational freedom of the guests and the complexes upon complexation.

The case of ditopic guests **12** and **15** must be considered in a different way. As determined by fluorescence titration of cavitand Tiiii[C_3H_7, CH_3, Ph] with methyl viologen $(PF_6^-)_2$, the two association constants are equivalent, therefore the two binding events are independent (no cooperativity either positive or negative). Therefore the enthalpy for a single complexation event can be obtained dividing in two the experimental values, (ΔH = -36.41/2 = -18.2 kJ.mol^{-1} for **15** and ΔH = -31.63/2 = 15.8 kJ.mol^{-1} for **12**). The ΔH = -18.2 kJ.mol^{-1} of **15** correlates very well with the ΔH = -16.1 kJ.mol^{-1} of **14A.** Even better is the

correlation between ΔH = -15.8 kJ.mol^{-1} of **12** and ΔH = -16.4 kJ.mol^{-1} of **9B.**

The difference between 1:1 complexes and 1:2 complexes lie in the entropic term, which for **12** and **15** are close to 0. Therefore the enthalpic gain is totally lost in moving from a monotopic to a ditopic guests. The overall effect is a slight increase in ΔG for ditopic guests. This is a typical example of enthalpy-entropy compensation (see later), where the stronger binding is balanced by the entropy loss of connecting three objects instead of two and of limiting the conformational freedom of the ditopic guests.

Thermodynamic parameters in methylene chloride.

The equivalence region should be well defined by the concentration range spanned by the injection, to determine accurately value of the association constant and the enthalpy of the process.[36] Working in methylene chloride, low concentrations < 0,25 mM and 5 mM respectively for the host and guest systems, that comply the above conditions are required. The average values for thermodynamic parameters in methylene chloride are given in Table 6.

The thermodynamic data related to the complexation of ammonium salts are not reported owing to the rapid saturation of the binding sites that lead to a reduced number of data in the flections points (Figure 31) and then to high errors in the valuation of thermodynamic parameters. The rapid saturation is due to the high association constant (> 10^8) recorded in the complexation of such ammonium salts and then the direct ITC titration cannot be the appropriated technique for the determination of thermodynamic data.[37]

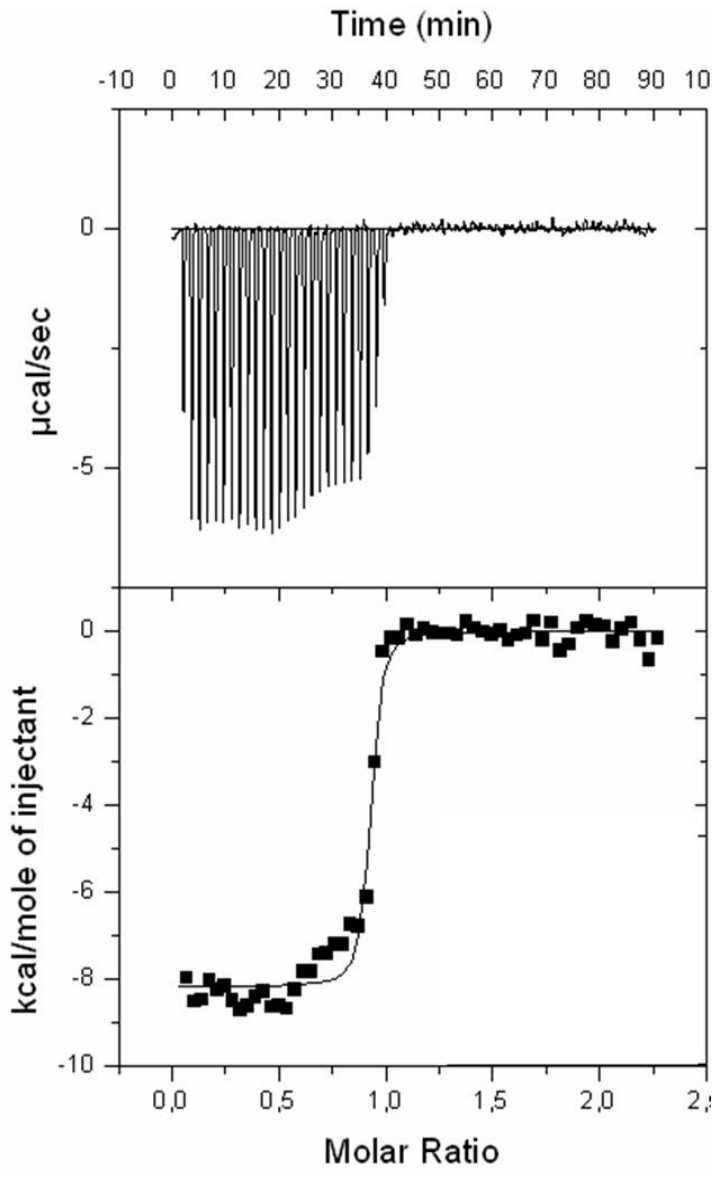

Figure 31. Titration of cavitand Tiiii[C_3H_7, CH_3, Ph] with N-methylbuthylammonium chloride via ITC in CH_2Cl_2.

	K_{ass} (M^{-1})	ΔH($KJmol^{-1}$)	TΔS($KJmol^{-1}$)	ΔG($KJmol^{-1}$)	n
9B: 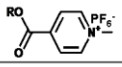	$(7.8 \pm 2.6)10^6$	-24 ± 0.4	15.1 ± 0.8	-39.1 ± 0.82	0.95 ± 0.01
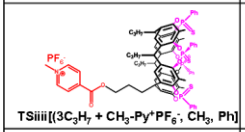 TSiiii[($3C_3H_7$ + CH_3-$Py^+PF_6^-$, CH_3, Ph]	$(4 \pm 0.1)10^7$	-30.0 ± 0.1	13.4 ± 0.5	-43.6 ± 0.06	0.81 ± 0.06
8B: 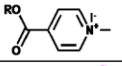	$(1.7 \pm 0.1)10^7$	-20.6 ± 0.1	20.8± 0.2	-41.3 ± 0.15	0.95 ± 0.14
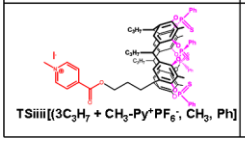 TSiiii[($3C_3H_7$ + CH_3-$Py^+PF_6^-$, CH_3, Ph]	$(1.9 \pm 0.6)10^7$	-26.1 ± 0.2	15.2 ± 0.01	-41.4 ± 0.78	0.96 ± 0.01

Table 6. Thermodynamics of complexation in methylene chloride via ITC.

Regarding methyl isonicotinium salts, the complexation processes are enthalpy driven with a considerable entropic contribution.

The following trends can be enucleated by comparing the data in Table 6:

1) The presence of a cavitand attached to the methyl pyridinium guest does not affect the observed K_{ass}.

2) The counterion overall influence on the K_{ass} is limited. However, if we compare the ΔH and TΔS data of **9B** υs **8B** or TSiiii[($3C_3H_7$ + CH_3-$Py^+PF_6^-$), CH_3, Ph] υs TSiiii[($3C_3H_7$ + CH_3-Py^+I^-), CH_3, Ph], the contribution of the counterion to the complexation can be evidenced. The entropic gain of 2-4 $kJmol^{-1}$ in favour of iodide in both cases is balanced by an equivalent in enthalpic loss. This effect is probably due to the larger lipophilia of the iodide that fits better than PF_6^- the alkyl chains of the host (observed by comparing the crystal structure determination of Tiiii[C_3H_7, CH_3, Ph]-TSiiii[($3C_3H_7$ + CH_3-$Py^+PF_6^-$), CH_3, Ph] dimer complex (see Chapter 3.2.1) and that of Tiiii[C_3H_7, CH_3, Ph]-N-methyltrifluoromethylpyridinium complex[38]): the evolving larger desolvation given to I^- an entropic advantage balanced by the enthalpic

loss of desolvation. The most relevant result enucleated from ITC measurements is the solvent effect.

CH_3OH					
	K_{ass} (M^{-1})	ΔH(KJmol^{-1})	$T\Delta S$(KJmol^{-1})	ΔG(KJmol^{-1})	n
9B: 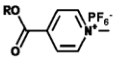	$(8.6 \pm 0.04)10^4$	-16.4 ± 0.03	11.73 ± 0.01	-28.13 ± 0.01	0.91 ± 0.02
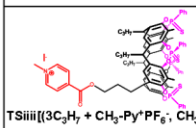 TSiii[($3C_3H_7$ + CH_3-$Py^+PF_6^-$, CH_3, Ph]	$(8.16 \pm 0.5)10^4$	-11.86 ± 0.4	16.1 ± 0.4	-28 ± 0.015	1.01 ± 0.01
8B: 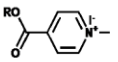	$(9.3 \pm 0.96)10^4$	-17.11 ± 0.05	11.21 ± 0.01	-28.74 ± 0.26	0.88 ± 0.01
CH_2Cl_2					
	K_{ass} (M^{-1})	ΔH(KJmol^{-1})	$T\Delta S$(KJmol^{-1})	ΔG(KJmol^{-1})	n
9B: 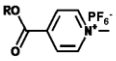	$(7.83 \pm 2.6)10^6$	-24 ± 0.4	15 ± 0.8	-39.1 ± 0.82	0.95 ± 0.02
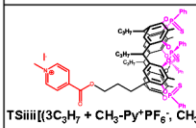 TSiii[($3C_3H_7$ + CH_3-$Py^+PF_6^-$, CH_3, Ph]	$(4.0 \pm 0.1)10^7$	-30.0 ± 0.1	13.4 ± 0.5	-43.6 ± 0.06	0.81 ± 0.01
8B: 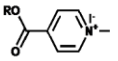	$(1.7 \pm 0.1)10^7$	-20.6 ± 0.1	20.8 ± 0.2	-41.3 ± 0.15	0.95 ± 0.09

Table 7. Comparison of thermodynamic data of isonicotinium guests in methanol and in methylene chloride via ITC.

The ITC data of methylisonicotinium guests in methanol and methylene chloride are compared in Table 7.

By moving from methanol to methylene chloride, a gain of two order magnitude is observed in all cases. This gain can be entirely attributed to the better solvation of the methyl pyridinium cation by methanol. In other words, in methylene chloride the guests prefer cavity inclusion to CH_2Cl_2

solvation. Also the host prefer methanol to methylene chloride solvation.[39] This means that the complexation in this class of compound can be defined as solvophobic.

Observing the compensation of enthalpic gain by entropic loss in the dimerization processes (**12**, and **15**), and the contrary entropic gain compensated by enthalpy loss (by comparing **8B** and **9B**), the study of the validity of the enthalpy-entropy compensation was made. This type of compensation is present in other host-guest systems.[40] Using the data reported in Table 6, the entropy changes TΔS are plotted against the enthalpy changes ΔH to give the reasonable straight line with a correlation coefficient of 0.903 as shown in Figure 32.

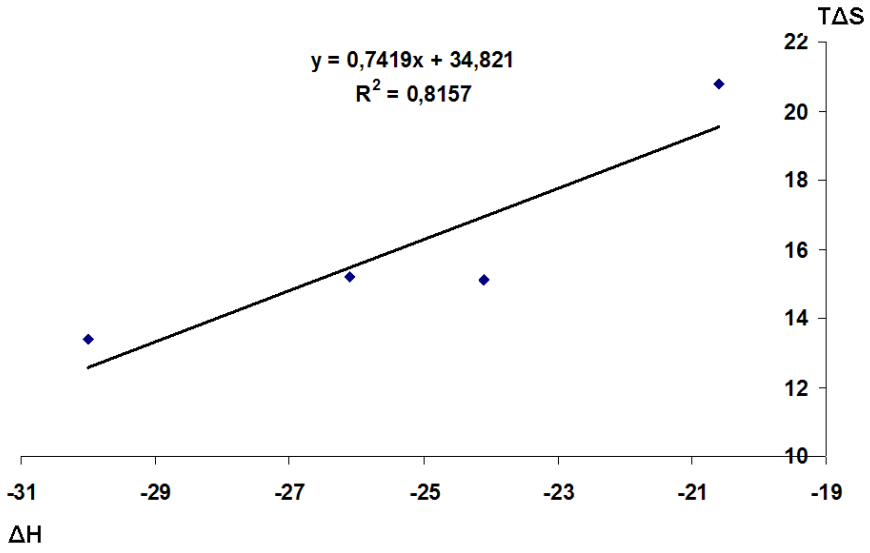

Figure 32. Enthalpy-entropy compensation of isonicotinium salts inclusion in the cavitand Tiiii[C_3H_7, CH_3, Ph] in CH_2Cl_2.

The empirical linear relationship between ΔH and ΔS mean that, whatever the cause is, the resulting change in TΔS is proportional to the accompanying change in ΔH, which leads to Equation 3.

$T\Delta(\Delta S) = \alpha\ \Delta(\Delta S)$ (3)

Integration of Equation 3 gives Equation 4, where α is the slope and T ΔS_o is the intercept of Figure 31.

$T(\Delta S) = \alpha\ \Delta H + T\Delta S_o$ (4)

Equation 4 indicates that the entropy change consists of two terms: the first one (α ΔH) proportional to the enthalpy change and the second one ($T\Delta S_o$) independent of it. By inserting equation 4 in the Gibb-Helmholtz equation, Equation 5 and 6 are obtained.

$\Delta(\Delta G) = \Delta(\Delta H) - T\ \Delta(\Delta S)$ (5)

$\Delta(\Delta G) = (1- \alpha)\Delta(\Delta H)$ (6)

Equation 3 indicates that the slope α is a quantitative measure of the entropic cancelling of the enthalpic gain from host-guest complexation. In other words, only a proportion (1- α) of the increment in ΔH contributes toward raising the complex stability (-ΔG). Equation 4 indicates that, as far as the intercept ($T\Delta S_o$) is positive as is indeed our case of complexation of the isonicotinium salts by Tiiii cavitands, the complex formation can take place even in the absence of enthalpic gain (-ΔH).[41] However, the small value of the slope (α = 0.73) (α is smaller respect to the high value of $T\Delta S_o$) and the very large value of intercept ($T\Delta S_o$ = 34,8) indicate respectively the rigidity of the host cavitand that cannot greatly change the original conformation and the extensive desolvation of both host and guest molecules that governs the entropic changes of the host-guest complexation.

2.3 Conclusions

A new synthetic procedure for stereoselective synthesis of the Tiiii cavitands has been performed leading to highly pure products.

The Complexation properties of Tiiii cavitands was studied using Tiiii[C_3H_7, CH_3, Ph] cavitand as host molecule, and different ammonium, N-methyl ammonium, and methyl pyridinium salts as guests. Different techniques were used to study and determine the association constants of the complexation processes.

1) The ^{1}H NMR and ^{31}P NMR experiments for a qualitative evaluation of the inclusion of the guests inside the cavity of the host cavitand.

2) The photophysical measurements led to the determination of the association constants in both polar and apolar solvents and the results obtained led to conclude that this type of host-guest complexation is solvent-driven.

3) The electrochemical experiments demonstrated the complete reversibility of this type of complexation by redox processes.

4) The ITC measurements led to the accurate determination of the thermodynamic parameters of the host-guest complexation processes in both methanol and methylene chloride. The association constants obtained with this technique are comparable with those determined photophysically in methylene chloride. By comparing ITC data of isonicotinium salts in methanol and in methylene chloride, the solvophobic nature of the host-guest complexation process is confirmed.

Enthalpy-entropy compensation effects have been observed in methylene chloride.

2.4 Experimental section

General Method: All commercial reagents were ACS reagent grade and use as received. All solvents were dried over 3Å and 4Å molecular sieves. ^{1}H NMR spectra were recorded on Bruker AC300 (300 MHz), AVANCE (300 MHz) and AMX400 (400 MHz) spectrometers and all chemical shift (δ) were reported in parts per million (ppm) relative to the proton resonances resulting from incomplete deuteration of the NMR solvents. ^{13}C NMR spectra were recorded on a Brucker AVANCE (75 MHz) spectrometer. Melting points were obtained with an electrothermal capillary melting points apparatus and were not corrected. Microanalyses were performed by the service of Parma University. Mass spectra of the organic compounds were measured with a Finningan-MAT SSQ 710 spectrometer, using CI (Chemical ionization) technique. Electrospray ionization (ESI)-MS experiments were performed on a Waters ZMD spectrometer equipped with an electrospray interface.

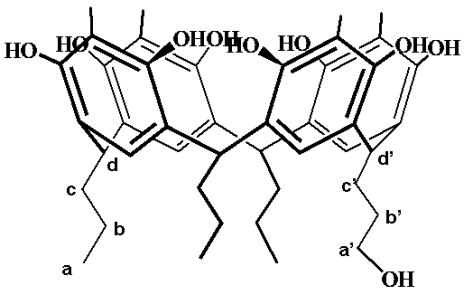

1

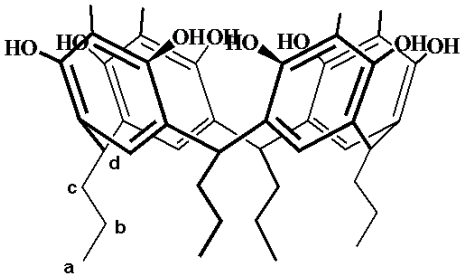

2

Synthesis of resorcinarenes 1 and 2: to a solution of methyl resorcinol (8.9 g, 72 mmol) dissolved in methanol (57 mL), butanal (4.73mL, 54 mmol) and 2,3-dihydrofuran (1.36 mL, 18 mmol) were added. The resulting yellow solution was stirred at room temperature, while 14.4 mL of a solution 12 M of HCl in water were slowly added in 30 min. The reaction mixture was stirred 6 day at 50°C then cooled at room temperature. 100 mL of water were added and the yellow suspension was filtered. Re-crystallisation from a mixture 9:1 of H_2O and CH_3OH followed by two sequential column chromatographic separations on silica gel with a mixture 93:7 of CH_2Cl_2 and CH_3OH as eluant gave rise to **1** (3.3 g, 4.5 mmol, 25%) and **2** (1.66 g, 2.34 mmol, 13%).

^{1}HNMR of 1 (300 MHz, 298 K, DMSO-d_6,) δ(ppm): 0.89 (t, 9H, $\mathbf{H_a}$, J = 7 Hz), 1.2 (m, 6H, $\mathbf{H_b}$), 1.3 (m, 2H, $\mathbf{H_{b'}}$), 1.9 (s, 12H, Ar$\mathbf{CH_3}$), 2.2 (m, (2+6)H, $\mathbf{H_{c'}}$ + $\mathbf{H_c}$), 3.4 (m, 2H, $\mathbf{H_{a'}}$), 4.2 (t, (1 + 3)H, $\mathbf{H_{d'}}$ + $\mathbf{H_d}$, J = 7.6 Hz), 4.3 (m, 1H, CH_2**OH**), 7.3 (s, 4H, Ar**H**), 8.6 (s, 8H, Ar**OH**).). **ESI-MS:** 730 $(M + H)^{+.}$

^{1}H NMR of 2 (300 MHz, acetone-d_6) δ (ppm): 0.93 (t, 12H, $\mathbf{H_a}$, J = 7.2 Hz), 1.2 (m, 8H, $\mathbf{H_b}$), 2.1 (s, 12H, ar$\mathbf{CH_3}$), 2.3 (m, 8H, $\mathbf{H_c}$), 4.4 (t, 4H, $\mathbf{H_d}$, J = 7.9 Hz), 7.4 (s, 4H, ar**H**), 7.9 (s, 8H, arO**H**). **ESI-MS:** $C_{44}H_{56}O_8$: 712.5 $(MH)^+$ and 736 $(M + Na^+)^{+.}$

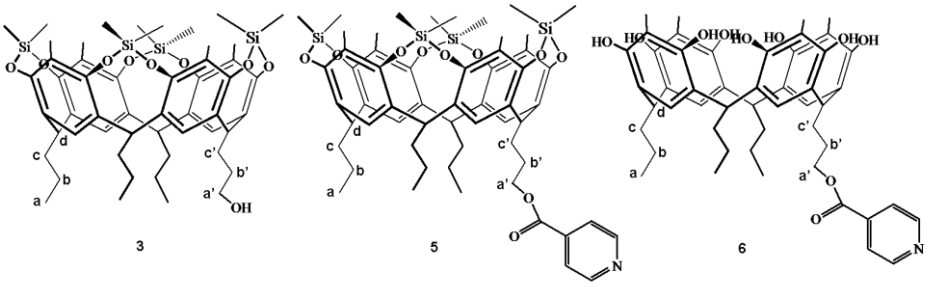

Synthesis of silyl-cavitand 3: to a solution of resorcinarene **1** (3.5 g, 4.8 mmol) dissolved in dry pyridine (120 ml), dimethyldichlorosilane (7 ml, 58 mmol) was added at 0 °C. The mixture was stirred at 70 °C for 3h; the solvent was removed under vacuum. 20 mL of methanol were added and then the yellow suspension was filtered. Purification by column chromatography on silica gel using a mixture 97:3 of CH_2Cl_2 and CH_3OH as eluant, yielded **3** (4.17 g, 4.37 mmol, 91%).

^{1}HNMR (300 MHz, 298 K, $CDCl_3$) δ(ppm): -0.71 (s, 12H, Si$\mathbf{CH_{3IN}}$), 0.50 (s, 12H, Si$\mathbf{CH_{3OUT}}$), 0.96 (t, 9H, $\mathbf{H_a}$, J=7.2 Hz), 1.3 (m, 6H, $\mathbf{H_b}$), 1.6 (m, 2H, $\mathbf{H_{b'}}$), 1.90 (s, 12H, Ar$\mathbf{CH_3}$), 2.1 (m, 6H, $\mathbf{H_c}$), 2.3 (m, 2H, $\mathbf{H_{c'}}$), 3.7 (t, 2H, $\mathbf{H_{a'}}$, J=6.3 Hz), 4.60 (t, 4H, Ar**CH,** J=7.9 Hz), 7.2 (s, 2H, Ar**H)**, 7.2 (s, 2H, Ar**H)**. **ESI-MS**: $C_{52}H_{72}O_9Si_4$, 954 $[M+H]^+$.

Synthesis of silyl-cavitand 5: isonicotinoyl chloride hydrochloride (0.25 g, 1.38 mmol) was dissolved in 15 mL of dried pyridine; silyl-cavitand **3** (0.44 g, 0.46 mmol) was added and stirred at 100 °C for 3h. The solvent was removed under vacuum and then 10 mL of water were added. The resulting suspension was filtered and purified by re-crystallisation from a mixture 9:1 of H_2O and CH_3OH yielding **5** (0.44g, 0.42mmol, 90%).

^{1}HNMR (300 MHz, 298 K, $CDCl_3$,) δ (ppm): -0.7 (s, 12H, Si$\mathbf{CH_{3\ IN}}$), 0.5 (s, 12H, Si$\mathbf{CH_{3\ OUT}}$), 0.9 (t, 9H, $\mathbf{H_a}$, J=7.2 Hz), 1.29 (m, 6H, $\mathbf{H_b}$), 1.78 (m, 2H, $\mathbf{H_{b'}}$), 1.89 (s, 12H,

ArC**H**$_3$), 2.16 (m, 6H, **H**$_c$), 2.35 (m, 2H, **H**$_{c'}$), 4.4 (t, 2H, **H**$_a$, , J=6.5 Hz), 4.6 (m, 4H, **H**$_d$), 7.16 (s, 4H, Ar**H**), 7.9 (d, 2H, **H**$_{mpy}$, J=5.1 Hz**)**, 8.8 (d, 2H, **H**$_{opy}$, J=5.1 Hz **)**: **ESI-MS:** $C_{58}H_{75}NO_{10}Si_4$: 1060 ($M+H^+$).

Synthesis resorcinarene 6: to a solution of silyl-cavitand **5** (1 g, 0.95 mmol) dissolved in 20 mL of DMF, 450 µL of a solution 55% of HF in water were added. The mixture was left to stir for 18h at 40 °C. The solvent was removed in vacuum. Purification by column chromatography on silica gel using a mixture 95:5 of H_2O and CH_3OH, yielded **6** (0,65g, 0,773 mmol, 81.5%).

^{1}HNMR (300 MHz, 298 K, Acetone-d_6) δ (ppm): 0.91 (t, 9H, **H**$_a$, J=7.4 Hz), 1.26 (m, 6H, **H**$_b$), 1.76 (m, 2H, **H**$_{b'}$), 2.04 (s, 12H, ArC**H**$_3$), 2.24 (m, 6H, **H**$_c$), 2.46 (m, 2H, **H**$_{c'}$), 4.4 (m, 4H, **H**$_a$, + **H**$_d$), 7.41 (s, 2H, Ar**H**), 7.47 (s, 2H, Ar**H**), 7.85 (d, 2H, **H**$_{mpy}$, J=6.4 Hz**)**, 7.93 (s, 4H, ArO**H**), 7.96 (s, 4H, ArO**H**), 8.78 (d, 2H, **H**$_{opy}$, J=6.4 Hz **)**. **ESI-MS**: $C_{50}H_{59}NO_{10}$: 834.9 ($M+H^+$) and 857,3 $(M+Na)^+$.

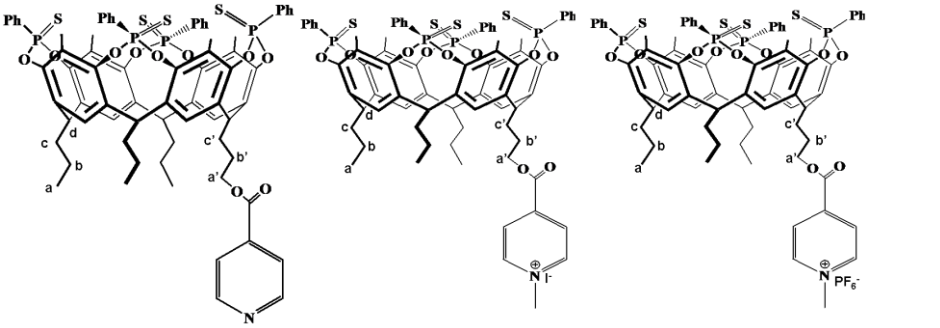

Synthesis of cavitand TSiiii[(3C$_3$H$_7$ + Py), CH$_3$, Ph]: to a solution of resorcinarene **6** (0.3 g, 0.36 mmol) dissolved in freshly distilled pyridine (15 mL), dichlorophenylphosphine (0.2 mL, 1.47 mmol) was slowly added at room temperature. The mixture was stirred for 3h at 80 °C and then cooled at room temperature. S_8 (0.11 g, 0.43 mmol) was added and left to stirred for 1 h at 50°C. The solvent was removed. Purification by column chromatography on silica gel from a mixture 98:2 of CH_2Cl_2 and CH_3OH yielded the Tiiii cavitand (0.3 g, 0.216 mmol, 60%).

^{1}HNMR (300 MHz, 298 K,$CDCl_3$) δ (ppm): 1.0 (m, 9H, **H**$_a$), 1.4 (m, 6H, **H**$_b$), 1.9 (m, 2H, **H**$_{b'}$), 2.1 (s, 12H, ArC**H**$_3$), 2.3 (m, 6H, **H**$_c$), 2.5 (m, 2H, **H**$_{c'}$), 4.5 (t, 2H, **H**$_{a'}$, J=6.4 Hz), 4.7 (m, 4H, **H**$_d$), 7.25 (s, 4H, Ar**H**), 7.55 (m, 12H, O=PAr**H**$_m$, O=PAr**H**$_p$), 7.83 (d,

2H, $\mathbf{H}_{mpy,}$ J=5.8 Hz**),** 8.2 (m, 8H, O=PAr$\mathbf{H}_o$), 8.8 (d, 2H, $\mathbf{H}_{opy}$, J=5.8 Hz **)**. **^{31}P NMR** (172 MHz, 298K, $CDCl_3$) δ (ppm): 72.0 (s, **P=S**). **ESI-MS** $C_{74}H_{71}NO_{10}P_4S_4$: 1425.61 $(M+K^+)^+$.

Synthesis of guest cavitand TSiiii[($3C_3H_7$ + CH_3-Py$^+$I), CH_3, Ph]: to a solution of TSiiii[($3C_3H_7$ + Py), CH_3, Ph] (0.3 g, 0.2 mmol) dissolved in 8 mL of a mixture 6:2 of acetonitrile and $CHCl_3$, methyl iodide (0.13 mL, 2 mmol) was added. The mixture was stirred at reflux for 18 h. The solvent was removed and the red crude reaction was purified by re-crystallization from a mixture 7:3 of acetonitrile and water yielding the product (0.3 g, 0.196 mmol, 90.7%).

^{1}HNMR (300 MHz, 298 K, $CDCl_3$) δ (ppm): 1.06 (m, 9H, $\mathbf{H_a}$), 1.37 (m, 6H, $\mathbf{H_b}$), 1.92 (m, 2H, $\mathbf{H_{b'}}$), 2.09 (s, 12H, ArC$\mathbf{H_3}$), 2.26 (m, 6H, $\mathbf{H_c}$), 2.7 (m, 2H, $\mathbf{H_{c'}}$), 4.6 (m, 2H, $\mathbf{H}_{a'}$), 4.75 (m 7H, C$\mathbf{H}_{3Py}$ + ArC**H**), 7.7-7.5 (m, 4H, P=SAr$\mathbf{H}_p$ + P=SAr$\mathbf{H}_m$ + Ar**H**), 8.13 (m, 8H, P=SAr$\mathbf{H}_o$), 8.43 (d, 2H, $\mathbf{H}_{mPy}$ J=5.5 Hz), 9.02 (d, 2H, $\mathbf{H}_{opy}$, J=5.5 Hz**)**. **^{31}PNMR** (172 MHz, 298K, $CDCl_3$) δ (ppm): 72.5 (s, **P=S**). **ESI-MS:** $C_{75}H_{74}INO_{10}P_4S_4$: 1400.74 $(M - I^-)^+$

Synthesis of the guest cavitand TSiiii[($3C_3H_7$ + CH_3-Py$^+$$PF_6^-$), CH_3, Ph]: to a solution of guest cavitand TSiiii[($3C_3H_7$ + CH_3-Py$^+$I$^-$), CH_3, Ph] (0.35 g, 0.23mmol) dissolved after heating in 5 mL of a mixture 3:2 of CH_3CN an H_2O, NH_4PF_6 (0.224 g, 1.4 mmol) was added. The mixture was stirred at 50 °C for 20 min and cooled at room temperature. The resulting yellow suspension was stirred until become white and filtered. Purification by re-crystallization from a mixture 1:1 of CH_3CN and H_2O mixture yielded the product (0.32 g, 0.21 mmol, 90.7%).

^{1}HNMR (300 MHz, 298 K, $CDCl_3$) δ (ppm): 1.06 (m, 9H, $\mathbf{H_a}$), 1.41 (m, 6H, $\mathbf{H_b}$), 1.89 (m, 2H, $\mathbf{H_{b'}}$), 2.14 (s, 12H, ArC$\mathbf{H_3}$), 2.55 (m, 6H, $\mathbf{H_c}$), 2.76 (m, 2H, $\mathbf{H_{c'}}$), 4.6 (m, 2H, $\mathbf{H}_{a'}$), 4.76 (m, 7H, C$\mathbf{H}_{3Py}$ + ArC**H**), 7. 9-7.52 (m, 16H, P=SAr$\mathbf{H}_p$ + P=SAr$\mathbf{H}_m$ + Ar**H**), 8.17 (m, 8H, P=SAr$\mathbf{H}_o$), 8.47 (d, 2H, $\mathbf{H}_{mPy}$ J=5.8 Hz), 9.13 (d, 2H, $\mathbf{H}_{opy}$, J=5.8 Hz**)**, **^{31}PNMR** (172 MHz, 298 K, $CDCl_3$) δ (ppm): 72.5 (s, 4P, **P**=S), -155 (m, 1P, **P**F_6, J_{P-F} = 810 Hz). **ESI-MS:** $C_{75}H_{74}F_6NO_{10}P_5S_4$: 1400.32 $(M - PF_6^-)^+$.

Crystal structure of cavitand TSiiii [($3C_3H_7$ + py$^+$ PF_6^-), CH_3, Ph]: The molecular structure of compound $C_{75}H_{74}NO_{10}P_4S_4$+$PF_6$+$CH_3CN$ was determined by single-crystal X-ray diffraction methods. Experimental details are summarized in Table 8. Intensity data were collected using Cu Kα radiation (λ= 1.5418 Å) equipped with a CCD area detector. The structure was solved by direct method using DENZO-SMN, SCALEPACK, and AMoRe SHELXL program. [42] The data for TSiiii [($3C_3H_7$ + py$^+$ PF_6^-), CH_3, Ph] were performed and refined using a reported programs. [43]

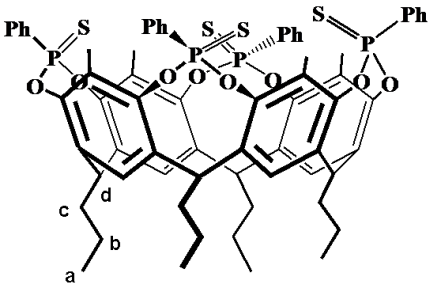

TSiiii[C_3H_7, CH_3, Ph]

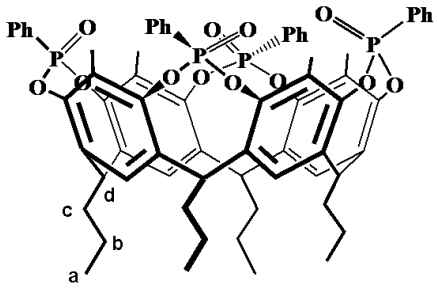

Tiiii[C_3H_7, CH_3, Ph]

Synthesis of the cavitand Tiiii[C_3H_7, CH_3, Ph]: to a solution of resorcinarene **2** (2.5 g, 3.5 mmol) dissolved in 20 mL of freshly distilled pyridine, dichlorophenylphosphine (1.93 mL, 14.3 mmol) was slowly added at room temperature. The mixture was stirred for 3h at 80°C then cooled at room temperature. An excess of H_2O_2 35% and $CHCl_3$ (5 mL) was added and left to stir for 30 min. The resulting bilayer was evaporated under vacuum. 50 mL of water were added and the white suspension was filtered. Purification by re-crystallization from a mixture 8:2 of H_2O and CH_3CN yielded the product (4 g, 3.33 mmol, 95%).

^{1}H NMR (300 MHz, $CDCl_3$) δ(ppm): 1.1 (t, 12H, **H_a**, J=7.1 Hz), 1.43 (m, 8H, **H_b**), 2.19 (s, 12H, Ar**CH_3**), 2.38 (m, 8H, **H_c**), 4.82 (t, 4H, **H_d**, J=7.4 Hz), 7.14 (s, 4H, Ar**H**), 7.62-7.5 (m, 12H, O=PAr**H*p*** + O=PAr**H_m**), 8.09 (m, 8H, O=PAr**H_o**). **^{31}P NMR:** (172 MHz, $CDCl_3$) δ(ppm): 4.02 (s, **P=O**). **ESI-MS**: $C_{68}H_{68}NO_{12}P_4$: 1201.6 $(M + H^+)^+$.

Synthesis of the TSiiii[C_3H_7, CH_3, Ph] : to a solution of resorcinarene **2** (2.5 g, 3.5 mmol) dissolved in 20 mL of freshly distilled pyridine, dichlorophenylphosphine (1.93 mL, 14.3 mmol) was slowly added at room temperature. The mixture was stirred for 3h at 80°C then cooled at room temperature. S_8 (0.72g, 2.81 mmol) was added and left to stir for 1h at 50°C. The solvent was removed in vacuum. 50 mL of water was added and the yellow suspension was filtered. Purification by column chromatography on silica gel with CH_2Cl_2 : hexane (9:1) yielded the product (2.74 g, 2,17 mmol, 62%)

^{1}H NMR (300 MHz, $CDCl_3$) δ(ppm): 1.0 (t, 12H, **H_a**, J=7.2 Hz), 1.4 (m, 8H, **H_b**), 2.1 (s, 12H, Ar**CH_3**), 2.3 (m, 8H, **H_c**, J=7.5 Hz), 4.7 (t, 4H, **H_d**, J=7.8 Hz), 7.2 (s, 4H, Ar**H**), 7.5 (m, 8H, O=PAr**H_m**), 7.6 (m, 4H, O=PAr**H*p***), 8.2 (m, 8H, O=PAr**H_o**). **^{31}P NMR:** (172 MHz, $CDCl_3$) δ(ppm): 72(s, **P=O**). **ESI-MS:** $C_{68}H_{68}NO_{12}P_4$: 1201.6 $(M+H^+)^+$.

Crystal structure of Tiiii [C_3H_7, CH_3, Ph] and TSiiii[C_3H_7, CH_3, Ph] : The molecular structure of compound $C_{68}H_{68}O_{12}P_4$+2C_2H_3N Tiiii [C3H7, CH3, Ph] and compound

$C_{68}H_{68}O_8P_4S_4$ +C_2H_3N+H_2O TSiiii [C_3H_7, CH_3, Ph] were determined by single-crystal X-ray diffraction methods. Experimental details are summarized in Table 9. Intensity data were collected using Mo Kα radiation on a Brucker AKS Smart 1000 single crystal diffractometer equipped with a CCD area detector at 173.3±2 K and 293±2 K respectively. The structures of both two compounds were solved by direct method using the SIR97 program,[44] refined on F_0^2 by full matrix least-squares procedures, using SHELXL-97.[45] The data reduction was performed using SAINT[46] and SADABS programs[47]. Geometric calculations and molecular graphics were performed with the PARST97 program[48], the DS ViewerPro 5.0 package the Mercury 1.4.2 program and the Gaussview 3.0 program.

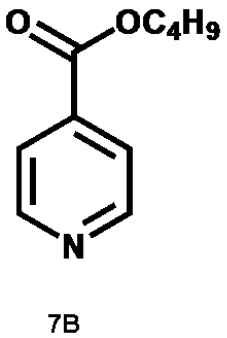

7B

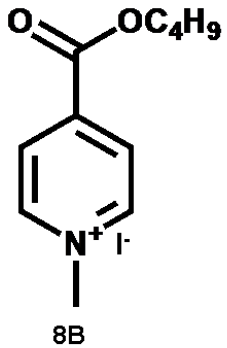

8B

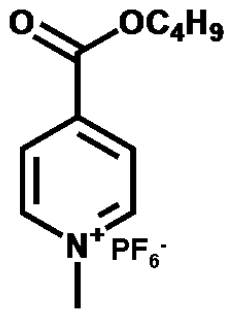

9B

Synthesis of 7B: to a solution of isonicotinoylchloride hydrochloride (2 g, 11.2 mmol) dissolved in 40 mL of pyridine, n-butanol (1.03 mL, 11.2 mmol) was added. The reaction mixture was stirred for 3h at 100°C. The solvent was removed under vacuum. 20 ml of a solution of sodium carbonate 5 mM was added and the resulting suspension was filtered. Purification by extraction (CH_2Cl_2 / H_2O) yielded **7B** (1.4 g, 7.84 mmol, 70%).

^{1}H NMR (300MHz, $CDCl_3$) δ(ppm): 0.93 (t, 2H, $OCH_2CH_2CH_2\mathbf{CH_3}$, J=7.3 Hz), 1.4 (m, 2H, $OCH_2CH_2\mathbf{CH_2}CH_3$), 1.7 (m, 2H, $OCH_2\mathbf{CH_2}CH_2CH_3$), 4.3 (t, 2H $O\mathbf{CH_2}CH_2CH_2CH_3$, J=6.6 Hz), 7.8 (d, 2H, $\mathbf{H}_{mpy}$, J=4.5 Hz), 8.7 (d, 2H, $\mathbf{H}_{opy}$, J=4.5 Hz) . **GC-MS (EI)**: rt = 7.59 min, *m/z (%)*: (M^+) = 179 (4), 106 (100), 124 (92), 78 (59), 56 (47), 51 (36.7), 123 (36.2), 137(12.2), 164 (10.2), 178 (10.2), 150 (2).

Synthesis of 8B: to a solution of butyl isonicotinate **7B** (2.17 g, 11.2 mmol) dissolved in 50 mL of acetonitrile, methyl iodide (12 mL, 22.4 mmol) was added. The reaction was stirred at reflux for 16h. The solvent was removed and the product was re-

crystallized from a mixture 1:1 of acetonitrile and ethyl acetate affording **8B** (2.86 g, 8.91 mmol, 80%).

^{1}H NMR: (300 MHz, $CDCl_3$) δ(ppm): 0.96 (t, 3H, **CH_3,** J=6.87 Hz), 1.43 (m, 2H, $OCH_2CH_2\mathbf{CH_2}CH_3$), 1.76 (m, 2H, $OCH_2\mathbf{CH_2}CH_2CH_3$), 4.43 (t, 2H, $O\mathbf{CH_2}CH_2CH_2CH_3$, J=6.7 Hz), 5.24 (s, 3H, N-CH_3), 8.45 (d, 2H, $\mathbf{H_{mPy}}$, J=6.6 Hz), 9.5 (d, 2H, $\mathbf{H_{oPy}}$, J=6.6 Hz). **ESI-MS:** $C_{11}H_{16}INO_2$: 195.1 $(M - I^-)^+$.

Synthesis of 9B: to a solution of ammonium hexafluorophosphate (3.65 g, 22.4 mmol) dissolved in a hot mixture 7:3 of acetonitrile and water, **8B** (3.6 g, 11.2 mmol) was added. The resulting yellow suspension was stirred at room temperature until the precipitate became white. Filtration and re-crystallisation from a mixture 9:1 of H_2O and CH_3CN yielded **9B** (3.6 g, 10.2 mmol, 95%).

^{1}H NMR: (300 MHz, $CDCl_3$) δ(ppm): 0.96 (t, 3H, **CH_3,** J=7.3 Hz), 1.43 (m, 2H, $OCH_2CH_2\mathbf{CH_2}CH_3$), 1.76 (m, 2H, $OCH_2\mathbf{CH_2}CH_2CH_3$), 4.4 (t, 2H, $O\mathbf{CH_2}CH_2CH_2CH_3$, J=6.7 Hz), 4.47 (s, 3H, N-CH_3), 8.4 (d, 2H, $\mathbf{H_{mPy}}$, J=5.6 Hz), 8.84 (d, 2H, $\mathbf{H_{oPy}}$, J=5.6 Hz). **^{31}P NMR** (172 MHz, DMSO-d_6) δ(ppm): -141.23 (m, $\mathbf{P}F_6^-$, $J_{P\text{-}F}$=713 Hz). **ESI-MS:** $C_{11}H_{16}INO_2$: 195$(M - PF_6^-)^+$.

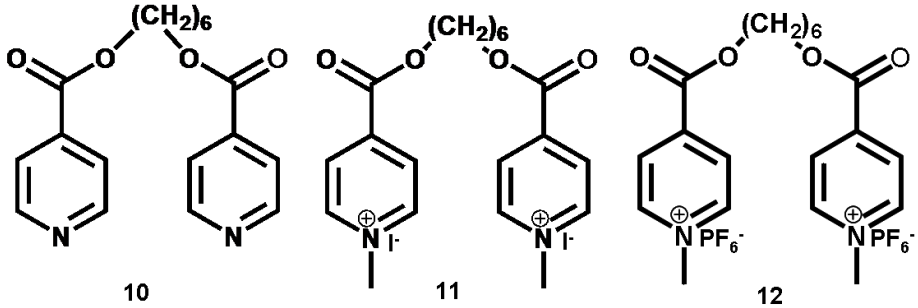

10 11 12

Synthesis of 10: to a solution of 1,6-hexandiol (99.6 mg, $8.43 \cdot 10^{-1}$ mmol) dissolved in 15 mL of pyridine, isonicotinoyl chloride hydrochloride (0.3 mg, 1.68 mmol) was added. The reaction mixture was stirred at 100°C for 3 hours. The solvent was removed and the crude reaction was purified by column chromatography on neutral aluminium oxide using first CH_2Cl_2/ hexane (60/ 40 *v/v*) then CH_2Cl_2/ ethanol (95/ 5 *v/v*) as eluant to give **10** (221.5 mg, $6.74 \cdot 10^{-1}$ mmol, 80%).

^{1}H NMR (DMSO-d_6, 300 MHz) δ (ppm): 1.3 (m, 4H, $OCOCH_2$-CH_2-$\mathbf{(CH_2)_2}$), 1.7 (m, 4H, $OCOCH_2$-$\mathbf{CH_2}$), 4.4 (t, 4H, $OCO\mathbf{CH_2}$, J=6.54 Hz), 7.9 (d, 4H, $\mathbf{H_{mPy}}$, J=4.9 Hz), 8.8

(d, 4H, $\mathbf{H}_{opy}$, J=4.9 Hz). **GC-MS (EI)**: rt = 14.14 min. *m/z (%)*: (M^+) = 329(2.3), 156(100), 106(80), 78(52), 124(27), 51(25), 184(18), 327(12), 255(11.2).

Synthesis of 11: to a solution of **10** (0.2 mg, 0.61 mmol) dissolved in 15 mL of acetonitrile, methyl iodide (0.2 mL, 3.05 mmol) was added and then stirred at reflux for 16h. After removal of the solvent, the product was re-crystallized from a mixture of acetonitrile and ethyl acetate 1:1 obtaining **11** (298 mg, $4.87 \cdot 10^{-1}$ mmol, 80%).

^{1}H NMR (DMSO-d_6, 300 MHz) δ(ppm): 1.5 (m, 4H, $OCOCH_2$-CH_2-($\mathbf{CH_2}$)$_2$), 1.8 (m, 4H, $OCOCH_2$-$\mathbf{CH_2}$), 4.3 (t, 4H, $OCO\mathbf{CH_2}$, J=6.6 Hz), 4.4 (s, 6H, $\mathbf{CH_3}$), 8.5 (d, 4H, $\mathbf{H}_{mPy}$, J=6.6 Hz), 9.2 (d, 4H, $\mathbf{H}_{oPy}$, J=6.5 Hz), **ESI-MS**: $C_{20}H_{26}I_2N_2O_4$: 179.3 $(M\text{-}2I^-)^{2+}$, 487.1 $(M\text{-}I^+)^+$.

Synthesis of 12: to a solution of **11** (0.4 g, 0.57 mmol) in a mixture 7:3 of water and acetonitrile, ammonium hexafluorophosphate (0.47, 2.87 mmol) was added. The resulting yellow suspension was stirred at room temperature until became white. Filtration and re-crystallisation from a mixture 9:1 of H_2O and CH_3CN yielded **12** (0.35 g, 0.54 mmol, 95%).

^{1}H NMR (DMSO-d_6, 300 MHz) δ (ppm): 1.5 (m, 4H, $OCOCH_2$-CH_2-($\mathbf{CH_2}$)$_2$), 1.8 (m, 4H, $OCOCH_2$-$\mathbf{CH_2}$), 4.4 (t, 4H, $OCO\mathbf{CH_2}$, J=6.6 Hz), 4.4 (s, 6H, $\mathbf{CH_3}$), 8.5 (d, 4H, $\mathbf{H}_{mPy}$, J=6.6 Hz), 9.2 (d, 4H, $\mathbf{H}_{oPy}$, J=6.5 Hz), **^{31}P NMR:** (DMSO-d_d, 172 MHz): -141.23 (m, $\mathbf{P}F_6^-$, $J_{P\text{-}F}$ = 755 Hz). **ESI-MS:** $C_{20}H_{26}I_2N_2O_4$: 179.5 $(M - 2PF_6^-)^{2+}$ and 504.1 $(M - PF_6^-)$

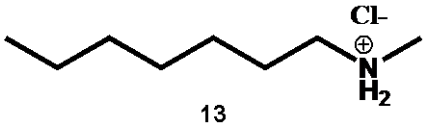

13

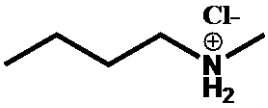

14A

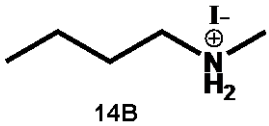

14B

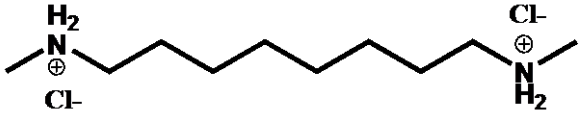

15

Synthesis of $C_7H_{15}NH_3Cl$ (13): an excess of a solution 12M of HCl in water was added to n-heptylamine (1 mL, 6.8 mmol) in 20 mL of methylene chloride. The resulting solution was stirred 30 min at room temperature. The solvent was removed and the product was re-crystallized from a mixture 99:1 of diethyl ether and acetonitrile yielding **13** (0.94 g, 6.2 mmol, 92%).

^{1}H NMR (300 MHz, CD_3CN) δ(ppm): 0.88 (t, 3H, $\mathbf{CH_3}CH_2$, J=6.5 Hz), 1.36-1.3 (m, 8H, $CH_3\mathbf{(CH_2)_4}CH_2CH_2NH_3$), 1.6-1.53 (m, 2H, $\mathbf{CH_2}CH_2NH_3$). 2.97-2.86 (m, 2H, $\mathbf{CH_2}NH_3$), 6.26-5.9 (t, 3H, $CH_2N\mathbf{H_3}$, J=52.8 Hz). **ESI-MS:** $C_7H_{18}ClN$: 1317.5 (M – Cl^- + tetraphosphonate cavitand)$^+$.

Synthesis of $CH_3NH_2C_4H_9Cl$ (14A): an excess of a solution 12M of HCl in water was added to N-methylbutylamine (1 mL, 1.69 mmol) dissolved in 20 mL of methylene chloride. The resulting solution was stirred for 30 min at room temperature. The solvent was removed and the product was re-crystallized from a mixture 99:1 of diethyl ether and acetonitrile yielding **14A** (1.97 g, 1.6 mmol, 95%).

^{1}H NMR (300 MHz, DMSO-d_6) δ (ppm): 0.87 (t, 3H, $\mathbf{CH_3}CH_2$, J=7.3 Hz), 1.3 (m, 2H, $CH_3\mathbf{CH_2}CH_2$), 1.52 (m, 2H, $CH_3CH_2\mathbf{CH_2}$), 2.46 (s, 3H, $NH_2\mathbf{CH_3}$), 2.78 (t, 2H, $CH_3CH_2\mathbf{CH_2}NH_2CH_3$, J=7.4 Hz), 9 (broad, 2H, $N\mathbf{H_2}CH_3$). **ESI-MS:** $C_5H_{14}IN$: 162 (M + $2Cl^-$)$^-$.

Synthesis of $CH_3NH_2C_4H_9I$ (14B): and excess of a solution 57% of HI in water was added to a solution of N-methylbutylamine (2 mL, 16.9 mmol) dissolved in 20 mL of in

diethyl ether. The resulting solution was stirred for 30 min at room temperature. The yellowish suspension was filtered. Re-crystallisation in a mixture 1:99 of acetonitrile and diethyl ether yielded **14B** (3.45 g, 1.6 mmol, 95%).

^{1}H NMR (300 MHz, CD_3CN) δ (ppm): 0.91 (t, 3H, $\mathbf{CH_3}CH_2$, J=7.3 Hz), 1.4 (m, 2H, $CH_3\mathbf{CH_2}$), 1.7 (m, 2H, $\mathbf{CH_2}CH_2NH_2CH_3$), 2.6 (s, 3H, $NH_2\mathbf{CH_3}$), 2.9 (t, 2H, $\mathbf{CH_2}NH_2CH_3$, J=7.5 Hz), 7.5 (broad, 2H, $N\mathbf{H_2}$). **ESI-MS:** $C_5H_{14}IN$: 342 $(M + 2I^-)^-$.

Synthesis of $CH_3NH2\text{-}C_8H_{16}\text{-}NH_2CH_3Cl_2$ (15): to a solution of octyl-1,8-diamine (200 µL, 1.16 mmol) dissolved in CH_2Cl_2, an excess of a solution 12 M of HCl was added. The reaction mixture was stirred at room temperature for 3h. The white suspension was filtered and re-crystallisation from a mixture 2:8 of CH_3CN and CH_2Cl_2 yielding **15** (0.27 g, 1.1 mmol, 95%).

^{1}H NMR (300 MHz, DMSO-d_6) δ (ppm): 1.2 (m, 8H, $(CH_3NH_2CH_2CH_2)_2$ **$(CH_2)_4$)**, 1.5 (m, 4H $NH_2CH_2\mathbf{CH_2}$**),** 2.8 (s, 4H, $CH_3NH_2\mathbf{CH_2}$), 2.5 (s, 6H, $\mathbf{CH_3}NH_2$), 7.0 (t, 4H, $N\mathbf{H_2}$, J = 51 Hz). **ESI-MS:** $C_{10}H_{26}Cl_2N_2$: 209.2 $(M - Cl^-)^+$, 105 $(M - 2Cl^-)^{2+}$.

	TSiiii[($3C_3H_7$ + CH_3-$Py^+PF_6^-$) , CH_3, Ph]
Formula	$C_{75}H_{74}NO_{10}P_4S_4$+$PF_6$+$C_2H_3N$
Formula weight	1546.44
Temperature	298 K
Wavelength	1.5418 Å
Crystal system	Monoclinic
Space Group	C2/c
***a*/Å**	24.4593±0.0875
***b*/Å**	23.8933±0.0359
***c*/Å**	29.3660±0.0456
α/°	90
β/°	108.2344±0.0707
γ/°	90
V/Å^3	16300.1
Z	8
D_c/g cm^{-3}	1.262
F(000)	6432
μ/mm^{-1}	2.569
$\theta_{min,max}$/°	2.65 – 37.38
Resolution	50.0 – 1.25 Å
Reflections collected	12150
Independent reflections	3695
Observed Reflections [F_o>4σ(F_o)]	2942
I/σ(I) (all data)	8.8
I/σ(I) (max resolution)	2.9
Completeness (all data)	98.7%
Completeness (max resolution)	96.2%
Multiplicity (all data)	1.7
Multiplicity (max resolution)	1.3
Data/restraint/parameters	3695/12/653
R[I>2.0σ(I)]	0.1045
R(all data)	0.1204
Goodness of fit	1.312

Table 8: crystallographic data of cavitand TSiiii[($3C_3H_7$ + CH_3-$Py^+PF_6^-$), CH_3, Ph]

	Tiiii[C_3H_7, CH_3, Ph]	TSiiii[C_3H_7, CH_3, Ph]
Formula	$C_{68}H_{68}O_{12}P_4 \cdot 2\ CH_3CN$	$C_{68}H_{68}O_8P_4S_4 \cdot CH_3CN \cdot H_2O$
Formula weight	1283.28	1324.48
Crystal system	Tetragonal	Monoclinic
Space group	*P4/n*	*P21/n*
***a*/Å**	15.053(4)	14.459(1)
***b*/Å**	15.053(6)	24.151(2)
***c*/Å**	14.652(8)	21.766(2)
***β*/°**	-	99.613(2)
***V*/Å³**	3320(2)	7494(1)
Z	2	4
D_c/g cm^{-3}	1.284	1.174
***F*(000)**	1352	2784
μ/mm^{-1}	1.568	0.263
$\theta_{min.max}$/°	3.02 - 69.84	1.27. 23.26
Reflections collected	3385	46155
Independent reflections	3138 [R(int) = 0.0431]	10724 (*R*int = 0.0943)
Obs. refl. [Fo>4σ(Fo)]	2520	4557
Data / restr. / param	3138 / 1 / 209	10724 / 3 / 772
R indeces [Fo>4σ(Fo)][a]	R1 = 0.0876. wR2 = 0.2503	R1 = 0.0671. *w*R2 = 0.1644
R indeces (all data)	R1 = 0.1000. wR2 = 0.2655	R1 = 0.1590. *w*R2 = 0.1910
$\Delta\rho_{min.max}$/e Å^{-3}	-0.384. 0.688	-0.437. 0.779
***S*[b]**	1.008	1.010

Table 9. Crystallographic data of cavitands Tiiii [C_3H_7, CH_3, Ph] and TSiiii [C_3H_7, CH_3, Ph].

Absorption and luminescence experiments. Measurements were carried out at room temperature (ca. 295 K) on air equilibrated CH_2Cl_2 (Merck Uvasol) or CH_3CN (Merck Uvasol) solutions in the concentration range from 1×10^{-6} to 2×10^{-5} M. UV-vis absorption spectra were recorded with a Perkin-Elmer λ40 spectrophotometer. Luminescence spectra were obtained with a LS-50 spectro-fluorimeter (Perkin-Elmer) equipped with a Hamamatsu R928 phototube. Correction of the luminescence intensity for inner filter effects was performed when necessary according to a previously reported procedure.[49] Luminescence lifetimes were measured by the time-correlated single-photon counting (TCSPC) technique with an Edinburgh Instruments FLS920 equipment. The spectrophotometric and spectrofluorimetric titration curves were analyzed with the SPECFIT software.[50] The experimental error on molar absorption coefficients, emission intensities, and luminescence lifetimes is estimated to be ±5%, on wavelength values, ± 1 nm.

Electrochemical experiments. Cyclic voltammoletric (CV) and differential pulse voltammoletric (DPV) experiments were carried out in argon-purged CH_2Cl_2 (Romil Hi-Dry) solution at room temperature with an Autolab 30 multipurpose instrument interfaced to a PC. The working electrode was a glassy carbon electrode (Amel; 0.07 cm^2), the counter electrode was a Pt wire, separated from the solution by a frit, and an Ag wire was employed as a quasi-reference electrode. Ferrocene was present as an internal standard ($E_{1/2}$ = +0.51 V vs SCE). The concentration of the compounds examined was on the order of 1×10^{-3} M; tetrabutylammonium hexafluorophosphate 0.1 M was added as supporting electrolyte. Under these conditions, the observed potential window ranged from –1.8 to +1.8 V vs SCE. CVs were obtained at sweep rates varying from 0.02 to 5 V s^{-1}. DPVs were obtained at a sweep rate of 0.02 mV s^{-1}, with a pulse height of 75 mV and a duration of 40

ms. The IR compensation implemented within the Autolab 30 was used, and every effort was made throughout the experiments to minimize the resistance of the solution. In any instance, the full electrochemical reversibility of the voltammoletric wave of ferrocene was taken as an indicator of the absence of uncompensated resistance effects. For reversible processes the halfwave potential values were calculated from an average of CV and DPV experiments, whereas the redox potential values in the case of irreversible processes were estimated from the DPV peaks. Experimental errors: potential values, ±10 mV for reversible processes, ±20 mV for irreversible processes. Spectroelectrochemical measurements were performed *in situ* with a custom-made optically transparent thin-layer electrochemical (OTTLE) cell by using an Autolab 30 potentiostat and a Hewlett-Packard diode array spectrophotometer. The working and counter electrodes were Pt minigrids, and the quasi-reference electrode was an Ag wire; all the electrodes were melt-sealed into a polyethylene spacer.

ITC Titrations: ITC titrations were performed using an isothermal titration microcalorimeter Microcal VP-ITC. All measurements were performed at (298 ±0,02) K. The host solution was filled into the cell of the ITC instrument and guest solutions were added with the syringe. In each case control experiments with dilution of guest in the solvent were performed and were found to be negligible. Concentration of cavitand Tiiii [C_3H_7, CH_3, Ph] range between 0.4 and 0.5 mmol in methanol while range between 0.125 and 0.3 in methylene chloride and the concentration of the guests (**8B, 9B, 21F, 12, 13, 14A, 14B)** range 4-10 mmol in methanol and 2.5-5 mmol in methylene chloride). The volume of injection was 10 μL and the stirring speed was 300 rpm. Samples were weight with a microbalance Mettler Toledo MX5. The solvent was previously degassed by sonication during 15 min. Titrations were made 3

times in order to be reproducible. Analysis and curve fitting were done using the software *MCS Origin-ITC 7.0* program.

^{1}H-NMR Titrations: Two standard solutions were prepared in methylene chloride, one with the cavitand Tiiii [C_3H_7, CH_3, Ph] (C= 0.02 mmol) and the other one with the guests (**14A, 14B)** (C = 0.32 mmol) in order to keep constant the concentration of host during the titration. All titrations were performed using an initial amount of 0.4 mL of host solution. To this solution increasing amounts of standard solution of the guest (20 uL, 0 up to 2 equivalents) were added.

2.5 references

[1] a) B. Dietrich, J.-M. Lehn, J. P. Sauvage *Tetraheddron Lett.* **1969**, 2885; b) B. Dietrich, J.-M. Lehn, J.-P. Sauvage, J. Blanzat, *Tetrahedron*, **1973**, 29, 1629; c) B. Dietrich, J.-M. Lehn, J.-P. Sauvage, J. Blanzat, *Tetrahedron*, **1973**, 29, 1647; J.-M. Lehn, *Struct. Bonding*, **1973,** 16, 1.

[2] a) C. J. Pedersen, *J. Am. Chem. Soc.* **1967**, 89, 7017; b) C. J. Pedersen, *Angew. Chem. Int. Ed.* **1988**, 27, 1053.

[3] a) S. Valliyaveettile, J. F. Engbersen, W. Verboom, D. N. Reinhoudt, *Angew. Chem. Int. Ed. Engl.* **1993,** 32, 900, b) P. D. Beer, P. A. Gale, D. Hesek, *Tetrahedron Lett.* **1995,** 36, 767, c) A. V. Eliseev, H. –J. Schneider, *Angew. Chem. Int. Engl*, **1993,** 32, 1331; d) K. Manabe. K. Okamura, T. Date, K. Koga, *J. Am. Chem. Soc.*, **1992,** 114, 6940

[4] a) R. Breslow, *Chem. Soc. Rev.*, **1972,** 1, 553; b) J.-M. Lehn, *Pure Appl. Chem.* **1979,** 51, 979.

[5] a) M. P. Mertes, K. B. Mertes, A*cc. Chem. Res.*, **1990,** 23, 230; b) M. W. Hosseini, J.-M. Lehn, *J. Am. Chem. Soc.*, **1991,** 451; c) M. W. Hosseini, J.-M. Lehn, K. C. Jones, K. E. Pluto, K. B. Mertes, M. P. Mertes, *J. Am. Chem. Soc.*, **1989,** 111, 6330.

[6] D. J. Cram, *Science*, **1983**, 219, 1177-1183

[7] a) R. J. M. Egbering, P. UH. M. Gobben, W. Verboom, S. Harkema, D. N. Reinhoudt, *J. Inclusion Phenom.* **1992,** 12, 151; b) E. U. Thoden van Velzen, J. F. J. Engbersen, D. N. J. reinhoudt, *j. Am. Chem. Soc.* **1994,** 116, 3597; c) D. J. Cram, S. Karbach, H.-E. Kim, C. B. Knobler, E. F. Marverick, J. L. Ericson, R. C. Helgeson, *J. Am. Chem. Soc.* **1988**, 110, 2229

[8] W. Xu, J. J. Vittal, R. J. Puddephatt, *J. Am. Chem. Soc.*, **1995,** 117, 8362-8371;.

[9] R. Pinalli, M. Suman, E. Dalcanale, *Eur. J. Org. Chem.*, **2004,** 451-462.

[10] A. G. S. Högberg, *J. Am. Chem. Soc.* **1980,** 102, 6046-6050; b) A. G. S. Högberg, *J. Org. Chem.* **1980,** 45, 4498-4500; c) L.M. Tunstadt, J.A Tucker, E. Dalcanale, J. Weiser, J.A. Bryant, J.C. Sherman, R.C. Helgeson, C.B. Knobler, D.J. Cram, *J. Org. Chem*. **1989**, 54, 1305-1312.

[11] K. D. Stewart. PH.D. Dissertation, University of California, Los Angeles, **1984.**

[12] T. Lippmann, G. Mann, E. Dalcanale, *Tetrahedron Lett.,* **1994,** 35, 1685-1688.

[13] T. Lippmann, H. Wilde, E. Dalcanale, L. Mavilla, G. Mann, U. Heyer, S. Spera, *J. Org. Chem.,* **1995,** 235-242.

[14] E. Dalcanale, P. Jacopozzi, F. Ugozzoli, G. Mann, S*upramol. Chem.,* **1998,** 9, 305-316.

[15] P. Delange, J.-P. Dutasta. *Tetrahedron Lett.,* **1995,** 60, 36, 9325-9328.

[16] P. Delange, J.-C. Mulatier, B. Tinant, J.-P. Declercq, J.-P. Dutasta, *Eur. J. Org. Chem.,* **2001,** 3695-3704 ; b) B. Bibal, J.-P. Declercq, J.-P. Dutasta, *Supramol. Chem.,* **2003,** 15, 25-32.

[17] W. Xu, J. P. Rourke, J. J. Vittal, R. J. Puddephatt, *J. Chem. Soc. Chem. Commun.*, **1993,** 145-147.

[18] **PCMODEL** Molecular Modeling Sofware, version 4.2, Serena Software **1992**

[19] a) W. Xu, J. J. Vittal, R. J. Puddephatt, *J. Am. Chem. Soc.,* **1993,** 115, 6456-6457; b) W. Xu, J. P. Rourke, J. J. Vittal, R. J. Puddephatt, *Inorg. Chem.,* **1995,** 34, 323-329; c) W. Xu, J. J. Vittal, R. J. Puddephatt, *Inorg. Chem.,* **1997,** 36, 86

[20] E. E. Nifantyev, V. I. Maslennikova, L. K. Vasyanina, E. V. Panina, *Rus, J. Gen. Chem.*. **1994,** 64, 142-143; b) E. E. Nifantyev, V. I. Maslennikova, E. V. Panina, A. R. Bekker, L. K. Vasyanina, K.A. Lyssenkov, M. Y. Stuchkov, *Mendeleev Commun.,* **1995,** 131-133; c) V. I. Maslennikova, E. V. Panina, R. Bekker, L. K. Vasyanina, E. E. Nifantyev, *Phosphorus Sulfur and Silicon,* **1996,** 113, 219-223.

[21] B. Bibal, B. Tinantb, J.-P. Declercq, J.-P. Dutasta, *Chem. Commun.,* **2002**, 432-433

[22] B. Bibal, B. Tinantb, A.-G. Valade, J.-P. Declercq, J.-P. Dutasta, *Tetrahedron.,* **2003**, 59, 5849-5854

[23] W. J. Stec, A. Okruszek, J. Michalski, *J. Org. Chem.,* **1976,** 41, 233-238

[24] A. W. Herriott, *J. Am. Chem. Soc.,* **1971,** 93, 3304-3305

[25] W. N. Setzer, M. L. Brown, X.-J. Yang, M. A. Thompson, K. W. Whitaker, *J. Org. Chem.,* **1992,** 57, 2812-2818

[26] B. Dubessy, Thèse de l'Ecole Normale Superiore de Lyon, **2006.**

[27] F. Hauke, A. J. Myles, J. Rebek, Jr., *Chem. Commun.,* **2005,** 4164-4166.

[28] B. C. Gibb, R. G. Chapman, J. C. Sherman, *J. Org. Chem.*, **1996,** 61, 1505-1509.

[29] H.-J. Schneider, R. Kramer, S. Simova, U. Schneider, *J. Am. Chem. Soc.*, **1988,** 110, 6442-6448; b) C. S. Wilcox, *In Frontiers in Supramolecular Chemistry and Photophysical*; H.-J. Schneider, H. Durr, , Eds., VCH: *Wienhien, Germany*, **1991,** 123-143, c) R. S. J. Macomber, J. Chem. Educ. **1992,** 69, 375-378.

[30] Busi Marco, PhD thesis in Science and Technology of Innovative Materials, **2006.**

[31]. R. Ballardini, A. Credi, M.T. Gandolfi, C. Giansante, G. Marconi, S. Silvi, M. Venturi, *Inorg. Chim. Acta* **2007**, *360*, 1072.

[32]. A. Credi, S. Dumas, S. Silvi, M. Venturi, A. Arduini, A. Pochini, A. Secchi, *J. Org. Chem.* **2004**, *69*, 5881.

[33] T. Wiseman, S. Williston, J. F. Brandts, L. N. Lin *Anal. Biochem.* **1989**, 179, 131-137. b) E. Freire, O. L. Mayorga, M. Straume, *Anal. Chem.* **1990,** 62, 950-959. c) D. S. Gill, D. J. Roush, K. A. Shick, R. C. Willson, *J. Chromatogr.* **1995,** 715, 81-93

[34] Ingemar Wadso, *Chem. Soc. Rev.*, **1997**, 79-86

[35] C. R. Yonker, R. D. Smith, *J. Phys. Chem.* **1988,** 92, 2374-2378

[36] M. M. Pierce, C. S. Raman, B. T. Nall, *Methods,* **1999,** 19, 213-221

[37] J. L. Sessler, D. E. Gross, W.-S. Cho, V. M. Lynch, F. P. Schmidtchen, G. W. Bates, M. E. Light, P. A. Gale, *J. Am. Chem. Soc.* **2006,** 128, 12281-12288.

[38] E. Biavardi, E. Dalcanale, Unpublished results.

[39] L. Pirondini, E. Dalcanale, *Chem. Soc. Rev.*, **2007**, 36, 695-706.

[40] a) Y. Inoue, T. Hakushi, *J. Chem. Soc. Perkin Trans.* **1985,** 2, 935-938; b) Y. Inoue, T. Hakushi, Y. Lui, L.-H. Tong, J. Hu, G.-D. Zhao, S. Huang, B.-Z. Tian, , *J. Phys. Chem.*, **1988,** 92, 2371-2375; c) Y. Lui, L.-H. Tong, S. Huang, B.-Z. Tian, Y. Inoue, T. Hakushi *J. Phys. Chem.,* **1990,** 94, 2666-2671; d) Y. Lui, L.-H. Tong, Y. Inoue, T. Hakushi, *J. Chem. Soc. Perkin Trans.* **1990,** 2, 1247-1257.

[41] Y. Inoue, T. Hakushi, Y. Lui, L.-H. Tong, B.-J. Shen, D. S. Jin, *J. Am. Chem. Soc.* **1993,** 115, 475-481.

[42] a) Z. Otwinowski, W. Minor, *Processing of X-ray Diffraction Data Collected in Oscillation Mode. Methods In Enzymology*, **1997**, 276, 307-326; b) J. Navaza,

Amore-an Automated Package for Molecular Replacement. Acte Crystallographica Section A, **1994,** 50, 157-163.

[43] DS viewerPro 5.0 *by accelry*. http://www.accelrys.com/com/about/msi.html.

44 A. Altomare, M. C. Burla, M. Cavalli, G. L. Cascarano,. C. Giacovazzo, A Guagliardi,. A. G. G. Moliterni, G. Polidori, R. Spagna .,. *J. Appl. Crystallogr*. 1999, 32, 115-119.

[45] G. M. Sheldrick, *SHELXL97. Program for Crystal Structure Refinement, University of* Göttingen: Göttingen, Germany, **1997**.

[46] SAINT, Software Users Guide, 6.0; Bruker Analytical X-ray Systems: **1999**.

[47] G. M. Sheldrick, *SADABS Area-Detector Absorption Correction, 2.03;* University of Göttingen: Göttingen, Germany, **1999**.

[48] Nardelli, M., *J. Appl. Crystallogr*. **1996,** *29*, 296-300

[49] A. Credi, L. Prodi, *Spectrochim. Acta A* **1998**, *54*, 159.

[50] R.A. Binstead, SPECFIT, Spectrum Software Associates, Chapel Hill, NC, 1996

Chapter 3

Host-guest driven self-assembly of supramolecular homopolymers

3.1 Introduction

Dynamic materials[1] featuring modular components, nano-scale dimensions and controlled responsiveness to external stimuli are among the most attractive targets of contemporary materials science. Since supramolecular polymers[2] fulfil nicely all these conditions, they are in a prominent position in the list of effective dynamic materials.

While the self-assembly of supramolecular polymers driven by H-bonding[3] and metal coordination[4] has undergone explosive development, the host-guest route is by far less travelled, despite of the many different options potentially available. The need of very high association constants for the self-assembly of truly polymeric materials greatly reduces the number of possibilities. So far, most of the activity has been centered on solvophobic interactions using cyclodextrins as hosts,[5] and, to a lesser extent, on pseudorotaxane treading with alkylammonium guests.[6] More recently calixarenes,[7] cavitands,[8] and donor-acceptor molecules[9] have been used as monomers, leading to the formation of oligomeric materials.

This Chapter will describe a new class of supramolecular polymers which self-assembly is driven by the outstanding complexing properties of tetraphosphonate cavitands toward methyl pyridinium guests.

Phosphonate cavitands are resorcinarene-based molecular receptors presenting one or more P(V) moieties as bridging units.[10] The tetraphosphonate ones in their all inward configuration[11] are able to complex positively charged species, such as ammonium salts or inorganic cations with very high association constants ($K_{ass}=10^7$-10^9 M^{-1}).[12]

3.1.1 Supramolecular polymers based on hydrogen bonding

One of the main approaches to build supramolecular architectures is based on the introduction of self-recognizing hydrogen-bonding patterns. As secondary interaction, the H-bond assures directionality and versatility. However, the weakness of single hydrogen bonding led the pioneering group of J.-M. Lehn[13] to design a system that combines complementary triple hydrogen-bonding (Figure 1). Only oligomeric chains were obtained with this combination of triple hydrogen-bonding due to the low association constant < 10^4.

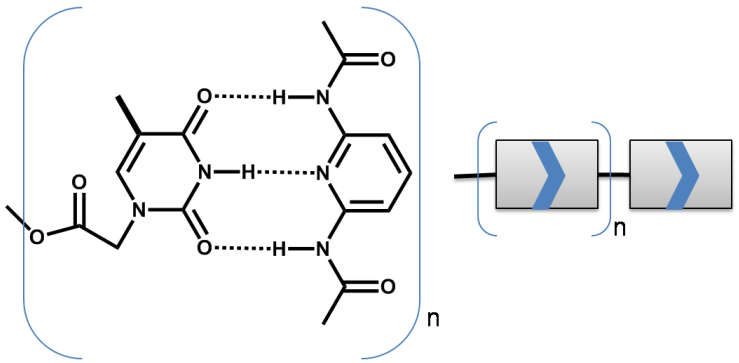

Figure 1. Supramolecular polymers based complementary triple hydrogen-bonding

In order to increase the strength of the interactions, Meijier and co-workers[14] proposed supramolecular polymers were complementary triple hydrogen-bonding, were expanded to self-complementary quadruple hydrogen-bonding (Figure 2). This system is based on bis-ureodopyrimidinones containing self-complementary hydrogen-bonding units which can form a donor-donor-acceptor-acceptor (DDAA) array of hydrogen-bonding sites. The formation of high molecular weight species due o the high association constant > 10^6 was shown by viscosimetry, which revealed an exponential relationship of the viscosity with concentration.[15] Improved material properties were demonstrated via reology and dynamic mechanical thermal analysis.[16]

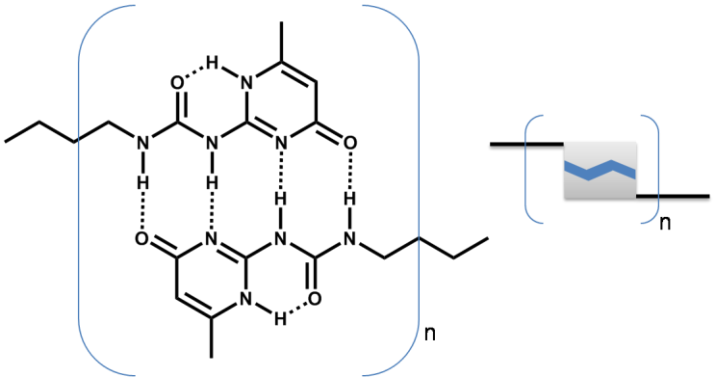

Figure 2. Self-complementary quadruple hydrogen-bonding for supramolecular polymers

More recently, sextuple hydrogen-bonds of diamino-pyridine-substituted isophthalamide and cyanuric acid, were employed by Lehn group to form supramolecular polymers in which molecular weight can be adjusted tuning the stoichiometry of the components.[17]

3.1.2 Supramolecular polymers based on metal-coordination.

Supramolecular polymers can be constructed exploiting the directionality and the tunable strength of metal complexes. The most used ligands or chelated systems reported in literature are based on pyridine, bi-pyridine, and ter-pyridine. The most used metals are zinc and palladium which forms labile reversible complexes, ruthenium, platinium and rhenium which complexes are very stable and become reversible by addition of competitive ligands.

Precursors containing *p*-bis(ter-pyridine) functionalized phenyl compounds were utilized by Rehahn and co-workers to prepare extended rod-like and linear coordination polymers.[18] Covalent oligomers or polymers (the most used is poly-ethylene glycol PEG) were functionalized at the two end-chains with ter-pyridine moieties and subsequently converted into linear metallo-supramolecular architectures and, as results there has been, an increase of molecular weight (Figure 3), with consequent, the improvement of the initial structural and mechanical properties.[19]

Figure 3. High molecular weight ter-pyridine- functionalized PEG copolymer after Ru(II) complexation

Recently Lehn et al. reported metallo-supramolecular polymers of polysiloxane oligomers functionalized with acylhydrazone-pyridine derivatives[20] (Figure 4). The oily polysiloxane oligomers (A and B), become the gum material (C, D, and E) by adding either Zn(II) or Ni(II). The molecular weight increases more than twenty times compared to the initial oligomers. The optical properties change after complexation. The

dynamic behaviour of the metallo-supramolecular polymers as result of the reversibility of the coordinated bonds was demonstrated at ^{1}H NMR spectroscopy by occurrence of ligand exchange and recombination of the mixture C and D.

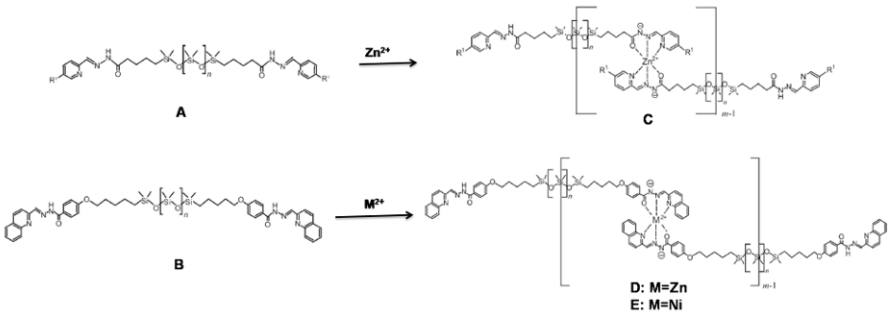

Figure 4. Metallo-supramolecular polymer of acylhydrazone functionalized polysiloxane.

Metal coordination was used to cross-link polymers bearing multiple metal-coordination sites. The first copolymers containing metal-coordination cross-linking were reported in the 1990s.[21] Redox-reversible and thermo-reversible hydrogels were obtained in this manner by metal-complexation of multi-terpyridine linked in the side-chains of the polymers. Recently the addition of Fe(II) and Zn(II) ions to terpyridine-containing copolymers in diluted solution resulted in drastically increased viscosities, showing the formation of cross-linked aggregates (Figure 5a). The low concentration is maintained to avoid precipitation.[22] Grafting copolymers approach was also reported (Figure 5b), using the directed complexation to terpyidine-side-chains polymer of asymmetric terpyridine end-chains functionalized polymers with Ru (II) or Ru(III).[23]

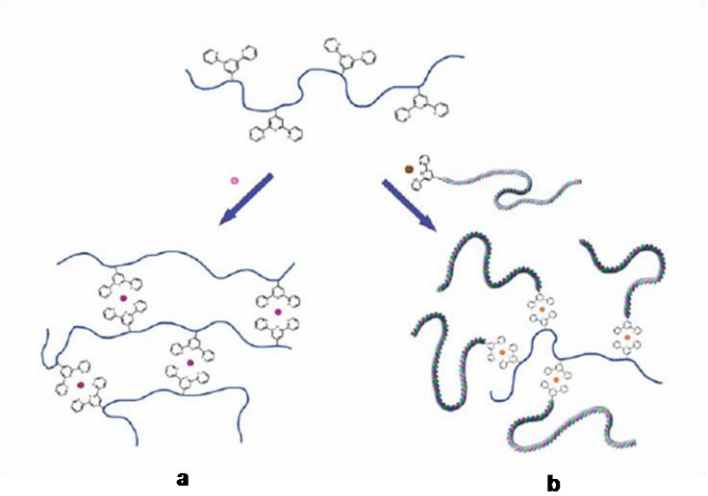

Figure 5. Cross-linking and grafting copolymers containing ter-pyridine moieties in the side-chains

3.1.3 Supramolecular polymers based on host-guest interactions.

Host-guest complexes are formed by non covalent interactions between a molecule named host (often the biggest one) and a smaller molecules named guest which lead reversible complexes. In many cases the host has a three-dimensional cavity that, interacts with the guests through the sum of weak but specific interactions such as, ion-ion, ion-dipole, dipole-dipole, π-π stacking, CH-π, hydrogen-bonds, etc... The sum of these weak interactions leads to the strong and specific non covalent bonds.

This type of interaction plays an important role in the construction of supramolecular architectures. Over time, scientists have synthesized many functional hosts capable to form strong host-guest interactions, with cations, ionic or neutral organic molecules which can be used to construct supramolecular architectures. Calixarenes for example, are widely studied. Their capacity to encapsulate small guests like benzene was used to construct linear supramolecular polymer (Figure 6) from bis-calixarenes.[24]

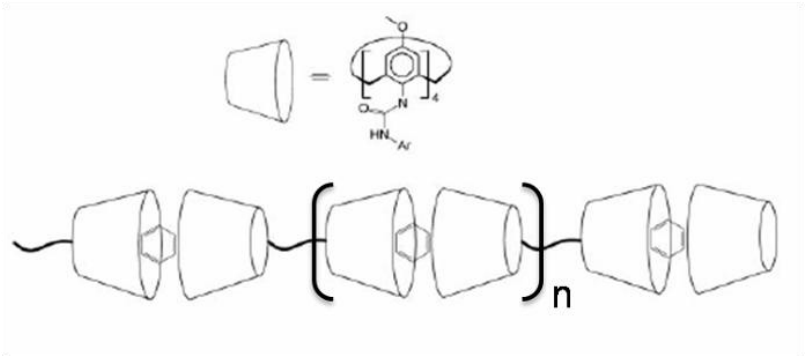

Figure 6. Linear supramolecular polimer through benzene incapsulation on bis-calixarene

Other supramolecular entities based on the calix[5]arene-primary alkylammonium ions recognition motif have been reported. The formation of inclusion motif networks derived from the self-assembly of a bis-calix[5]arene receptor and long-chain α,ω-alkyldiammonium ions have been reported.[25] The degree of polymerization was modulated by varying the counterions. Supramolecular homopolymer based on cone calix[5]arene derivative, bearing a long-chain alkylamino pendant group on the lower rim has also been reported by Parisi group.[26] Another contribution describes supramolecular polymers containing cyclodextrins as host molecules and adamantane or *p-(tert*-butyl) phenyl groups as guests. Supramolecular architectures based on this type of host-guest interactions have been widely studied. Harada and co-workers[27] reported a homopolymers containing α-cyclodextrin and *p-t*-butoxyamonociannamoylamino group. The same group has reported linear supramolecular polymer based on recognition between α-cyclodextrin-ß-cyclodextrin hetero-dimer and hetero-cyannamamide guest dimer.[28] Recently supramolecular polymers based on ß-cyclodextrin in which assembly and disassembly processes (Figure 7) are photochemically controlled have been reported in the literature.[29]

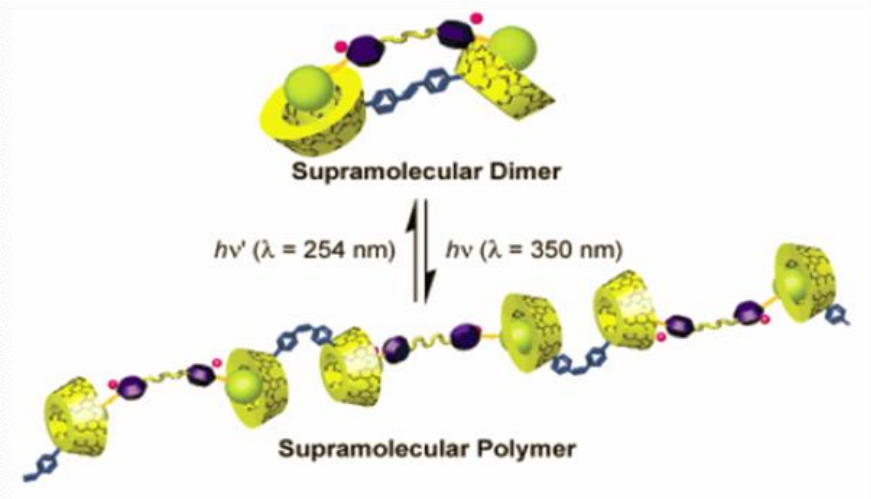

Figure 7. Photochemical control of bis- α-cyclodextrin-bis-adamantane assembly-disassembly

The ß-cyclodextrin dimer assumes reversibly the cis or trans-conformation if photochemically stimulated. In the trans shape, the ditopic adamantane guest make the intramolecular complex while in the cis shape linear supramolecular polymeric chains are formed.

There is also an example of simultaneous use of two different interactions. The combination of different orthogonal non covalent interactions can be introduced in a highly defined way by controlled self-assembly processes. Thus hydrogen bonding and unidirectional electrostatic interaction between complementary units were combined in order to generate supramolecular architectures in the solid state.[30]

In order to generate dynamic polymeric materials we designed and prepared a molecule that contains both the host and the guest functionalities. In this way, such molecule can auto-assemble through host-guest self-complementarity toward linear supramolecular architectures.

In previous work from our laboratory, cavitand-based supramolecular oligomers were made (see Chapter 4). The drawback of these materials

was the low K_{ass} for polymer formation. To avoid this problem we resolved to the very strong host-guest association like the ones described in Chapter 2.

3.2 Results and discussion.

3.2.1 Host-guest dimerisation.

The ITC studies previously reported in Chapter 2 and summarized in Table 1 showed that, the thermodynamic parameters of formation of the host-guest dimer between the phosphonate-cavitand Tiiii[C_3H_7, CH_3, Ph] and the thiophosphonate-cavitands TSiiii[($3C_3H_7$ + CH_3-Py^+ x^-), CH_3, Ph] were similar to that of the complex between Tiiii[C_3H_7, CH_3, Ph] and *N*-methyl pyridinium guest. Since the thiophosphonate cavitands TSiiii cannot form host-guest interactions with pyridinium guests (see crystal structure of TSiiii[($3C_3H_7$ + CH_3-Py^+ PF_6^-), CH_3, Ph] in Chapter two), we started studying the dimerisation process between the thiophosphonate cavitand TSiiii[($3C_3H_7$ + CH_3-Py^+ PF_6^-), CH_3, Ph] and the model phosphonate cavitand Tiiii[C_3H_7, CH_3, Ph] (Figure 8) both synthesized in the previous chapter.

Guests	ΔH (kJmol^{-1})	TΔs (kJmol^{-1})	ΔG (kJmol^{-1})	K_{aSS}(M^{-1})
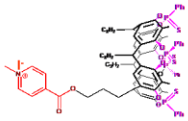 TSiiii [($3C_3H_7$ + CH_3-Py^+ I^-). CH_3. Ph]	-26.1±0.2[a]	15.2±0.9[a]	-41.4±0.78[a]	(1.9±0.6)•10^7[a]
	-11.86±0.4[b]	16.1±0.4[b]	-28±0.2[b]	(8.16±0.6)• 10^4[b]
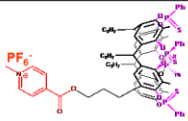 TSiiii [($3C_3H_7$ + CH_3-Py^+ PF_6^-). CH_3. Ph]	-30.0±0.1[a]	13.4±0.5[a]	-43.6±0.06[a]	(4.0±0.1)•10^7[a]
Dimer disassembly with C_4H_9-NH_2^+-CH_3 Cl^-	-99.7±10.3[c]	-77.9±11[c]	-21.75±0.45[c]	(6±1.1)•10^3[c]

Table 1. Thermodynamic parameters of [a] dimerization process in CH_2Cl_2, [b] dimerization process in methanol, [c] disassembly of the host guest dimer 1 in methanol via ITC calorimetry.

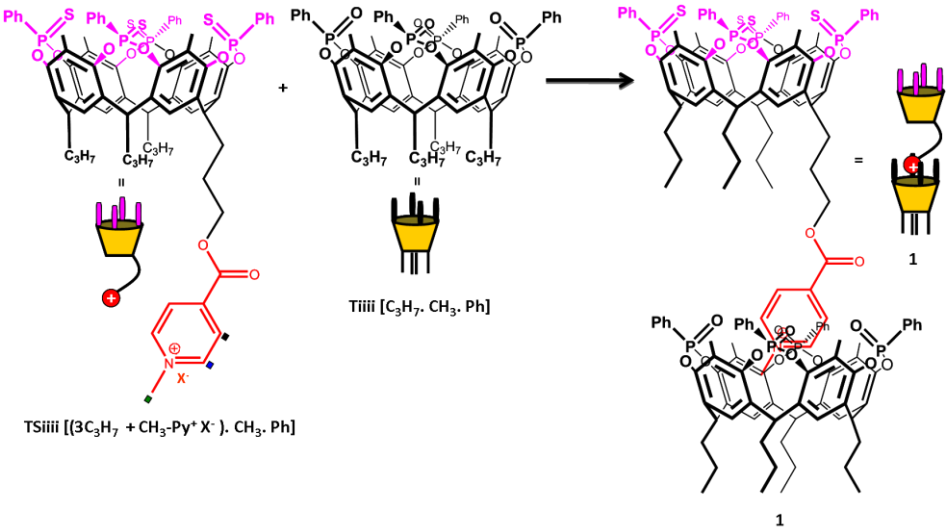

Figure 8. Dimerization process between Tiiii[C_3H_7, CH_3, Ph] and TSiiii[($3C_3H_7$ + CH_3-Py^+ x^-), CH_3, Ph] to form 1.

The ^{1}H NMR data confirm the inclusion of pyridinium moiety inside the cavity of phosphonate-cavitand Tiiii[C_3H_7, CH_3, Ph]**.** This assertion is verified by observing the ortho, meta and CH_3 pyridinic protons. As reported in the previous chapter in the case of methyl-isonicotinium butyl ester, the CH_3 (green square in Figure 9) is shifted more than 3 ppm up-field, the ortho (blue square) 1.3 ppm in the same direction and meta (black square) shift 0.7 ppm always in the same direction. These shifts are reported in Table 2. There are also the shift of the signals of the cavitand Tiiii[C_3H_7, CH_3, Ph], not highlighted because less obvious. The attribution of the signals highlighted in Figure 9 was defined based on the information obtained from the NOESY of the self-complementary head-to-tail homopolymer (see later).

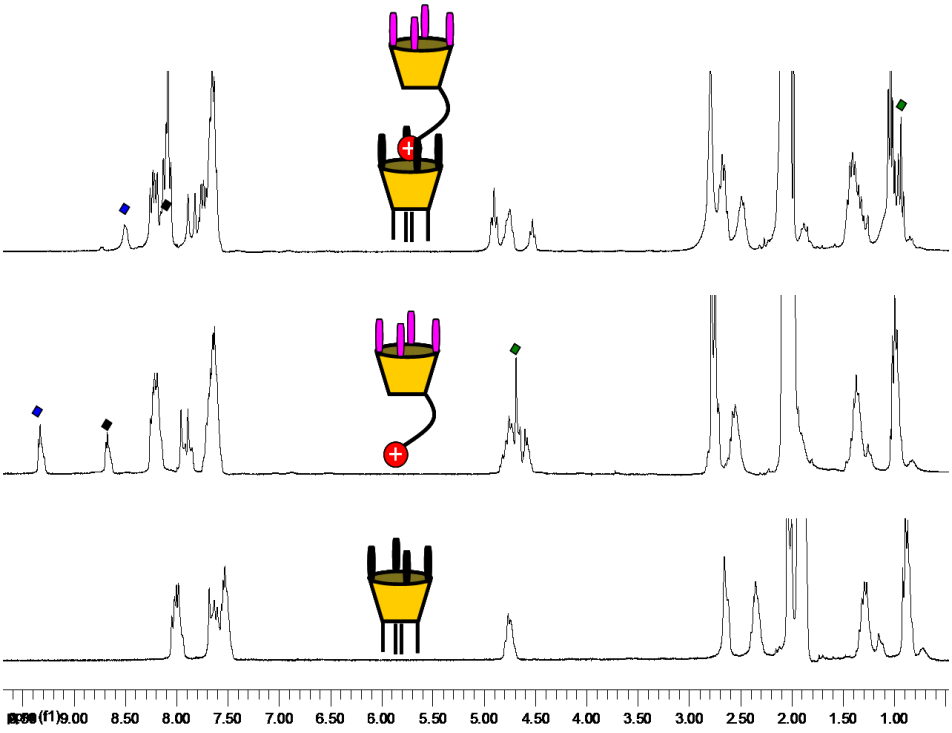

Figure 9. Host-guest self-assembly of the dimer complex monitored via ^{1}H NMR

groups	H_{oPy}	H_{mPy}	CH_3	ArH
Δδ (ppm)	1.3	0.7	3.6	- 0.35

Table 2. Shifts of the guest protons and of the aromatic protons of resorcinarene skeleton.

The SLS (static light scattering) studies, made on the one-to-one mixture of Tiiii[C_3H_7, CH_3, Ph] and TSiiii[($3C_3H_7$ + CH_3-Py^+ PF_6^-), CH_3, Ph], indicated the formation of the dimer complex, and the experimental molecular weight measured of 2730 ± 22 Da, close to the theoretical one of 2743 Da**.** The formation of host guest dimer complex was also observed in gas phase, by conducting a study at the ESI-MS (Figure 10). The mass spectrum, obtained by analysing a solution similar to that used for the SLS, displays a characteristic peak of free cavitand TSiiii[($3C_3H_7$ + CH_3-$Py^+PF_6^-$), CH_3, Ph] and a peak of host guest dimer **1** without counterion.

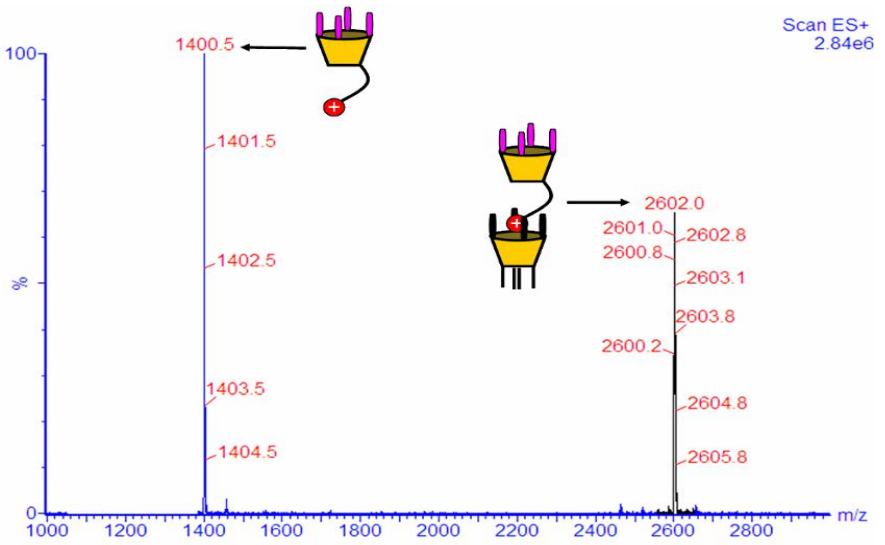

Figure 10. Host-guest self-assembly of dimer in gas phase montored via ESI-MS.

In collaboration with prof. Geremia of the University of Trieste, the crystal structure of host guest dimer complex **1** has been obtained by slow diffusion of water in a solution containing a mixture 1 to 1 of Tiiii[C_3H_7, CH_3, Ph] and TSiiii[($3C_3H_7$ + CH_3-Py^+ PF_6^-), CH_3, Ph] in acetonitrile. The crystal structure clearly shows the pyridinium tail of the cavitand TSiiii[($3C_3H_7$ + CH_3-Py^+ PF_6^-), CH_3, Ph] inside the cavity of the cavitand Tiiii[C_3H_7, CH_3, Ph] (Figure 11). Such inclusion is mainly stabilized by two interactions: the first one is the ion-dipole interactions between the oxygen of the P=O bonds and the positive charge of the nitrogen of methyl pyridinium moiety. The minimum distance N^+-O=P has been calculated to be 2.83±0.02 (green line Figure 11). The second interaction that stabilizes the complex is the CH-π interaction between the CH_3 hydrogens of the methyl pyridinium moiety and the π electrons of the aromatic ring of resorcinarene scaffold. The minimum distance between the CH_3 and the plane of the aromatic ring is 3.49±0.02. The crystal structure also displays one molecule of acetonitrile inside the cavity of the TSiiii[($3C_3H_7$ + CH_3-Py^+ PF_6^-), CH_3, Ph].

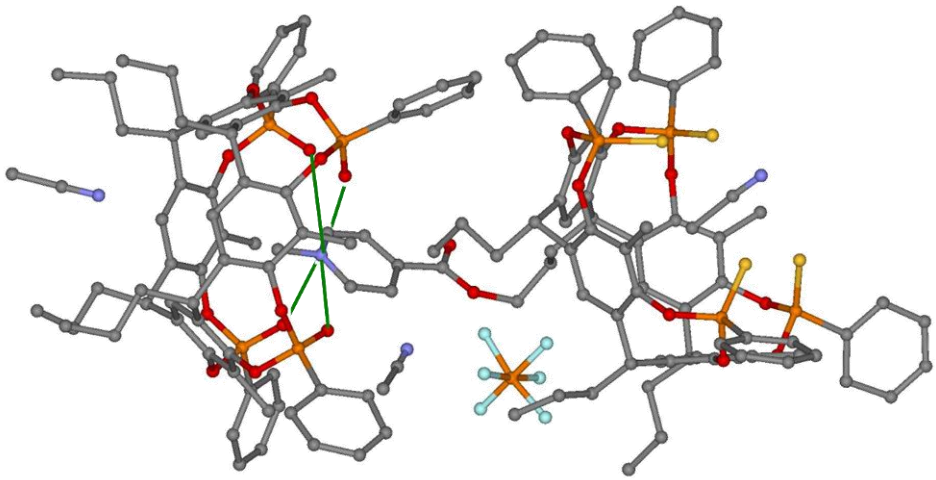

Figure 11. Crystal Structure of Host-guest dimer complex 1.

3.2.2 Homopolymer Based on host-guest self-complementarity.

3.2.2.1 Synthesis of the monomer.

In order to obtain homopolymer by host-guest self-complementarity, we designed a molecule containing both host and guest functionalities. [31] We chose Tiiii tetraphosphonate cavitands as host functionality, to exploit their high association constant recorded in both polar and apolar solvents by complexing ammonium and *N*-methyl pyridinium salts (see ITC in Chapter 2). Self-complementarity is obtained by linking covalently a methyl pyridinium moiety at the lower of a tetraphosphonate cavitand (Figure 12).

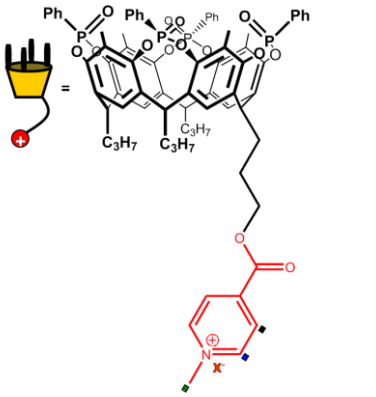

Figure 12. Monomer units for homopolymerization process.

In order to obtain these targets, we devised a six steps synthetic procedure:

Synthesis of mixed-footed resorcinarene. This class of resorcinarenes are obtained from acid-catalyzed condensation reaction of methyl resorcinol with a mixture 1:3 of 2,3-dihydrofuran and an aldehyde.[32] In

the specific case, a mixture 3:1 of butanal and 2,3-dihydrofuran was added to a solution of methyl resorcinol in methanol, and then a mixture 1:1 of a solution of HCl 12M in water and methanol was slowly added and heated at reflux (Scheme 1). Two sequential chromatographic separations on silica gel are necessary to isolate the pure mono-hydroxyl footed resorcinarene **2** in low yield 15%. Propyl-footed resorcinarene has also been separated in 13% yield.

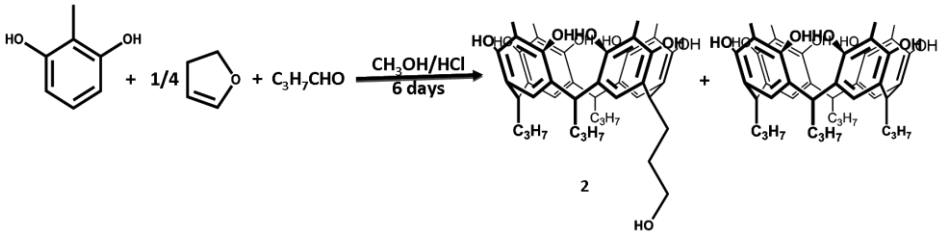

Scheme 1. Synthesis of mono-hydroxyl-footed resorcinarene.

Selective upper rim protection of the mono-hydroxyl footed resorcinarene 2. Since the eight phenolic hydroxyl groups at the upper rim can interfere with the functionalization of the hydroxyl group at the lower rim, the preliminary protection of the upper is necessary before lower rim functionalization.[33] We adopted the silyl-bridge protection because it is easy to introduce, stable enough to allow the lower rim functionalization and easy to remove. We chose a resorcinarene with four methyls in apical positions for three reasons: i) to deepen the cavity, ii) strengthen the CH-π interactions between the target molecules and the methyl pyridinium group, and especially iii) to obtain a silyl-bridged cavitand stable enough to support further reaction conditions until deprotection reaction. Since the hydroxyl phenol groups on resorcinarene decreases the yield of the purification on silica gel, we performed the silyl-bridged reaction on the crude reaction of the condensation. The reaction preceded well using dichlorodimethyl silane as bridging agent in dry pyridine (Scheme 2).

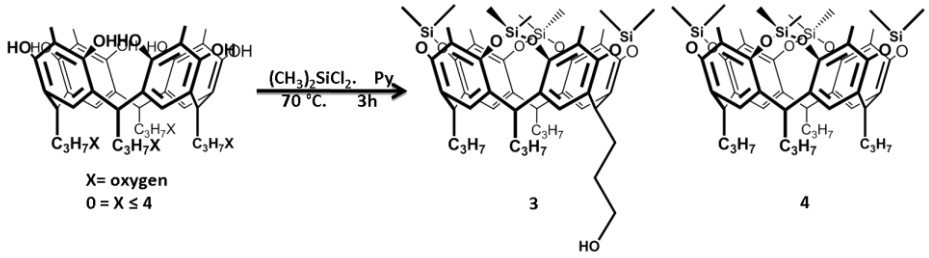

Scheme 2. Upper rim protection of resorcinarenes

Easy purification on silica gel chromatography leads to mono-hydroxyl footed silyl-bridged cavitand **3** with a total yield between the first and the second step of 29% while the propyl-footed silyl-bridged cavitand **4** is obtained with a total yield of 16%. The ^{1}H NMR spectrum of the product shows the presence of two new singlets, one at -0.7 ppm characteristic of Si-CH_3 that point inside the cavity and the other one at 0.4 ppm characteristic of Si-CH_3 that point outside of the cavity.

Lower rim functionalization. The isonicotinoyl moiety was introduced at lower rim by reacting, the mono-hydroxyl footed silyl-cavitand **3** with an excess of isonicotinoyl chloride hydrochloride in pyridine, affording the product as yellowish powder in 90% yield, after crystallization from a mixture 2:1 of water and acetonitrile (Scheme 3).

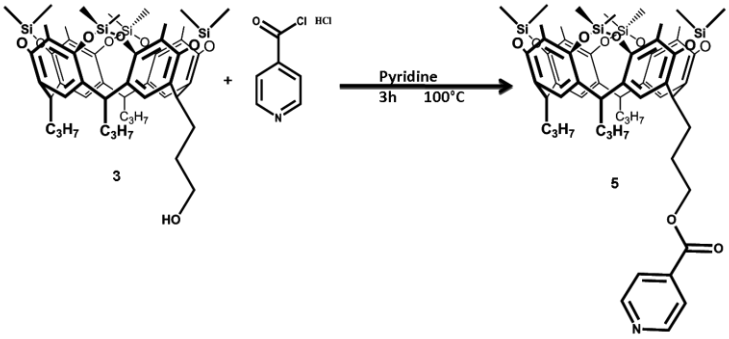

Scheme 3. Lower rim functionalization of mono-hydroxyl-footed silyl-cavitand 3.

Upper rim deprotection. The upper rim deprotection is a very easy reaction that occurs using a solution of HF as deprotection agent in DMF (Scheme 4). The crude product is purified by simply crystallization from a mixture 1:1 of acetonitrile and water, affording the mono-pyridyl footed resorcinarene **6** in 81% yield.

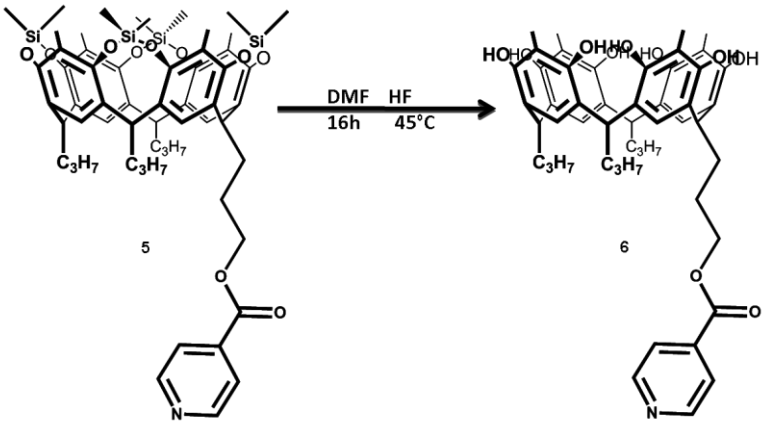

Scheme 4. Upper rim deprotection of mono-pyridyl footed silyl-cavitand 6.

Upper rim functionalization. We used the new procedure described in Chapter 2 to bridge the upper rim of mono-pyridyl footed resorcinarene with phosphonate moieties. In the reaction with the mono-pyridyl-footed resorcinarene **6**, the phosphoryl groups were attached to the resorcinarene skeleton to produce phosphonate-cavitand Tiiii [($3C_3H_7$ + py), CH_3, Ph] by using a two step synthesis (Scheme 5).[34] The phosphonito-cavitand P(III) Tiiii [($3C_3H_7$ + py), CH_3, Ph], which was obtained by reacting mono-pyridyl-footed resorcinarene with 4.1 equivalents of dichlorophenylphosphine (Scheme 5a), gave the phosphonate-cavitand Tiiii [($3C_3H_7$ + py), CH_3, Ph] after in situ treatment with an excess of a solution 35% of H_2O_2 in water (Scheme 5b). Purification by re-crystallization from a mixture 1:2 of water and acetonitrile affords cavitand Tiiii [($3C_3H_7$ + py), CH_3, Ph] as white powder in 95% yield.

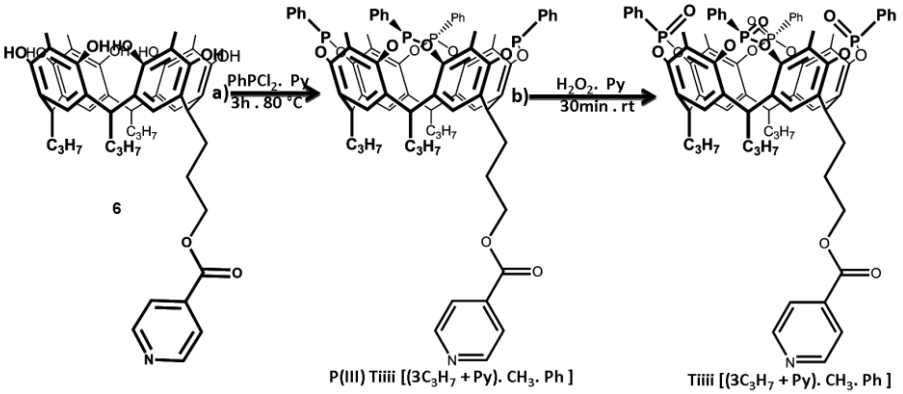

Scheme 5. Two step synthesis of phosphonate-cavitand Tiiii [(3C_3H_7 + py), CH_3, Ph].

Methylation of the pyridine moiety. The last step of this multi-stage synthesis was the methylation of the pyridine moiety to methyl pyridinium salt. We used two methylating agents leading to methyl pyridinium moieties with different counterions. The presence of different counterions was necessary to study their effect on the homopolymerization processes.

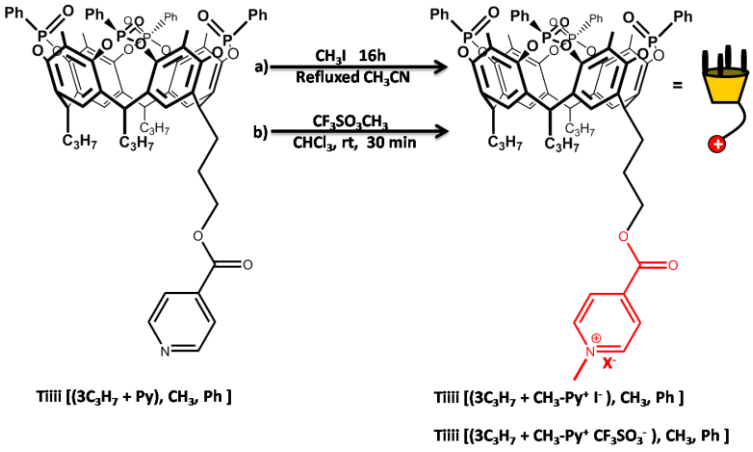

Scheme 6. Methylation reactions of Tiiii [(3C_3H_7 + py), CH_3, Ph].

The first methylating agent utilized was an excess of methyl iodide and the reaction occurred in refluxing acetonitrile. Purification by crystallization from a mixture 1:1 of acetonitrile and water afforded quantitatively the Tiiii [($3C_3H_7$ + CH_3-py^+ I^-), CH_3, Ph] (Scheme 6a). In the second case, $CF_3SO_3CH_3$ was used as methylating agent in chloroform at room temperature. The reaction afforded quantitatively after 30 minutes the product Tiiii [($3C_3H_7$ + CH_3-py^+ $CF_3SO_3^-$), CH_3, Ph] (Scheme 6b).

In all cases the homopolymer is the real product of the methylation reaction since the monomer immediately polymerizes both in solution and in the solid state (see later). Characterization of the polymer was obtained via ^{1}H NMR, ^{31}P NMR, NOESY, HOESY, Static Light Scattering, PGSE, viscosimetry, AFM and crystal structure.

3.2.2.2 Characterization via NMR

The NMR technique is a powerful tool for polymer characterization. In the specific case of supramolecular polymers, two are the most relevant techniques: i) NOESY, HOESY NMR spectroscopy for the spatial investigation of the host-guest complexation made in solution; ii) PGSE (Pulsed Gradient Spin Echo) for the diffusion studies leading to size and shape definition of the polymer in solution.

Figure 13 reports the ^{1}H NMR spectra of the homopolymer Tiiii [($3C_3H_7$ + CH_3-py^+ $CF_3SO_3^-$), CH_3, Ph] compared to that of thiophosphonate cavitand called stopper TSiiii [($3C_3H_7$ + CH_3-py^+ PF_6^-), CH_3, Ph].

The up-field shift of the pyridinium protons due to the shielding effect of the cavities in the homopolymer Tiiii [($3C_3H_7$ + CH_3-py^+ $CF_3SO_3^-$), CH_3, Ph] in acetonitrile demonstrates that this group interacts with the cavity. In the case of TSiiii [($3C_3H_7$ + CH_3-py^+ PF_6^-), CH_3, Ph] which cavity is

small and cannot complex methyl pyridinium guests (see crystal structure in Chapter 2), the methyl group resonates at 4.87 ppm.

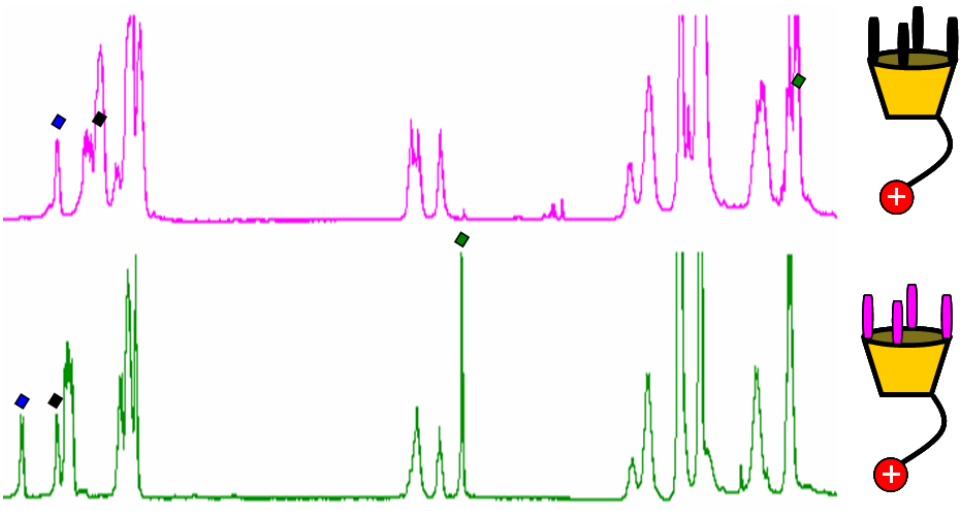

Figure 13. ^{1}H NMR spectra comparison between the homopolymer Tiiii [($3C_3H_7$ + CH_3-py^+ $CF_3SO_3^-$), CH_3, Ph] and the cavitand TSiiii [($3C_3H_7$ + CH_3-py^+ PF_6^-), CH_3, Ph] in CD_3CN.

The inclusion of the methyl pyridinium tail inside the cavity has been proved by performing the NOESY analysis in chloroform (Figure 14). The spectrum highlights the correlation between the ortho pyridinic protons of the tail of a cavitand, and the CH_3 in apical position of the resorcinarene scaffold of the head of the following cavitand. Further evidence of the inclusion comes from the correlation between the CH_3 pyridinic signal of the tail of a cavitand, and the aromatic protons of the resorcinarene scaffold of the following cavitand, in the head-to-tail mode (red arrows).

In order to study the position of the triflate counterion in the homopolymer Tiiii [($3C_3H_7$ + CH_3-py^+ $CF_3SO_3^-$), CH_3, Ph], we carried out the HOESY analysis in chloroform. The spectrum in Figure 15 highlights the strong interactions between the signals of the fluorine of

the counterion and those of the alkyl chains and the aromatic protons of the resorcinarene scaffold (red arrows).

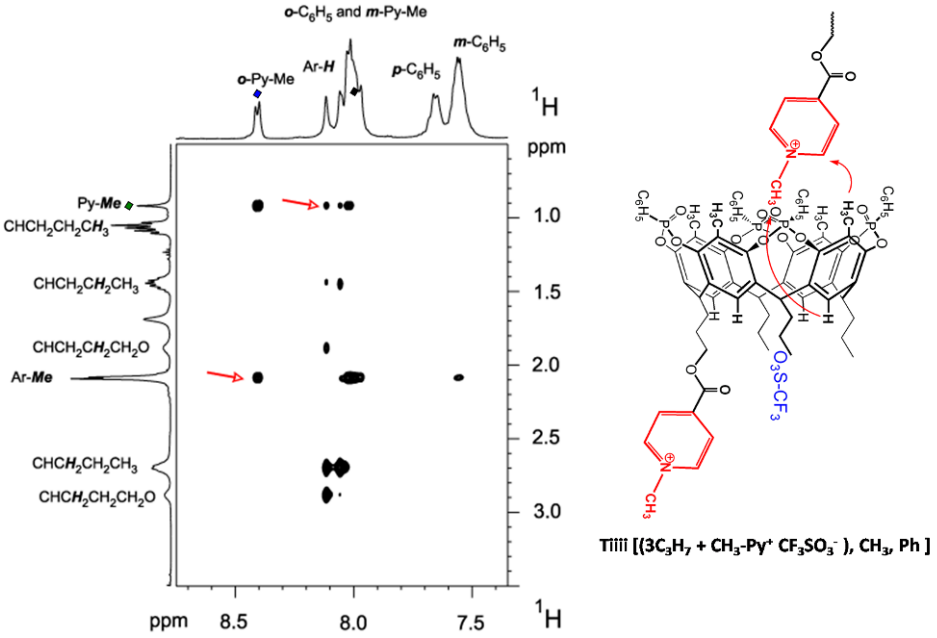

Figure 14. Spatial correlation between the methyl-pyridinium tail of a cavitand and the following cavity of other cavitand in the homopolymer [($3C_3H_7$ + CH_3-py^+ $CF_3SO_3^-$), CH_3, Ph] via NOESY in $CDCl_3$

This fact demonstrates the fitting of the triflate counterion among the lower rim chains. The triflate counterion and the CH_3 of the methyl pyridinium moiety pointing toward the center of the cavity interact weakly, demonstrating the deep inclusion of the pyridinium moiety inside the cavity. This fact also demonstrates that, the inclusion does not prevent the formation of the ion pair in chloroform between the pyridinium moiety and its counterion.

The formation of the head-to-tail homopolymer and the fitting of the triflate counterion among the lower rim chain by dissolving Tiiii [($3C_3H_7$

+ CH_3-py$^+$ $CF_3SO_3^-$), CH_3, Ph] in solution was also observed in the solid state (see crystal structure later).

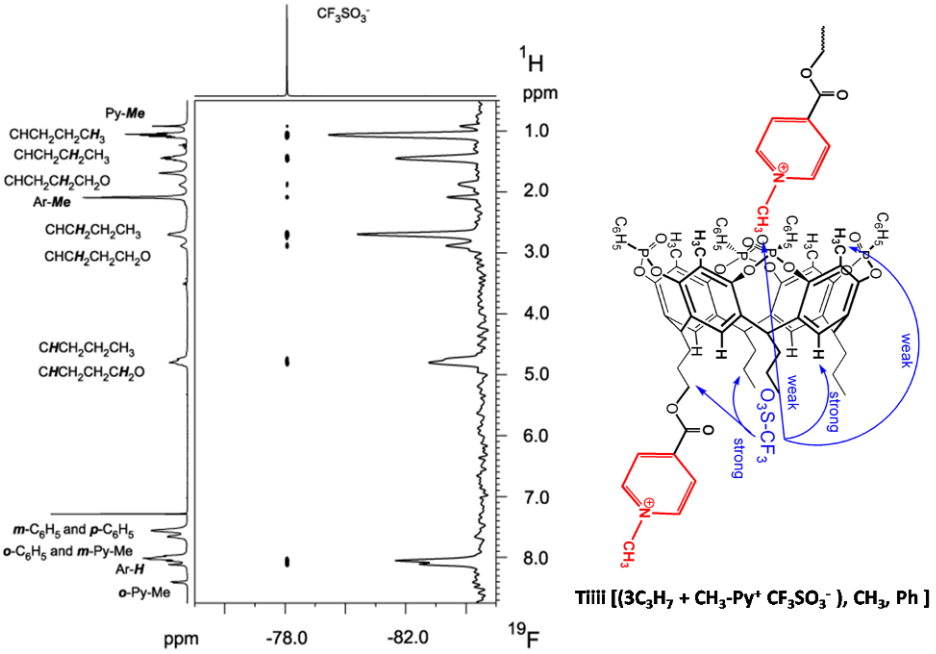

Figure 15. HOESY highlights the fitting of the triflate counterion among the lower rim chains and thus the formation of complexed ion pair in $CDCl_3$.

3.2.2.3 Static Light Scattering

The Static Light Scattering (SLS) measurements have been made in collaboration with the Group of Prof. Mendichi of the CNR of Milano.

SLS is a technique that uses the time-average scattered intensity at different scattering angles to derive information about the gyration radius (Rg), weight-average molecular weight (Mw) of polymers and aggregates, and the second virial coefficient (A_2);[35] it can also derive information about a contour length of the polymeric structure.[36] With this technique the applicable molecular weight measurement range, is from

few hundred g.mol^{-1} to 500,000 g.mol^{-1} for linear polymers, and over 20,000,000 g.mol^{-1} for near spherical polymers and proteins. The intensity of scattered light, produced by macromolecules, is proportional to the product of the weight-average, and the concentration of the macromolecules. Moreover, since the molecular weight of supramolecular architectures grows by concentrating the solution, this technique can be used in the field of supramolecular polymers only at low concentrations due to the achievement of the instrumental limit. So the use of SLS technique has been limited for the characterization of supramolecular polymers.[37] We performed SLS measurements in chloroform in concentration in the range 1.05 g.L^{-1} (0.71 mM) - 15 g.L^{-1} (10.2 mM) (Figure 16). We stopped the measurement at 15 g.L^{-1} because, beyond this concentration, the instrumental limit is reached.

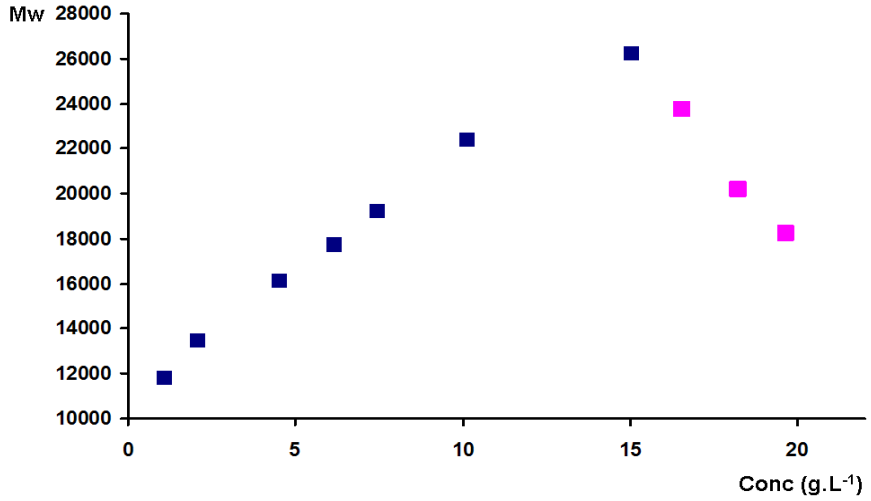

Figure 16. SLS measurements: the blue square shows the increase molecular weight by concentrating the solution of homopolymer Tiiii [($3C_3H_7$ + CH_3-py^+ I^-), CH_3, Ph] in chloroform, and the magenta triangle shows the molecular weight decrease by adding the chain stopper TSiiii [($3C_3H_7$ + CH_3-py^+ I^-), CH_3, Ph] in chloroform.

The SLS measurements show that the hopolymer Tiiii [($3C_3H_7$ + CH_3-py^+ I^-), CH_3, Ph] has the typical behaviour of the supramolecular polymers which degree of polymerization (dp) is concentration dependent[38] (blue square Figure 16). At 15 $g.L^{-1}$ concentration, the homopolymer Tiiii [($3C_3H_7$ + CH_3-py^+ I^-), CH_3, Ph] reaches 26270 Da corresponding to an average dp =18 (Table 3).

Tiiii [($3C_3H_7$ + CH_3-Py^+ I^-). CH_3. Ph] dn/dc = 1.52		
gL^{-1}	M_W	dp
1.045	11850	8.1
2.05	13490	9.2
4.487	16140	11
6.129	17740	12.1
7.408	19280	13.2
10.110	22410	15.3
14.990	26270	17.9

Table 3. Static Light Scattering Data of the homopolymer Tiiii [($3C_3H_7$ + CH_3-py^+ I^-), CH_3, Ph].

In the literature, models relating the degree of polymerization to the concentration and especially to the strength of interactions between the monomer units for supramolecular polymers are reported.[39] The EK model describes supramolecular polymers with isodesmic behaviour in the multi-stage association (K_1 = K_2 = ...= K_i). This model relates the degrees of polymerization to the concentration and to the association constant following the Equation 1.[40]

$$dp \approx \alpha\sqrt{KC} \quad (1)$$

Where α is a parameter comprised between 1 and 2, K is the association constant, and C is the concentration of the monomer.

The AK model describes supramolecular polymers in which the association of the following monomer to the polymer chain occurs with attenuation of the association constant, compared to the previous one $K_{i+1} < K_i$; the equations that simulate the model are complex.[41]

The homopolymer Tiiii [($3C_3H_7$ + CH_3-py^+ I^-), CH_3, Ph] does not follow the isodesmic EK model likely because, by increasing the concentration, the ionic strength of the solution increases due to the increase of dissolved salts. Consequently the association constant of the successive addition of the monomer to the homopolymer chain decreases. Then we concluded that, this system grows following an AK model.

Many research groups reported the devastating effects on the solution and material properties of the presence of small amount of mono-functional monomer (called chain stopper because prevents the further growth of the polymer chain) as impurity linked at the supramolecular polymers.[15,42] Many other research groups, added deliberately, a controlled amount of chain stopper in order to control the average-length of the chains and then the properties of the supramolecular systems.[43] Since the mono-pyridyl-footed thiophosphonate-cavitand TSiiii [($3C_3H_7$ + CH_3-py^+ I^-), CH_3, Ph] cannot self-assembly via host-guest interactions, we used it to study the effect of the addition of chain stopper on static and dynamic properties of a solution of homopolymer. To this purpose to a solution of homopolymer Tiiii [($3C_3H_7$ + CH_3-py^+ I^-), CH_3, Ph] 15 $g.L^{-1}$, increase amount of stopper TSiiii [($3C_3H_7$ + CH_3-py^+ I^-), CH_3, Ph] (10%, 20%, and 30% mol/mol) was added. By increasing the stopper concentration, the molecular weight undergoes a linear decrease (magenta triangle Figure 16). This because mono-functional stopper, decreases the average-chain length by forming non-functional chain ends. The use of chain stopper is the only way to get variation of the properties

of the system (such as chain length) independently of other parameters such as the overall concentration, and temperature, that is otherwise impossible in supramolecular polymers.[38c] Table 4 shows the data obtained by adding the chain stopper to the solution of homopolymer. It is important to notice that homopolymers Tiiii [($3C_3H_7$ + CH_3-py^+ X^-), CH_3, Ph] have two independent stopper sites that can be used for the independent growth of polymeric chains in one direction or another (Figure 17).

Static Light scattering of disassembled polymer				
H (gL^{-1})	**S (gL^{-1})**	**H+S (gL^{-1})**	**M_W (Da)**	**dn/dc**
15.055	**1.613**	**16.667**	**23720 ± 90**	**0.1507**
15.055	**3.291**	**18.344**	**20160 ± 70**	**0.1496**
15.055	**4.7310**	**19.7860**	**18230 ± 50**	**0.1489**
H = Tiiii [($3C_3H_7$ + CH_3-Py^+ I^-). CH_3. Ph] S = TSiiii [($3C_3H_7$ + CH_3-Py^+ I^-). CH_3. Ph]				

Table 4. Mw reduction of the homopolymer by addition of chain stopper.

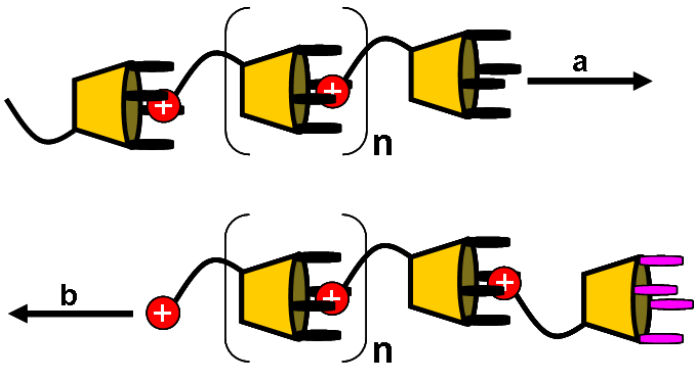

Figure 17. a) Addition of Tiiii cavitand without lower rim functionalization as chain stopper ; b) addition of cavitands TSiiii [($3C_3H_7$ + CH_3-py^+ X^-), CH_3, Ph] as chain stopper.

In order to obtain high molecular weights without reaching the instrumental limit at the SLS, small amount of tetratopic guest able to complex tetraphosphonate-cavitand such as tetrakis(N-methylpyridinium)porphyrin[44] is added to the less concentrated solutions of homopolymers Tiiii [($3C_3H_7$ + CH_3-py+ X-), CH_3, Ph]. This technique has been utilized to increase the Mw of polymers by imposing covalent star shapes[45] and supramolecular star shapes.[46] Following this purpose, solutions of the homopolymer Tiiii [($3C_3H_7$ + CH_3-py+ I-), CH_3, Ph] in chloroform were prepared and the 5,10,15,20-tetrakis(1-methyl-4-pyridinio) porphyrin tetra(p-toluenesulfonate) was added as template leading to a substantial increase in Mw. The porphyrin acts as nucleation unit for the formation of a star polymer via its four meso pyridinium groups (Figure 18). Additions of 2.5% molar[47] of this porphyrin to solutions of the homopolymer Tiiii [($3C_3H_7$ + CH_3-py+ I-), CH_3, Ph] at different concentrations: 1.05 $g.L^{-1}$, 2.05 $g.L^{-1}$, and 4.1 $g.L^{-1}$ induced a three/fourfold increase of Mw (Table 5). Only in the lower concentration regime (1.04 g/L) the stoichiometric Mw/Mw_0 ratio was reached. Interestingly, it is the only case in which the porphyrin was fully solubilized in the homopolymer solution; since it is driven into chloroform by complexation (it is insoluble in pure chloroform).[48] This trend can be rationalized assuming that at higher concentrations of homopolymer Tiiii [($3C_3H_7$ + CH_3-py+ I-), CH_3, Ph] the ionic strength increases the polarity of the medium, thereby opposing the complexation driven solubilization.

Star shaped polymer					
H (gL^{-1})	P (gL^{-1})	(H + P) (gL^{-1})	M_{w0} (Da)	M_w (Da)	$R = M_w/M_{w0}$
1.045	0.01216	1.05716	11850	46210 ± 580	3.9
2.049	0.02384	2.07283	13490	41600 ± 180	3.1
4.09488	0.04764	4.14252	15940	49700 ± 180	3.1
H = Tiiii [($3C_3H_7$ + CH_3-Py^+ I^-). CH_3. Ph]; P = 5,10,15,20-tetrakis(1-methyl-4-pyridinio) porphyrin tetra(p-toluenesulfonate)					

Table 5. Static Light Scattering data of the star shaped homopolymer.

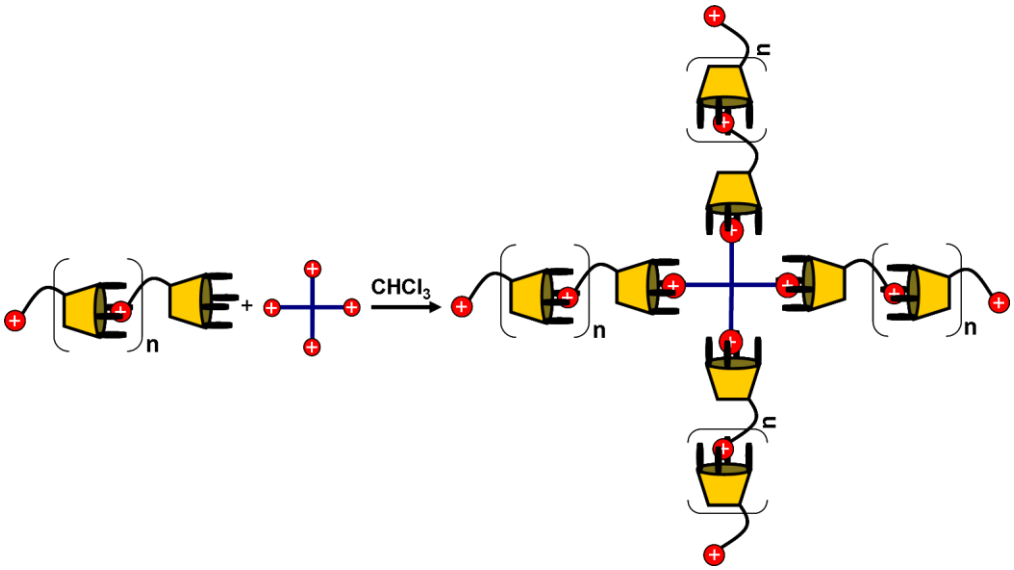

Figure 18. Star shaped supramolecular polymer.

3.2.2.4 Pulsed-Field-Gradient- Spin- Echo NMR Spectroscopy.

In collaboration with Prof. Alceo Macchioni and Dr. Daniele Zuccaccia of the University of Perugia, the self-diffusion studies and the application of different models to define the size and the shape of the homopolymers

in solution via NMR by using the PGSE NMR spectroscopy has been performed.

A valuable methodology to study the aggregation of molecular species in solution is based on the determination of molecular self-diffusion coefficients by PGSE (Pulsed-Field-Gradient-spin-Echo) [49] Spectroscopy. The measured parameter by this technique is the D_t (self-diffusion coefficient) that completely characterizes the spatial Gaussian distribution of the moving particles after the investigated time t. D_t can be measured by a number of pulse sequences[50] based on standard stimulated Spin-Echo. By applying that sequence, and combining it with different equations reported in literature,[51] it comes out that the dependence of the resonance intensity (I) on a constant waiting time and on a varied gradient strength (G) is described by the equation (2).

$$\ln\left(\frac{I}{I_0}\right) = -(\gamma\delta)^2 D_t\left[\Delta - \frac{\delta}{3}\right]G^2 \quad (2)$$

Where I, is the intensity of the observed Spin-Echo, I_0 is the intensity of the Spin-Echo without gradient, D_t is the diffusion coefficient, Δ is the delay between the midpoint of the gradient, δ is the length of the gradient pulse and γ is the magnetogyric ratio. D_t is directly proportional to the slope of the line obtained by plotting $\ln(I/I_0)$ vs G^2.

PGSE is very versatile and describes well different shape and size systems, therefore it has been widely used in supramolecular chemistry to measure the diffusion coefficient and consequently the volume (the size) of the supramolecular polymers.[52]

Assuming that homopolymer Tiiii [($3C_3H_7$ + CH_3-py^+ I^-), CH_3, Ph] forms rod-like objects in solution, we used the prolated model[53] to calculate the volume and the degree of polymerization. Applying this model, the size of the cavitand TSiiii [($3C_3H_7$ + CH_3-py^+ I^-), CH_3, Ph] corresponding to

dp = 0.99 and that of dimer complex **1** corresponding to dp = 1.96 have been measured and used as monomer and dimer units reference.
Since the association of the monomer units is weak in polar solvents, we made the measurements only in apolar solvents. We started comparing the SLS data with the PGSE ones obtained in chloroform. The results are plotted in Figure 19.

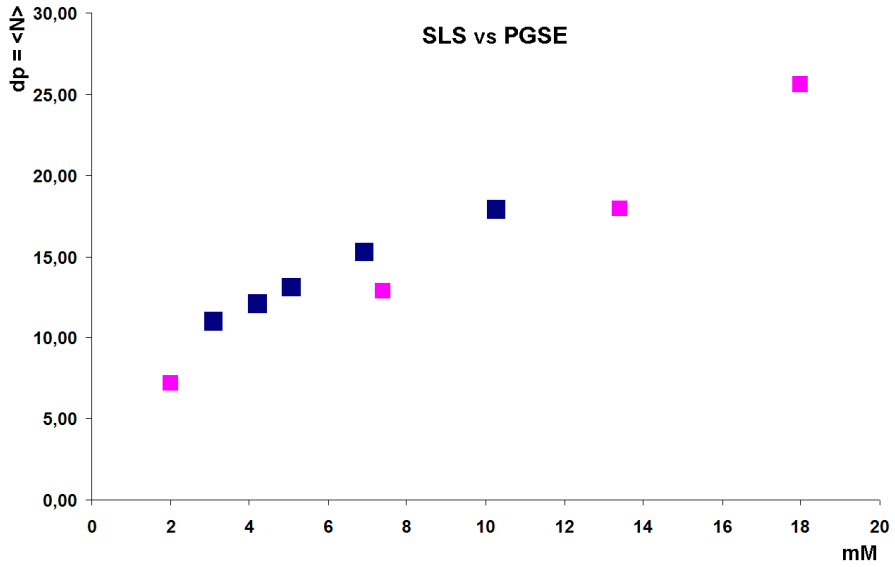

Figure 19. SLS vs PGSE; blue squares represent the data obtained from the SLS, magenta square represent the PGSE ones.

The dp via SLS are obtained by dividing the experimental molecular weight with that of the single monomeric unit (1465 Da). Figure 19 shows that the PGSE data using the prolated model are slightly underestimated. In fact, the dp obtained via PGSE are calculated dividing the volume of the measured prolated polymer by the PGSE volume of the stopper assumed as monomer. In doing so, PGSE never considers the volume of the solvent lost by complexing the methyl pyridinium moiety inside the cavity by growing the polymer (Figure 20).

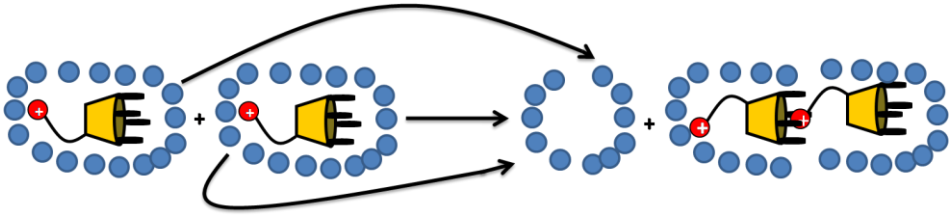

Figure 20. Desolvation volume lost by growing the polymer chain.

Such volume becomes unimportant when the homopolymer assumes large dimensions. In fact by concentrating the polymeric solution (2 to 10 mM) the difference between the two data decreases (29 to 5 %). In order to measure the effect of the counterion on the polymerization process using the prolated model, we compared the PGSE data of the homopolymer Tiiii [($3C_3H_7$ + CH_3-py^+ I^-), CH_3, Ph] with those of homopolymer Tiiii [($3C_3H_7$ + CH_3-py^+ $CF_3SO_3^-$), CH_3, Ph]. The results obtained are plotted in Figure 21.

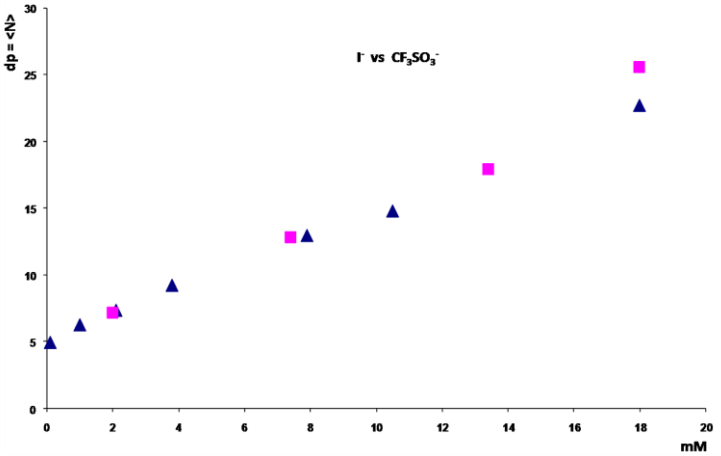

Figure 21. Degree of polymerization versus concentration via PGSE spectroscopy in $CDCl_3$ of Tiiii [($3C_3H_7$ + CH_3-py^+ I^-), CH_3, Ph] (magenta square) and Tiiii [($3C_3H_7$ + CH_3-py^+ $CF_3SO_3^-$), CH_3, Ph] (blue triangle).

The solution of the homopolymer Tiiii [($3C_3H_7$ + CH_3-py^+ I^-), CH_3, Ph] grows slightly faster that of the Tiiii [($3C_3H_7$ + CH_3-py^+ $CF_3SO_3^-$), CH_3, Ph], since the ion pair between the iodide and the complexed methyl pyridinium is more associated than that formed with the triflate as counterion.

Since the purpose was to determine the Mw of the homopolymer at high concentrations not accessible via SLS, the measurements were carried out until 88 mM using solutions of the homopolymer Tiiii [($3C_3H_7$ + CH_3-py^+ I^-), CH_3, Ph] in chloroform. The degree of polymerization continuous to grow linearly, with the concentration (Figure 22). At 88 mM concentration of the homopolymer, the solubility is still good and the degrees of polymerization reached dp = 114 units corresponds to a molecular weight higher than 160,000 (Table 6). It is important to notice that the prolated model is very conservative, underestimating the real Mw.

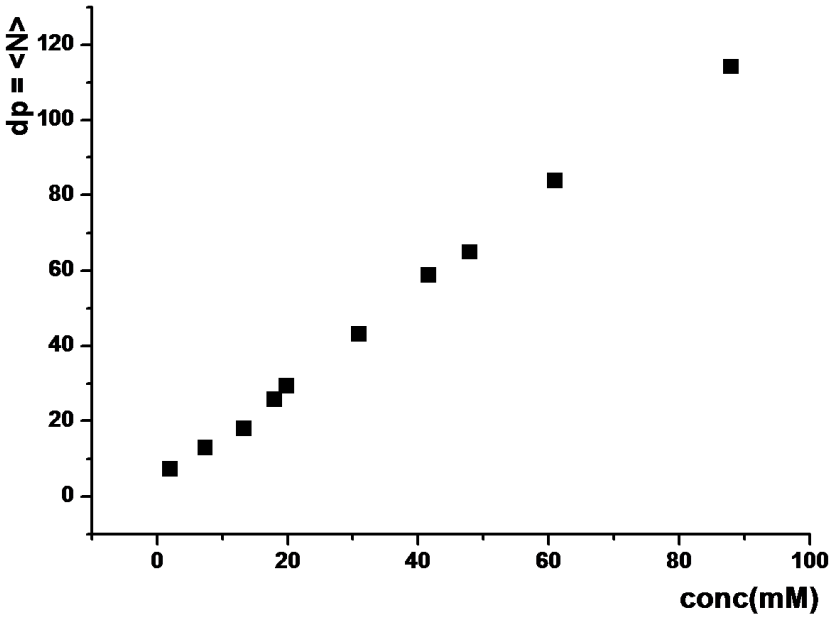

Figure 22. dp vs concentration via PGSE spectroscopy.

Conc (mM)	dp	MW
2	7.2	10519
7.4	13.0	18825
13.4	18.0	26297
18	26.0	37504
20.0	29.0	42954
31	43.1	63127
41.7	59.0	86010
48	65.0	95035
61	84.0	122591
88	114.1	167098

Table 6. PGSE data obtained considering the prolated model, MW is calculated by multiplication of the dp with the molecular weight of the monomer unit.

Plotting dp(dp-1), derived from PGSE NMR measurements, versus concentration in mol/L, linear trends fitted with Equation 1 could be obtained, and the association constant of the homopolymerization process could be the slope of the line obtained from linear regression.[54] The fitting of the PGSE NMR data of the homopolymer Tiiii [($3C_3H_7$ + CH_3-py^+ I^-), CH_3, Ph] displays two trends (Figure 23), indicating two different association modes.

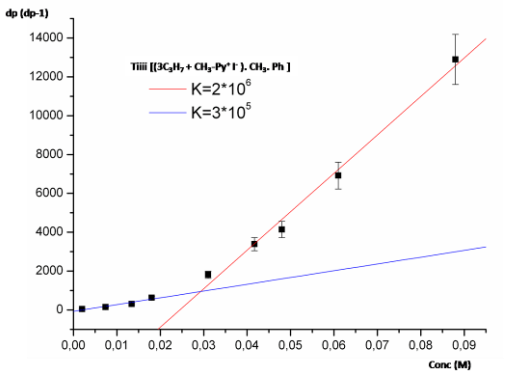

Figure 23. PGSE derived dual association mode of the monomer Tiiii [($3C_3H_7$ + CH_3-py^+ I^-), CH_3, Ph]

Observing this strange behaviour, we paid attention to the large deviation from the linearity of the plot $\ln(I/I_0)$ vs G^2 (Figure 24a) that suggests the presence in solution of more than one distribution species.[55] So, we carried out, other PGSE NMR experiments with a large number of points and applied the exponential-fitting[55] that take into account the multi-distribution of the species in solution (Figure 24b).

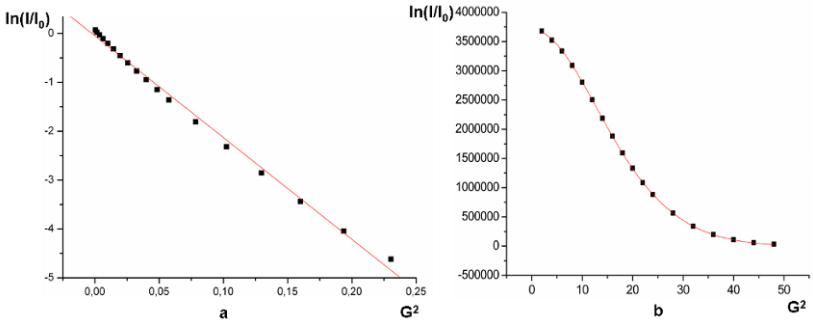

Figure 24. $\ln(I/I_0)$ vs G^2 a) linear fitting that consider a single distribution, b) exponential-fitting that take into account the multi-distribution of the species in solution.

With the exponential-fitting the presence of two distributions of the species that exchange slowly at the NMR time scale was revealed in solution at each concentration investigated. We assumed that, the distribution of the species with largest diffusion coefficient correspond to the polymer that grows linearly by complexing the monomer units or small oligomers in solution (Figure 25a), while the smallest one, is formed by four linear polymeric or oligomeric chains held together by quadruplar interactions between the positive charged chains and the negative charged of the counterions (Figure 25b). Table 7 reported the diffusion coefficients of the each distribution at the investigated concentrations of homopolymer Tiiii [($3C_3H_7$ + CH_3-py$^+$ I$^-$), CH_3, Ph] and those of the reference monomer unit TSiiii [($3C_3H_7$ + CH_3-py$^+$ I$^-$), CH_3, Ph] and of dimer complex **1**.

Conc (mM) / D_t(m^2s^{-1})	1.5mM	3mM	5.5mM	10.5mM	13.4mM	22.3mM	41mM	64.7mM
D_{t1}(*10^{-10})	2.3[a]	-	2.00[a]	1,6[a]	1.40[a]	1.34[a]	0.85[a]	0.61[a]
D_{t1}(*10^{-10})	0.96[c]	-	0.95[b]	0.68[b]	0.65[b]	0.50[b]	0.34[b]	0.26[b]
D_{tm}(*10^{-10})	-	4.8 [c]	-	-	-	-	-	-
D_{td}(*10^{-10})	-	3.8 [d]	-	-	-	-	-	-

Table 7. [a] Diffusion coefficients of the faster diffusing species in solution, [b] diffusion coefficients of the slower diffusing species, [c] diffusion coefficient of the single species in solution of the stopper, and [d] diffusion coefficient of the single species in the solution of dimer complex 1 in $CDCl_3$.

As reported in the Table 7, the diffusion coefficient of the two distributions decreases by increasing the concentration of the solution. It can be also observed that the two distributions in solution of Tiiii [($3C_3H_7$ + CH_3-py^+ I⁻), CH_3, Ph], diffuse very slowly compared to those of the two references.

In order to calculate the average degree of polymerisation in the two distributions, we assumed that the two systems in solution form cylindrical rod-like objects[56] and the base of the smallest distribution corresponds to the width of the monomer unit reference, while the base of the largest one is four time that of the smaller one.

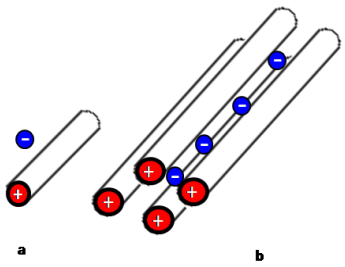

Figure 25. a) Smallest distribution formed by subsequent complexation of monomer units; b) largest distribution formed by quadrupolar interaction between four polymeric chains and the counterion

Taking into account these assumptions, we plotted in Figure 26, the degree of polymerization versus concentration of the two distributions. The two distributions grow linearly by increasing the concentration but, the smallest grows very slowly due to the progressive increase of the polarity of the solution that progressively weakens the association constant of the complexation of the monomeric units to the polymer chain. While the growth of the largest one is faster because promoted by the multiplicity of the quadrupolar interactions that stabilize the final structure. The largest distribution reach dp = 260 corresponding to almost 400000 of molecular weight (Table 8).

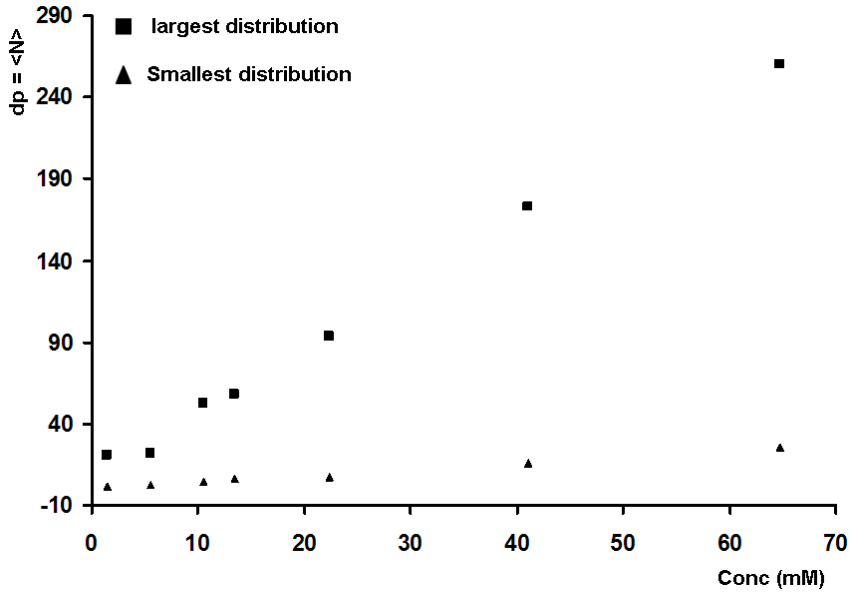

Figure 26. dp in $CDCl_3$ of the solution of Tiiii [($3C_3H_7$ + CH_3-py^+ I^-), CH_3, Ph] versus concentration, assuming the cylindrical shape of the two distributions.

This complex behaviour can be rationalized considering the different trend of the two association modes. The small object is formed by a sequence of host-guest association constants which progressively

decrease in strength with concentration. The large object is held together by quadrupolar interactions which increase in number with polymer elongation. At a certain level of growth of the smaller object (linear chain), the sum of possible lateral quadrupolar interactions overrides energetically the single K_{ass} of host-guest interaction. At this point, the system prefers lateral aggregation to linear growth.

conc (mM)	Dt_S (m^2s^{-1})	$<N>_S$	MW_S (Da)	Dt_L (m^2s^{-1})	$<N>_L$	MW_L (Da)
1,5	2,29E-10	1,38	2022	9,67E-11	20,67	30282
5,5	1,97E-10	2,27	3326	9,55E-11	21,47	31454
10,5	1,61E-10	4,49	6578	6,80E-11	52,73	77250
13,4	1,41E-10	6,08	8907	6,48E-11	58,33	85454
22,3	1,34E-10	6,80	9962	5,029E-11	93,33	136729
41,0	8,52E-11	15,40	22561	3,42E-11	173,33	253929
64,7	6,08E-11	25,90	37944	2,59E-11	260,13	381091
S = smallest distribution L = largest distribution						

Table 8. Diffusion coefficients, degrees of polymerization, and molecular weight of the each distribution at investigated concentration.

In order to verify the presence of the quadrupolar interactions between the polymer chains of the largest distribution, a polar solvent has been added to the starting solutions of homopolymer Tiiii [($3C_3H_7$ + CH_3-py^+ I^-), CH_3, Ph] and PGSE NMR has been performed. This experiment was made on solutions of the homopolymer at three different concentrations 5, 13 and 22 mM in $CDCl_3$ which show bi-distribution of species. By adding 8% of CD_3OD to each solution, the largest distribution disappears in all three cases. The CD_3OD increases the polarity of the solutions as well as shields the charges by solvating them. In this way, interactions between positive charges of the homopolymer chains and negative charges of the counterions are minimized. Figure 27 reported the $\ln(I/I_0)$

versus G^2 after and before addition of CD_3OD in the case of the solution 13 mM concentration.

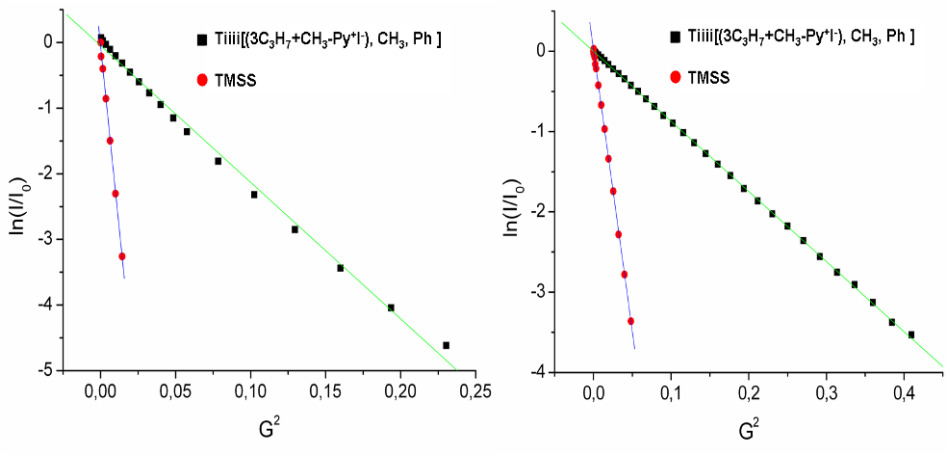

Figure 27. ln(I/I$_0$) Vs G^2 after and before addition of CD_3OD to polymer solution at 13 mM.

3.2.2.5 Viscosimetry studies

Viscosimetry studies made on the solution of Tiiii [($3C_3H_7$ + CH_3-py^+ I^-), CH_3, Ph] in methylene chloride, shows the growth of the specific viscosity of the solution by increasing the concentration (Figure 28a), thus confirming SLS and PGSE experiments. The maximum slope of the regression line corresponding to the blue square (Figure 28a) is very small (0.06). The system forms rod-like without entanglement; the absence of the entanglement is also confirmed by the perfect linearity (R^2 = 0.99) of the plot Log(specific viscosimetry) versus Log(concentration) (Figure 27b)[57].

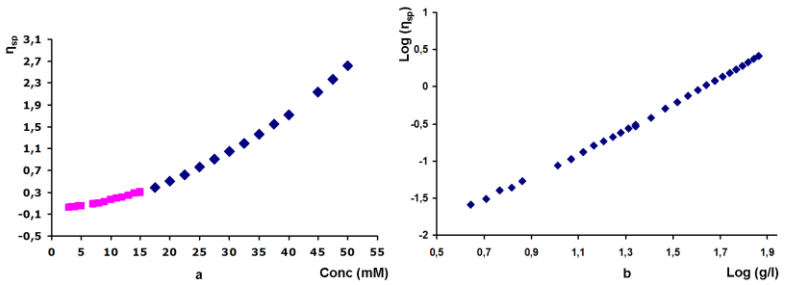

Figure 28. Viscosimetry measurements of the Tiiii [($3C_3H_7$ + CH_3-py^+ I^-), CH_3, Ph] solutions in CH_2Cl_2 a) specific viscosity versus concentration b) Log(specific viscosity) versus Log(concentration).

In parallel to characterization of the homopolymers in solution, attention was given to the behaviour in solid state. Some assumptions and conclusions made by studying the homopolymers in solution were verified and confirmed by the studies in the solid state.

3.2.2.6 Crystal structure of the homopolymer Tiiii [($3C_3H_7$ + CH_3-py^+ $CF_3SO_3^-$), CH_3, Ph].

In collaboration with the Prof. Geremia of the CEB-Centre of Excellence in Biocrystallography of the University of Trieste, the homopolymer Tiiii [($3C_3H_7$ + CH_3-py^+ $CF_3SO_3^-$), CH_3, Ph] was crystallized from a very slow vapour diffusion from a liquid mixture 1:2 of methanol and ethanol in a trifluoro ethanol solution of the homopolymer.

The homopolymer crystal structure shows the linear supramolecular architectures arranged in an anti-parallel fashion. The monomer units are held together by self-complementarity of host-guest interactions between the tetraphosphonate cavity of a cavitand and the methyl pyridinium tail of the following cavitand (Figure 29). The host-guest interactions are mainly stabilized by the ion-dipole interactions between the nitrogen

positively charged of the methyl pyridinium moiety and the oxygen of the P=O bonds of the cavitand. CH-π interactions between the CH_3 of the methyl pyridinium moiety and the π electrons of the aromatic rings of the resorcinarene skeleton are also present. The crystallographic structure shows that the minimum distance between the CH_3 of the methyl pyridinium moiety inside the cavity and the aromatic systems plans of the resorcinarenic unit is 3.49 ± 0.02 Å, while the minimum distance between the N^+ of the methy pyridinium group and the oxygen of the P=O bonds is 2.83 ± 0.02 Å.

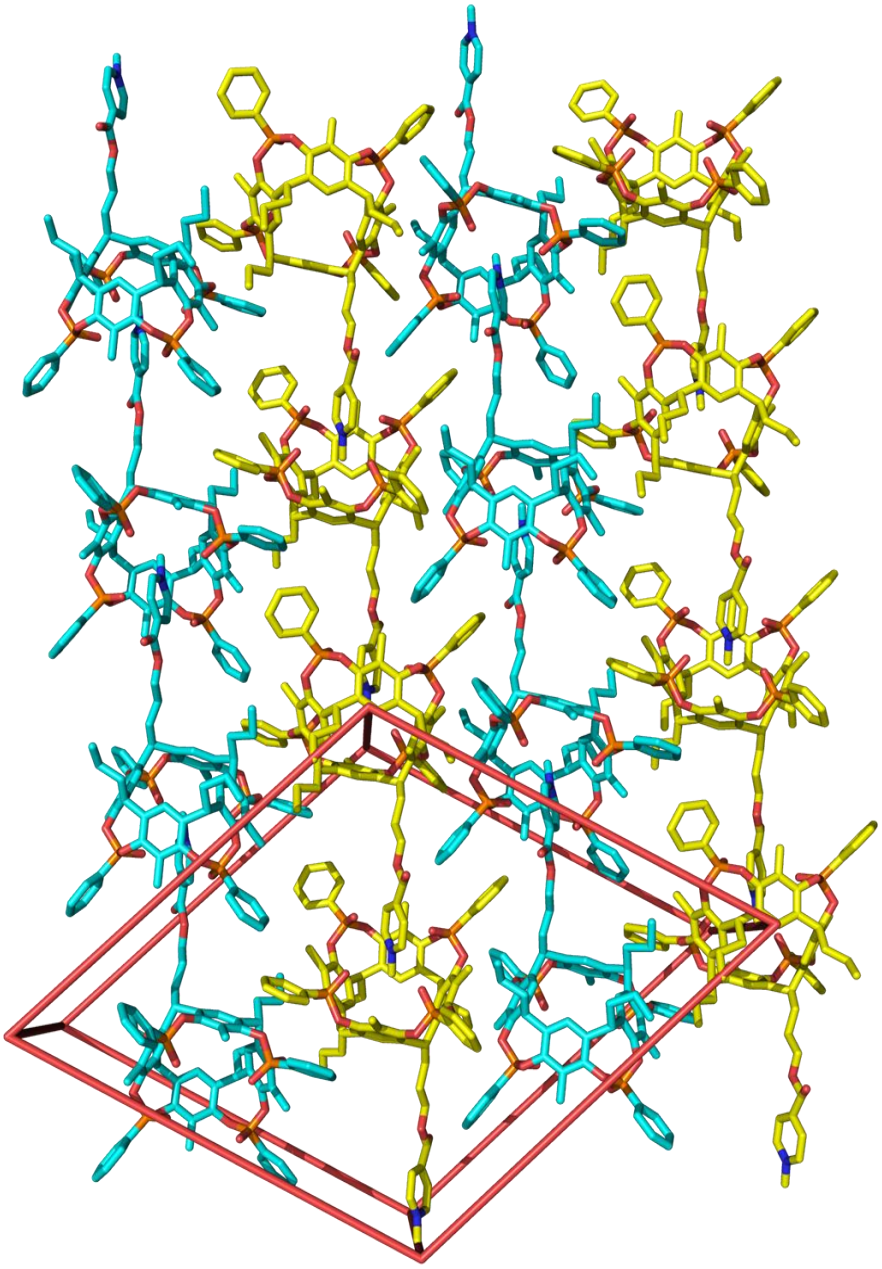

Figure 29. Anti-parallel arranged polymeric chains of Tiiii [($3C_3H_7$ + CH_3-py^+ $CF_3SO_3^-$), CH_3, Ph].

The HOESY NMR reported above (Figure 15) shows the strong interactions between the triflate counterions and the lower rim chains and the aromatic protons of the resorcinarene skeleton. It also reported the weak interactions of the triflate counterions with the CH_3 of the methyl pyridinium moiety. We concluded above that these interactions indicate the fitting of the triflate counterions at lower rim chain with the SO_3 group pointing toward the center of the cavity, forming a ion pair between the methyl pyridinium of the residue **i** inside the cavity of the residue **i+1** and its counterion.

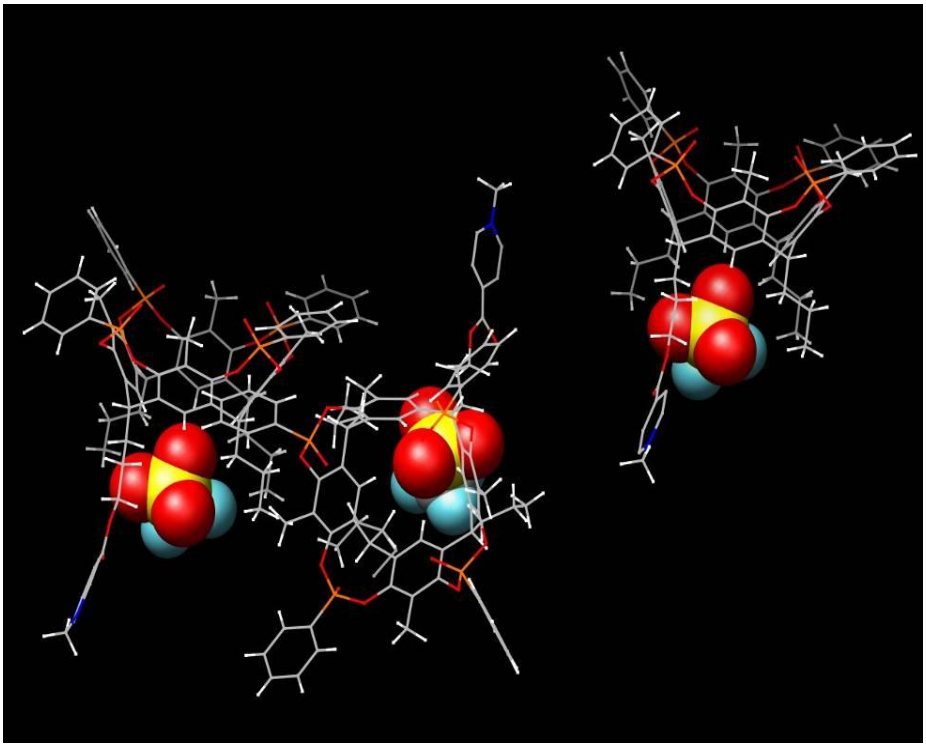

Figure 30. Simplified crystal packing of the homopolymer with triflate counterion between the lower rim chain and the SO_3^- group pointing toward the center of the cavity

Such conclusion are confirmed in the solid state by observing a simplified crystal packing in Figure 30 that shows the triflate counterion

among the lower rim chains and the SO_3 group pointing toward the center of the cavity where is present the methyl pyridinium moiety. The average distance between the N^+ of the methyl piridinium moiety of the residue **i** inside the cavity of the residue **i+1** and the O^- of the triflate counterion under the chain of the residue **i+1** is 6.92 Å; the average distance between the N^+ of the methyl pyridinium of the residue **i** and the O^- of the triflate counterion under the lower rim chain of the residue **i** is 8.73 Å. The solvent molecules of the solvents (trifluoroethanol, methanol and ethanol) removed in the crystal packing (Figure 30) for clarity, fill the interstices between the polymer chains. Each polymeric chain is surrounded by other eight polymeric chains (Figure 31).

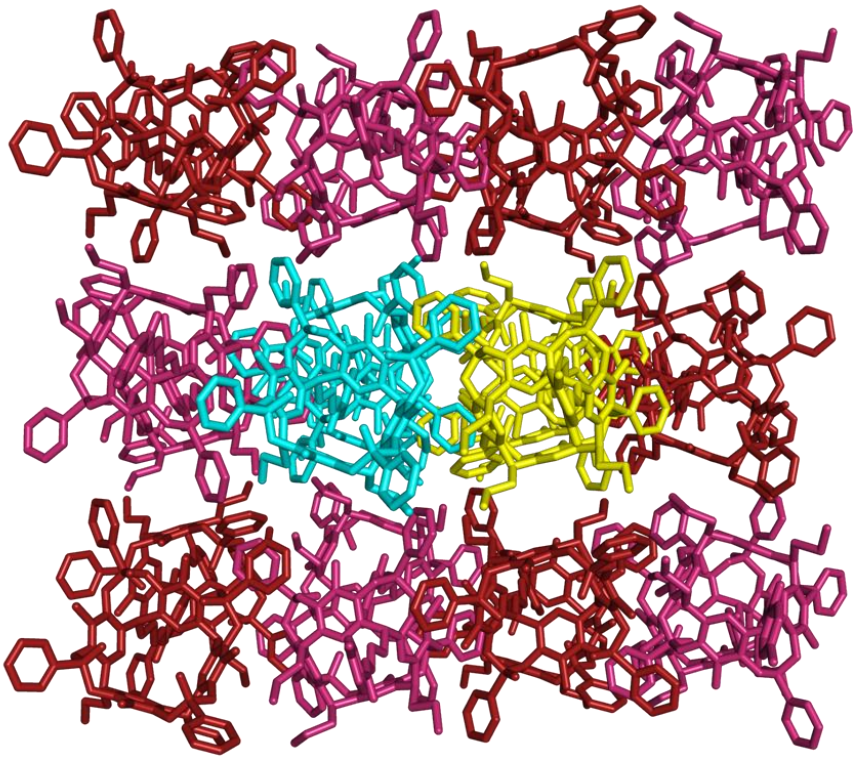

Figure 31. Homopolymer crystal structure: antiparallel polymer stacking.

The polymeric chains are anti-parallel each other to exploit the electrostatic interactions (quadrupolar interactions) that stabilize the polymeric chains in the final supramolecular structure (Figure 32).

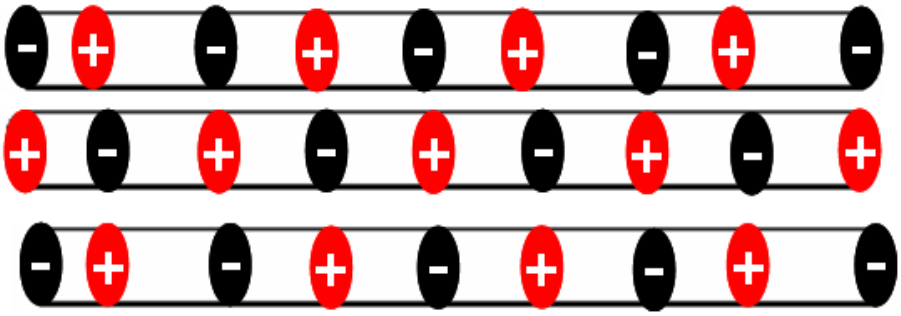

Figure 32. Electrostatic interactions stabilize the polymeric chains in the final quadrupolar supramolecular structure.

In order to investigate the presence of the quadrupolar interactions between the polymeric chains, some distances have been measured from the crystallographic data. Considering two anti-parallel polymeric chain, yellow, and blue that are crystallographically independent (Figure 29), the average distance between N^+ of the residues of the yellow polymeric chain and the O^- of the triflate counterions of the blue chain is 11.51 Å. At this distance, the ionic interactions between the polymeric chains are weak, but the combination of many of these weak interactions stabilizes the quadrupolar association.

3.2.2.7 SFM Investigation of casted homopolymer Tiiii [($3C_3H_7$ + CH_3-py^+ $CF_3SO_3^-$), CH_3, Ph] on solid surface

In collaboration with Dr. Matteo Palma and Prof. Paolo Samori of Laboratory of Nanochemistry, Institut de Science et d' Ingenierie Supramolecolaires (I.S.I.S) Université Louis Pasteur, Strasbourg (France) Scanning Force Microscopy experiments were performed.

Preliminary experiments to study the nanostructures in the solid state have been performed using Scanning Force Microscopy (SFM).[58] This technique provides an independent evaluation of the shape and the molecular weight distribution for the polymeric species once deposited on a solid support. Thin dry organic films have been grown from methylene chloride and acetone diluted solutions of the homopolymer Tiiii [($3C_3H_7$ + CH_3-py^+ $CF_3SO_3^-$), CH_3, Ph] on different surfaces namely: mica, and modified mica.

From CH_2Cl_2 solution 10^{-4} M, cast on mica by dipping the solid surface directly in the investigated solution, rod-like objects (Figure 33) with a certain degrees of anisotropy, have been observed; interestingly on uncovered (by such layer) mica areas, the rods weren't observed (see uncovered areas Figure 33). Such rods exhibit an average height of (2.8 ± 0.5) nm and average width of (10.0 ± 5.5) nm. This width is averagely four times than the single polymer chain. This large deviation can be explained with the formation of the quadrupolar supramolecular architectures cast on the mica surface then confirming the PGSE and the crystallographic data (Figure 34).

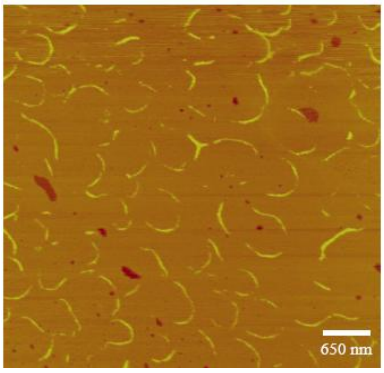

Figure 33. Solution 10^{-4} M in CH_2Cl_2 of the homopolymer Tiiii [($3C_3H_7$ + CH_3-py^+ $CF_3SO_3^-$), CH_3, Ph] in CH_2Cl_2 casted on mica.

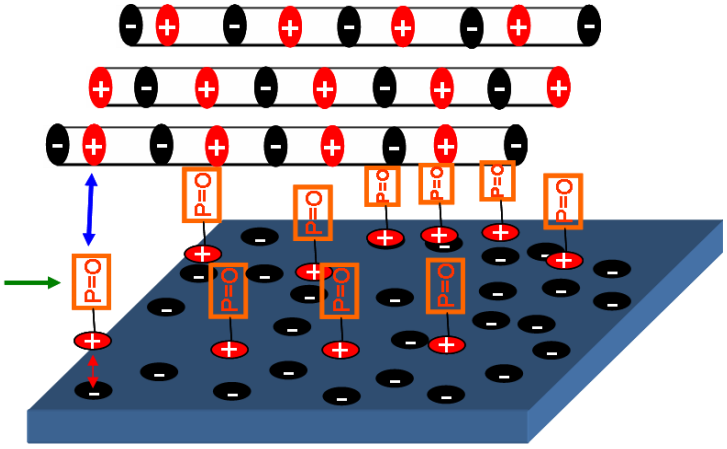

Figure 34. Quadrupolar polymer chains cast on mica deposited on a layer of monomer unit (green arrow), ion-dipole interactions (blue arrow) stabilize the deposition on the layers, the monolayer is stabilized by electrostatic interactions (red arrow) between the positive charges of the methyl-pyridinium tail and the negative charges of the mica surface.

The height is compared with the width of the cavitand taken from the crystal structure (≈2.7 nm). The length of the observed rod-like objects is not mono-dispersed and was found to vary in a wide range 200 (> 130 units >190,000 Da) – 1800 nm (> 1200 units > 1700,000 Da) (Figure 35).

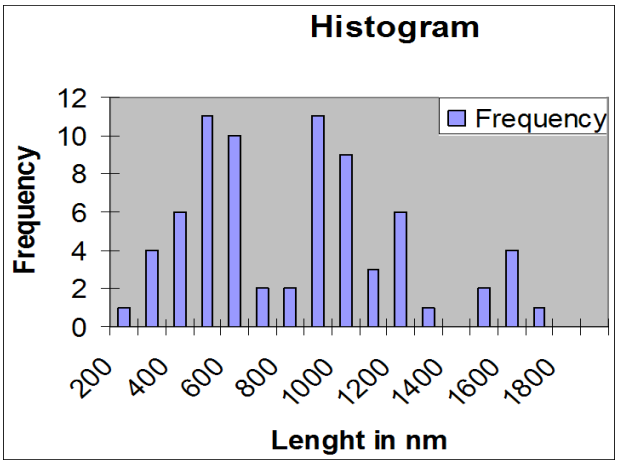

Figure 35. Distribution of the length of the rod-like objects on mica surface.

The rods were found to be positioned on top of a (1.2 ±0.3) nm thick layer performed on the mica surface (Figure 34). The two structures, i.e. the rods and the layer, possess different viscoelastic properties as highlighted by phase imaging (Figure 36), pointing toward different structures at the supramolecular level.

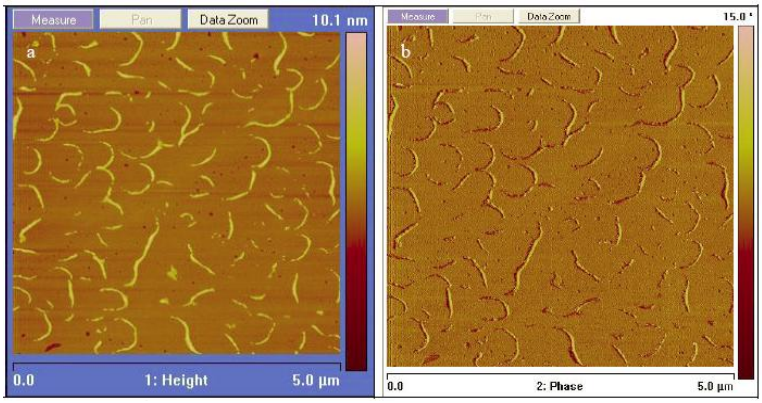

Figure 36. Solution 10^{-4} M^{-1} of the homopolymer Tiiii [($3C_3H_7$ + CH_3-py^+ $CF_3SO_3^-$), CH_3, Ph] in CH_2Cl_2 cast on mica, a) topographical, b) phased images.

The 1.2 nm height of the observed layer is in agreement with a rough estimation of the monomer length, i.e. ≈ 1.5 nm. It can be speculated that the methyl pyridinium cation preferentially and initially forms a layer on the surface of mica due to the interactions between the negative charges on the substrate surface and the positive charge of the monomer tail group. This strong interaction leads to the uniform dewetting toward the formation of homogeneous film. Then, when such a layer is formed, the polymer chains deposit on the surface. In fact, casting the same solution on a treated mica surface on which a positively charged and continuous layer of poly-L-ornithine was deposited, the behaviour is completely different. In this case, the rods occupy uniformly the surface of the modified mica (Figure 37), the layer disappears and the height was found to be 1.5 nm. This behaviour can be interpreted as being due to the small interactions between the rods and the substrate as compared to the interactions between the rods themselves. This situation destabilizes the layer.

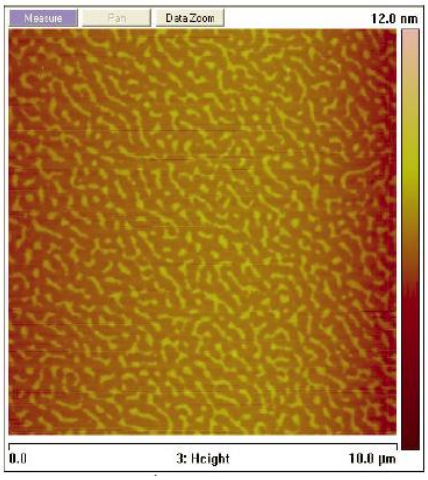

Figure 37. Solution 10^{-4} M of the homopolymer Tiiii [($3C_3H_7$ + CH_3-py^+ $CF_3SO_3^-$), CH_3, Ph] in CH_2Cl_2 casted on a positively charged layer of poly-L-ornithine on mica.

In order to observe the polarity effect of the solvent on surface, a solution 10^{-4} M of the homopolymer Tiiii [($3C_3H_7$ + CH_3-py^+ $CF_3SO_3^-$), CH_3, Ph] in acetone was deposited on mica surface and as expected only smaller oligomers was observed (Figure 38).

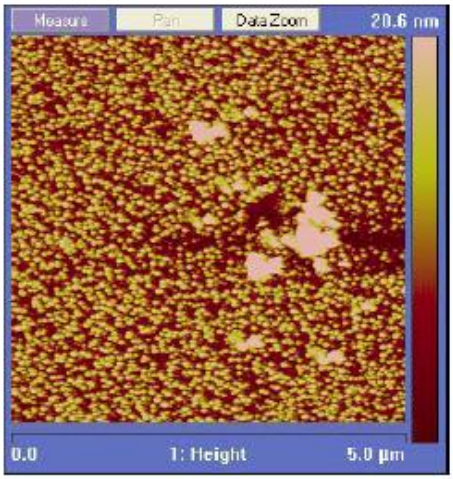

Figure 38. Solution 10^{-4} M of the homopolymer Tiiii [($3C_3H_7$ + CH_3-py^+ $CF_3SO_3^-$), CH_3, Ph] in acetone cast on mica.

In conclusion, the STM measurements on mica supported the PGSE data in solution about the formation of larger aggregates held together by quadrupolar interactions. On mica, only aggregated polymeric chains are present. Moreover the homopolymer formation in solid state is confirmed. The very large dp values observed on mica are due to the solvent evaporation which trigger further polymerization among already formed polymers and oligomers present in solution.

3.2.2.8 Guest-driven reversible assembly-disassembly of homopolymer in solution.

We demonstrated above the self-complementarity between the *N*-methyl pyridinium moiety of a residue **i** and the tetraphosphonate-cavity of following residue **i +1** in the homopolymers Tiiii [($3C_3H_7$ + CH_3-py^+ I^-), CH_3, Ph] and Tiiii [($3C_3H_7$ + CH_3-py^+ $CF_3SO_3^-$), CH_3, Ph]. Such self-complementarity is characterized by the shielding of the protons of the *N*-methyl pyridinium moiety that lead to the upfield shift of their ^{1}H NMR signals. Now our purpose is to probe the reversible assembly-disassembly of the polymeric chains, monitoring at the ^{1}H NMR the deshielding of *N*-methylpyrinidinium and the deshielding of the P=O signals at the ^{31}P NMR (Figure 40).

The reversible disassembly of the homopolymer has been triggered by addition of a competitive guest, N-butylmethylammonium iodide. The K_{ass} of the complex between this guest and the Tiiii cavitand could not be measured via ITC, since its value exceeds 10^8 M^{-1}, the upper limit of reliable ITC K_{ass} determination.[59] Therefore its affinity for the cavitand Tiiii [C_3H_7, CH_3, Ph] was evaluated by ITC via guest exchange experiments of the corresponding chloride with dimer complex **1** in methanol (Table 1). The recorded ΔG value (-21.46 $kJmol^{-1}$) indicates a large preference for N-butylmethylammonium complexation, justifying a complete guest exchange close to the stoichiometric ratio. The homopolymer Tiiii [($3C_3H_7$ + CH_3-py^+ $CF_3SO_3^-$), CH_3, Ph] disassembly monitored by ^{1}H NMR (Figure 38) and ^{31}P NMR (Figure 39) in $CDCl_3$, is recorded. The methylpyridiunium complexation inside the host cavity is proved by some significant variations of chemical shift. By comparing the spectra of stopper TSiiii [($3C_3H_7$ + CH_3-py^+ PF_6^-), CH_3, Ph] (Figure 38a) and of homopolymer Tiiii [($3C_3H_7$ + CH_3-py^+ $CF_3SO_3^-$), CH_3, Ph] (figure 38b), an upfield shift of the pyridine aromatic signals of the latter

was observed, due to a shielding effect of the cavity. The same effect explains the shift from 4.35 ppm to 0.87 ppm of the N-CH_3 signal (see NOESY Figure 14). Addition of two equivalents of N-methylbutylammonium iodide to a solution of homopolymer Tiiii [($3C_3H_7$ + CH_3-py^+ $CF_3SO_3^-$), CH_3, Ph] led to the complete disassembly of the polymer (Figure 38e). The chemical shifts of pyridine aromatic and N-CH_3 protons are comparable to those of the stopper TSiiii [($3C_3H_7$ + CH_3-py^+ PF_6^-), CH_3, Ph] (Figure 39a), while the NH and N-CH3 peaks of the ammonium salt undergo large upfield shifts. The P=O peak at ^{31}P NMR undergoes slight downfield shift (from 7.86 to 8.72) (Figure 40b) due to the greater deshielding effect likely related to the formation of P=O----H H-bonding. These changes prove that the competitive guest replaced the methylpyridinium moiety inside the cavity, inducing the depolymerisation. Finally, addition of two equivalents of DBU (1,8-diazobicyclo(5,4,0)-undec-7-en) restored the original polymer quantitatively (Figure 39f and 40c). DBU breaks the ammonium-cavitand complex by deprotonating the guest. Since DBU is a hindered base, it cannot enter the cavity, therefore the affinity of its protonated form for Tiiii [($3C_3H_7$ + CH_3-py^+ $CF_3SO_3^-$), CH_3, Ph] is very low.

The same protocol can be followed visually by suspending the investigated homopolymer in acetonitrile, where it is insoluble (see vials in Figure 39). Addition of one equivalent of N-butylmethylammonium iodide was sufficient to obtain a perfectly homogeneous solution, as expected for disassembled small oligomeric and monomeric species. The solution became again heterogeneous after addition of one equivalent of DBU, for the presence of the reassembled polymer.

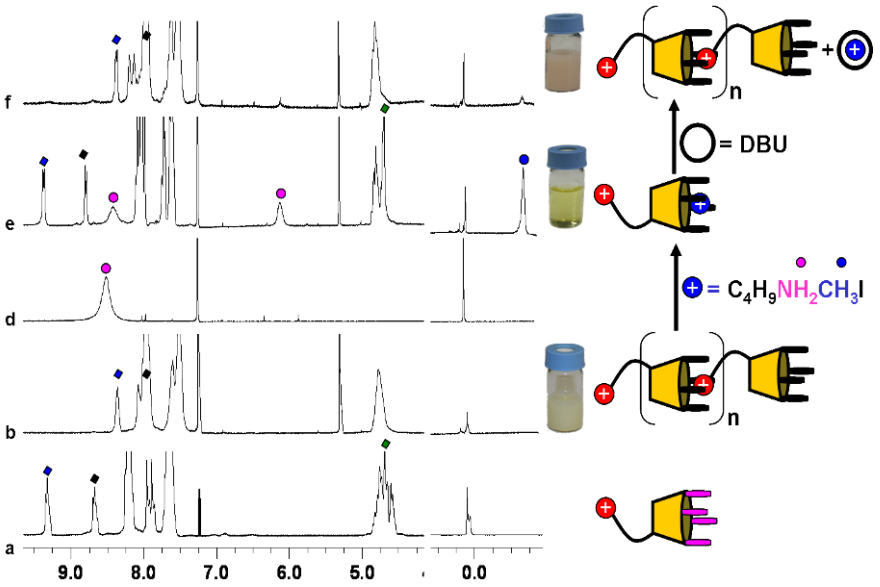

Figure 39. Guest-driven assembly-disassembly of the homopolymer Tiiii [($3C_3H_7$ + CH_3-py^+ $CF_3SO_3^-$), CH_3, Ph] in chloroform monitored by ^{1}H NMR.

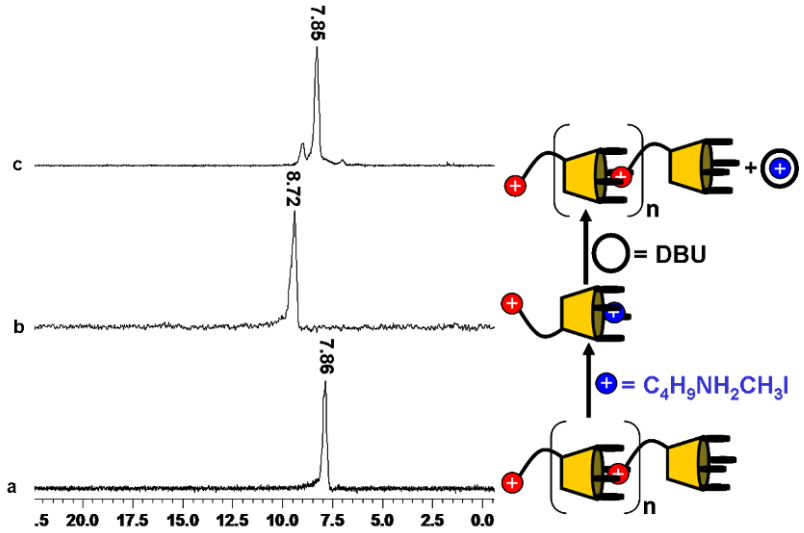

Figure 40. Guest-driven assembly-disassembly of the homopolymer Tiiii [($3C_3H_7$ + CH_3-py^+ $CF_3SO_3^-$), CH_3, Ph] in chloroform monitored by ^{31}P NMR.

3.3 Conclusions

A new class of host-guest supramolecular polymers has been designed, prepared, and characterized. The monomeric unit presents the host moiety at the upper rim of a cavitand in the form of cavity surrounded by four inward facing P=O groups, and the guest moiety at the lower rim as methyl pyridinium unit. The self association of this monomer to give the corresponding homopolymer has been studied with several different solution and solid state techniques. The overall picture emerging from these studies shows that the formation of the polymer is both enthalpy and entropy driven and is solvent dependent.

The remarkable plasticity of the system ha been proven by the guest triggered reversible assembly-disassembly and by the formation of star polymers by addition of a tetra-functionalized porphyrin template.

Crystal structure and STM experiments clearly indicate that these homopolymers have a remarkable tendency to aggregate in the solid state. PGSE measurements evidence the same behaviour in $CDCl_3$ where two different sizes objects in slow exchange are present. Quadrupolar interactions are the driving force for this remarkable aggregation mode among ionic polymer chains, as proven by the suppression of the largest aggregates upon addition of CD_3OD to the $CDCl_3$ solution of homopolymer.

The polymer chains in solution and their aggregates tend to be quite rigid with minimal entanglement as shown by viscosimetry.

The peculiar feature of this new homopolymer can be exploited in the formation of new composite materials featuring both covalent polymeric and non covalent supramolecular characteristics.

3.4 Experimental section

General Method: All reagents were purchased from Sigma-Aldrich Co. All solvents were dried over 3Å and 4Å molecular sieves by standard procedures. Pyridine was distilled on potassium hydroxide and dried over 3Å molecular sieves. ^{1}H NMR spectra were recorded at Bruker AC300 (300 MHz), AVANCE (300 MHz) and AMX400 (400 MHz) spectrometers and all chemical shift (δ) were reported in parts per million (ppm) relative to the proton resonances resulting from incomplete deuteration of the NMR solvents. Microanalyses were performed by the service of Parma University. Electrospray ionization (ESI)-MS experiments were performed on a Waters ZMD spectrometer equipped with an electrospray interface. Column chromatography was performed using silica gel 60 (Merck 70-230 mesh) equipped with

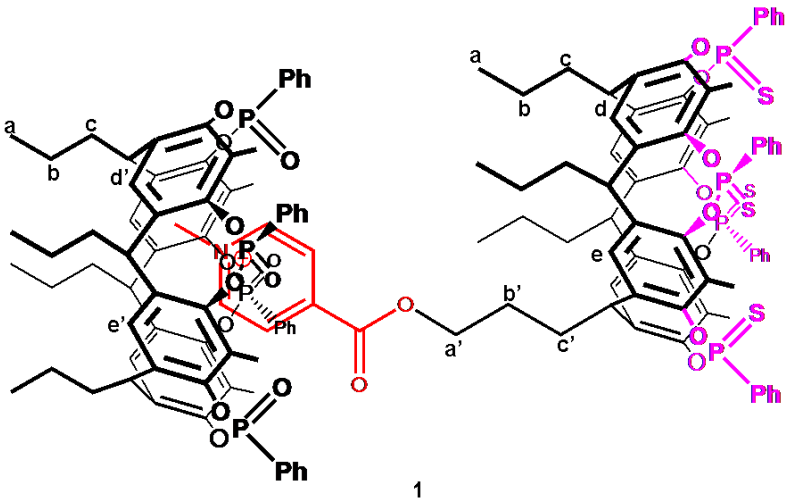

1

Titration of phosphonate cavitand Tiiii [C_3H_7, CH_3, Ph] with thiophosphonate cavitand TSiiii [($3C_3H_7$ + CH_3-$Py^+PF_6^-$), CH_3, Ph] to form the dimer complex 1: to a solution of phosphonate cavitand Tiiii [C_3H_7, CH_3, Ph] (5 mg, 4.210^{-3} mmol) dissolved in 500 µL of CD_3CN, 50 µL of a solution 0.08 mM (4.210^{-3} mmol) of the cavitand TSiiii [($3C_3H_7$ + CH_3-$Py^+PF_6^-$), CH_3, Ph] in CD_3CN was added in five aliquot of 10 µL.

^{1}H NMR (300 MHz, CD_3CN): δ (ppm): 0.91 (s, 3H, **CH_{3py}**), 1.06-0.90 (broad , 21H, **H_a**), 1.43-1.35 (broad , 14H, **H_b**), 1.86 (m, 2H, **$H_{b'}$**), 2.03-1.98 (broad s, 24H, Ar**CH_3**), 2.7-2.4 (broad , 16H, **H_c +$H_{c'}$**), 4.51 (t, 2H, **$H_{a'}$**, J=4.8 Hz), 4.74 (broad t, 4H, **H_d**), 4.9 (t, 4H, **$H_{d'}$**, J=5.2 Hz), 7.73-7.63 (broad , 24H, S=PAr**H_m** +O=PAr**H_m** O=PAr**H_p**

+S=PAr$\mathbf{H}_p$), 7.82(s 2x2H, $\mathbf{H}_e$), 8.18-8.05 (broad , 22H, S=PAr$\mathbf{H}_o$ +O=PAr$\mathbf{H}_o$ +$\mathbf{H}_c$, +$\mathbf{H}_{mPy}$), 8.52 (d, 2H, $\mathbf{H}_{oPy}$)). **^{31}PNMR** (172 MHz, 298 K, CD_3CN) δ(ppm): -141.2 (m, 1P, PF_6^-, J = 751 Hz), 12,87 (s, 4P, P=O), 73.02 (s, 4P, P=S). **ESI-MS:** $C_{143}H_{142}F_6NO_{22}P_9S_4$: 1400.3 (TSiiii [($3C_3H_7$ + CH_3-$Py^+PF_6^-$), CH_3, Ph]- PF_6^-)$^+$, 2683.2 (M-PF_6^-)$^+$.

Crystallographic data of dimer complex 1: The molecular structure of compound $C_{143}H_{142}NO_{22}P_8S_4$+$PF_6$+$3C_2H_3N$ **1** was determined by single-crystal X-ray diffraction method. Experimental details are summarized in Table 8. Intensity data were collected using Cu Kα radiation (λ= 1.5418 Å) at 100K equipped with a CCD area detector. The structure was solved by direct method using SHELXL program.[60] The data of **1** were performed and refined using DENZO-SMN, SCALEPACK, and AMoRe programs.[61]

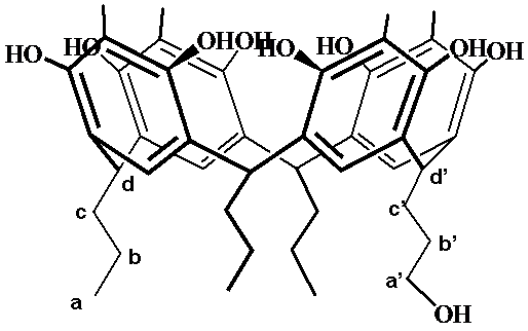

Resorcinarene 2

Synthesis of resorcinarene 2: to a solution of methyl resorcinol (8.9 g, 72 mM) dissolved in 57 mL of methanol, butanal (4.73 mL, 54 mmol) and 2,3-dihydrofuran (1.36 mL, 18 mmol) were added. The resulting yellow solution was stirred at room temperature, while 14.4 mL of a solution 12 M of HCl in water were slowly added in 30 min. The reaction mixture was stirred 6 day at 50°C then cooled at room temperature. 100 mL of water were added and the yellow suspension was filtered. Re-crystallisation from a mixture 9:1 of H_2O and CH_3OH followed by two sequential column chromatographic separations on silica gel with a mixture 93:7 of CH_2Cl_2 and CH_3OH as eluant gave rise to product as yellowish powder (3.3 g, 4.5 mmol, 25%).

^{1}HNMR 8B (300 MHz, 298 K, DMSO-d_6,) δ (ppm): 0.89 (t, 9H, $\mathbf{H}_a$, J= 7 Hz), 1.17 (m, 6H, $\mathbf{H}_b$), 1.32 (m, 2H, $\mathbf{H}_{b'}$), 1.91 (s, 12H, Ar$\mathbf{CH_3}$), 2.2 (m, (2+6)H, $\mathbf{H}_c$, + $\mathbf{H}_c$), 3.41(m, 2H, $\mathbf{H}_{a'}$), 4.2 (t, (1 + 3)H, $\mathbf{H}_{d'}$ + $\mathbf{H}_d$, J = 7.6 Hz), 4.33 (m, 1H, $CH_2\mathbf{OH}$), 7.27 (s, 4H, Ar**H**), 8.64 (s, 8H, Ar**OH**).). **ESI-MS:** 730 (M + H)$^{+\cdot}$

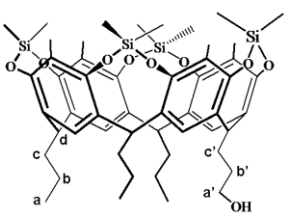

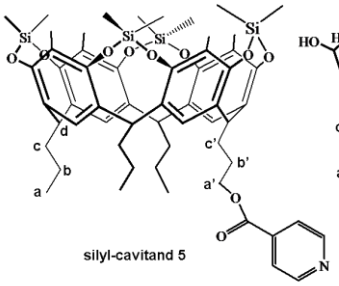

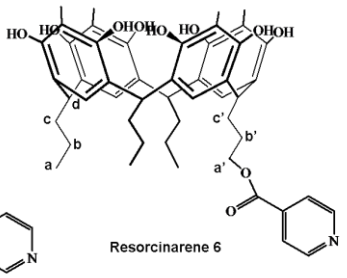

Synthesis of silyl-cavitand 3: to a solution of resorcinarene **2** (3.5 g, 4.8 mmol) dissolved in dry pyridine (120 ml), dimethyldichlorosilane (7 ml, 58 mmol) was added at 0 °C. The mixture was stirred at 70 °C for 3h; the solvent was removed under vacuum. 20 mL of methanol were added and then the yellow suspension was filtered. Purification by column chromatography on silica gel using a mixture 97:3 of CH_2Cl_2 and CH_3OH as eluant yielded the product (4.17 g, 4.37 mmol, 91%).

^{1}HNMR (300 MHz, 298 K, $CDCl_3$) δ (ppm): -0.71 (s, 12H, SiC**H$_{3IN}$**), 0.50 (s, 12H, SiC**H$_{3OUT}$**), 0.96 (t, 9H, **H$_a$**, J=7.2 Hz), 1.27 (m, 6H, **H$_b$**), 1.56 (m, 2H, **H$_{b'}$**), 1.90 (s, 12H, ArC**H$_3$**), 2.14 (m, 6H, **H$_c$**), 2.31 (m, 2H, **H$_{c'}$**), 3.71 (t, 2H, **H$_{a'}$**, J=6.3 Hz), 4.60 (t, 4H, ArC**H,** J=7.9 Hz), 7.16 (s, 2H, Ar**H)**, 7.19 (s, 2H, Ar**H)**. **ESI-MS**: $C_{52}H_{72}O_9Si_4$: 954 $[M+H]^+$.

Synthesis of silyl-cavitand 5: to a solution of isonicotinoyl chloride hydrochloride (0.25 g, 1.38 mmol) dissolved in 15 mL of dry pyridine; silyl-cavitand **3** (0.44 g, 0.46 mmol) was added and stirred at 100 °C for 3h. The solvent was removed under vacuum and then 10 mL of water were added. The resulting suspension was filtered and purified by re-crystallisation from a mixture 9:1 of H_2O and CH_3OH yielding **5** (0.44g, 0.42mmol, 90%).

^{1}HNMR (300 MHz, 298 K, $CDCl_3$,) δ (ppm): -0.7 (s, 12H, SiC**H$_{3\ IN}$**), 0.5 (s, 12H, SiC**H$_{3\ OUT}$**), 0.9 (t, 9H, **H$_a$**, J=7.2 Hz), 1.29 (m, 6H, **H$_b$**), 1.78 (m, 2H, **H$_{b'}$**), 1.89 (s, 12H, ArC**H$_3$**), 2.16 (m, 6H, **H$_c$**), 2.35 (m, 2H, **H$_{c'}$**), 4.4 (t, 2H, **H$_{a'}$** , J=6.5 Hz), 4.6 (m, 4H, **H$_d$**), 7.16 (s, 4H, Ar**H**), 7.9 (d, 2H, **H$_{mpy}$**, J=5.1 Hz**)**, 8.8 (d, 2H, **H$_{opy}$**, J=5.1 Hz **)**: **ESI-MS:** $C_{58}H_{75}NO_{10}Si_4$: 1060 $(M+H^+)$.

Synthesis resorcinarene 6: to a solution of silyl-cavitand **5** (1 g, 0.95 mmol) dissolved in 20 mL of DMF, 450 μL of a solution 55% of HF in water were added. The mixture was left to stir for 18 h at 40 °C. The solvent was removed under vacuum. Purification by column chromatography on silica gel using a mixture 95:5 of H_2O and CH_3OH, yielded **6** (0,65g, 0,773 mmol, 81.5%).

^{1}HNMR (300 MHz, 298 K, Acetone-d_6) δ (ppm): 0.91 (t, 9H, $\mathbf{H_a}$, J=7.4 Hz), 1.26 (m, 6H, $\mathbf{H_b}$), 1.76 (m, 2H, $\mathbf{H_{b'}}$), 2.04 (s, 12H, ArC$\mathbf{H_3}$), 2.24 (m, 6H, $\mathbf{H_c}$), 2.46 (m, 2H, $\mathbf{H_{c'}}$), 4.4 (m, 4H, $\mathbf{H_a}$, + $\mathbf{H_d}$), 7.41 (s, 2H, Ar**H**), 7.47 (s, 2H, Ar**H**), 7.85 (d, 2H, $\mathbf{H_{mpy}}$, J=6.4 Hz**)**, 7.93 (s, 4H, ArO**H**), 7.96 (s, 4H, ArO**H**), 8.78 (d, 2H, $\mathbf{H_{opy}}$, J=6.4 Hz **)**. **ESI-MS**: $C_{50}H_{59}NO_{10}$: 834.9 $(M+H^+)$ and 857,3 $(M+Na)^+$.

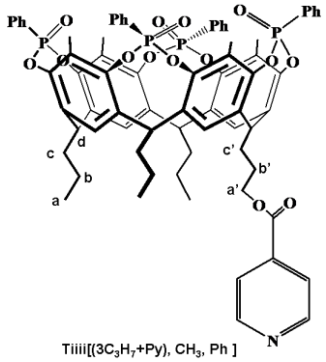

Tiiii[(3C_3H_7+Py), CH_3, Ph]

Synthesis of the cavitand Tiiii[(3C_3H_7 + Py), CH_3, Ph] : to a solution of mono-pyridyl-footed resorcinarene (0.5 g, 0.6 mmol) dissolved in 20 mL of fresh distilled pyridine, dichlorophenylphosphine (0.332 mL, 2.45 mmol) was slowly added at room temperature. The mixture was stirred for 3h at 70 °C and then cooled at 0 °C. An excess of a solution 35% of H_2O_2, and 5 mL of $CHCl_3$ were added and left to stir for 30 min. The resulting bilayer was evaporated and dried under vacuum. 50 mL of water were added and the white suspension was filtered. Purification by re-crystallization from a mixture 8:2 of H_2O and CH_3CN yielded the product (0.753 g, 0.57 mmol, 95%).

^{1}H NMR (300 MHz, $CDCl_3$) δ (ppm): 1.05 (t, 9H, $\mathbf{H_a}$ J = 7.32 Hz), 1.43 (m, 6H, $\mathbf{H_b}$), 1.91 (m, 2H, $\mathbf{H_{b'}}$), 2.3 (s, 12H, Ar$\mathbf{CH_3}$), 2.3 (m, 6H, $\mathbf{H_c}$), 2.46 (m, 2H, $\mathbf{H_{c'}}$), 4.5 (t, 2H, $\mathbf{H_{a'}}$, J = 6.3 Hz), 4.86 (t, 4H, $\mathbf{H_d}$, J = 7.8 Hz), 7.12 (s, 4H, Ar**H**), 7.52 (m, 8H, O=PAr$\mathbf{H_m}$), 7.65 (m, 4H, O=PAr$\mathbf{Hp}$), 8.08 (d, 2H, $\mathbf{H_{mPy}}$, J = 5.4 Hz), 8.12 (m, 8H, O=PAr$\mathbf{H_o}$), 8.73 (d, 2H, $\mathbf{H_{oPy}}$). **^{31}P NMR** (172 MHz, $CDCl_3$) δ (ppm): 4.2 (s, O=**P**). **ESI-MS**: $C_{74}H_{71}NO_{14}P_4$: 1322.30 $(M + H^+)^+$.

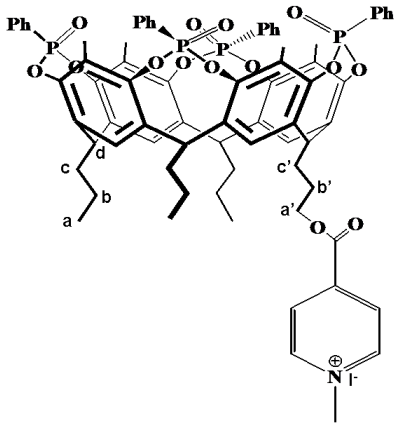

Tiiii[($3C_3H_7$+CH_3-Py$^+I^-$), CH_3, Ph]

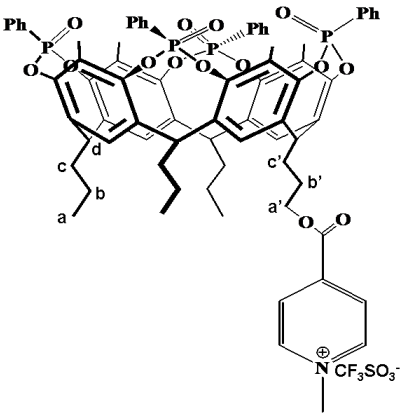

Tiiii[($3C_3H_7$+CH_3-Py$^+CF_3SO_3^-$), CH_3, Ph]

Synthesis of the homopolymer Tiiii[($3C_3H_7$ + CH_3-Py$^+I^-$), CH_3, Ph]: to a solution of cavitand Tiiii[($3C_3H_7$ + Py), CH_3, Ph] (0.3 g, 0.23 mmol) dissolved in 8 mL of a mixture 6:2 of acetonitrile and chloroform, methyl iodide (0.14 mL, 2.3 mmol) was added. The mixture was stirred at reflux for 18 h. The solvent was removed and the resulting yellowish powder was purified by re-crystallization from a mixture 1:1 of H_2O and CH_3CN yielding the product (0.3 g, 0.205 mmol, 90%).

^{1}H NMR (300 MHz, $CDCl_3$) δ (ppm): 0.89 (s, 3H, **CH_{3py}**), 1.10-1.06 (broad m, 9H, **H_a**), 1.36-1.42 (broad m, 6H, **H_b**), 1.86 (m, 2H, **$H_{b'}$**), 2.07 (s, 12H, Ar**CH_3**), 2.94 (broad m, 6H, **H_c**); 3.2 (broad m, 2H, **$H_{c'}$**), 4.82-4.76 (broad m, 6H, **H_a**, **+H_d**), 7.51 (broad m, 8H, O=PAr**H_m**), 7.60 (broad m, 4H, O=PAr**H*p***), 8.98 – 7.91 (m, (8 + 2)H, O=PAr**H_o** + **H_{mPy}**), 8.3 – 8.22(broad 2, 2x2H, ArH), 8.37 (d, 2H, **H_{oPy}**). **^{31}PNMR** (172 MHz, 298 K, $CDCl_3$) δ (ppm): 7.87 (s, **O=P**). **ESI-MS:** $C_{75}H_{74}NO_{14}P_4I$: 1336.77 $(M\text{-}I^-)^+$

Synthesis of the homopolymer Tiiii[($3C_3H_7$ + CH_3-Py$^+CF_3SO_3^-$), CH_3, Ph]: to a solution of cavitand Tiiii[($3C_3H_7$ + Py), CH_3, Ph] (0.4 g, 0.302 mmol) dissolved in 8 mL of Chloroform, $CH_3OSO_2CF_3$ (0.103 mL, 0.91 mmol) was added. The mixture was stirred 30 min at room temperature. The solvent was removed. Purification by crystallization from a mixture 1:1 of acetonitrile and water yielded the product (0.413 g, 0.278 mmol, 92%).

^{1}H NMR (300 MHz, $CDCl_3$) δ (ppm): 0.87 (s, 3H, **CH_{3Py}**), 1.03-0.98 (broad m, 9H, **H_a**), 1.38 (m, 6H, **H_b**), 1.82 (m, 2H, **$H_{b'}$**), 2.13 (s, 12H, **CH_{3Py}**), 2.64 (m, 6H, **H_c**) 2.71-2.64 (brod m, 2H, **$H_{c'}$**), 4.74 (broad m, 6H, **H_a**, **+H_d**), 7.62 -7.51 (b, (8 + 4)H, O=PAr**H_m** + O=PAr**H_p**), 8.0 – 8.2 (broad m, (2+ 4+ 8)H, **H_{mPy}** + Ar**H** + O=PAr**H_o**), 8.07 (m, 2H,

H_{oPy}). **^{31}PNMR** (172 MHz, 298K, $CDCl_3$) δ (ppm): 7.86 (s, **P=O**). **ESI-MS:** $C_{76}H_{74}F_3NO_{17}P_4S$: 1337.4 (M - $CF_3SO_3^-$)$^+$.

Crystallographic data for the homopolymer Tiiii [($3C_3H_7$ + CH_3-py$^+$ $CF_3SO_3^-$), CH_3, Ph]: The molecular structure of compound $C_{76}H_{74}F_3NO_{17}P_4S$ was determined by single-crystal X-ray diffraction methods. Experimental details are summarized in table 8. Intensity data were collected using Elettra XRD1 beamline diffractometer double crystal Si(111) radiation (λ= 1.2 Å) at 100 K equipped with a CCD area detector. The structure was solved by direct method using SHELXL program.[60] The data for 24B were performed and refined using DENZO-SMN, SCALEPACK, and AMoRe programs.[61] Cryosystem: Oxford Cryosystems Cryocooler 700 (liquid nitrogen).

Static Light Scattering (SLS): The molecular characterization of polymers was performed by static (or elastic) light scattering technique. A multi-angle laser light scattering (MALS) Dawn DSP-F photometer from Wyatt (Santa Barbara, CA, USA) in off-line (batch) mode in chloroform solvent at room temperature was used. All polymeric solutions were accurately filtered through 0.2 μm PTFE filters. The MALS photometer uses a vertically polarized He-Ne laser (wavelength λ=632.8 nm) and simultaneously measures the intensity of the scattered light at 18 angular locations ranging in chloroform solvent from 19.2° to 149.2°. It is well known that MALS is a quick and reliable technique for determining the molecular weight (M) and, when the angular dependence of the scattered light is experimentally measurable, also the molecular size generally known as radius of gyration (Rg). The MALS calibration constant was calculated using toluene as standard assuming a Rayleigh Factor of 1.406·10-5 cm-1. The normalization of the different photodiodes was performed by measuring the scattering intensity of a narrow molecular weight distribution (MWD) polystyrene standards (Mp=10.3 kg/mol, Mw/Mn=1.03, Rg=2.6 nm) in the solvent assumed to act as an isotropic scatterer. Details of the MALS photometer were described elsewhere.[62] The specific refractive index increment, dn/dc, of polymers with respect to the solvent at 25 °C of temperature was measured by a KMX-16 differential refractometer from LDC Milton Roy (Riviera Beach, FL, USA).

Pulse gradient spin echo (PGSE) spectroscopy: All the PGSE NMR measurements were performed by using the standard stimulated echo pulse sequence on a Brucker Avance DRX 400 spectrometer equipped with a Great 1/10 gradient unit and QNP probe with a Z-gradient coil, at 296K without spinning. The shape of the gradient was rectangular, their duration (δ) was 4-5 ms, and their strength was varied during the experiments. Different values of relaxtion time were used for different samples and ranging between 130 us and 900 us. The semi-logaririthmic plots of $\ln(I/I_0)$ vs G^2 were fitted using the linear regression for the thiophosphonate-cavitands TSiiii [($3C_3H_7$ +

CH_3-py^+ I^-), CH_3, Ph], TSiiii [($3C_3H_7$ + CH_3-py^+ PF_6^-), CH_3, Ph]**,** and the dimeric complex **1** and both linear and exponential fitting for the homopolymers Tiiii [($3C_3H_7$ + CH_3-py^+ $CF_3SO_3^-$), CH_3, Ph], and the homopolymer Tiiii [($3C_3H_7$ + CH_3-py^+ I^-), CH_3, Ph]. Different values of Δ, "nt" (number of transients) and number of different gradient strengths (G) were used for different samples. The diffusion coefficient D_t that is directly proportional to the slope of the regression line obtained plotting $\log(I/I_0)$ vs G^2 (eq 1), was estimated by measuring the proportional constant using a TMSS that is introduced as internal standard.[63]

	Homopolymer Tiiii[($3C_3H_7$ + CH_3-$Py^+CF_3SO_3^-$), CH_3, Ph]	**Host-guest dimer complex 1**
Formula	$C_{76}H_{74}F_3NO_{17}P_4S$	$C_{143}H_{142}NO_{22}P_8S_4$+$PF_6$+$3C_2H_3N$
Formula weight	1485.36	2861.64
Temperature	100 K	100 K
Wavelength	1.2 Å	1.5418 Å
Crystal system	Monoclinic	Monoclinic
Space Group	$P2_1/n$	$P2_1/a$
a/Å	26.3391±0.0015	15.9619±0.0011
b/Å	28.4212±0.0026	49.5064±0.0031
c/Å	27.2131±0.0020	21.2934±0.0009
α/°	90	90
β/°	111.6149±0.0039	107.0161±0.0039
γ/°	90	90
V/Å^3	18942.449	16089.47
Z	8	4
D_c/g cm^{-3}	1.327	1.181
F(000)	7786	5972
μ/mm^{-1}	0.79	1.955
$\theta_{min,max}$/°	1.55 31.43	1.78 – 36.30
Resolution	50.0 – 1.15 Å	50.0 – 1.30 Å
Reflections collected	379973	39524
Independent reflections	12912	7458
Observed Reflections [F_o>4σ(F_o)]	7530	4876
I/σ(I) (all data)	5	9.6
I/σ(I) (max resolution)	1.1	2.0
Completeness (all data)	99.4%	98.1%
Completeness (max resolution)	98.3%	90.1%
Multiplicity (all data)	7.2	3.8
Multiplicity (max resolution)	5.2	1.7
Data/restraint/parameters	12912/38/1734	7458/0/754
R[I>2.0σ(I)]	0.1479	0.1248
R(all data)	0.1772	0.1880
Goodness of fit	1.491	1.559

Table 9. Crystallographic data of dimeric complex 1 and the homopolymer Tiiii [($3C_3H_7$ + CH_3-py^+ $CF_3SO_3^-$), CH_3, Ph].

3.5 References

[1] J.-M. Lehn in *Supramolecular Science: Where It Is and Where It Is going (*Eds.: R. Ungaro, E. Dalcanale), Kluwer Academic Publishers, Dordrecht, **1999,** 287-304; J.-M. Lehn, *Chem. Eur. J.* **1999,** 5, 2455-2463.

[2] *Supramolecular Polymers* 2 nd ed. (Ed.: A. Cifferi), Taylor & Francis, New York, **2005.**

[3] a) a) H. Xu, D. M. Rudkevich, *Chem. Eur. J.* **2004,** 10, 5432-5442; b) T. Park, S. C. Zimmerman, *J. Am. Chem. Soc.*, **2006,** 128, 11582-11590.

[4] a) J.-P. Sauvage, *Chem. Rev.* **1994,** 94, 993-1019; b) I. Manners, *Angew. Chim. Int. Ed. Engl.* **1996**, 35, 1603-1621.

[5] a) M. Miyauchi, Y. Takashima, H. Yamaguchi, A. Harada, *J. Am. Chem. Soc.*, **2004,** 127, 2984-2989; b) V. H. S. Tellini, A. Jover, J. C. Garcia, L. Gallatini, F. Meijide, J. V. Tato, *J. Am. Chem. Soc.*, **2006,** 128, 5728-5734.

[6] a) N. Yamaguchi, H. W. Gibson, *Angew. Chem. Int. Ed.*, **1999,** 38, 143-147; b) E. N. Guidry, J. Li, F. Stoddart, R. H. Grubbs, *J. Am. Chem. Soc.* **2007,** 129, 8444-8945.

[7] T. Haino, Y. Matsumoto, Y. Fukazawa, *J. Am. Chem. Soc.*, **2005,** 127, 8936-8937.

[8] H. Ihm, J.-S. Ahm, M. S. Lah, Y. H. Ko, K. Paek, *Org. Lett.*, **2004,** 6, 3896.

[9] G. Fernàndez, E. M. Pérez, L. Sànchez, N. Martìn, *Angew. Chem. Int. Ed.*, **2007**, 46, 1-5.

[10] R. Pinalli, M. Suman, E. Dalcanale, *Eur. J. Org. Chem.*, **2004,** 3, 451-462.

[11] P. Delangle, J.-P. Dutasta, *Tetrahedron Lett.*, **1995,** 36, 9325-9328.

[12] a) P. Delangle, J.-C. Mulatier, B. Tinant, J.-P. Declercq, J.-P. Dutasta, *Eur. J. Org. Chem.*, **2001,** 19, 3695-3704; b) J.-P. Dutasta, *Top. Curr. Chem.*, **2004,** 232, 55-91.

[13] C. Fouquey, A.-M. Levelut, J.-M. Lehn, *Adv. Mater.* **1990,** 2, 254-257.

[14] F. H. Beijer, R. P. Sijbesma, H. Kooijman, A. L. Spek, E. W Meijer, *J. Am. Chem. Soc.*, **1998,** 120, 6761-6767.

[15] R. P. Sijbesma, F. H. Beijer, L. Brunsveld, B. L. Folmer, J. H. Hirschberg, R. F. Lange, J. K Lower, E. W. Meijer, *Science,* **1997,** 278, 1601-1604.

[16] B. J. B. Folmer, R. P. Sijbesma, R. M. Versteegen, J. A. J. v. d. Rijt, E. W. Meijer, *Adv. Mater.* **2000**, 12, 874-878.

[17] V. Bert, M. Schmutz, M. J. Krische, R. G. Khoury, J. –M. Lehn, *Chem. Eur. J.*, **2002,** 8, 1227-1244.

[18] S. Kelch, M. Rehahn, *Macromolecules*,**1998,** 31, 4102-4106.

[19] S. Schmatloch, M. Fernandez-Gonzàlez, U. S. Schubert, *Macromol. Rapid Commun.*, **2002,** 23, 957-961; b) H. Hofmeier, S. Smatloch, D. Wouters, U. S. Schubert, *Macromol. Chem. Phys.*, **2003,** 36, 9943-9949; c) S. Schmaloch, A. A. M. v. d. Berg, M. W. M. Fijen, U. S. Schubert, *Macromol. Rapid Commun.*, **2004**, 25,321-325.

[20] C.-F. Chow, S. Fujii, J. –M. Lehn, *Angew. Chem. Int. Ed.* **2007,** 46, 5007-5010.

[21] R. Stadler, M. A. D. Araujo, M. Kuhrau, J. Rösch, *Macromol. Chem.* **1989,** 190, 1433-1443; b) Y. Chujo, K. Sada, T. Saegusa, *Macromoles*, **1993,** 26, 6315-6319; c) Y. Chujo, K. Sada, T. Saegusa, *Macromoles*, **1993,** 26, 6320-6323.

[22] H. Hofmeier, U. S. Schubert, *Macromol. Chem.* **2003,** 204, 1391-1397.

[23] U. S. Schubert, H. Hofmeier, *Macromol. Rapid Commun.*, **2002**, 23, 561-566.

[24] R. K. Castellano, D. M. Rudkevich, J. Rebeck, *Proc. Natl. Acad. Sci. USA* **1997,** 94, 7132-7137.

[25] D. Garozzo, G. Gattuso, F. H. Kohnkes, A. Notti, S. Pappalaro, I. Pisagatti, A. J. P. white, D. J. Williams, M. F. Parisi, *Org. Lett.* **2003,** 22, 4025-4028.

[26] S. Pappalardo, V. Villari, S. Slovak, Y. Cohen, G. Gattuso, A. Notti, A. Pappalardo, I. Pisagatti, M. F. Parisi, *Chem. Eur. J.*, **2007**, 8164-8173.

[27] a) M. Miyauchi, Y. Takashima, H. Yamaguchi, A. Harada, *J. Am. Chem. Soc.***, 2005,** 127, 2984-2989; b) M. Miyauchi, T. Hoshino, H. Yamaguchi, S. Kamitori, A. Harada *J. Am. Chem. Soc.***, 2005,** 127, 2034-2035.

[28] H. Takahashi, Y. Takashima, H. Yamaguchi, A. Harada, *J. Org. Chem.*, **2006,** 76, 4878-4883.

[29] P. Kuad, A. Miyawaki, Y. Takasima, H. Yamaguchi, A. Harada, *J. Am. Chem. Soc.* **2007,** 42, 12630-12631.

[30] O. Félix, M. W. Hosseini, A. De Cian, J. Fischer, *Angew. Chem. Int. Ed. Engl.*, **1997,** 36, 102-104.

[31] a) M. C. Jiménez, C. Dietrich-Buchecker, J. P Sauvage, A. De Cian, *Angew. Chem.* **2000,** 112, 1351-1354; *Angew. Chem. Int. Ed.,* **2000,** 39, 1295-1298; b) T. Hoshino, M. Miyauchi, Y. Kawaguchi, H. Yamaguchi, A. Harada, *J. Am. Chem. Soc.* **2002,** 124, 9876-9877.

[32] F. Hauke, A. J. Myles, J. Rebek, Jr. *Chem. Commun.,* **2005,** 4164-4166.

[33] B. C. Gibb, R. G. Chapman, J. C. Sherman, *J. Org. Chem.,* **1996,** 61, 1505-1509.

[34] B. Bibal, B. Tinant, J.-P. Declercq, J.-P. Dutasta, *Chem. Commun.,* **2002**, 432-433

[35] a) A. Einstein, *Ann. Phys.* **1910,** 33, 1275 ; b) C. V. Raman, *Indian J. Phys,* **1927**, 2, 1 ; b) P. Debye, *J. Appl. Phys.* **1944,** 15, 338; c) B. H. Zimm, *J. Chem. Phys.,* **1945,** 13, 141; d) B. H. Zimm, *J. Chem. Phys.,* **1948,** 16, 1093.

[36] a) R. C. Oberthür, Makromol. Chem. **2003,** 36, 7857-7872; b) P. G. De Gennes, Scaling concepts in polymer physics, Cornell University Press, Ithaca, NY, **1979.**

[37] a) C. Leggio, M. Anselmi, A. Di Nola, L. Galantini, A. Jover, F. Meijide, N. V. Pavel, V. H. S. Tellini, J. V. Tato, *Macromolecules,* **2007,** 40, 5899-5906; b) Y. Lui, L. Li, H.-Y. Zhang, Y.-L. Zhao, X. Wu, *Macromolecules,***2002,** 35, 9934-9938.

[38] A. W. Bosman, R. P. Sijbesma, E. W. Meijer, *Material Today,* **2004,** 34-39**.**

[39] L. Brunsveld, B. J. B. Folmer, E. W. Meijer, R. P. Sijbesma, *Chem. Rev.,* **2001,** 101, 4071-4097.

[40] Bruce Martin, *Chem. Rev.,* **1996,** 96, 3043-3059.

[41] F. Garland, S. D. Christian, *J. Phys. Chem.* **1975,** 1247-1252.

[42] G. Amstrong, M. Buggy, *J. Mater. Sci.,* **2005,** 40, 547-559.

[43] a) W. Knoben, N. A. M. Besseling, L. Bouteiller, A. M. S. Cohen, *Phys. Chem. Chem. Phys.* **2005,** 7, 2390-2398; b) F. Lortier, S. Boileau, L. Bouteiller, C. Chassenieux, F. Lauprêtre, *Macromolecules,* **2005,** 38, 5283-5287 ; C) W. Knoben, N. A. M. Besseling, M. A. C. Stuart, *Macromolecules,* **2006,** 38, 2643-2653.

[44] R. De Zorzi, B. Dubessy, J.-C. Mulatier, S. Geremia, L. Randaccio, J.-P. Dutasta, *J. Org. Chem.,* **2007**, 72, 4528-4531.

[45] a) Xuo Lijing *PHD Thesis, Technische Universiteit Eindhoven,* **2005;** b) W. R. William, K.-Y. Beak, J.M.J Fréchet, I. B. Rietveld, S. A. Vinogradov, *Journal of Polymer Science,* **2006,** 44, 4939-4951; c) X.-H. Dai, C.-M. Dong, H.-B. Fa, D. Yan,

Y. Wei, *Biomacromolecules*, **2006,** 7, 3527-3533; d)) R. Hoogenboom, B. C. Moore, U. S. Schubert *Chem. Commun.* **2006,** 4010-4012.

[46] a) C. Slebodnick, H. W. Gibson, D. S. Negvekar, *J. Am. Chem. Soc.*, **2005,** 127, 484-485; b) R. Hoogenboom, B. C. Moore, U. S. Schubert, *Polymeric Materials: Science & Ingineering*, **2005,** 93, 873, c) R. Hoogenboom, B. C. Moore, U. S. Schubert, *Chem. Soc. Rev.*, **2005**, 35, 622-629; d) E. M. Todd, S. C. Zimmerman, *J. Am. Chem. Soc.*, **2007,** 129, 14534-14535.

[47] The molar ratio porphyrin: Tiiii [($3C_3H_7$ + CH_3-py^+ I^-), CH_3, Ph] 1:40 has been calculated considering: (i) an average degree of polymerization of 10 units in the concentration range 1.04-4.10 gL-1 of Tiiii [($3C_3H_7$ + CH_3-py^+ I^-), CH_3, Ph] employed (Figure 16) for the estimate of the number of end groups available for porphyrin complexation; (ii) a 1:4 porphyrin:end group stoichiometric ratio for the complexation.

[48] At higher concentrations, only partial solubilisation of the porphyrin has been obtained after six hours.

[49] a) L. Avram, Y. Cohen, *J. Am. Chem. Soc.*, **2002,** 124, 15148-15149; b) H. Ihre, A. Hult, E. So Derlind, *J. Am. Chem. Soc.* **1996,** 118, 6388-6395.

[50] a) E. O. Stejskal, J. E. Tanner, *J. Chem. Phys.* **1965,** 42, 288-292, b) P. Stilbs, *Prog. in Nucl. Magn. Reson. Spectrosc.* **1987,** 19, 1-45; c) W. S. Price *Concepts Magn. Rev.*, **1997,** 9, 299-336; d) W. S. Price *Concepts Magn. Rev.*, **1998,** 10, 197-231; e) Jr. C. S. Johnson, *Prog. Nucl. Magn. Res. Spectrosc.* **1999,** 34, 203-256; f) M. Valentini, H. Rüegger, P. S. Pregosin, *Helv. Chem. Act.* **2001,** 84, 2833-2853.

[51] a) A. Gierer, K. Z. Wirtz, *Naturforsch, A.* **1953**, 8, 522; b) A. Gierer, K. Z. Wirtz, *Naturforsch, A.* **1953**, 8, 532; c) H.-C Chen, S.-H. Chen, *J. Phys. Chem.* **1984,** 88, 5118-5123, d) J. T. Edward, *J. Chem. Educ.*, **1970,** 47, 261; e) A. Bondi, *J. Phys. Chem.* **1964,** 68, 441-448.

[52] a) C. Ihm, Y.-J. Ko, J.-H. Shin, K. Paek, *Tetrahedron Letters*, **2006,** 47, 8847-8850; b) Y. Hasegawa, M. Miyauchi, Y. Takashima, H. Yamaguchi, A. Harada, *Macromolecules*, **2005,** 38, 3724-3730.

[53] a) F. Perrin, *J. Phys. Radium (Paris)* **1934,** 5, 497-511; b) F. Perrin, *J. Phys. Radium (Paris)* **1936,** 7, 1-11.

[54] G. Ciancaleoni, Ilone De Maio, D. Zuccaccia, A. Macchioni, *Organometallics*, **2007,** 26, 489-496.

[55] a) E. Sauvage, N. Plucktaveesak, R. H. Colby, D. A. Amos, B. Antalek, K. M. Schroeder, J. S. Tan, *J. Pol. Science*, **2004,** 42, 3584-3597; b) E. Sauvage, N. Plucktaveesak, R. H. Colby, D. A. Amos, B. Antalek, K. M. Schroeder, J. S. Tan, *J. Pol. Science,*, **2004,** 42, 3571-3583; c) A. Yaghmur, A. Aserin, B. Antalek, N. Garti, *Langmuir*, **2003,** 19, 1063-1068, d) B. Antalek, J. M. Hewitt, W. Winding, P. D Yacobucci, T. Maurey, K. Le, *Magnetic Resonance in Chemistry*, **2002,** 40, S60-S71, e) B. Antalek, *Concepts in Magnetic Resonance*, **2002,** 14, 225-258, f) B. Antalek, *J. Am. Chem. Soc.* **2006,** 128, 8402-8403.

[56] a) A. Wong, *J. Am. Chem. Soc.*, **2005,** 127, 6990-6998; b) M. M. Troado, C. L. Matinez, J. Garcia de la Torre, *J. Chem. Phys.*, **1984,** 81, 2047-2052.

[57] M. E. Cates, *Macromolecules*, **1987,** 2289-2296.

[58] a) J. Tomayo, R. Garcia, *Langmuir*, **1996,** 12, 4430-4435; b) P. Samorì, V. Francke, K. Müllen, J. P. Rabe, *Chem. Eur. J.*, **1999,** 5, 2312-2317.

[59] J. L. Sessler, D. E. Gross, W. –S. Cho, V. M. Lynch, F. P. Schmidtchen, *J. Am. Chem. Soc.*, **2006,** 128, 12281-12288.

[60] J. March, (1985) *Advance Organic Chemistry*, Third Ed., Wiley-Interscience Publication, New York, **1985,** 353.

[61] a) Z. Otwinowski, W. Minor, Processing of X-ray Diffraction Data Collected in Oscillation Mode. Methods In Enzymology, **1997**, 276, 307-326; b) J. Navaza, Amore-an Automated Package for Molecular Replacement. Acte Crystallographica Section A, **1994,** 50, 157-163.

[62] a) R. Mendichi, A. G. Schieroni, *Current Trends in Polymer Science*, Pandalai S. G. Ed., TWR Network: Trivandrum India, **2001**, 6, 17-32; b) P. J. Wyatt, *Anal. Chim. Acta* **1993**, 272, 1-40

[63] a) M. Corti, V. Degiorgio, *Phys. Rev. Lett.* **1980,**, 45, 1045-1048, b) M. Corti, V. Degiorgio, *J. Phys. Chem.* **1981**, 85, 711-717.

Chapter 4

Self-assembly of Supramolecular Copolymers via Host-guest Interactions and Metal-coordination

4.1 Introduction

Biomolecules are characterized by a combination of different supramolecular interactions. These non-covalent binding sites are highly selective. Orthogonal supramolecular interactions describe non-covalent interactions that do not interfere with each other directly.[1] The combination of different orthogonal supramolecular binding units allows control of the self-assembly step, leading to well defined architectures presenting specific functionalities.

In contrast to biological systems, only few examples of synthetic supramolecular polymers that combine orthogonal supramolecular interactions are reported. Hydrogen-bonding and unidirectional electrostatic interactions between complementary units were combined in order to generate supramolecular polymers, but only in the solid state[2] (Figure 1).

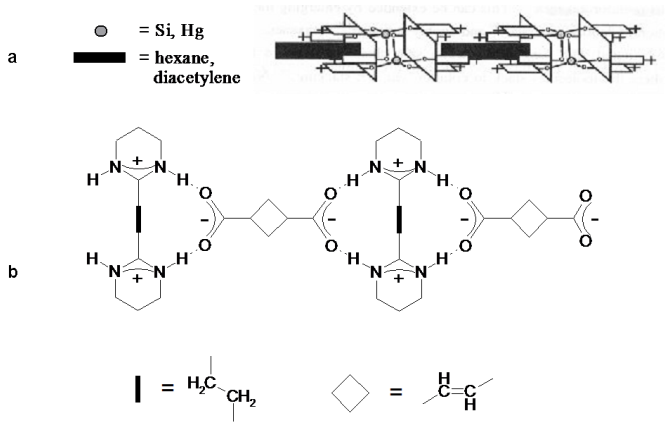

Figure 1. a) Presentation of a linear array formed by connection of biconcave receptors through convex molecules; b) Schematic representation of α-network between dicarboxylate di-anionic and di-cationic organic connectors through both electrostatic interactions and directionally controlled H-bonding.

Poly(norbonene) bearing hydrogen-bonding moieties as well as metal complex units in the side-chain were reported. The supramolecular cross-linked polymers (Figure 2), obtained by addition of a molecule containing complementary hydrogen-bonding units and a suitable metal find applications in high-impact corrosion resistant materials.[3]

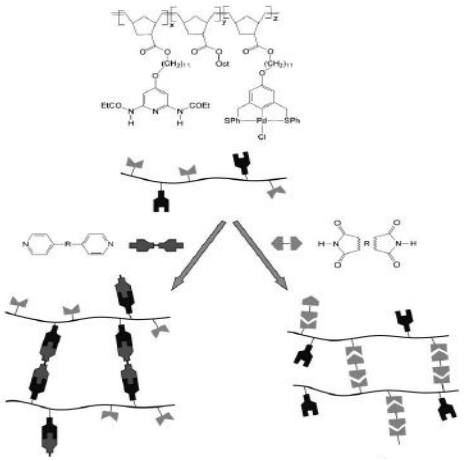

Figure 2. Cross-linked supramolecular polymer based on combination of hydrogen-bonding and metal-coordination interactions.

The group of Dalcanale reported a linear supramolecular oligomer that combines the metal-coordination of a pyridine system and the solvophobic interactions of quinoxaline kite cavitand[4] (Figure 3). Only oligomers have been observed due to the weakness of the solvophobic interactions with a $K_{ass} < 10^4$ M^{-1}.[5]

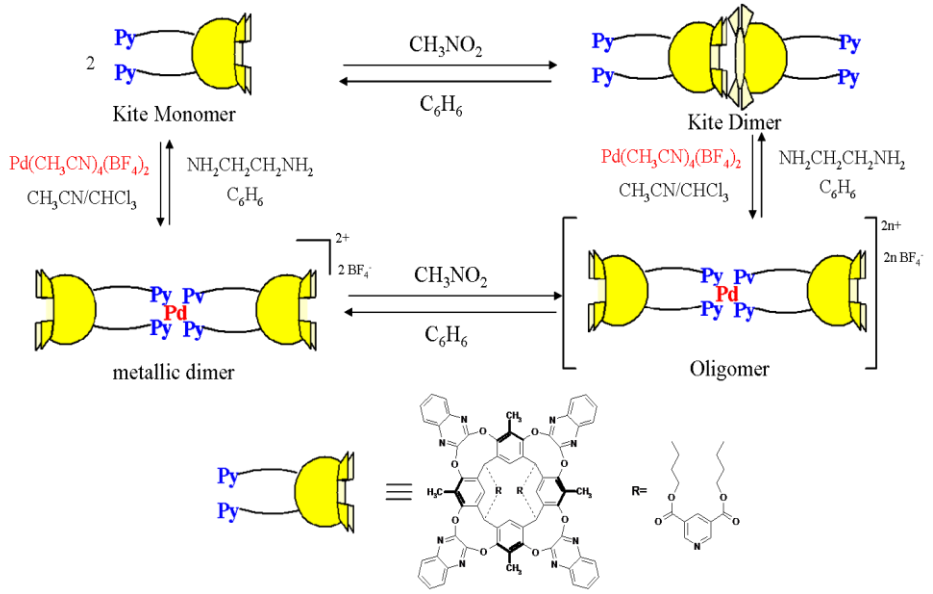

Figure 3. Supramolecular oligomer based on combination of solvophobic and metal-coordination interactions.

Biotin, one of the most prominent natural non-covalent binding units that forms stable complexes with the proteins avidin or streptavin as host structures with association constant $K_{ass} > 10^{15}$ M^{-1}, was combined with terpyridine moieties. A non polymeric as well as a polymeric poly (ethylene glycol) linker was used (Figure 4).[6] Such systems are suitable building blocks for the construction of functional nano-architectures for devices that find applications as biosensors.

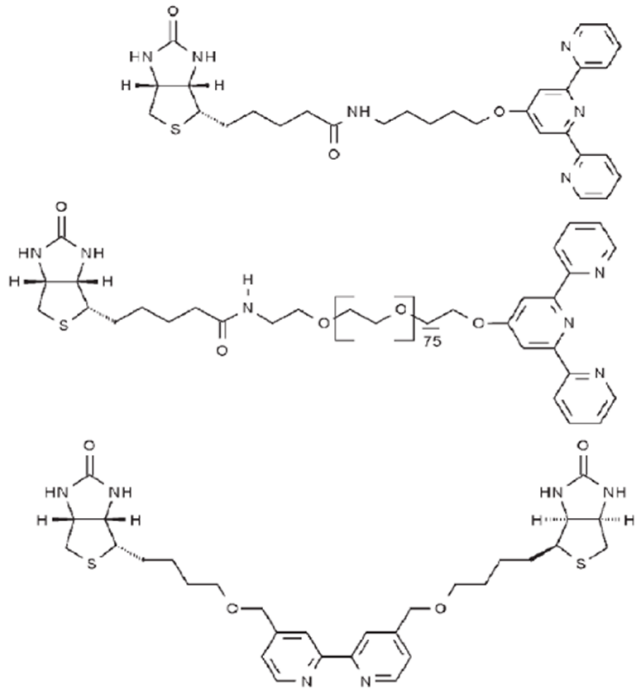

Figure 4. Molecules containing biotin groups and metal chelator.

4.2 Results and Discussion

In order to generate dynamic polymeric materials we designed and prepared functionalised cavitands capable of bimodal independent self-assembling interactions namely host-guest and metal coordination. Two are the systems chosen: i) the first one is a functionalized phosphonate-cavitand Tiiii[($3C_3H_7$ + Py), CH_3, Ph] that leads to reversible host-guest dimer **2** (Figure 5) by addition of ditopic guests, or reversible metal-coordinated dimer **3** (Figure 5) by addition of an appropriated metal. Combination of host- guest and metal-coordination, leads to reversible linear supramolecular copolymer **4** (Figure 5).

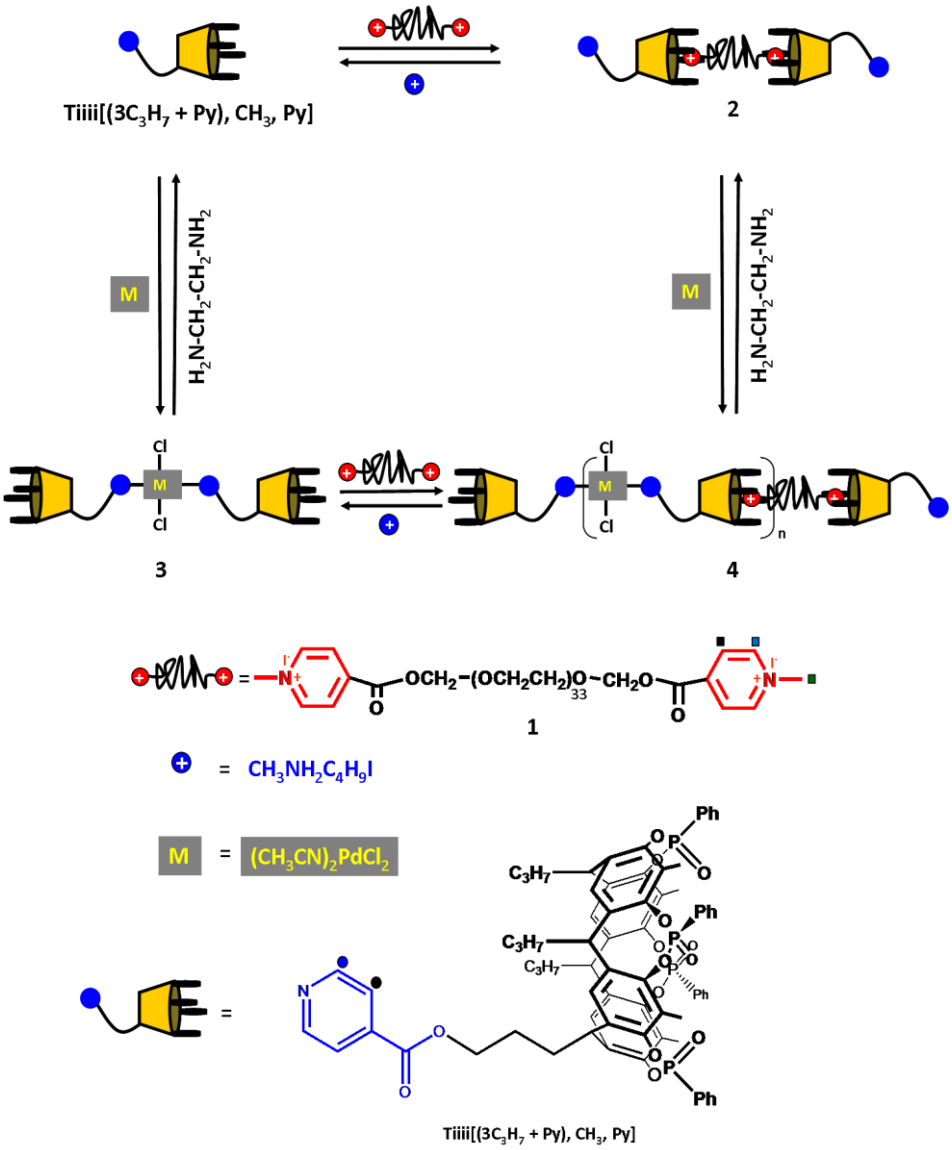

Figure 5. Bimodal self-assembly cycle of the cavitand Tiiii[(3C_3H_7 + Py), CH_3, Ph] to form linear supramolecular copolymers.

ii) The second one is a bis-cavitand Tiiii[C_3H_7, CH_3, Ph]-Py- [Ph, CH_3, C_3H_7]Tiiii that leads to linear reversible supramolecular polymer **6** by addition of a ditopic guest, and, in the presence of an appropriated metal, to cross-linked reversible supramolecular copolymer **7** (Figure 6).

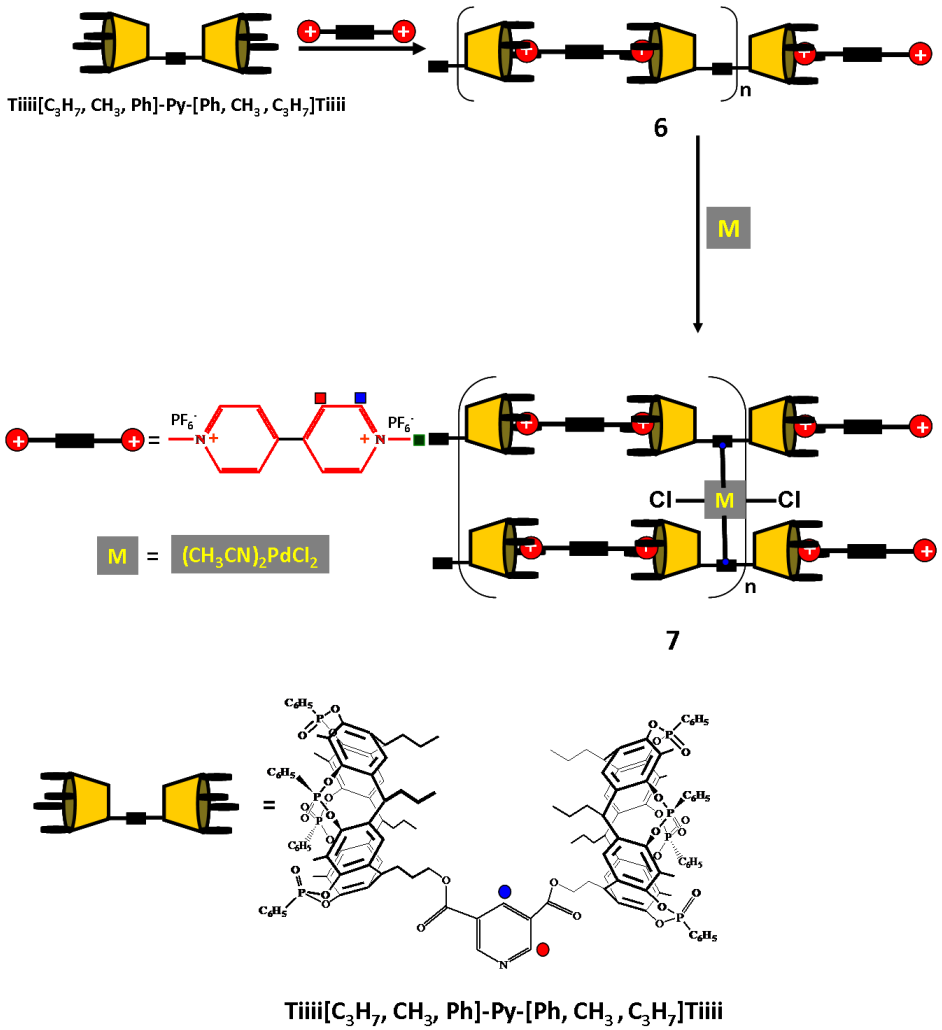

Figure 6. Cross-linked supramolecular copolymer based on bimodal self-assembly.

4.2.1 Synthesis of bis-cavitand Tiiii[C_3H_7, CH_3, Ph]-Py-[Ph, CH_3, C_3H_7]Tiiii and ditopic guest 1.

The preparation of cavitand Tiiii[(3C_3H_7 + Py), CH_3, Ph] is reported in Chapter 3.

The ditopic guest **1** has been obtained by esterification reaction of the polyethylene glycol (Mn = 1500 Da) with isonicotinoyl chloride hydrochloride followed by methylation reaction of the pyridine moieties with methyl iodide (see experimental part).

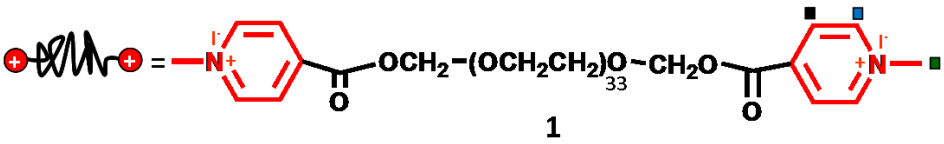

1

In order to obtain the target molecule Tiiii[C_3H_7, CH_3, Ph]-Py-[Ph, CH_3, C_3H_7]Tiiii (Figure 6), we devised a five steps synthetic procedure.

Synthesis of the starting resorcinarene and upper rim functionalization. The syntheses of the starting resorcinarene and the upper rim protection (Scheme 1) have been reported in the Chapter 3.

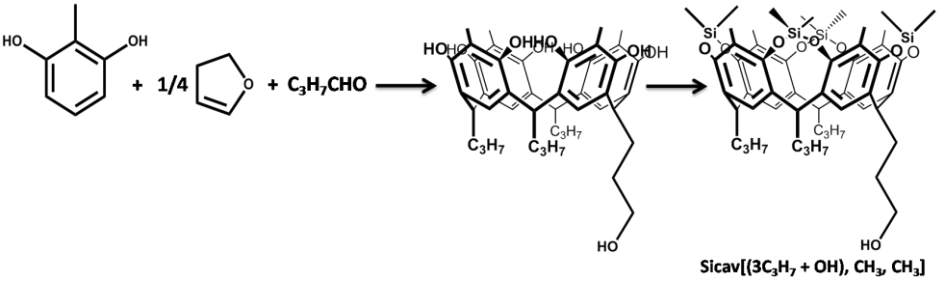

Scheme 1. Syntheses of the mono-hydroxyl-footed resorcinarene and the cavitand Sicav[(3C_3H_7 + OH), CH_3, CH_3].

Dimerization of silyl-cavitand Sicav[($3C_3H_7$ + OH), CH_3, CH_3] . In order to work out the best reaction conditions for the introduction of the pyridine linker group between two cavitands, we performed an esterification reaction with 3,5-pyridinedicarboxylic acid in a mixture 1:6 of DMF/CH_2Cl_2 in the presence of DCC (1,3-dichlohexylcarbodiimide) and DMAP (4-dimethylaminopyridine) (Scheme 2) as promoters and catalyst. The DMF is necessary to dissolve the 3,5-pyridinedicarboxylic acid. After purification by column chromatography, the bis-cavitand Sicav[C_3H_7, CH_3, CH_3]-Py-[CH_3, CH_3, C_3H_7]cavSi was isolated in 42% yield.

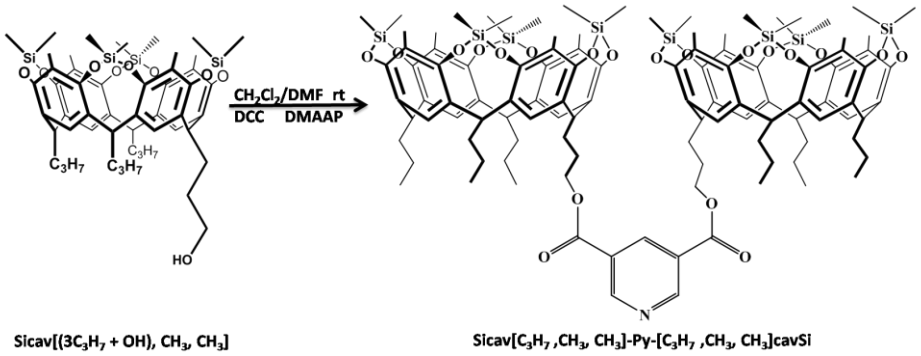

Scheme 2. Dimerization process.

Upper rim deprotection. The breaking of the silyl-bridged occurs by adding a water solution of HF to the solution of bis-cavitand Sicav[C_3H_7, CH_3, CH_3]-Py-[CH_3, CH_3, C_3H_7,]cavSi in DMF. The reaction yields quantitatively the bis-resorcinarene **5** (Scheme 3).

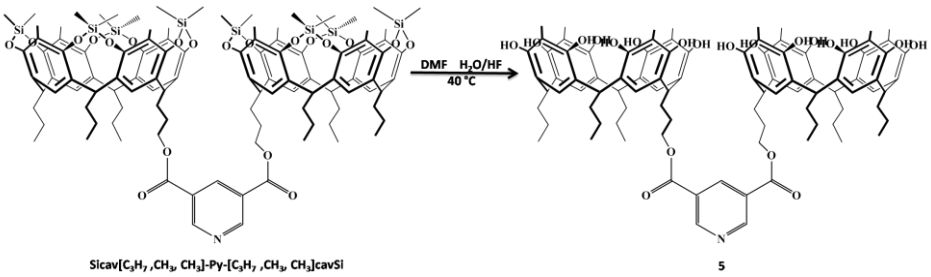

Scheme 3. Upper rim deprotection.

Upper rim functionalization. The new procedure described in Chapter 2 has been used to introduce phosphonate groups at the upper of the bis-resorcinarene **5** following the two steps synthesis in Scheme 4. The first step requires the reaction of the bis-resorcinarene **5** with 8.2 equivalents of dichlorophenylphosphine in dry pyridine. The progress of the reaction has been monitored via ^{31}P NMR. The reaction affords the bis-phosphonito-cavitand **5a** which, after cooling to room temperature, undergoes in a second step, an in situ oxidation by adding an excess of a solution of H_2O_2 and chloroform (Scheme 4). The reaction affords the bis-cavitand Tiiii[C_3H_7, CH_3, Ph]-Py- [Ph, CH_3, C_3H_7] Tiiii in 90% yield. All eight P=O bridges are orientated inward.

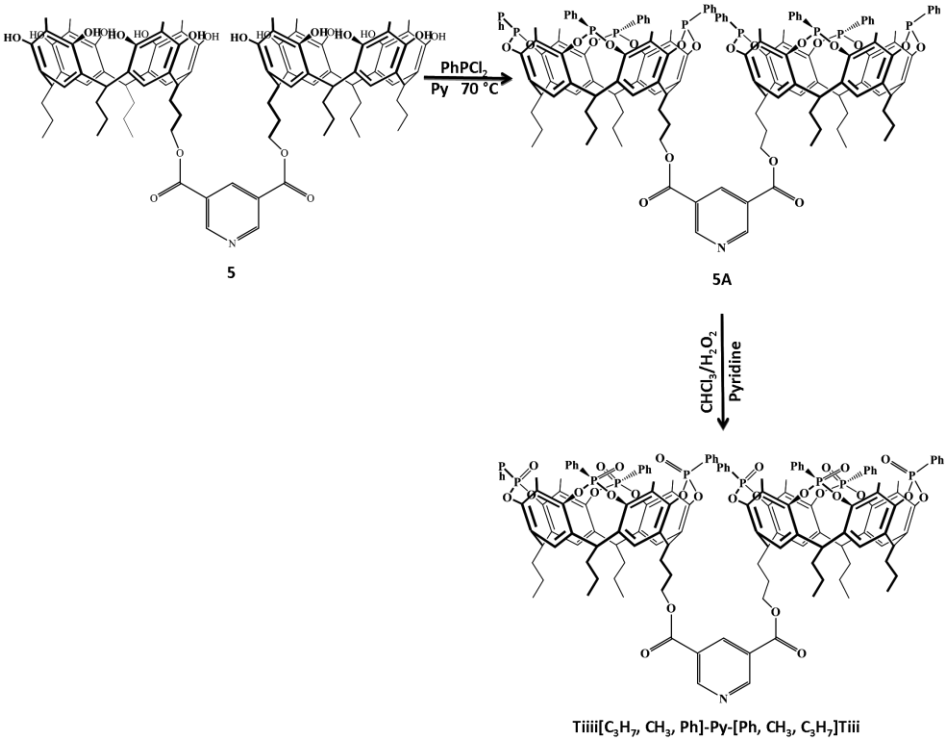

Scheme 4. Upper rim functionalization.

4.2.2 Linear Supramolecular Copolymer from Host-guest and Metal-coordination Interactions.

As shown in Figure 5, cavitand Tiiii[($3C_3H_7$ + Py), CH_3, Ph] bears two independent binding sites. The first one is the phosphonate-cavity that recognises ammonium and methyl-pyridinium salts with high association constants $K_{ass} > 10^7$ (see Chapter 2). The second binding site is the pyridine moiety that acts as ligand in the presence of a suitable metal.

4.2.2.1 Host-guest-driven dimerization of the cavitand Tiiii[(3C_3H_7 + Py), CH_3, Ph]

The dimerization process occurs spontaneously by adding 0.5 equivalents of the ditopic guest **1** to a solution of Tiiii[(3C_3H_7 + Py), CH_3, Ph] in $CDCl_3$. The choice of $CDCl_3$ is due to the high association constants recorded in chlorinated solvents (see Chapter 2).

The host-guest dimerization process was monitored via ^{1}H NMR. The large up-field shift of methyl-pyridinium signals of the ditopic guest (green, blue, and black squares) and the slight down-field shift of the host protons at the ^{1}H NMR (Figure 7) confirm the formation of the host guest dimeric complex. It is interesting to observe that, the ^{1}H NMR signals of the pyridine moiety of the cavitand Tiiii[(3C_3H_7 + Py), CH_3, Ph] do not change upon complexation. This indicates the independence of the two binding sites.

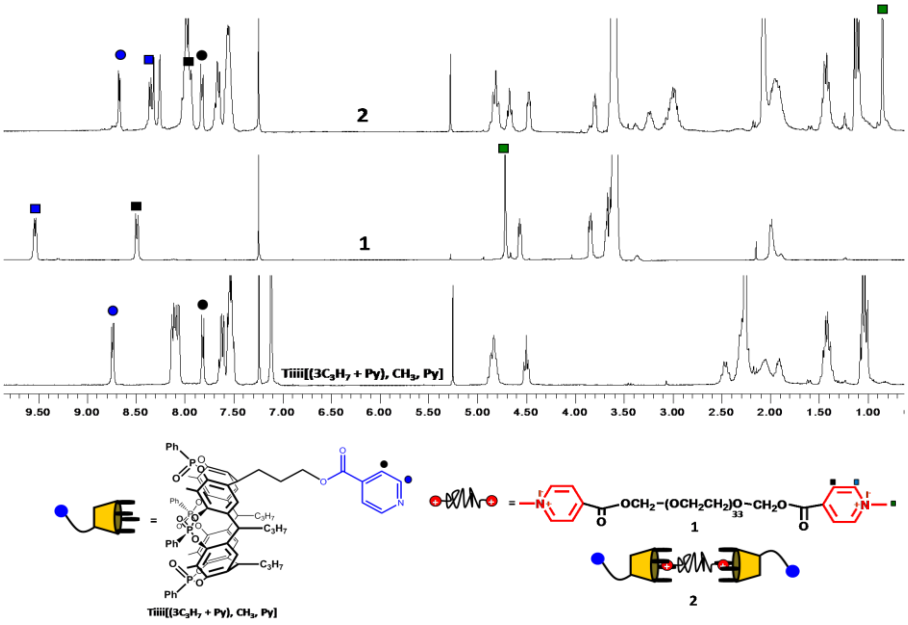

Figure 7. Host-guest dimerization monitored via ^{1}H NMR in $CDCl_3$.

The Figure 8 shows the host-guest dimerization process monitored via ^{31}P NMR. The down-field shift from 4.28 ppm to 7.83 ppm of the phosphorous signals of the cavity (Figure 8) confirms the inclusion of the methyl pyridinium moiety inside the cavity and then the formation of the host-guest dimeric complex.

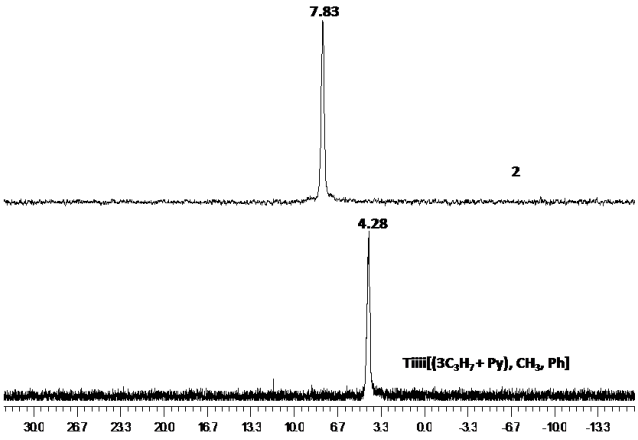

Figure 8. Host-guest dimerization process monitored via ^{31}P NMR in $CDCl_3$.

4.2.2.2 Metal-directed dimerization of the cavitand Tiiii[(3C$_3$H$_7$ + Py), CH$_3$, Ph]

As second interaction mode, we exploited the pyridine foot at the lower rim of cavitand Tiiii[($3C_3H_7$ + Py), CH_3, Ph] which, in the presence of an appropriated metal, led to the dimerization process through metal-coordination. We chose $(CH_3CN)_2PdCl_2$ as metal complex for the metal-dimerization of the cavitand Tiiii[($3C_3H_7$ + Py), CH_3, Ph], for two reasons: i) the very easy exchange of the two acetonitrile of the metal complex with two pyridine of two cavitand.[7] ii) The trans effect of the pyridine ligand that leads to the desire trans geometry[7,8] of the metallic-

dimer complex. The dimerization process was monitored via ^{1}H NMR that showed the typical low down-field shift of the pyridine signals indicating the coordination to the Pd center (Figure 9).

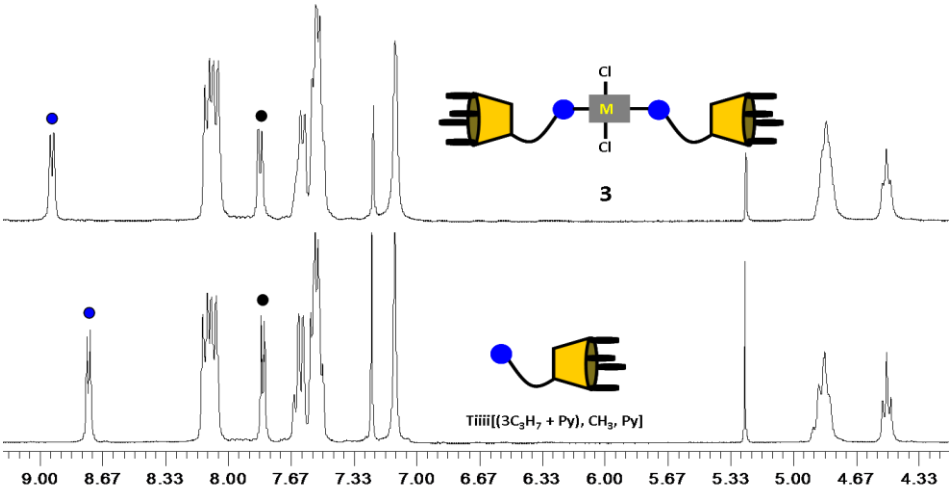

Figure 9. Metal-directed dimerization monitored via ^{1}H NMR in $CDCl_3$.

In order to verify the non inclusion of the metal inside the cavity, the ^{31}P NMR was performed (Figure 10). The stability of the position of the phosphorous signal upon metal-driven dimerization process demonstrates that, the cavity do not interfere with the metal-coordination process.

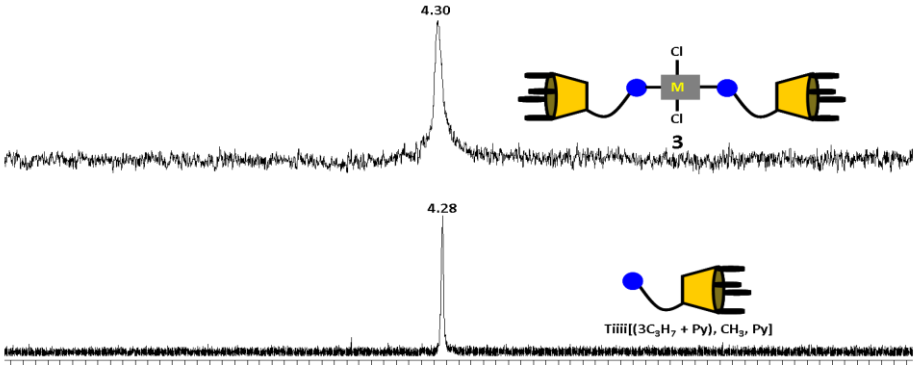

Figure 10. Metal-directed dimerization monitored via ^{31}P NMR in $CDCl_3$.

4.2.2.3 Host-guest dimerization followed by metal-directed polymerization

In order to obtain a supramolecular polymer, the two independent interactions are combined.

We started by making the host-guest dimerization process followed by metal-coordination that led to the polymerization process (Figure 11). This process was monitored via ^{1}H NMR (Figure 11A) that shows the characteristic up-field shift of the methyl-pyridinium signals of the ditopic guest, followed by down-field shift of the pyridine signals of the cavitand Tiiii[($3C_3H_7$ + Py), CH_3, Ph] by adding 0.5 equivalents of the metal complex precursor. While the ^{31}P NMR (Figure 11B) shows the characteristic down-field shift of the phosphorous signals indicating that the host-guest dimerization occurs, and no change is observed by adding the metal precursor. This fact confirms the orthogonality of the two interactions. The broadening of the proton signals after addition of the metal, demonstrated the occurred polymerization process.

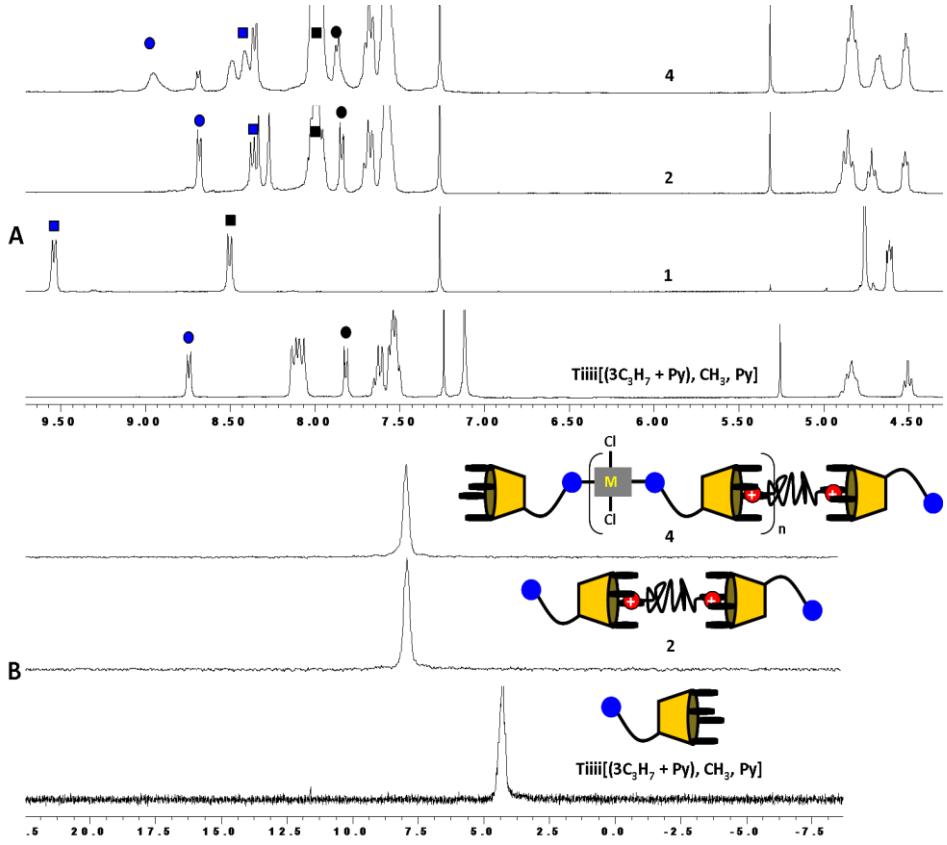

Figure 11. Host-guest dimerization followed by metal-directed polymerization monitored via ^{1}H NMR and ^{31}P NMR in $CDCl_3$.

4.2.2.4 Metal-directed dimerization followed by host-guest polymerization

In another experiment, the reverse ordering of the assembly steps is followed: 1) metal-directed dimerization; 2) host-guest polymerization. Also in this case the experiment was monitored via ^{31}H NMR (Figure 12A) and the characteristic down-field shift of the pyridine signals was observed, while no change occurred by observing the ^{31}P NMR spectrum (Figure 12B). Addition of 0.5 equivalents of ditopic guest, led to the

polymerization confirmed by the broadening of the signals, and the remarkable up-field shift of the methyl pyridinium signal in the ^{1}H NMR spectrum, as well as the down-field shift of the phosphorous signal in the ^{31}P NMR spectrum.

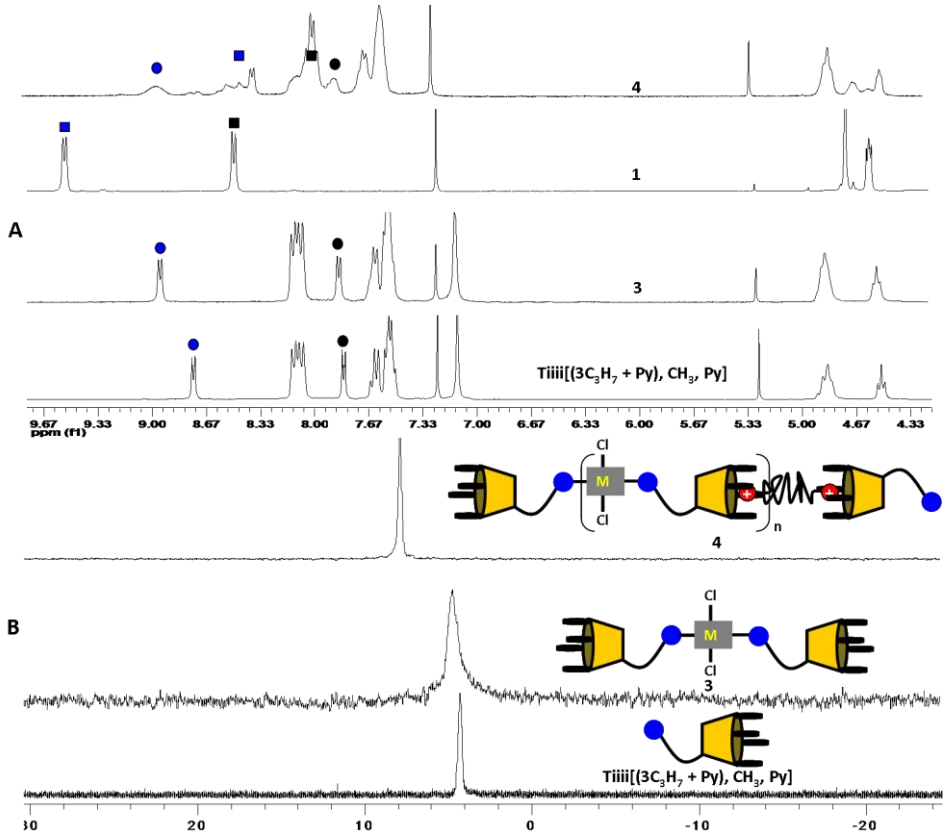

Figure 12. Metal-directed dimerization followed by host-guest polymerization monitored via ^{1}H NMR and ^{31}P NMR in $CDCl_3$.

4.2.2.5 Metal-directed depolymerimerization

In this experiment, one equivalent of a competitive ligand is added to a solution of the polymer **4** to disassemble it.

Addition of ethylenediamine to copolymer **4** as competitive ligand led to the disassembly of the metal connection, leaving dimer **2** (Figure 13B). This experiment proves that the assembly of copolymer **4** is reversible and then the two interactions connecting the monomer units of **4** are completely orthogonal.

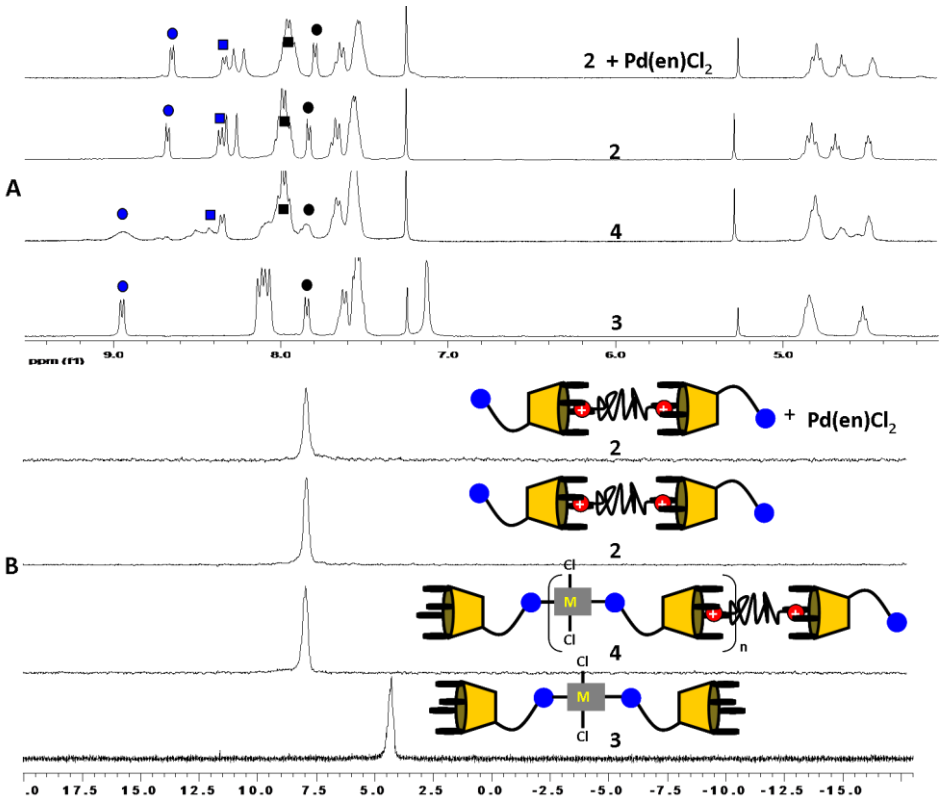

Figure 13. Metal-directed disassembly of the copolymer 4 monitored via ^{1}H NMR and ^{31}P NMR in $CDCl_3$.

The reversible self-assembly via breaking of host-guest interactions first is in progress. The molecular weight characterization of copolymer **4** via PGSE spectroscopy, DLS, SLS, and viscosimetry is in progress.

4.2.3 Cross-linked polymer via Host-guest interactions followed by Metal-coordination.

Cross-linking is a powerful tool to improve the chemical, physical, and mechanical properties of the polymers.[9] Supramolecular polymers capable of reversible cross-linking are extremely interesting for their potential self-healing properties.

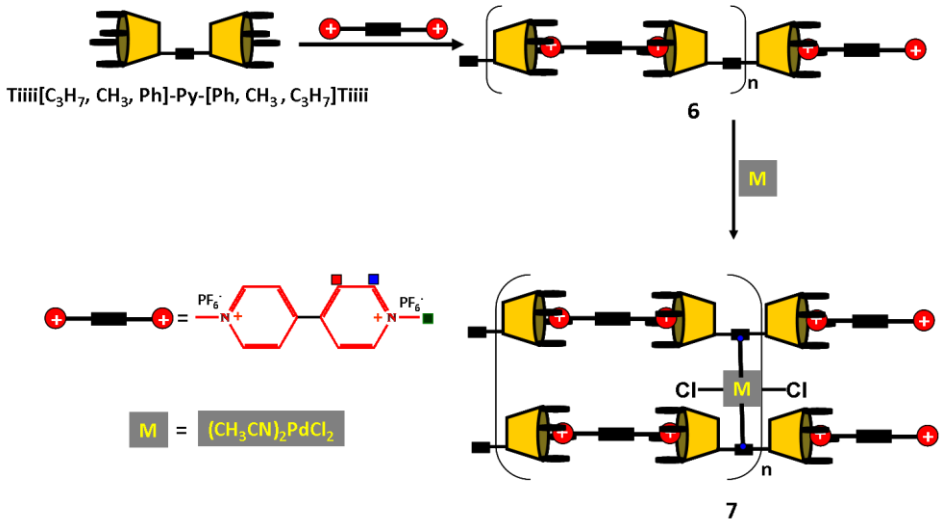

Figure 14. Host-guest polymerization followed by metal-coordinated cross-linking.

To this purpose we designed and synthesized a monomer unit able to generate linear supramolecular polymers via host-guest interactions, followed by cross-linking between the polymeric chains directed by metal-coordination. Such monomer is the bis-cavitand Tiiii[C_3H_7, CH_3, Ph]-Py-[Ph, CH_3, C_3H_7]Tiiii that can polymerize in the presence of

ditopic guests leading to a linear supramolecular architecture. Such architecture undergoes cross-linking through metal-coordination (Figure 14).

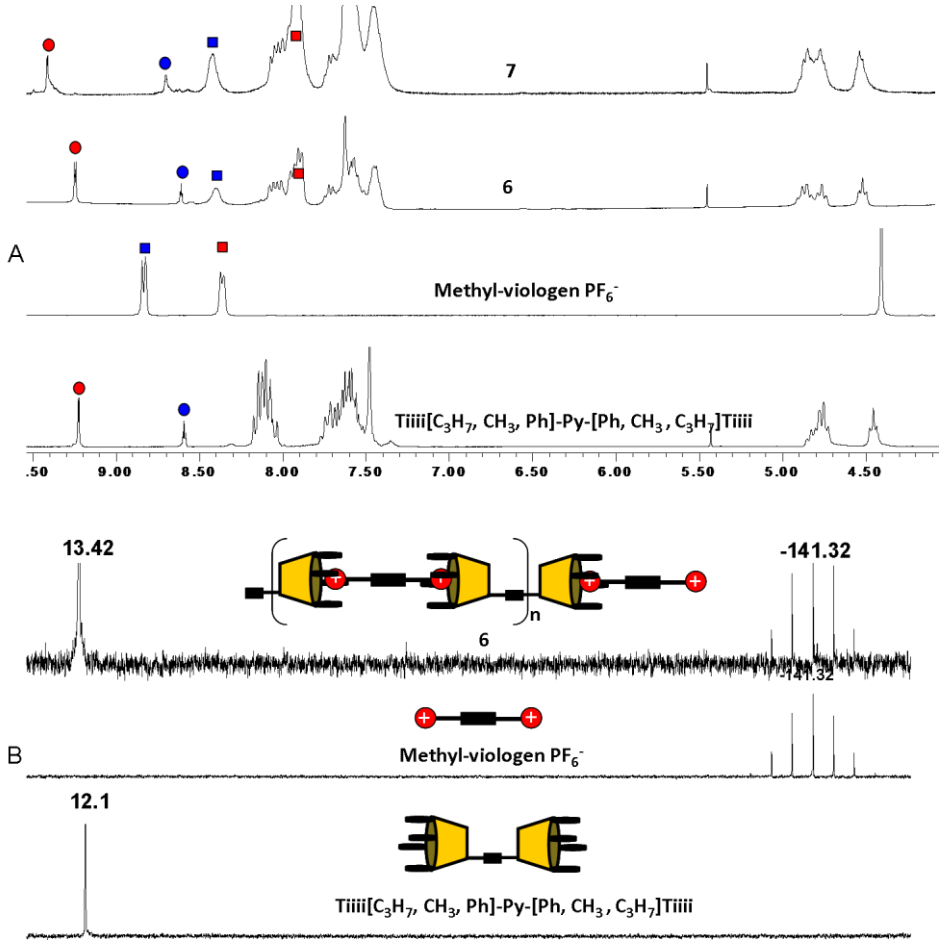

Figure 15. Host Guest polymerization, followed by metal-directed cross-linking monitored by ^{1}H NMR and ^{31}P NMR in CD_3CN.

Owing to the low solubility of the methyl viologen in apolar solvents, we used acetonitrile as solvent to perform this experiment. The ^{1}H NMR spectra, shows the up-field shift of methyl-pyridinium signals, and the

down-field shift of the aromatic signals of the cavity (Figure 15A), while the ^{31}P NMR displays the classical down-field shift of the phosphorous signal (Figure 15B). Such shift confirms the inclusion of the methyl viologen guest inside the cavity in a polar and competitive solvent. The broadening of the signals after addition of the ditopic guest indicates the formation of oligomeric/polymeric species. The addition of $(CH_3CN)_2PdCl_2$ led to the typical down-field shift of the pyridine signals that links together two cavitands (Figure 15A), cross-linking the polymer-chains. The extension of the polymer network is confirmed by the further broadening of the signals at the ^1H NMR (Figure 15A).

Because of the conformational freedom of the pyridine bi-carboxylate moiety that links together the two cavitands in the bis-cavitand Tiiii[C_3H_7, CH_3, Ph]-Py-[Ph, CH_3, C_3H_7]Tiiii, and the rigidity of the methyl viologen, the formation of the host-guest tetrameric complex by adding methyl viologen to a solution of bis-cavitand Tiiii[C_3H_7, CH_3, Ph]-Py-[Ph, CH_3, C_3H_7]Tiiii could not be excluded (Figure 16).

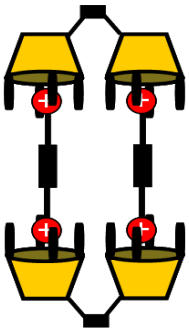

Figure 16. Host-guest tetrameric complex from a mixture 1:1 of bis-cavitand Tiiii[C_3H_7, CH_3, Ph]-Py-[Ph, CH_3, C_3H_7]Tiiii and methyl viologen.

In collaboration with Prof. Geremia of the university of Trieste, a mixture 1:1 of bis-cavitand Tiiii[C_3H_7, CH_3, Ph]-Py-[Ph, CH_3, C_3H_7]Tiiii, and methyl viologen hexafluorophosphate was crystallized from a mixture 9:1 of acetonitrile and water and the crystal structure was solved.

The X-ray analysis clearly shows the formation of linear polymeric chains in which monomer units are held together by ion-dipole and CH-π interactions (Figure 18). A section of the crystal packing clearly shows the eight P=O groups that points inside the cavity, making ion-dipole interactions with the positive charged nitrogen of methyl viologen guest, and the average distance N^+-O=P measured is 3.04 ± 0.03 (green arrows Figure 17). The CH-π interactions between the CH protons of the methyl viologen guest and the π electrons of the aromatic rings of the cavity were investigated. The average distance between the protons of the CH_3 of the methyl viologen and the plane of the aromatic rings is 3.6 ± 0.02 (blue arrows Figure 17).

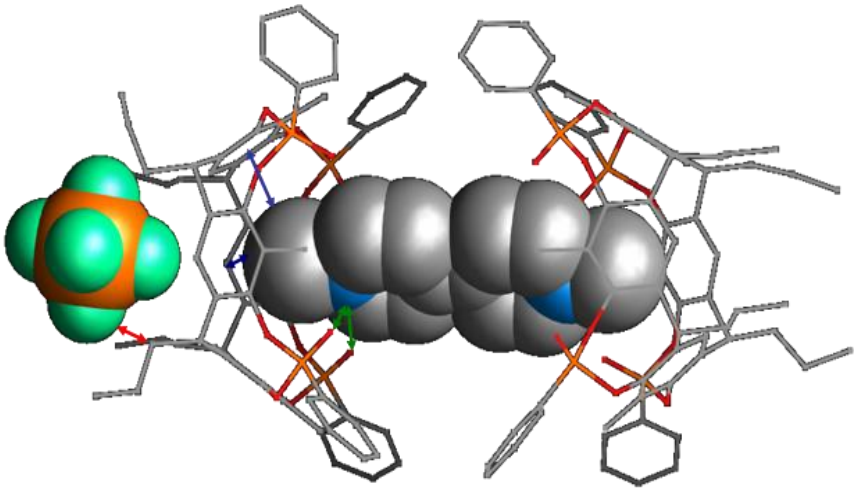

Figure 17. Section of the linear polymer that shows ion-dipole, CH-π and the fitting of the counterion among the alkyl chains of the cavitands.

The PF_6^- counterion fits among the alkyl chains at the lower rim of the cavitands interacting with them (red arrows) and a P-F bond points toward the center of the cavity stabilizing the ion pair with the complexed methyl pyridinium moiety.

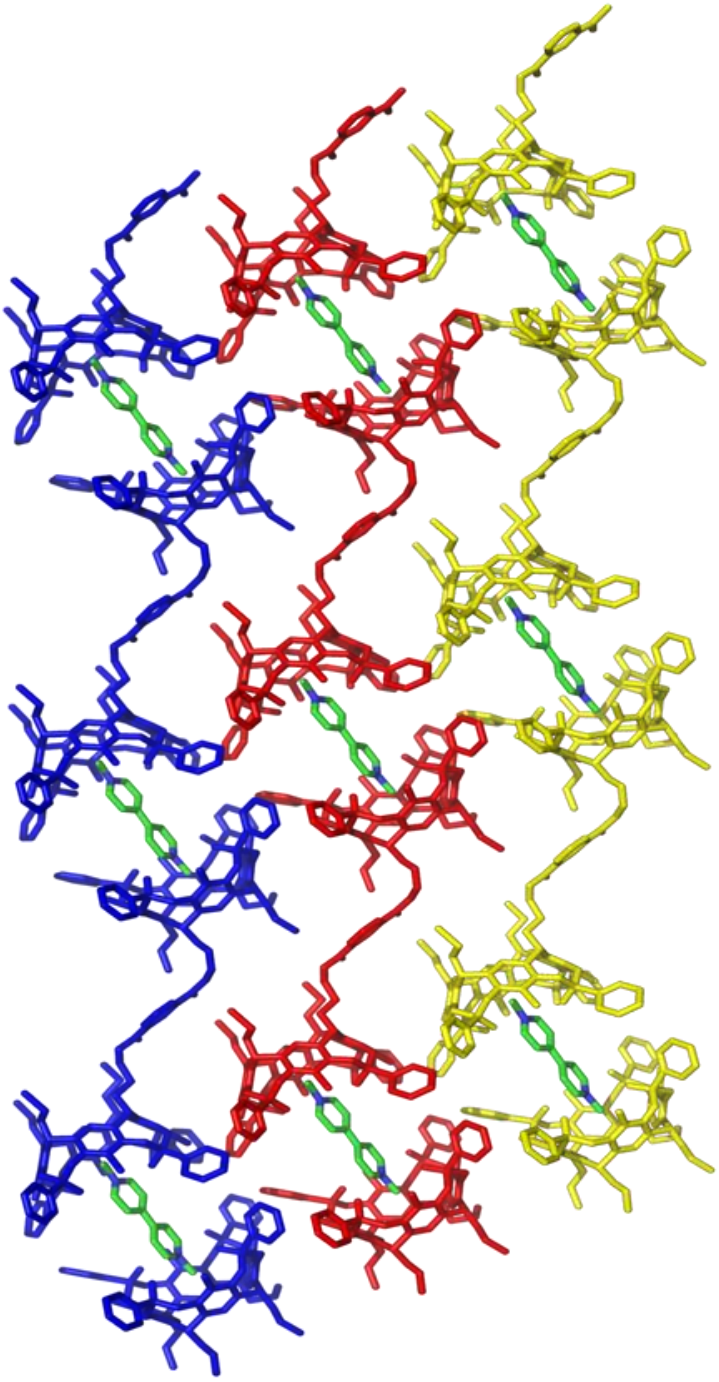

Figure 18. X-ray crystal structure of the linear supramolecular copolymer 6.

4.3 Conclusions

We designed and synthesized molecules able to self-assemble through combination of orthogonal host-guest and metal-coordination interactions. Linear and cross-linked supramolecular copolymers were obtained monitoring the polymerization process via ^{1}H NMR and ^{31}P NMR. The interaction modes employed are fully orthogonal to each other and completely reversible. These two properties make this class of linear and cross-linked copolymers attractive for the emerging field of self-healing polymers. We are now performing molecular weight characterization studies of these systems via PGSE, DLS, and SLS.

4.4 Experimental section

General Method: All reagents were purchased from Sigma-Aldrich Co. All solvents were dried over 3Å and 4Å molecular sieves by standard procedures. Pyridine was distilled on potassium hydroxide and dried over 3Å molecular sieves. ^{1}H NMR spectra were recorded at Bruker AC300 (300 MHz), AVANCE (300 MHz) and AMX400 (400 MHz) spectrometers and all chemical shift (δ) were reported in parts per million (ppm) relative to the proton resonances resulting from incomplete deuteration of the NMR solvents. Microanalyses were performed by the service of Parma University. Electrospray ionization (ESI)-MS experiments were performed on a Waters ZMD spectrometer equipped with an electrospray interface. Column chromatography was performed using silica gel 60 (Merck 70-230 mesh) equipped with.

Synthesis 1A: to a solution of isonicotinoyl chloride hydrochloride (0.6 g, 3.4 mmol) dissolved in dry pyridine, PEG (PM = 1500) (1.26g, 0.84 mmol) was added. The reaction mixture was stirred at 100 °C for 3h and the solvent was removed under vacuum. 20 mL of a solution of potassium carbonate in water were added and extracted with methylene chloride. The crude reaction crystallized from diethyl ether at 0 °C and filtered maintaining low temperature yielded **1A** (1.3 g, 0.71 mmol, 85%).

^{1}H NMR (300 MHz, $CDCl_3$) δ (ppm): 3.6 (broad, 62H, O(**CH_2CH_2**O)$_{31}$), 3.8 (t, 4H, OOCCH_2**CH_2**, J = 4.7 Hz), 4.4 (t, 4H, OOC**CH_2**, J = 4.7 Hz), 7.8 (d, 2H, **H_{mPy}**, J =5.9 Hz), 8.7 (d, 2H, **H_{oPy}**, J =5.9 Hz). **ESI-MS:** $C_{82}H_{148}N_2O_{39}$: 1786.7 (M^+).

Synthesis of the ditopic guest 1: to a solution of **1A** (0.75 g, 0.42 mmol) dissolved in acetonitrile, CH_3I (0.26 mL, 4.22 mmol) was added. The reaction mixture was stirred at reflux overnight. The solvent was removed and the gel obtained was purified by crystallisation from a cooled mixture 3:7 of acetonitrile and ethyl ether yielding **1A** (0.73 g, 0.35 mmol, 84%).

^{1}H NMR (300 MHz, $CDCl_3$) δ (ppm): 3.62 (broad, 62H, O(**CH_2CH_2**O)$_{31}$), 3.86 (t, 4H, OOCCH_2**CH_2**, J = 4.8 Hz), 4.6 (t, 4H, OOC**CH_2**, J = 4.8 Hz), 5.3 (s, 6H, **CH_{3py}**), 8.52 (d, 2H, **H_{mPy}**, J = 6.5 Hz), 9.53 (d, 2H, **H_{oPy}**, J = 6.5 Hz). **ESI-MS:** $C_{84}H_{154}N_2O_{39}I_2$: 2069.7 $(M\text{-}I^-)^+$.

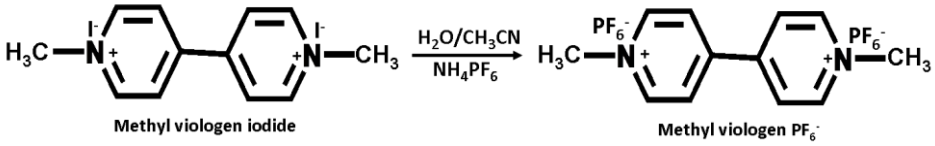

Synthesis of methyl viologen iodide: to a solution of 2,2-bipyridine (0.7 g, 4.5 mmol) dissolved in 25 mL of acetonitrile, methyl iodide (1.4 mL, 22.4 mmol) was added and the solution heated to reflux over night. The solvent was removed and the product was purified by crystallization from a mixture 8:2 methylene choride and acetotonitrile yielding the product (1.85 g, 4.23 mmol, 94%).

^{1}H NMR (300 MHz, DMSO-d_6) δ (ppm): 4.4 (s, 6H, **CH_{3py}**), 8.8 (d, 4H, **H_{mPy}**, J = 6.7 Hz), 9.3 (d, 4H, **H_{oPy}**, J = 6.7 Hz). **ESI-MS:** $C_{12}H_{14}F_{12}N_2$. 313.2 $(M\text{-}I^-)^+$, 186.1 $(M\text{-}2I^-)^{2+}$.

Synthesis of methyl viologen hexafluorophosphate: to a solution of methyl viologen iodide (1.7 g, 3.87 mmol) dissolved in 6 mL of H_2O, ammonium hexafluorophosphate (1.6 mL, 9.7 mmol) was added. The yellow suspension formed was stirred until became white and then, it was filtered and washed with an excess of water. Purification by crystallization from a mixture 9:1 water and acetonitrile gave the product (1.77 g, 3.7 mmol, 96%).

^{1}H NMR (300 MHz, CD_3CN) δ (ppm): 4.38 (s, 6H, **CH_{3py}**), 8.36 (d, 4H, **H_{mPy}**, J = 6.6 Hz), 8.8 (d, 4H, **H_{oPy}**, J = 6.6 Hz). **^{31}P NMR** (172 MHz, CD_3CN): -141.1 (m, **PF_6^-**, $J_{P\text{-}F}$ = 752 Hz). **ESI-MS:** $C_{12}H_{14}F_{12}N_2P$. 313.5 $(M\text{-}PF_6^-)^+$, 186.1 $(M\text{-}2PF_6^-)^{2+}$.

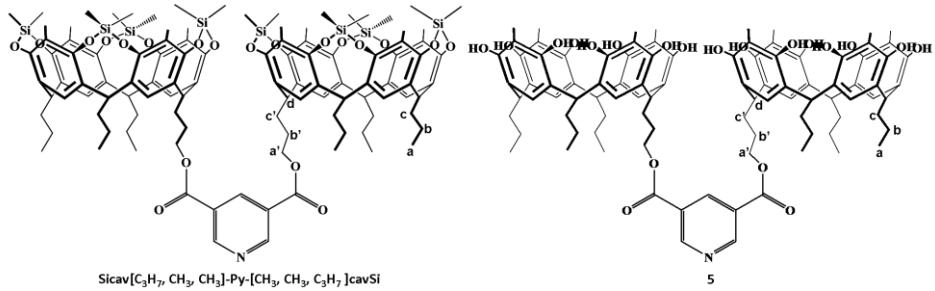

Synthesis of bis-cavitand Sicav[C_3H_7, CH_3, CH_3]-Py-[CH_3, CH_3, C_3H_7]cavSi: to a solution of 3,5-pyridinedicarboxylic acid (0.022 g, 0.13 mmol) dissolved in 9 mL of a dry mixture 1:8 of DMF and CH_2Cl_2, DCC (0.054 g, 0.26 mmol) and DMAP (0.01 g, 0.087 mmol) were added. The resulting suspension was stirred at room temperature

until complete dissolution. Silyl-bridged cavitand Sicav[($3C_3H_7$ + OH), CH_3, CH_3] (0.25 g, 0.26 mmol) was added. The reaction mixture was stirred at room temperature for 24 h and the solvent was removed. 10 mL of water were added and the resulting suspension was filtered. Purification by column chromatography on silica gel from a mixture 99:1 of CH_2Cl_2 and C_2H_5OH as eluant yielded the desired product (0.22 g, 0.11 mmol, 42%).

^{1}H NMR (300 MHz, $CDCl_3$) δ (ppm): -0.68 (s, 24H, **$CH_3Si_{(in)}$**), 0.51 (s, 24H, **$CH_3Si_{(out)}$**), 0.94 (t, 18H, **H_a**, J = 6.5 Hz), 1.27 (m, 12H, **H_b**), 1.82 (m, 4H, **$H_{b'}$**), 1.87 (s, 24H, ar**CH_3**), 2.17 (m, 12H, **H_c**) , 2.32 (m, 4H, **$H_{c'}$**), 4.45 (t, 4H, **$H_{a'}$**, J = 6.7 Hz), 4.6 (t, 8H, **H_d**, J = 8.16 Hz), 7.16 (s, 8H, ar**H**), 8.8 (d, 1H, **H_{oPy}**, J = 2.0 Hz), 9.3 (d, 2H, **H_{mPy}**, J = 2.0 Hz). **ESI-MS:** $C_{111}H_{145}NO_{20}Si_8$: 2037.83 $(MH)^+$ and 2062.8 $(M + Na^+)^+$.

Synthesis of bis-resorcinarene 5: to a solution of bis-cavitand Sicav[C_3H_7, CH_3, CH_3]-Py-[CH_3, CH_3, C_3H_7]cavSi (1 g, 0,5 mmol) dissolved in 30 mL of DMF in a polypropylene flask, 0.72 mL of a solution 40% of HF in water were added. The mixture was stirred for 16h at 50°C, and the solvent was removed. 20 mL of water were added and the resulting suspension was filtered. Purification by re-crystallisation from a mixture 7:3 of water and acetonitrile yielded **5** (0.75 g, 0.47 mmol, 96%).

^{1}H NMR (300 MHz, DMSO-d_6) δ (ppm): 0.87 (t, 18H, **H_a**, J = 6.5 Hz), 1.2 (m, 12H, **H_b**), 1.80 (m, 4H, **$H_{b'}$**), 1.91 (s, 24H, ar**CH_3**), 2.18 (m, 12H, **H_c**) , 2.35 (m, 4H, **$H_{c'}$**), 4.19 (t, 4H, **$H_{a'}$**, J = 6.7 Hz), 4.37 (t, 8H, **H_d**, J = 8.2 Hz), 7.25 (s, 8H, ar**H**), 7.93 (d, 1H, **H_{oPy}**, J = 2.0 Hz), 8.63 (s, 16H, **OH**), 9.25 (d, 2H, **H_{mPy}**, J = 2.0 Hz), **ESI-MS:** $C_{95}H_{113}NO_{20}$: 1589.8 $(M+H)^+$.

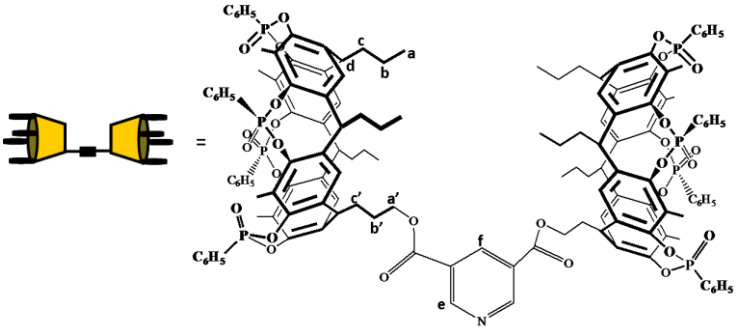

Synthesis of bis-cavitand Tiiii[C_3H_7, CH_3, Ph]-Py-[Ph, CH_3, C_3H_7]Tiiii: to a solution of bis-resorcinarene **5** (0.2 g, 0.13 mmol) dissolved under argon in 10 mL of freshly distilled pyridine, $PhPCl_2$ (0.14 mL, 1.03 mmol) was slowly added at room temperature. The reaction mixture was stirred for 3h at 70°C and then cooled at room temperature. An excess of H_2O_2 35% and 4 mL of $CHCl_3$ were added and stirred for 30 min at room temperature. The solvent was removed under vacuum, 20 mL of water were added and the resulting white suspension was filtered. Purification by re-crystallisation from a mixture 8:2 of H_2O and CH_3CN gave the desired product (0.31 g, 0.12 mmol, 90%).

^{1}H NMR (300 MHz, $CDCl_3$) δ (ppm): 1.0 (t, 18H, $\mathbf{H_a}$, J = 7.6 Hz), 1.2 (m, 12H, $\mathbf{H_b}$), 1.92 (m, 4H, $\mathbf{H_{b'}}$), 2.2 (s, 24H, ar$\mathbf{CH_3}$), 2.33 (m, 12H, $\mathbf{H_c}$), 2.5 (m, 4H, $\mathbf{H_{c'}}$), 4.53 (t, 4H, $\mathbf{H_{a'}}$, J = 6.3 Hz), 4.8 (t, 8H, $\mathbf{H_d}$, J = 7.4 Hz), 7.24 (s, 8H, ar**H**), 7.63-7.53 (m, (8 + 16)H, O=PAr$\mathbf{H_p}$ + O=PAr$\mathbf{H_m}$), 8.1-8.0 (m, 8H, O=PAr$\mathbf{H_o}$), 8.8 (d, 1H, $\mathbf{H_{oPy}}$, J = 2 Hz), 9.25 (d, 2H, $\mathbf{H_{mPy}}$, J = 2 Hz). **^{31}P NMR** (172 MHz, $CDCl_3$) δ (ppm): 4.02 (s, **P**=O). **ESI-MS:** $C_{142}H_{135}NO_{28}P_8$: 2587.09 $(M + K^+)^+$, 1306.07 $(M + Na^+ + K^+)^{2+}$ and 1283.56 $(M + Na^+ + H^+)^{2+}$.

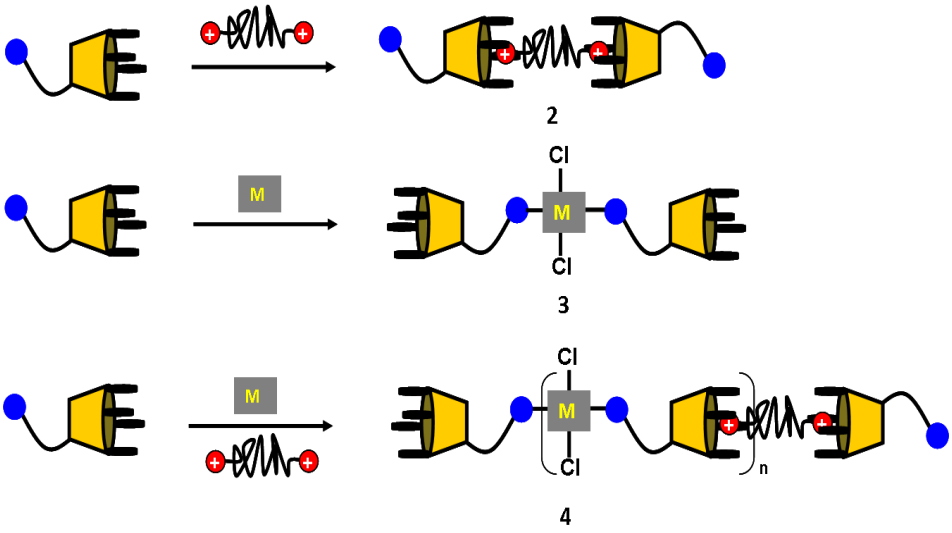

Host-guest-driven self-assembly of dimer complex 2: to a solution of cavitand Tiiii[($3C_3H_7$ + Py), CH_3, Ph] (9.5 mg, $7.2*10^{-3}$ mmol) dissolved in 500 µL of $CDCl_3$, 40 µL of a solution 0.09 mM of ditopic guest **1** in $CDCl_3$ were added in four aliquots of 10 µL, leading to the complete formation of dimer complex **2**.

^{1}H NMR (300 MHz, $CDCl_3$) δ (ppm): 0.84 (s, 6H, $\mathbf{CH_{3Py}}$), 1.05 (t, 18H, $\mathbf{H_a}$, J = 7.3 Hz), 1.45 (broad m, 12H, $\mathbf{H_b}$), 1.92 (broad m, 4H, $\mathbf{H_{b'}}$), 2.05 (s, 24H, Ar$\mathbf{CH_3}$), 2.99 (m,

12H, $\mathbf{H_c}$), 3.35 (m, 4H, $\mathbf{H_{c'}}$), 3.59 (m, 62H, O$\mathbf{(CH_2CH_2O)_{31}}$), 3.80 (t, 4H, $OOCCH_2\mathbf{CH_2}O$, J= 4.5 Hz), 4.5 (t, 4H, $OOC\mathbf{CH_2}CH_2O$, J= 4.5 Hz), 4.66 (t, 4H, $\mathbf{H_{a'}}$, J = 6.2 Hz), 4.80 (t, 4H, $\mathbf{H_d}$, J = 7.9 Hz), 7.55 (m, 16H, O=PAr$\mathbf{H_{\textit{m}}}$), 7.66 (m, 8H, O=PAr$\mathbf{H\textit{p}}$), 7.83 (d, 4H, $\mathbf{H_f}$, J = 5.9 Hz), 7.96 (broad m, (4+16)H, $\mathbf{H_i}$+O=PAr$\mathbf{H_o}$), 8.33 (s, (4+4)H, Ar**H**), 8.36 (broad, 4H, $\mathbf{H_h}$), 8.67 (d, 4H, $\mathbf{H_e}$, J = 5.9 Hz). ^{31}**P NMR:** (172 MHz, $CDCl_3$) δ (ppm): 7.8 (s, O=**P**Ar).

Metal-directed self-assembly of dimer complex 3: To a solution of cavitand Tiiii[($3C_3H_7$ + Py), CH_3, Ph] (9.5 mg, $7.2*10^{-3}$ mmol) dissolved in 500 μL of $CDCl_3$, 25 μL of a suspension 0.144 mM of $\mathbf{(CH_3CN)_2PdCl_2}$ in $CDCl_3$ were added in two aliquots of 12.5 μL, leading to the complete formation of metal-dimer complex **3**.

^{1}**H NMR** (300 MHz, $CDCl_3$) δ (ppm): 1.05 (t, 18H, $\mathbf{H_a}$ J = 7.3 Hz), 1.43 (m, 12H, $\mathbf{H_b}$), 1.91 (m, 2H, $\mathbf{H_{b'}}$), 2.04 (broad, (12+24)H, $\mathbf{H_c}$+Ar$\mathbf{CH_3}$), 2.43 (m, 4H, $\mathbf{H_{c'}}$), 4.51 (t, 4H, $\mathbf{H_{a'}}$, J = 5.9 Hz), 4.83 (broad t, 8H, $\mathbf{H_d}$), 7.12 (s, 8H, Ar**H**), 7.54 (m, 16H, O=PAr$\mathbf{H_{\textit{m}}}$), 7.64 (m, 8H, O=PAr$\mathbf{H\textit{p}}$), 7.84 (d, 4H, $\mathbf{H_f}$, J = 5.9 Hz), 8.11 (m, 16H, O=PAr$\mathbf{H_o}$), 8.94 (d, 4H, $\mathbf{H_e}$, J = 5.9 Hz). ^{31}**P NMR**(172MHz, $CDCl_3$) δ (ppm): 4.64 (s, O=**P**Ar).

Self-assembly of linear copolymer 4: to a solution of cavitand Tiiii[($3C_3H_7$ + Py), CH_3, Ph] (9.5 mg, $7.2*10^{-3}$ mmol) dissolved in 500 μL of $CDCl_3$, 40 μL of a solution 0.09 mM of ditopic guest **1** and 25 μL of a suspension 0.144 mM of metallic complex $(CH_3CN)_2PdCl_2$ both in $CDCl_3$ were added leading to the formation of the supramolecular copolymer **4.**

^{1}**H NMR** (300 MHz, $CDCl_3$) δ (ppm): 0.83 (s, $\mathbf{CH_{3\textit{Py}}}$), 1.06 (broad, $\mathbf{H_a}$), 1.44 (broad m, $\mathbf{H_b}$), 1.92 (broad m, $\mathbf{H_{b'}}$), 2.05 (s, Ar$\mathbf{CH_3}$), 2.92 (broad, $\mathbf{H_c}$), 3.33(broad, $\mathbf{H_{c'}}$), 3.59 (broad, O$\mathbf{(CH_2CH_2O)_{31}}$), 3.78 (broad, $OOCCH_2\mathbf{CH_2}O$), 4.46 (broad, $OOC\mathbf{CH_2}CH_2O$), 4.6 (broad, $\mathbf{H_{a'}}$), 4.80 (t, $\mathbf{H_d}$, J = 7.9 Hz), 7.55 (broad, O=PAr$\mathbf{H_{\textit{m}}}$), 7.68 (broad m, O=PAr$\mathbf{H\textit{p}}$), 7.85 (broad, $\mathbf{H_f}$), 7.96 (broad , ($\mathbf{H_i}$+O=PAr$\mathbf{H_o}$), 8.33 (broad, , Ar**H**), 8.36 (broad, $\mathbf{H_h}$), 8.95 (broad, $\mathbf{H_e}$). ^{31}**P NMR** (172MHz, $CDCl_3$) δ (ppm): 7.78 (s, O=**P**Ar).

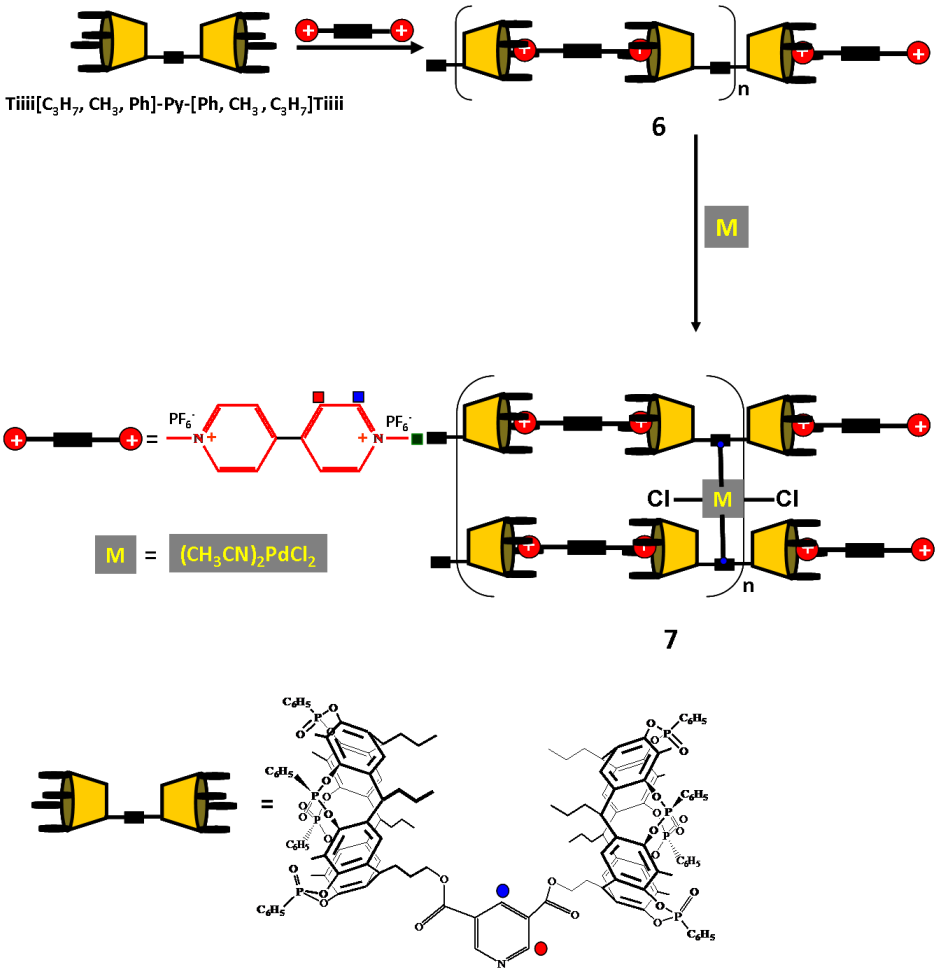

Host-guest-driven self-assembly of linear copolymer 6: to a solution of bis-cavitand Tiiii[C_3H_7, CH_3, Ph]-Py-[Ph, CH_3, C_3H_7]Tiiii (5 mg, $2*10^{-3}$ mmol) dissolved in 400 µL of CD_3CN, 20 µL of a solution $9.74*10^{-2}$ mM of the methyl viologen PF_6^- were added in two aliquots of 10 µL leading to the complete formation of the linear copolymer **6.**

^{1}H NMR (300 MHz, CD_3CN) δ (ppm): 0.96 (s, 6H, **CH_{3Py}**), 1.05 (broad, 18H, **H_a**), 1.3 (m, 12H, **H_b**), 1.92 (broad, 4H, **$H_{b'}$**), 2.04 (s, 24H, ar**CH_3**), 2.43 (broad, 12H, **H_c**), 2.6 (broad, 4H, **$H_{c'}$**), 4.42 (t, 4H, **$H_{a'}$**, J = 6.2 Hz), 4.80 (broad, 8H, **H_d**), 7.61-7.42 (broad, (8 + 16)H, O=PAr**H_p** + O=PAr**H_m**), 8.07-7.83 (broad, (4+8+16)H, **H_g**+ar**H**+O=PAr**H_o**), 8,38 (broad, 4H, **H_h**), 8.62 (d, 1H, **H_f**, J = 1.95 Hz), 9.25 (d, 2H, **H_e**, J = 1.95 Hz). **^{31}P**

NMR (172 MHz, $CDCl_3$) δ (ppm): -141.1 (m, 1P, **P**F_6, J_{P-F} = 750 Hz), 13.4 (s, 4P, O=**P**). **ESI-MS:** 1374.74 [Tiiii[C_3H_7, CH_3, Ph]-Py-[Ph, CH_3, C_3H_7]Tiiii + 2 viologen]$^{4+}$, 1881 [Tiiii[C_3H_7, CH_3, Ph]-Py-[Ph, CH_3, C_3H_7]Tiiii + 2 viologen + PF_6^-]$^{3+}$, 2895.5 [Tiiii[C_3H_7, CH_3, Ph]-Py-[Ph, CH_3, C_3H_7]Tiiii + 2 viologen + $2PF_6^-$]$^{2+}$.

Crystallographic data of linear polymer 6: The molecular structure of the compound $C_{156}H_{153}N_3O_{28}P_8$ + $2PF_6^-$ + $2.5CH_3CN$ **6,** was determined by single-crystal X-ray diffraction methods. Experimental details are summarized in Table 1. Intensity data were collected using Cu Kα radiation (λ= 1.54 Å) equipped with a CCD area detector at 100K. The structure was solved by direct method using DENZO-SMN, SCALEPACK, and AMoRe SHELXL program.[10] The data of **6** were performed and refined using programs.[11]

Self-assembly of cross-linked supramolecular polymer 7: to a solution of bis-cavitand Tiiii[C_3H_7, CH_3, Ph]-Py-[Ph, CH_3, C_3H_7]Tiiii (5 mg, $2*10^{-3}$ mmol) dissolved in 400 µL of CD_3CN, 20 µL of a solution $9.74*10^{-2}$ mM of methyl viologen hexafluorophosphate in CD_3CN were added. To the resulting solution, 20 µL of a solution $4.9*10^{-2}$ mM of $(CH_3CN)_2PdCl_2$ in CD_3CN were added leading to the formation of the cross-linked polymer **7.**

^{1}H NMR (300 MHz, CD_3CN) δ (ppm): 0.98 (broad, **CH_{3Py}**), 1.05 (broad, **H_a**), 1.35 (broad, **H_b**), 1.9 (broad, **$H_{b'}$**), 1.94 (broad, ar**CH_3**), 2.47 (broad, **H_c**), 2.61 (broad, 4H, **$H_{c'}$**), 4.51 (broad, **$H_{a'}$**), 4.94-4.68 (broad, **H_d**), 7.9-7.40 (broad, O=PAr**H_p** + O=PAr**H_m**), 8.07-7.82 (broad, **H_g**+ar**H**+O=PAr**H_o**), 8,42 (broad, **H_h**), 8.69 (d, **H_f**, J = 1.8 Hz), 9.41 (d, 2H, **H_e**, J = 1.8 Hz). **^{31}P NMR**(172 MHz, $CDCl_3$) δ (ppm): -141.1 (m, 1P, PF_6, J= 750 Hz), 13.44 (s, 4P, O=**P**).

	Host-guest linear supramolecular polymer 6
Formula	$C_{156}H_{153}N_3O_{28}P_8+2PF_6+C_2H_3N$
Formula weight	12626.12
Temperature	100 K
Wavelength	1.54 Å
Crystal system	Monoclinic
Space Group	$P2_1/c$
a/Å	13.7267±0.0007
b/Å	27.4467±0.0019
c/Å	42.02920±0.0025
α/°	90
β/°	108.2344±0.0707
γ/°	90
V/Å^3	15823.8
Z	4
D_c/g cm^{-3}	1.262
F(000)	6432
μ/mm^{-1}	2.569
$\theta_{min,max}$/°	1.5
Resolution	1.5 – 200.0 Å
Reflections collected	4835
Independent reflections	2928
Observed Reflections [$F_o>4\sigma(F_o)$]	75147
I/σ(I) (all data)	11.9
I/σ(I) (max resolution)	2.3
Completeness (all data)	94.2%
Completeness (max resolution)	80.4%
Multiplicity (all data)	2.5
Multiplicity (max resolution)	1.5
Data/restraint/parameters	4646/494/540
R[I>2.0σ(I)]	0.2111
R(all data)	0.2603
Goodness of fit	2.352

Table 1. Crystallographic data of host-guest linear supramolecular polymer 6.

3.5 References.

[1] H. Hofmeier, U. S. Schubert, *Chem. Commun.,* **2005**, 2423-2432.

[2] O. Félix, M. W. Hosseini, A. De Cian, J. Fischer, *Angew. Chem. Int. Ed. Engl.*, **1997,** 36, 102-104.

[3] a) J. M. Pollino, M. Weck, *Pol. Prepr.*, **2004**, 45, 339-340; b) L. P. Stubbs, M. Weck, *Chem. Eur. J.*, **2003,** 9, 992-999; c) J. M. Pollino, L. P. Stubbs, M. Weck, *Macromolecules*, **2003,** 36, 2230-2234; d) J. M. Pollino, L. P. Stubbs, M. Weck, *Pol. Prepr.*, **2003**, 44, 730-731; e) J. M. Pollino, M. Weck, *J. Am. Chem. Soc.*, **2004,** 126, 563-567.

[4] J. R. Moran, J. L. Ericson, E. Dalcanale, J. A. Bryant, C. B. Knobler, D. J. Cram, *J. Am. Chem. Soc.* **1991,** 114, 7748-7765.

[5] L. Pirondini, A. G. Stendardo, S. Geremia, M. Campagnolo, P. Saporì, J. P. Rabe, R. Fokkens, E. Dalcanale, *Angew. Chem. Int. Ed.* **2003,** 42,1384-1387.

[6] a) H. Hofmeier, J. Pahnker, C. H. Weild, U. S. Schubert, *Biomacromolecules,* **2004,** 5, 2055-2064; b) N. Haddour, C. Gondron, S. Cosnier, *Chem. Commun.,* **2004,** 324-325.

[7] E. Menozzi, M. Busi, R. Ramingo, M. Campagnola, S. Geremia, E. Dalcanale, *Chem. Eur. J.* **2005,** 11, 3136-3148.

[8] P. C. Kong, F. D. Rochon, *Can. J. Chem.* **1978**, 56, 441-445.

[9] a) D. I. Pererad, R. A. Shanks, *Polym. Int.* **1996**, 39, 121-127; b) H. Schmid, B. Michel, *Macromolecules* **2000,** 33, 3042-3049; c) S. Wang, J. E. Mark, *J. Polym. Sci.*, **1992,** 30, 801; d) S. A Visser, *J. Appl. Polym. Sci.*, **1997,** 63, 1805.

[10] a) Z. Otwinowski, W. Minor, *Processing of X-ray Diffraction Data Collected in Oscillation Mode. Methods In Enzymology*, **1997**, 276, 307-326; b) J. Navaza, *Amore-an Automated Package for Molecular Replacement. Acte Crystallographica Section A,* **1994,** 50, 157-163.

[11] DS viewerPro 5.0 *by accelry*. http://www.accelrys.com/com/about/msi.html.

Chapter 5

Highly selective Monomethylation of Primary Amines promoted by Host-guest complexation.

5.1 Introduction

Amines are an important class of organic compounds which synthesis have received wider attention than the preparation of many other functional groups in organic chemistry.[1] In particular secondary amines are important pharmacophores in numerous biologically active compounds since they possess interesting physiological activities. They are utilized as important precursors in the synthesis of functional groups in organic and organometallic chemistry.[2] However, despite the widespread interest, traditional methods for secondary amines formation are often problematic because of harsh reaction conditions, generally poor yields and/or low chemical selectivities.[3] Scheme 1 illustrates for the major traditional methods for the synthesis of secondary amines. Among these, suitable procedures and conditions can be properly chosen to prepare particular amines with acceptable efficiency.

At the top of scheme 1, the masked alcohols such as sulfonates, alkyl phosphates, and alkyl phosphites are known to act as suitable leaving groups in monoalkylation of primary amines,[4] however harsh reaction conditions are required and these methods suffer from lack of selectivity.

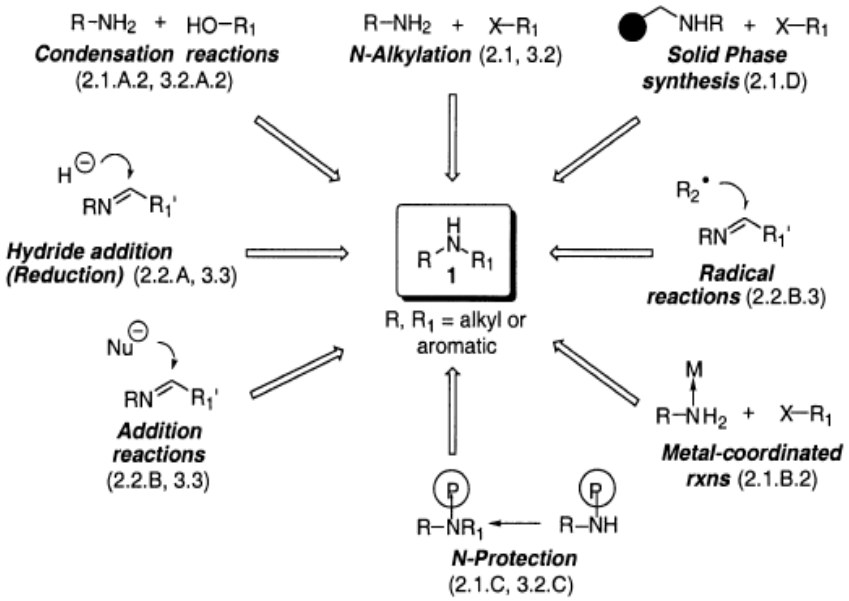

Scheme 1. Traditional methods for the synthesis of secondary amines.

Procedures employing the alkylating agents as the limiting reagents in order to obtain the selective synthesis of secondary amines are employed; however, the desired mono-alkylated products are more reactive than the starting amine and move the equilibrium toward multi-alkylation, leading obviously to the lack of selectivity.[5] The direct base-promoted N-alkylation of primary amines performed with traditional alkylating agents are less used because of the formation of mixture of secondary and tertiary amines along with the corresponding ammonium salt that are difficult to separate.[3] Many methods have been developed for the straightforward N-methylation of primary aromatic amines employing dimethyl sulphate or dimethyl carbonate over zeolite,[6] or methanol in either gas[7] or supercritical phase[8]. These processes need high temperature and high pressure, and they do not exclude the formation of by-products derived from further methylation even if in a low yield.

The difficulties associated with direct N-monoalkylation in general and especially with direct N-monomethylation using conventional or nonconventional alkylating agents, have led to the development of indirect N-alkylation procedures through partially protected amines or amino-derivatives. The indirect N-monomethylation is a multi-step process based on the synthesis of suitable amine derivative that are subjected to the N-methylation reaction, or to the reductive N-methylation followed by the release of the modified amine function. Some indirect methods exploit the low nucleophilicity of the coordinated amines compared to the free ones,[9] whose alkylation reactions rarely proceed beyond the monoalkylated stage. Following this purpose, Rh(III)[10] and organoborane derivatives[11] have been used giving monoalkylated products in good yield. Reduction of N-arylformamide,[12] N-arylformimidate[13] derivatives almost yields selectively N-monomethylated anilines and derivatives also without isolating the reaction intermediates before reduction. N-protection with 4-nitrobenzenesulfonyl which is able to enhance the acidity of the amine proton and N-methylation with diazomethane as methylating agent followed by deprotection is a three step indirect valid approach to the rapid and high selective N-methylation of aromatic primary amines.[14] Addition of chloromethyltrialkoxysilanes followed by hydrolitic cleavage of Si-C bond is another indirect method for selective N-methylation of both aromatic and aliphatic amines.[15]

Typically supramolecular objects have been used as catalysts or nano-vessels, capable of controlling reactivity and selectivity of organic reactions[16]

As alternative to known methodologies reviewed above we considered the possibility of stopping the methylation reaction at the monomethylation level by segregating the desired product via host guest complexation. Since Tiiii phosphonate cavitands strongly and selectively

complex the *N*-methylammonium salt ($K_{ass} > 10^7$),[17] we used them for high selective *N*-monomethylation of primary amines, as segregating nano-vessels that surround and shield the desired product, avoiding the contact with the reagents in solution.

5.2 Results and discussions

Three cavitands were used as complexing agents for *N*-methyl ammonium salts with increasing complexing ability from left to right (Figure 1).

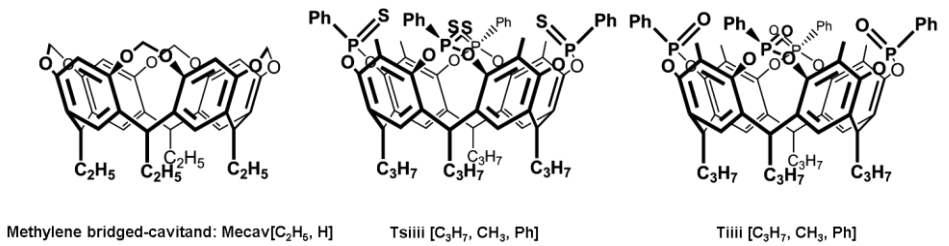

Figure 1. Three cavitands used as segregating agents.

Phosphonate cavitand Tiiii [C_3H_7, CH_3, Ph] in particular bind *N*-methylammonium salts with $K_{ass} > 10^7$ in chlorinated hydrocarbons (see Chapter 2). This large K_{ass} is due to three synergistic interaction modes: ion-dipole interactions between the N^+ and the four P=O groups, two H-bonds between the NH protons and the two adjacent P=O,[18] and the CH_3-π interactions between the cavity and the N-CH_3 moiety (Figure 2).

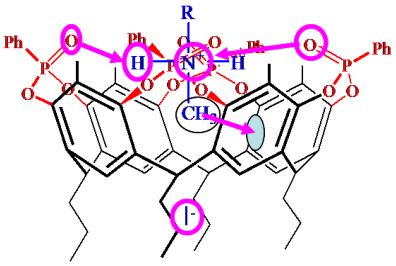

Figure 2. Interactions that stabilize the complex between cavitand Tiiii [C_3H_7, CH_3, Ph] and the N-methylammonium salts.

5.2.1 Synthesis of the segregating agents

The methylene-bridged cavitand is synthesized by bridging the corresponding ethyl-footed resorcinarene[19] using CH_2Br_2 as bridging agent in polar solvents under basic condition as reported in the literature[20] (Scheme 1).

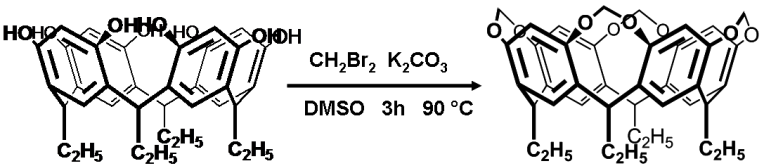

Scheme 2. Synthesis of the methylene-bridged cavitand Mecav[C_2H_5, H]

Thiophosphonate cavitand TSiiii[C_3H_7, CH_3, Ph] was prepared following a published two steps procedure (Scheme 3). [21]

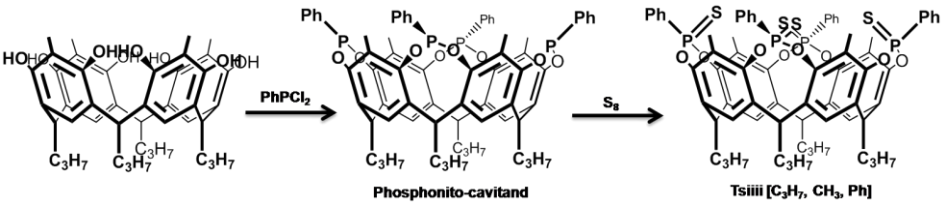

Scheme 3. Two step synthesis of the cavitand TSiiii [C_3H_7, CH_3, Ph].

Phosphonate cavitand Tiiii [C_3H_7, CH_3, Ph] has been previously synthesized (see Chapter 3).

5.2.2 Segregating agents effects on the selectivity of the monomethylation reactions.

The traditional *N*-monomethylation reaction of the primary amines occurs by mixing one equivalent of amine with an equimolar or a slightly excess of the methylating agent, CH_3I in our case. As reported above, after methylation, the methylating agent preferably reacts with the *N*-monomethylated product rather than with the starting amine, leading to subsequent alkylation until formation of quaternary ammonium salt. Consequently, low yield and especially low selectivity is observed. By adding to the reaction solution an equimolar amount of a suitable host, the desired monomethylated product, is made un-reactive via complexation. The effectiveness of this host-guest sequestration is governed by the equilibrium between free and complexed *N*-methylammonium salt in solution. The selectivity of the monomethylation reaction of the primary amines depends on this equilibrium. As shown in Figure 3, the first step is the formation of monomethylated product. Such product is complexed by the segregating agent. If the equilibrium is completely shifted toward the complex, further methylation will be prevented. In the intermediate cases, the observed selectivity of the monomethylation reaction will depend on the degrees of the complexation.

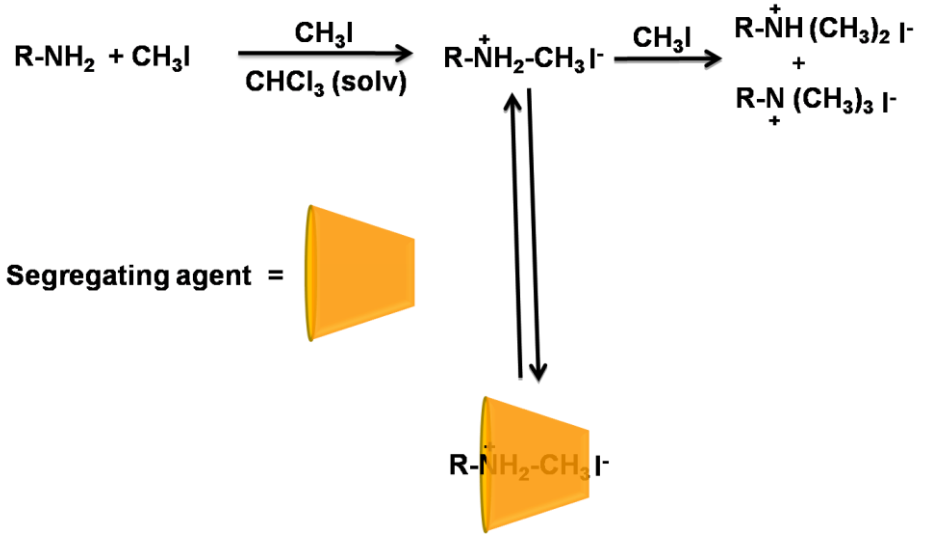

Figure 3. *N*-monomethylation with cavitands as segregating agents

The influence of the three cavitands on the selectivity of the monomethylation reaction was studied using butylamine as substrate. The reactions occur by adding three equivalents of methyl iodide to a solution containing one equivalent of cavitand and one equivalent of butylamine in chloroform. The results obtained are plotted in Figure 4 and summarized in Table 1.

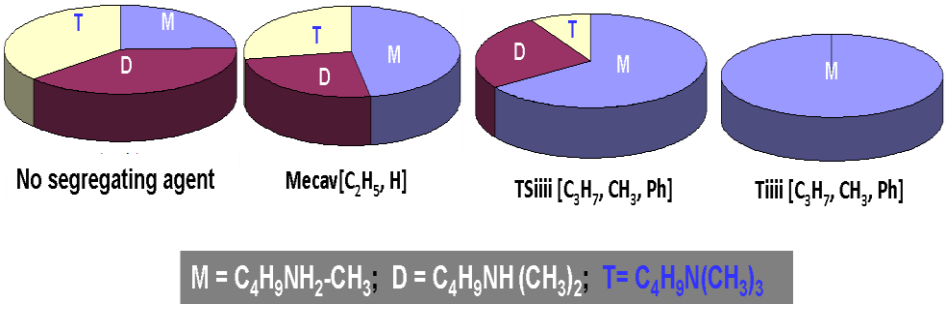

Figure 4. Pie graph of the selectivity of the monomethylation reaction in the presence of cavitands Mecav[C_2H_5, H], TSiiii[C_3H_7, CH_3, Ph] and Tiiii[C_3H_7, CH_3, Ph] as segregating agents

Entry	segregating agents	$CH_3N^+H_2C_4H_9\,I^-$ (M)	$(CH_3)_2\,N^+HC_4H_9I^-$ (D)	$(CH_3)_3\,N^+C_4H_9\,I^-$ (T)
1	Tiiii [C_3H_7, CH_3, Ph]	100	0	0
2	TSiiii [C_3H_7, CH_3, Ph]	65.5	26	8.5
3	Mecav [C_2H_5, H]	45.4	28.1	26.5
4	Control reaction	24.7	38.8	36.5

Table 1. Yield of the methylation reaction of butylamine, in the presence of cavitands as segregating agents. The conversion, calculated via GC-MS is 100%.

In the control reaction (entry 4), the selectivity is low as expected. The methylene-bridged cavitand (entry 3), that can form only CH-π interactions between the CH_3 of *N*-methylbutylammonium salt and the π electrons of the cavity, slightly improves the selectivity of the *N*-monomethylation reaction (see the second pie graph in Figure 4). Only weak CH-π interactions stabilize the complex between the Mecav[C_3H_7, H] and *N*-methylbutylammonium salt. Therefore the concentration of the non-complexed *N*-methylbutylammonium salt is still high in solution, enabling the subsequent per-methylation. Cavitand TSiiii [C_3H_7, CH_3, Ph] forms weak ion-dipole (N^+ - S=P) interactions with *N*-methylbutylammonium salt, and probably very weak hydrogen bonds between the NH of ammonium salt and the sulphurs of the P=S bonds.[21] The weakness of these two secondary interactions is due to the low polarity of the P=S bonds. The combination of these three interactions stabilizes the complex between cavitand TSiiii [C_3H_7, CH_3, Ph] and the desired product leading to an increase of selectivity (entry 2) in the monomethylation of butylamine (see the third pie graph, in Figure 4). It is interesting to notice that the ratio bis-methylated/ter-methylated is shifted in favour of the bis in the TSiiii [C_3H_7, CH_3, Ph] case with respect

to the control (entry 3) and the Mecav[C_3H_7, H] (entry 4) reactions (from 1.06 to 3.05). This difference indicates that the TSiiii [C_3H_7, CH_3, Ph] is able to complex also $(CH_3)_2N^+C_4H_9$ I^- via ion-dipole interactions. The polarity of the P=O bonds leads to the formation of strong hydrogen-bonding (N-H---O=P) and strong ion-dipole interactions (N^+---O=P) between the phosphonate cavitand Tiiii [C_3H_7, CH_3, Ph] and the *N*-methylbutylammonium salt. Such interactions combined to the CH-π interactions between the CH_3 of the *N*-methylbutylammonium salt and the π electrons of the cavity afford a very stable complex (Figure 2). Such stability moves the equilibrium entirely toward the complexed ammonium salt leading to 100% of selectivity in the monomethylation reaction of butylamine (last pie graph in Figure 4).

5.2.3 Procedure for the quantification of products distribution.

i) Quantification of the monomethylated product. The yields of the monomethylated product in all four cases reported in Table 1 are obtained by GC-MS injections in the presence of an internal standard from the following procedure summarized in Scheme 4.

Primary and secondary amines are very polar and can interact with the stationary phase of the GC-MS column, therefore, for a correct quantification, derivatization reactions are often used to reduce the polarity and especially to improve the GC properties.[22] The derivatization reaction occurs by adding to the crude reaction (Scheme 4a) in pyridine as solvent, one equivalent of butanol as internal standard, and an excess of isonicotinoyl chloride hydrochloride as derivatizing agent. This mixture is stirred three hours at 100 °C (Scheme 4b). The pyridine is used as solvent because is basic and can slightly deprotonate the ammonium salt affording amine that can successively react with the derivative agent. The butanol added, become isonicotinate butyl ester which is the real internal standard. Since total conversion is observed in

the monomethylation reaction of butylamine (GC-MS analysis of the derivatization reaction), the derivatization reaction affords only the product of amidification of *N*-methylbutylammonium salt and the internal standard. After the derivatization reaction, the cavitand used as segregating agent in the methylation reaction is removed by filtration of the suspension in water of crude reaction. The product and the internal standard are extracted in chloroform and then injected in GC-MS. The internal standard is prepared in situ to take into account the matrix effect[23] (differences in work up procedures and in the progress of the reactions).

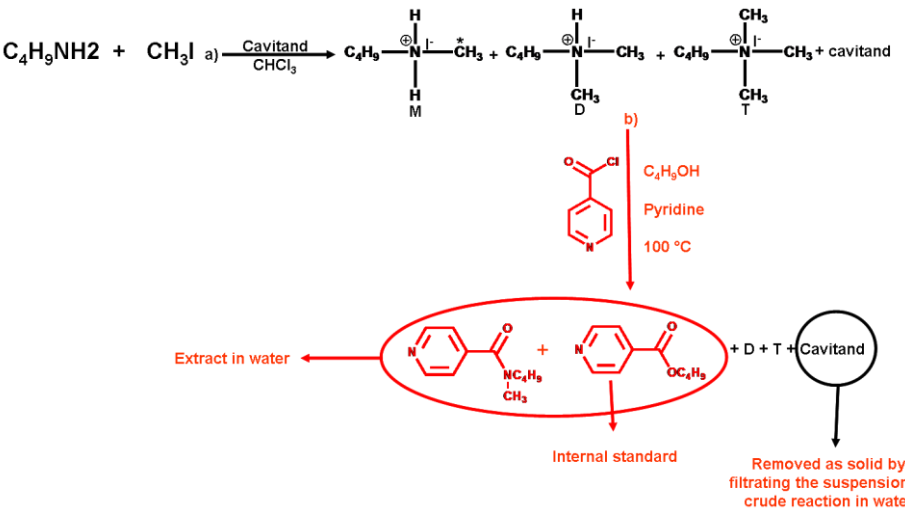

Scheme 4. Monomethylation reaction and derivatization reaction in the presence of the internal standard.

ii) Indirect quantification of the dimethylated and the trimethylated products. The distribution of the dimethylated and trimethylated product in Table 1 was obtained from the following indirect procedure summarized in Scheme 5.

In a different batch, the monomethylation reaction is made under the same conditions as before affording the three products M, D, and T (Scheme 5a). The flask containing the cavitand is weighted before starting the reaction. At the end of the reaction, the solvent is removed and dried under vacuum. The weight (S) of the three products M, D, T, and the starting cavitand was determined gravimetrically by weighting the flask of the crude reaction (Equation 1).

$S = M + D + T + \text{cavitand}$ (1).

An excess of DBU (1,8-diazobicyclo(5,4,0)-undec-7-en) dissolved in chloroform was added. The DBU is a hindered base that deprotonates the ammonium salts affording amines which were eliminated heating under vacuum together with the excess of non protonated DBU. The sum of the weight (R) of quaternary ammonium salt that cannot be deprotonated (T), the protonated DBU remained in the flask (Q), and the cavitand was determined gravimetrically (Equation 2).

$R = T + Q + \text{cavitand}$ (2).

Where Q is the weight of the protonated DBU that can be expressed following the Equation 3

$Q = (M/W_M + D/W_D)*W_Q$ (3).

Where W_M is the molecular weight of the monomethylated product, W_D is that of the dimethylated by-product, and W_Q is that of the protonated DBU salt. Since M was calculated from the GC-MS injection with the internal standard, and the weight of the cavitand was known, solving the equation system 4, D and T can be determined.

$$\begin{cases} S = M + D + T + \text{Cavitand} \\ R = T + (M/W_M + D/W_D)*W_Q + \text{Cavitand} \end{cases} \quad (4)$$

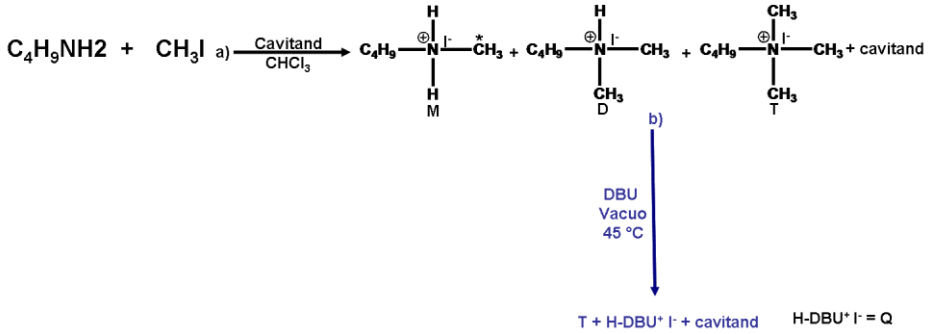

Scheme 5. Deprotonation of secondary and ternary amines by DBU.

Since the cavitand Tiiii [C_3H_7, CH_3, Ph] results to be the best segregating agent to obtain high selectivities, we tested it for *N*-monomethylation of different aliphatic, cycloaliphatic amines and aniline. The results obtained are summarized in Table 2.

				R-N$^+$H$_2$-CH$_3$ I$^-$	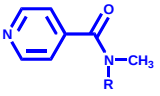	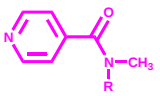
entry	**amines**	**T(°C)**	**Time**	**Yield[(a)]**	**Yield[(a)]**	**Yield from IS[(b)]**
1	$C_2H_5NH_2$	30	16	68	74.8	96.4
2	$C_3H_7NH_2$	40	16	62	79	98.2
3	$C_4H_9NH_2$	45	16	62	87.2	100
4	$C_7H_{15}NH_2$	50	16	-	74.6	99.6
5	$C_6H_{11}NH_2$	reflux	16	-	63.7	97.4
6	$C_6H_5NH_2$	reflux	20	-	82.1	99.3

Table 2. Yield of *N*-monomethylation of different amines determined using different approaches a) pure compounds characterized via ^{1}H NMR and GC-MS; b) Yield obtained from GC-MS with the IS (internal standard).

The red column in Table 2 represents the yields obtained by weighting and characterizing (^{1}H NMR and ESI-MS) the pure *N*-methylammonium salt (^{1}H NMR). After the monomethylation, the crude reaction was

suspended in water, sonicated and the cavitand was filtered out. The water containing the ammonium salt was removed and re-crystallization from a mixture methylene chloride and ethyl ether yielding the product which was then weighted. The blue column represents the yields obtained by weighting and characterizing (^{1}H NMR and GC-MS) the pure derivative products. After methylation reactions, the solvent was removed; the pyridine and successively the derivative agent were added and left to react. The solvent was removed, then the water was added and the resulting suspension was filtered eliminating the cavitand. The filtrate was extracted in basic medium with chloroform. The organic layer was rinsed with acidic water and then, with neutral water. The pure product obtained was weighted and characterized via ^{1}H NMR and GC-MS.

The magenta column represents the yields obtained by injection in GC-MS of a solution containing the internal standard after derivatization reactions.

For the quantitative analysis via GC-MS, a mixture 1:1 (mol/mol) of pure n-butanol and pure N-methylammonium salts were derivatizated in the presence of 1 equivalent of cavitand. The cavitand was eliminated by filtrating the suspension of crude reaction in water and after extraction of the derivative products in methylene chloride, a solution 20 $\mu g.L^{-1}$ was injected in GC-MS. The calibrations were performed by calculating the ratios (X) between the peak areas of the derivative internal standard and the derivative *N*-methylammonium salts. Figure 5 shows the example made using pure *N*-methylbutylammonium iodide. After monomethylation, derivatization reaction in the presence of one equivalence respect to the starting amine of n-butanol (IS) and the same work-up above described, a solution 20 $\mu g.L^{-1}$ is injected in GC-MS (Figure 6). The moles of the N-methylammonium salts were determined from the Equation 5.

$$n_a = n_b A_a / A_s X \qquad (5)$$

Where n_b are the stating moles of the normal butanol, A_a, and A_s are the area peaks of the respective derivative N-methylammonium salts, and derivative butanol.

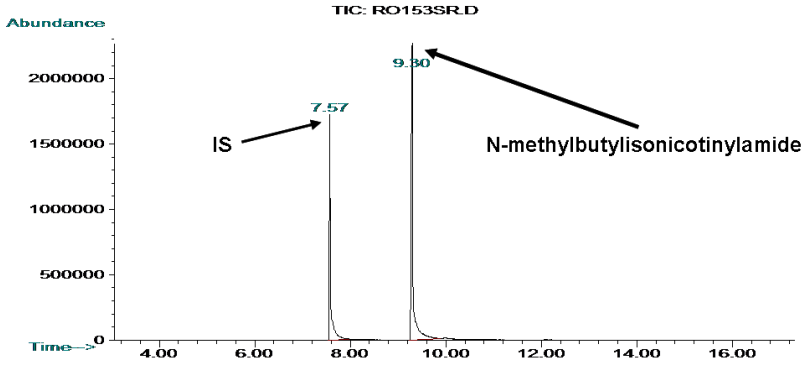

Peak#	Ret Time	Type	Width	Area	Start Time	End Time
1	7.574	BB	0.037	33512540	7.529	7.995
2	9.297	BB	0.044	65386554	9.230	9.897

Figure 5. GC-MS for the calibration in the case of monomethylation reaction of butylamine.

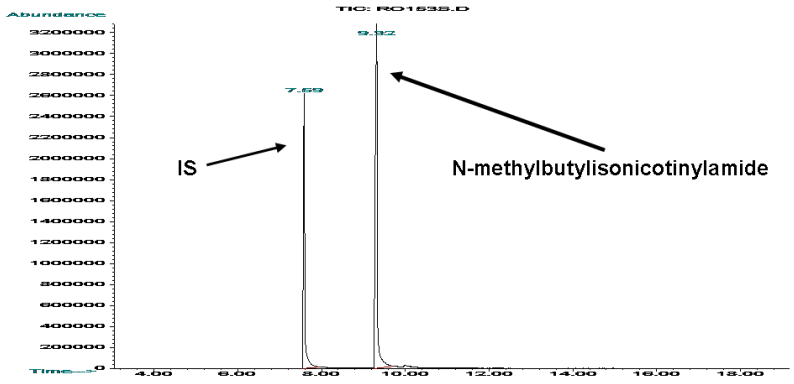

Peak#	Ret Time	Type	Width	Area	Start Time	End Time
1	7.587	BB	0.038	60278968	7.528	7.994
2	9.320	BB	0.056	118055516	9.237	9.750

Figure 6. GC-MS of the monomethylation reaction of butylamine.

As observe in Table 2, this monomethylation reaction is applicable to aliphatic (entry 1-4 Table 2), cycloaliphatic (entry 5 Table 2) and aromatic amines (entry 6 Table 2).

5.2.4 Preliminary thermodynamic and kinetic studies.

We made the preliminary kinetic studies at ^{31}P NMR by observing in the time, the appearance and the progressive growth of the new peak characteristic of the complex $CH_3N^+C_4H_9I^-$-Tiiii [C_3H_7, CH_3, Ph] (Figure 7a), and the progressive disappear of the free cavitand Tiiii [C_3H_7, CH_3, Ph] (Figure 7b). We plotted the intensity of each peak versus time and, as observed in Figure 8, the free cavitand completely disappears after less than 4500 s (1h 30min).

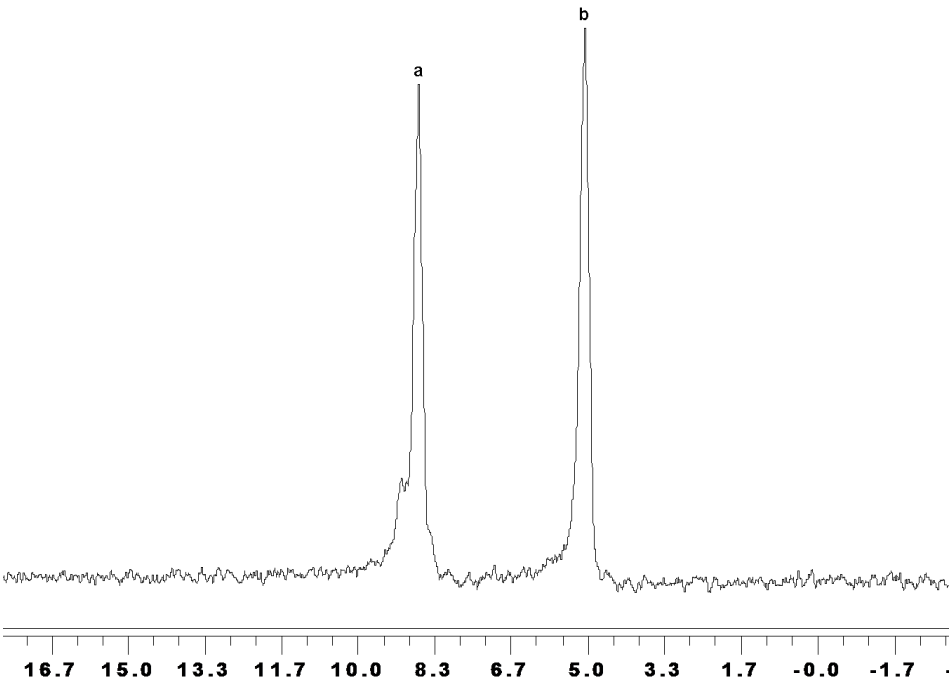

Figure 7. ^{31}P NMR monitoring of the monomethylation reaction after 10 min in $CDCl_3$.

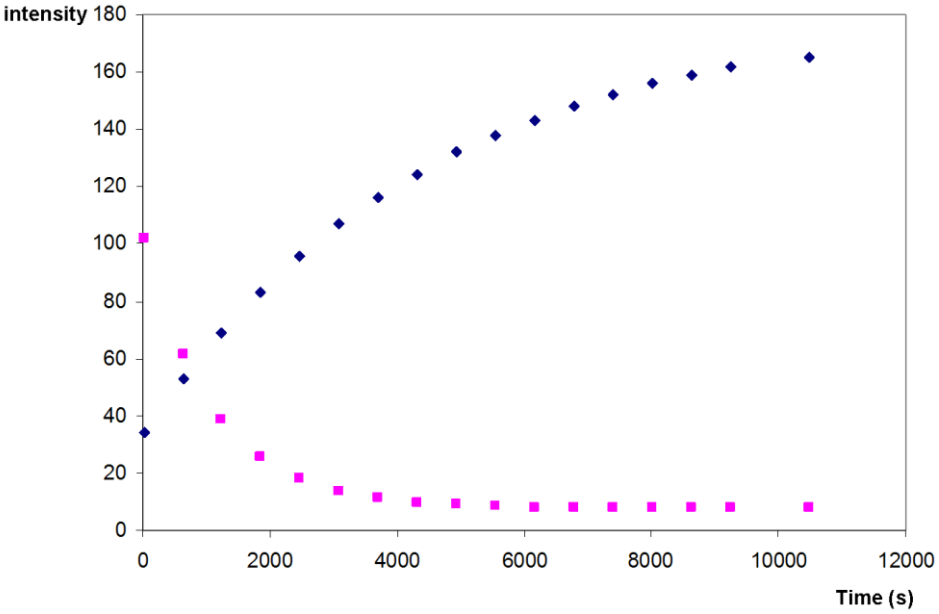

Figure 8. ^{31}P NMR monitoring of monomethylation reaction of butylamine in $CDCl_3$. Intensity υs time (s) of the free Tiiii cavitand (magenta squares); intensity υs time (s) of the N-methylammonium salt-Tiiii cavitand complex (blue squares).

5.3 Conclusions

In contrast to several other methods currently used for the *N*-monomethylation of primary aliphatic or aromatic amines, the use of the Tiiii cavitand as segregating agents presents some appreciable advantages. The application of this approach permits to control the selectivity of the reaction by controlling the strength of the interactions between the desired product and the segregating agent. High selective *N*-monomethylation of primary amines is achieved under mild conditions when the K_{ass} between the monomethylated product and the cavitand is above 10^7 M. At lower K_{ass} values like for TSiiii [C_3H_7, CH_3, Ph], the product monomethylated is biased, but the outcome is an any more univocal. This approach appears quite general and compatible with a

wide range of both aliphatic and aromatic amines. We are now performing the kinetic studies of these reactions.

5.4 Experimental Section

General Method: All reagents were purchased from Sigma-Aldrich Co. All solvents were dried over 3Å and 4Å molecular sieves by standard procedures. Pyridine was distilled on potassium hydroxide and dried over 3Å molecular sieves. ^{1}H NMR spectra were recorded at Bruker AC300 (300 MHz), AVANCE (300 MHz) and ^{31}P NMR at the AMX400 (172 MHz) spectrometers and all chemical shift (δ) were reported in parts per million (ppm) relative to the proton resonances resulting from incomplete deuteration of the NMR solvents. Microanalyses were performed by the service of Parma University. Electrospray ionization (ESI)-MS experiments were performed on a Waters ZMD spectrometer equipped with an electrospray interface. The GC-MS were performed on Agilent Technologies (mod.6890N) equipped with MS HEWLETT-PACKARD (mod. 5970) detector. The temperature programme used for the separation of derivative of ammonium salts and the internal standard started at 60 °C (held 3 min), set at 20 °C /min from 60 °C to 260 °C and held isothermally at 260 for 5 min. Column chromatography was performed using silica gel 60 (Merck 70-230 mesh).

Synthesis of thiophosphonate cavitand TSiiii [C_3H_7, CH_3, Ph]: to a solution of resorcinarene (2.5 g, 3.5 mmol) dissolved 20 mL of freshly distilled pyridine, dichlorophenylphosphine (1.93 mL, 14.3 mmol) was slowly added at room temperature. The reaction mixture was stirred for 3h at 80°C then cooled at room temperature. An excess of S_8 was added and left to stir for 1h. The solvent was removed under vacuum. 50 mL of water were added and the resulting yellow suspension was filtered. Purification by column chromatography on silica gel with a mixture 9:1 of methylene chloride and hexane yielded the product (2.74 g, 2,17 mmol, 62%)

^{1}H NMR (300 MHz, $CDCl_3$) δ (ppm): 1.05 (t, 12H, $CH_2\mathbf{CH_3}$, J = 7.2 Hz), 1.43 (m, 8H, $\mathbf{CH_2}CH_3$), 2.1 (s, 12H, Ar$\mathbf{CH_3}$), 2.31 (m, 8H, $\mathbf{CH_2}CH_2CH_3$, J = 7.5 Hz), 4.72 (t, 4H, $\mathbf{CH}CH_2$, J = 7.8 Hz), 7.24 (s, 4H, Ar**H**), 7.53 (m, 8H, O=PAr$\mathbf{H_m}$), 7.6 (m, 4H, O=PAr$\mathbf{H}p$), 8.2 (m, 8H, O=PAr$\mathbf{H_o}$). **^{31}P NMR** (172 MHz, $CDCl_3$) δ (ppm): 72 (s, **P=S**). **ESI-MS**: $C_{68}H_{68}NO_8P_4S_4$: 1265.3 $(M + H^+)^+$ and 1304.6 $(M + K^+)^+$.

Synthesis cavitand Mecav[C_2H_5, H] : to a solution of ethyl-footed resorcinarene (3.0 g, 5 mmol) dissolved in 20 mL of dry DMSO, K_2CO_3 **(**11.06 g, 80·mmol) and CH_2Br_2

(2.0 mL, 36·mmol) were added, under nitrogen. The purple mixture was stirred in a sealed tube at 90°C for 3 hours. The reaction was quenched by addition of 10 % $HCl_{(aq)}$ solution and the resulting mixture was extracted with CH_2Cl_2. The organic layer was washed with water (3 x 15 mL), dried over Na_2SO_4 and evaporated. The crude product was purified by column chromatography on silica gel by using hexane/ethyl acetate (6/4) as eluant to give the product (2.85 g, 88 %).

^{1}H NMR (300 MHz, $CDCl_3$) δ (ppm): 1.0 (t, 12H, C*H*$_3$), 2.3 (m, 8H, CHC*H*$_2$CH$_3$), 4.4 (d, 4H, C*H*$_{in}$, J = 7.2 Hz), 4.7 (t, 4H, C*H*Ar$_2$, J = 8.1 Hz), 5.7 (d, 4H, C*H*$_{out}$, J = 7.2 Hz), 6.5 (s, 4H, Ar*H*), 7.1 (s, 4H, Ar*H*) **ESI-MS**: *m/z* (%): 671 $(M+Na^+)^+$ and 637 $(M+H^+)^+$.

Synthesis of internal standard: to a solution of isonicotinoyl chloride hydrochloride (2 g, 11.2 mmol) dissolved in 80 mL of pyridine, n-butanol (1.03 mL, 11.2 mmol) was added. The reaction mixture was stirred for 3h at 100°C. The solvent was removed under vacuum. 50 ml of water solution containing 5 mmol of sodium carbonate were added and the resulting suspension was filtered. Purification by extraction (CH_2Cl_2 / H_2O) yielded the product (1.4 g, 7.84 mmol, 70%).

^{1}H NMR (300 MHz, $CDCl_3$) δ (ppm): 0.93 (t, 2H, $OCH_2CH_2CH_2\mathbf{CH_3}$, J = 7.3 Hz), 1.43 (m, 2H, $OCH_2CH_2\mathbf{CH_2}CH_3$), 1.71 (m, 2H, $OCH_2\mathbf{CH_2}CH_2CH_3$), 4.31 (t, 2H $O\mathbf{CH_2}CH_2CH_2CH_3$, J = 6.7 Hz), 7.79 (d, 2H, $\mathbf{H}_{mpy}$, J = 4.5 Hz), 8.72 (d, 2H, $\mathbf{H}_{opy}$, J = 4.5 Hz). **GC-MS**: rt = 7.59 min, *m/z (%)*: (M^+) = 179 (4), 106 (100), 124 (92), 78 (59), 56 (47), 51 (36.7), 123 (36.2), 137(12.2), 164 (10.2), 178 (10.2), 150 (2).

General procedure for the synthesis of N-methylammonium iodide salts.

To a solution of one equivalent of Tiiii [C_3H_7, CH_3, Ph] dissolved in chloroform, 3 equivalents of methyl iodide and one equivalent of primary amine were added at room temperature. The mixture was stirred for 16 h at 40°C. The solvent and the excess of methyl iodide were removed under vacuum. 5 mL of water were added and the resulting suspension of the cavitand Tiiii [C_3H_7, CH_3, Ph] was filtered. The resulting colourless water solution was evaporated and purified by crystallisation from a mixture methylene chloride:ethyl ether.

***N*-methylethylammonium iodide (68%)**: **^{1}H NMR** (300 MHz, CD_3CN) δ (ppm): 1.32 (t, 3H, $\mathbf{CH_3}CH_2NH_2CH_3$, J = 7.3 Hz), 2.99 (m, 2H, $CH_3\mathbf{CH_2}NH_2CH_3$), 2.55 (s, 3H, $NH_2\mathbf{CH_3}$), 7.24 (broad, 2H, $CH_3CH_2N\mathbf{H_2}CH_3$). **ESI-MS:** $C_3H_{10}IN$: 313.9 $(M + 2I^-)^-$.

***N*-methylpropylammonium iodide (62%): ^{1}H NMR** (300 MHz, CD_3CN) δ (ppm): 0.95 (t, 3H, $\mathbf{CH_3}CH_2$, J = 7.3 Hz), 1.73 (m, 2H, $CH_3\mathbf{CH_2}$), 2.55 (s, 3H, $NH_2\mathbf{CH_3}$), 2.9 (t, 2H, $\mathbf{CH_2}NH_2CH_3$, J = 7.5 Hz), 7.44 (broad, 2H, $CH_2N\mathbf{H_2}CH_3$). **ESI-MS**: $C_4H_{12}IN$: 328 $(M + 2I^-)^{2-}$.

***N*-methylbutylammonium iodide (62%): ^{1}H NMR** (300 MHz, CD_3CN) δ (ppm): 0.91 (t, 3H, $\mathbf{CH_3}CH_2$, J = 7.3 Hz), 1.4 (m, 2H, $CH_3\mathbf{CH_2}$), 1.7 (m, 2H, $CH_2\mathbf{CH_2}CH_2NH_2$), 2.55 (s, 3H, $CH_2NH_2\mathbf{CH_3}$), 2.9 (t, 2H, $\mathbf{CH_2}NH_2CH_3$, J = 7.5 Hz), 7.5 (broad, 2H, $N\mathbf{H_2}CH_3$). **ESI-MS:** $C_5H_{14}IN$: 342 $(M + 2I^-)^-$.

General procedure for the synthesis of N-methylisonicotinylamide.

To a solution of one equivalent of Tiiii [C_3H_7, CH_3, Ph] dissolved in chloroform, one equivalent of primary amine and 3 equivalents of methyl iodide were added. The reaction mixture was stirred for 16h at 40°C for aliphatic amines and for 20 h at reflux for cyclohexylamine and aromatic amine. The solvent and the excess of methyl iodide were removed under vacuum. The crude reaction was dissolved in pyridine; four equivalents of isonicotinoylchloride hydrochloride were added and stirred for 3h at 100°C. The pyridine was removed under vacuum. The water was added and the suspension of the cavitand was filtered. K_2CO_3 was added to the resulting colourless water solution and extracted with CH_2Cl_2. Purification by rinsing the organic layer with acidic water and neutral water and evaporation yielded colourless liquid for aliphatic amines, white and yellow crystals for respectively cyclohexylamine and aniline.

***N*-methylethylisonicotinylamide (74.8%): ^{1}H NMR** (300 MHz, CD_3CN) δ (ppm): 1.16 and 1.06 (t, 3H, $CH_3N(CO)CH_2$ **(2xCH_3),** J = 7.2 Hz), 2.97 and 2.82 (s, 3H, **(2xCH_3)**N(CO)), 3.48 and 3.15 (t, 2H, $CH_3N(CO)$**(2xCH_2)**CH_3, J = 7.2 Hz), 7.26 (d, 2H, $\mathbf{H}_{mpy}$, J = 4.5 Hz), 8.62 (d, $\mathbf{H}_{opy}$, J = 4.5 Hz). **GC-MS:** rt = 8.23 min. *m/z (%)*: (M^+) = 164 (27.2), 106 (100), 163 (51.2), 78(50.9), 51 (23.6), 58 (8.7), 79 (5.9), 135 (5.3), 149 (3.6).

***N*-methylpropylisonicotinylamide (79%): ^{1}H NMR** (300 MHz, CD_3CN) δ (ppm): 0.93 and 0.70 (t, 3H, CH_2CH_2 **(2xCH_3),** J = 7.2 Hz), 1.62 and 1.50 (m, 2H, CH_2 **(2xCH_2)**CH_3), 2.97 and 2.82 (s, 3H, **(2xCH_3)**N(CO)), 3.43 and 3.09 (t, 2H, $CH_3N(CO)$**(2xCH_2)**CH_2, J = 7.2 Hz), 7.26 (d, 2H, $\mathbf{H}_{mpy}$, J = 4.5 Hz), 8.62 (d, 2H, $\mathbf{H}_{opy}$, J = 4.5 Hz). **GC-MS**: rt = 8.77 min. *m/z (%)*: (M^+) = 178 (12.5), 106 (100), 78(29.4), 177 (10.7), 149 (12.5), 51 (12.5), 107 (6.25), 135 (5.3), 163 (1.7).

***N*-methylbutylisonicotinylamide (87.2%): ^{1}H NMR** (300 MHz, CD_3CN) δ (ppm): 0.95 and 0.76 (t, 3H, CH_2 **(2xCH_3)**, J = 7.2 Hz), 1.38 and 1.12 (m, 2H, CH_2

(2xCH$_2$)CH$_3$), 1.60 and 1.5 (m, 2H, CH$_2$ **(2xCH$_2$)**CH$_2$CH$_3$), 2.97 and 2.82 (s, 3H, **(2xCH$_3$)**N), 3.46 and 3.11 (t, 2H, **(2xCH$_2$)**CH$_2$CH$_2$CH$_3$, J = 7.2 Hz), 7.26 (d, 2H, **H$_{mpy}$**, J = 4.5 Hz), 8.61 (d, 2H, **H$_{opy}$**, J = 4.5 Hz). **GC-MS**: rt = 9.28 min. *m/z (%)*: (M^+) = 192 (3.6), 106 (100), 78(28.6), 149 (19.6), 51 (10.7), 114 (8.9), 135 (5.3), 163 (2.9), 191 (2.5).

***N*-methylheptylisonicotinylamide (74.6%): ^{1}H NMR** (300 MHz, CDCl$_3$) δ (ppm): 1.33 - 0.81 (broad, 2H, CH$_2$CH$_2$**CH$_3$**), 1.33 - 1.17 (broad, 6H, CH$_2$**CH$_2$CH$_2$CH$_2$CH$_2$**CH$_3$), 1.62 and 1.50 (m, 2H, CH$_3$N(CO)CH$_2$**(2xCH$_2$)**CH$_2$), 3.05 and 2.87 (s, 3H, **(2xCH$_3$)**N), 3.45 and 3.13 (t, 2H, CH$_3$N(CO)**(2xCH$_2$)**CH$_2$, J = 7.2 Hz), 7.24 (d, 2H, **H$_{mpy}$**, J = 4.5 Hz), 8.66 (d, 2H, **H$_{opy}$**, J = 4.2 Hz). **GC-MS:** rt = 10.87 min. *m/z (%)*: (M^+) = 234 (3.8), 106 (100), 149 (37.7), 78 (32), 51 (9.4), 156 (9.4), 135 (7.1), 177 (1.8), 233 (1.8).

***N*-methylciclohexylisonicotinylamide (63.7%): ^{1}H NMR** (300 MHz, CD$_3$CN) δ (ppm): 1.85 - 1.02 (broad, 10H, CH$_3$NCH **(CH$_2$)$_2$(CH$_2$)$_2$CH$_2$**), 2.88 and 2.69 (s, 3H, (**2xCH$_3$**)NCH), 4.35 and 3.24 (m, 1H, CH$_3$N(**2xCH)**), 7.25 (d, 2H, **H$_{mpy}$**, J = 4.5 Hz), 8.62 (d, 2H, **H$_{opy}$**, J = 4.5 Hz). **GC-MS**: rt = 10.76 min. *m/z (%)*: (M^+) = 218 (25.3), 106 (100), 137 (60.16), 78(41.6), 161 (16.6), 175 (15), 51 (14.2), 217 (6.6), 55 (6.6), 123 (4.5), 219 (3.3).

***N*-methylanilylisonicotinylamide (82.1%): ^{1}H NMR** (300 MHz, CD$_3$CN) δ (ppm): 3.41 (s, **CH$_3$**N), 7.02 (d, 2H, **H$_p$**, J = 7.2 Hz), 7.11 (d, 2H, **H$_{mpy}$**, J = 4.5 Hz), 7.26 – 7.17 (broad, 4H, **H$_m$** + **H$_o$**), 8.43 (d, 2H, **H$_{opy}$**, J = 4.5 Hz). **GC-MS**: rt = 10.25 min. *m/z (%)*: (M^+) = 212 (34.4), 106 (100), 78(60.6), 119 (24.6), 51 (23.7), 77 (16.4), 211 (8.2), 213 (3.2).

5.5 References

[1] B. R. Brown, *The Organic Chemistry of Aliphatic Nitrogen Compounds;* Oxford University: New York, **1994.**

[2] R. N. Salvatore, C. H. Yoon, K. W. Jung., *Tetrahedron,* **2001,** 57, 7785-7811.

[3] a) M. S. Gibson, *The Chemistry of the Amino Group,* Patai, S., Ed., Interscience: London, UK, **1968**, Chapter 2, 45-62; b) F. G. Willson, T. S. Wheeler, *Organic Syntheses,* Wiley: New York, NY, **1941,** 1, 102.

[4] a) D. D. Reynolds, W. O. Kenyon, *J. Am. Chem. Soc.* **1950,** 72, 1591; b) L. F. Tietze, H. Schirok, *J. Am. Chem. Soc.* **1990,** 121, 10264

[5] a)F. A. Carey, R. J. Sndberg, *Advanced Organic Chemistry, Part B;* 3th ed; Plenum: New York, **1990,** 132; b) R. O. C. Norman, J. M. Coxon, *Principles of Organic Syntheses, 3rd, ed.,* Blackie Academic: New York, **1993,** 301; c) H. Beyer, W. Walter, *Handbook of Organic Chemistry,* Printice Hall: New York, **1996,** 158.

[6] a) M. Selva, P. Tundo, A. Perosa, *J. Org. Chem.*, **2001,** 66, 677-680; b) Z.-H. Fu, Y. Ono, *Catal. Lett.,* **1993,** 22, 277-283; c) P. R. Hari, Presad Rao, P. Massiani, D Barthomeuf, *Catal. Lett.*, **1995,** 31, 115-120; d) M. Selva, A. Bomben, P. Tundo, *J. Chem. Soc., Perkin, Trans. 1* **1997,** 1041-1045; e) M. Onaka, K. Ishikawa, Y. Izumi, *Chem. Lett.* **1982**, 1783-1786; f) M. Onaka, A. Umezono, M. Kawai, Y. Izumi, *J. Chem. Soc. Chem. Commun.* **1985,** 1202-1203; g) M. Selva, P. Tundo, *Tetrahedron Lett.,* **2003,** 44, 8139-8142.

[7] a) J. Santhanalakshmi, T. Raja, *Appl. Catal.*,**1996**, 147, 69-80, b) F. Valot, F. Fache, R. Jacquot, M. Spagnol, M. Lemaire, *Tetrahedron Lett.* **1999,** 40, 3689-369.

[8] T. Oku, T. Ikariya, *Angew. Chem. Int. Ed.,* **2002,** 3476-3479.

[9] J. R. Browser, *Inorganic Chemistry;* Brooks/Cole: California, **1993,** 406

[10] E. C. Constable, *Metal and Ligand Reactivity;* VHC: New York, **1996,** 102.

[11] a) G. Bar-Haim, M. Kol, *Tetrahedron Lett.* **1998,** 39, 2663; b) H. C. Brown, A. M. Salunkhe, B. Singaram, *J. Org. Chem.* **1991,** 56, 1170-2666.

[12] a) S. Krishnamurthy, *Tetrahedron Lett.*, **1982,** 23, 3315-3318; b) P. Hamel, Y. Girard, *Tetrahedron Lett.*, **1994,** 35, 8101-8102.

[13] R. A. Crochet J.r., C. Dewitt Blanton J.r. *Synthesis,* **1974,** 55-56.

[14] A. Le Pera, A. Leggio, A. Liguori, *Tetrahedron*, **2006**, 62, 6100-6106.

[15] A. Adima, C. Bied, J. J. E. Moreau, M. W. C. Man, *Eur. J. Org. Chem.*, **2004,** 2582-2588.

[16] a) A. Gissot, J. Rebek, Jr. *J. Am. Chem. Soc.*, **2004,** 7424-7425, b) D. H. Leung, D. Fiedler, R. G. Bergman, K. N. Raymond, *Angwe. Chem. Int., Ed.* **2004,** 43, 963-966, J. Kang, J. Rebek, Jr., *Nature,* **1997,** 50-52; d) Y. Nishioka, T. Yamaguchi, M. Yoshizawa, M. Fujita, *J. Am. Chem. Soc.*, **2007,** 7000-7001.

[17] P. Delange, J.-C. Mulatier, B. Tinant, J. P. Declercq, J.-P. Dutasta, *Eur. J. Org. Chem.*, **2001,** 3695-3704.

[18] E. Kalenius, D. Moiani, E. Dalcanale, P. Vainiotalo, *Chem. Commun.*, **2007**, 3865-3867.

[19] L. Tunstad, J. A. Tucker, E. Dalcanale, J. Weiser, J. A. Briant, J. C. Sherman, R. C. Helgeson, C. B. Knobler, D. J. Cram, *J. Org. Chem.* **1989,** 54, 1305-1312.

[20] B. C. Gibb, R. G. Chapman, J. C. Sherman, *J. Org. Chem.* **1996,** 61, 1505-1509.

[21] B. Bibal, B. Tinantb, J.-P. Declercq, J.-P. Dutasta, *Chem. Commun.*, **2002**, 432-433.

[22] a) Hiroyuki Kataoka, *Journal of Chromatography A,* **1996,** 733, 19-34; b) F. Sacher, S. Lenz, H.-J. Brauch, *Journal of Chromatography A,* **1997,** 764, 85-93; c) J. M. Halket, D. Waterman, A. M. Przyborowska, R. K. P. Patel, P. D. Fraser, P. M. Bramley, *Journal of Experiment Botany*, 56, 219-243.

[23] H. G. J. Mol, S. Sumarto, O. M. Steijger *Journal of Chromatography A,* **2000,** 879, 97-112.

Abstract

Supramolecular polymers are the main topic of this thesis. Such polymers are based on well defined architectures in which the building blocks are held together by non-covalent interactions. Such interactions result to be reversible and tunable. Consequently supramolecular polymers may have many advantages over traditional polymers because of easy workability both in solution and in the melt. Also they might respond differently to high levels of stress since the secondary interactions holding the chains together are constantly being broken and reformed.

Chapter 2 reports the diastereoselective synthesis of tetraphosphonate cavitands and their complexation properties toward charged N-methyl derivatives. Chapter 3 and 4 report the synthesis of the monomer units based on functionalized tetraphosphonate cavitands for self-assembly-disassembly of polymers and the characterization of the supramolecular architectures obtained. In Chapter 5, the Tiiii cavitands that form very stable complexes with N-methylammonium salts were used as sequestrant agents in the monomethylation reactions of primary amines, achieving very high selectivity.

Abstract

Argomento principale di questa tesi è la sintesi e lo studio di sistemi polimerici supramolecolari. Tali sistemi presentano architetture ben definite in cui le singole unità costituenti sono legate tra loro mediante interazioni non covalenti, reversibili e modulabili. Per questo motivo i polimeri supramolecolari annoverano numerosi vantaggi rispetto a quelli tradizionali, tra cui la più facile lavorabilità, sia in soluzione che da fuso. Inoltre questi sistemi sono in grado di sopportare anche elevati stress applicati, grazie alla loro capacità di rompere e riformare in modo continuo le interazioni tra le unità monomeriche.

Il capitolo due riporta la sintesi diastereoselettiva di cavitandi tetrafosfonati e lo studio delle loro proprietà complessanti nei confronti di sali di N-metil piridinio e di N-metilammonio. I capitoli tre e quattro illustrano la sintesi di cavitandi tetrafosfonati diversamente funzionalizzati usate come unità monomeriche per il self-assembly-disassembly di polimeri. Si riporta inoltre la caratterizzazione delle architetture supramolecolari ottenute. Nel capitolo cinque, i cavitandi tetrafosfonati che formano complessi stabili con sali di N-metilammonio sono stati utilizzati come agenti sequestranti in processi di monometilazione di ammine primarie, raggiungendo altissime selettività per questo tipo di reazioni.

About the Author

Roger Yebeutchou Mbanda was born in Ntonga-Camerun in 1976. He graduated in Industrial Chemistry at the University of Parma in 2003. His research focused on the catalytic reaction in water. In 2005, he started his PhD course in Material Science in the group of Professor Enrico Dalcanale at the University of Parma; his research interests involve on the Host-guest Supramolecular polymer based on phosphonate cavitands.